CR 111769

[redacted]

(NASA-CR-111769) HYPERSONIC RESEARCH ENGINE PROJECT. PHASE 2A: STRUCTURES AND COOLING DEVELOPMENT Interim Technical Data Report, 3 May - 2 Aug. 1969 (AiResearch Mfg. Co., Los Angeles, Calif.) 167 p

N76-77236

Unclas
00/98 49645

GARRETT

AIRESEARCH MANUFACTURING COMPANY
A DIVISION OF THE GARRETT CORPORATION
9851-9951 SEPULVEDA BLVD. • LOS ANGELES, CALIFORNIA 90009
TELEPHONE: SPRING 6-1010, ORCHARD 0-0131 • CABLE: GARRETTAIR LOS ANGELES

AIRESEARCH MANUFACTURING COMPANY

Los Angeles, California

HYPERSONIC RESEARCH ENGINE PROJECT-PHASE IIA
STRUCTURES AND COOLING DEVELOPMENT
TENTH INTERIM TECHNICAL DATA REPORT
DATA ITEM NO. 55-7.10
3 MAY THROUGH 2 AUGUST 1969
NASA CONTRACT NO. NAS1-6666

DOCUMENT NO. AP-69-5390

Number of pages 167

Original date 26 August 1969

Attachments: AiResearch
Drawings L980628 and
L980630

Prepared by Engineering Staff

Edited by L. F. Jilly

Approved by Henry J. Lopez
HRE Program Manager

Revision	Date	Pages Affected (Revised, Added, Eliminated)

FOREWORD

This interim technical data report is submitted to the NASA-Langley Research Center by the AiResearch Manufacturing Company, Los Angeles, California. The document was prepared in accordance with the guidelines established by paragraph 6.3.3.2 of NASA Statement of Work L-4947-B.

Interim technical data reports are generated on a quarterly basis for major program tasks under the Hypersonic Research Engine Project. Upon completion of a given task effort, a final technical data report will be submitted.

The document in hand presents a detailed technical discussion of the structures and cooling development for the period of 3 May through 2 August 1969.

ACKNOWLEDGMENTS

Acknowledgments for completion of this document are herewith extended to the following contributors:

Design and Development:	O. A. Buchmann
	J. C. Gibson
	L. H. King
	C. M. Lee
	A. I. Stern
Heat Transfer Analyses:	S. M. Cho
	A. A. Vuigner
	F. M. Walters
	C. F. Young
Stress Analyses:	W. G. Flieder
	E. Katinszky
Materials Engineering:	O. Jones

CONTENTS

Section		Page
1.	SUMMARY OF STATUS	1-1
	1.1 Structural Assembled Model Design	1-1
	1.2 Full-Scale Component Manufacture	1-1
	1.3 Inlet Spike Actuation System	1-1
	1.4 Structural Elements and Models	1-1
2.	PROBLEM STATEMENT	2-1
3.	TOPICAL BACKGROUND	3-1
	3.1 General Design Guidelines	3-1
	3.2 Operational Boundaries	3-3
4.	OVERALL APPROACH	4-1
	4.1 Thermal Design	4-2
	4.2 Structural Design	4-3
	4.3 Mechanical Design	4-4
	4.4 Manufacturing	4-5
5.	ANALYTICAL DESIGN	5-1
	5.1 SAM Water-Cooled Cowl/Pylon	5-1
	5.2 SAM Water-Cooled Mounting Structure	5-5
	5.3 SAM Coolant Regulating Valves	5-19
	5.4 Leading Edge Thermal Performance	5-24
6.	DESIGN EFFORT	6-1
	6.1 Water-Cooled Cowl/Pylon	6-1
	6.2 Water-Cooled Mounting Structure	6-1
7.	MANUFACTURING	7-1
	7.1 Inlet Spike	7-1
	7.2 Innerbody (Inner Shell)	7-6
	7.3 Innerbody (Nozzle)	7-12
	7.4 Leading Edge	7-19

CONTENTS (Continued)

Section		Page
	7.5 Outer Shell	7-24
	7.6 Strut	7-26
	7.7 HRE Experimental Assembly	7-28
	7.8 Component Test Summary	7-28
8.	TESTING	8-1
	8.1 Full-Scale Strut	8-1
	8.2 Component Pressure Drop and Flow Distribution	8-41
	8.3 Inlet Spike Actuator	8-69
9.	FUTURE ACTION	9-1
	REFERENCES	R-1

ILLUSTRATIONS

Figure		Page
3.0-1	Cooled Structures Nomenclature	3-2
3.2-1	Typical Engine Operating Cycles	3-5
5.1-1	EASE HRE Cowl/Pylon Analysis	5-2
5.1-2	EASE HRE Cowl/Pylon Analysis	5-3
5.1-3	SAM Cowl/Pylon Aerodynamic Loads	5-4
5.2-1	External Flow Properties on Mounting Structure	5-8
5.2-2	Cooling of Flat Bottom Surface of Pylon and Part of Mounting Structure (Reference Figure 5.2-3)	5-9
5.2-3	Cooling of Remaining Part of Mounting Structure (Reference Figure 5.2-2)	5-10
5.2-4	Heat Flux Along Side Surface of Mounting Structure	5-12
5.2-5	Heat Flux on Pylon Bottom Surface at Pylon/Mounting Structure Interface with T (WALL) = 700°R	5-13
5.2-6	SAM Support Structure	5-16
5.2-7	SAM Aerodynamic Loads	5-17
5.2-8	SAM Weight Distribution, Spike Retracted	5-18
5.3-1	SAM Hydrogen Coolant Schematic	5-20
5.3-2	CRV Effective Areas at SAM Design Point Flow Rate	5-21
5.3-3	Spike Coolant Regulating Valve (CRV 1) Characteristics	5-22
5.3-4	Innerbody Coolant Regulating Valve (CRV 2) Characteristics	5-23
5.4-1	Leading Edge Hot Surface Temperatures	5-25
7.1-1	Major Components of Inlet Spike Brazed Assembly	7-2
7.1-2	Inlet Spike Assembly	7-3
7.1-3	Inlet Spike Assembly	7-4

ILLUSTRATIONS (Continued)

Figure		Page
7.2-1	HRE Innerbody	7-7
7.2-2	Inner Shell Assembly - View into Aft End Showing Actuator Mounting Pads, Strut Mounting Pads, and Nozzle Mounting Flange	7-8
7.2-3	Inner Shell Assembly - View of Forward End	7-9
7.2-4	Fabrication Sequence - Inner Shell Assembly Strut Openings	7-11
7.3-1	Aft Nozzle Assembly Viewed from Small (Aft) End	7-13
7.3-2	SAM Nozzle Assembly Viewed from Large (Forward) End	7-14
7.3-3	Nozzle Baffle Assembly	7-15
7.3-4	Nozzle Cover Assembly	7-16
7.3-5	Nozzle Cap	7-17
7.3-6	SAM Nozzle Assembly	7-18
7.4-1	Leading Edge Assembly	7-20
7.4-2	Components of Leading Edge Structural Assembly (Inlet and Outlet Manifold Assemblies, Mating Ring, Ring Stiffener)	7-21
7.4-3	Leading Edge Assembly After Completion of all Brazing Operations	7-22
7.5-1	SAM Outer Shell Assembly	7-25
7.6-1	Struts Internal Details	7-27
7.7-1	HRE Experimental Assembly - Engine Profile, Spike Retracted	7-29
7.7-2	HRE Experimental Assembly - View Looking Into Aft End	7-30
7.7-3	HRE Experimental Assembly - View Looking Into Forward End, Spike Retracted	7-31

ILLUSTRATIONS (Continued)

Figure		Page
8.1-1	Strut Configuration No. 1, SN 5 Prior to Thermal Cycling (Coated Leading Edge)	8-2
8.1-2	Strut Configuration No. 1, SN 5 After Thermal Cycle 102 (Coated Leading Edge)	8-3
8.1-3	Strut Configuration No. 1, SN 5 After Thermal Cycle 102	8-4
8.1-4	Strut Configuration No. 1, SN 5 Showing Braze Alloy Plugging in Leading Edge	8-5
8.1-5	Strut Configuration No. 2, SN 2 After Thermal Cycle 44	8-6
8.1-6	Strut Configuration No. 2, SN 2 After Thermal Cycle 44	8-7
8.1-7	SK 51509-1 Support Panel After Thermal Cycle 106	8-8
8.1-8	SK 51509-1 Support Panel After Thermal Cycle 106 Showing Heating Pattern on Edges of Cold Side	8-9
8.1-9	SK 51322-1 Panel Schematic and Flow Distribution Instrumentation	8-10
8.1-10	SK 51509-1 Panel Schematic and Flow Distribution Instrumentation	8-11
8.1-11	Configuration 2, SN 2 Strut Thermal Cycle Test Conditions	8-13
8.1-12	Configuration 1, SN 5 Strut Thermal Cycle Test Conditions	8-14
8.1-13	Configuration 2, SN 2 Strut Leading Edge Temperature vs Burner Hydrogen Flow Rates	8-16
8.1-14	Configuration 1, SN 5 Strut Leading Edge Temperature vs Burner Hydrogen Flow Rates	8-17
8.1-15	Configuration 1, SN 6 Strut Leading Edge Temperature vs Burner Hydrogen Flow Rates	8-18
8.1-16	Typical Thermal Cycle Temperatures	8-19

ILLUSTRATIONS (Continued)

Figure		Page
8.1-17	Wall Temperature vs Cycle	8-20
8.1-18	Configuration 2, SN 2 Strut Isotherms	8-21
8.1-19	Configuration 1, SN 5 Strut Isotherms	8-22
8.1-20	Configuration 1, SN 6 Strut Isotherms	8-23
8.1-21	Heat Flux Distribution	8-24
8.1-22	Simplified Heat Transfer Model for Finned Leading Edge Coolant Passage	8-26
8.1-23	Configuration 2, SN 2 Strut Wall Temperature vs Heat Load	8-29
8.1-24	Para-Hydrogen History	8-30
8.1-25	Para-Hydrogen History	8-31
8.1-26	Gas Chromatograph and Continuous Reading Single-Channel Recorder at NATS Laboratory	8-33
8.1-27	Support Panel Temperature Distribution for Thermal Cycle 5	8-35
8.1-28	Support Panels Flow Distribution	8-36
8.1-29	Strut Thermal Fatigue Temperatures	8-38
8.2-1	SAM Spike Air-Pressure-Drop Test Setup	8-42
8.2-2	SAM Spike Air-Pressure-Drop Test Setup	8-43
8.2-3	SAM Spike Air-Pressure-Drop Test Results	8-44
8.2-4	SAM Spike Injector Manifold Inlet Lines Pressure-Drop-Test Results	8-45
8.2-5	Strut Sides Air-Pressure-Drop Test Setup	8-48
8.2-6	Strut Sides Air-Pressure-Drop Test Results	8-49
8.2-7	Nozzle and Inner Shell Air-Pressure-Drop Test Setup	8-50
8.2-8	Innerbody Air-Pressure-Drop Test Setup	8-51

ILLUSTRATIONS (Continued)

Figure		Page
8.2-9	Nozzle Air-Pressure-Drop Test Results	8-52
8.2-10	Innerbody and Inner Shell Air-Pressure-Drop Test Results	8-53
8.2-11	Leading Edge Air-Pressure-Drop Test Setup	8-56
8.2-12	Leading Edge Air-Pressure-Drop Test Results	8-57
8.2-13	SAM Leading Edge Flow Distribution and Outlet Manifold Pressure	8-58
8.2-14	Outer Shell Assembly Air-Pressure-Drop Test Setup	8-61
8.2-15	Outer Shell Assembly Air-Pressure-Drop Test Setup	8-62
8.2-16	SN 1 Forward Outer Shell Air-Pressure-Drop Test Results	8-63
8.2-17	Aft Outer Shell Air-Pressure-Drop Test Results	8-64
8.2-18	SN 1 Outer Shell Manifolds Pressure Distributions	8-65
8.2-19	SN 2 (SAM) Outer Shell Injectors Air-Pressure-Drop Test Results	8-66
8.3-1	Inlet Spike Actuation System Assembly	8-71
8.3-2	Hydraulic Actuator for Inlet Spike Actuation System Assembly	8-72
8.3-3	Fabroid Journal Bearing in Structural Housing After Endurance Test	8-73
8.3-4	Fabroid Journal Bearing in Slide Assembly After Endurance Test	8-74
8.3-5	Actuator Piston Assembly After Endurance Test	8-75
8.3-6	Actuator Locking Cams and Piston After Endurance Test	8-76
8.3-7	Actuator Rod-End Assembly After Endurance Test Showing Extruded Fabroid	8-77

Figure		Page
8.3-8	Actuator Universal Hub and Pin After Endurance Test Showing Deformation of Pin	8-78

TABLES

Table		Page
5.1-1	SAM Cowl/Pylon Maximum Stress Due to Pressure and Inertia Loads	5-6
5.2-1	Sectional Pressure Drops for Cooling System of Mounting Structure L980628	5-14
7.8-1	Component Test Summary	7-33
8.1-1	Summary of Strut and Support Panel Testing	8-12
8.1-2	Errors Due to Erroneous Hydrogen Composition	8-32
8.2-1	Summary and Comparison of Results for Innerbody Air-Pressure-Drop Tests	8-54

NOMENCLATURE

Section 8.1.2

A_1	strut leading edge external effective area, 0.0041 ft^2
A_f/A_t	ratio of fin to total internal area, $\frac{\ell}{(\ell + 0.0025)}$ see Figure 8.1 -22b
A_w/A_1	ratio of the average heat conduction area to the external area, $\frac{\text{external area + internal area}}{2 \times \text{external area}}$
B_1, B_2 and B_3	coefficients defined in Equations (8.1-1) (8.1-2), and (8.1-3), respectively.
h_o	stagnation line heat transfer coefficient, Btu/ft^2 sec ^0R
h_c	internal heat transfer coefficient, Btu/ft^2 sec ^0R
K	stagnation zone heat transfer ratio of conditions with freestream turbulence to conditions without turbulence.
k	conductivity, Btu/ft sec ^0R
ℓ	fin height, ft (see Figure 8.1 -22b)
q	heat rate, Btu/sec
r_1, r_2	strut leading edge external and internal radii respectively
s	distance measured from the strut stagnation line, in.
T_{w1}, T_{w2}	strut stagnation line wall temperatures. Subscription 1 and 2 designate the external surface and the internal surface, respectively.
T_B	coolant temperature, ^0R
T_T	hot gas total temperature, ^0R
U	overall heat transfer coefficient, Btu/ft^2 sec ^0R
W_s, W_c	strut sidewall coolant flow rates and leading edge coolant flow rates respectively, lb/sec
δ	fin width, ft
η_f	fin effectiveness
η_2	overall fin effectiveness, Equation (8.1-4)

1. SUMMARY OF STATUS

All activity preparatory to assembly of the Structural Assembled Model (SAM) and fabrication of the water-cooled wind tunnel adapters has been completed. The fabrication of the adapters and assembly of the SAM will be delayed pending design reviews for the wind tunnel configuration of the design.

1.1 STRUCTURAL ASSEMBLED MODEL DESIGN

Detail design of all SAM components has been completed. The design effort included a water-cooled cowl and pylon and a water-cooled structural mounting, assembly drawings for the flightweight components, and a top assembly drawing for the flightweight and water-cooled components.

1.2 FULL-SCALE COMPONENT MANUFACTURE

Manufacture of all of the flightweight, full-scale components has now been completed, with one each of the components manufactured specifically to the SAM configuration. The components completed during the reporting period include the outer shell, the inlet spike, and the leading edge. These, along with the previously completed inner shell and nozzle, provide the necessary flightweight components for the SAM. All of the components have been satisfactorily proof-pressure tested with StressCoat to 1050 psig and leak-tested with gaseous nitrogen at 1050 psig. Acceptability for leakage is defined as absence of bubbles for a period of 5 min when the part is immersed in water. Structural acceptability in the StressCoat test requires absence of evidence of yielding.

Isothernal pressure drop and flow distribution tests, using air as the test fluid, also have been completed for all of the components. Data is presented to the extent that it has been reduced. Results indicate satisfactory performance within the boundaries of the design.

1.3 INLET SPIKE ACTUATION SYSTEM

Following completion of the test, as reported in the previous TDR, no additional work has been performed. This report does include a number of photographs not available at the time of publication of the previous TDR. They show the condition of various actuator components after post-test teardown.

1.4 STRUCTURAL ELEMENTS AND MODELS

The remaining effort in this category involved wind tunnel testing of the full-scale strut. This testing has been completed. The final testing, using a fourth strut in the test series, was aimed at accumulating 100 cycles

on the strut support panels. Evidence of leakage in these panels proved to be erroneous, and the panels survived 100 cycles without leakage. The panels used in the test were of a configuration simulating the configurations used in the full-scale inner and outer shell components.

2. PROBLEM STATEMENT

The objective of the structures and cooling development program is to analyze, design, and fabricate the regeneratively cooled surfaces and their associated structures and to verify the performance of these surfaces and structures at conditions that simulate the operating conditions expected in the flight test engine.

The Hypersonic Research Engine requires regenerative cooling on all surfaces that contact the engine airstream. The use of ablative coating on the engine aerodynamic surfaces is barred by the Statement of Work to minimize extraneous effects on engine performance. No such restriction is imposed on the engine cowl; therefore, ablative protection is used for this component.

The characteristic design problem in regeneratively cooled structures for this type of application is associated with the large heat fluxes encountered over major portions of the engine surfaces. These heat fluxes range from values of approximately 10 Btu/sec-ft^2 to 1800 Btu/sec-ft^2 on the stagnation line of the support strut leading edge. The conservation of fuel requires that these heat fluxes be accommodated at temperature differences across the regeneratively cooled surfaces which range up to approximately 800^{0}F in flat surfaces and 1200^{0}F in leading-edge areas. These temperature differences, in turn, result in strains that cause plastic deformation of the hot surfaces. Design therefore is governed by low-cycle fatigue conditions. Uncertainties associated with the prediction of low-cycle fatigue performance have led to heavy emphasis, in the experimental portion of the program, on the evaluation of the low-cycle fatigue performance of the engine components.

The general performance objectives set for the cooled structures are as follows:

Design life - 10 hr of hot operation, of which 3 hr are to be taken at Mach 7 to 8 flight conditions

Cycle life - 100 cycles, at conditions which produce the highest plastic strain

3. TOPICAL BACKGROUND

The cooled structures, which are being designed, fabricated, and tested as part of this task, and the associated connecting structures constitute the basic structural elements of the engine. The cooled surfaces of these structures form the aerodynamic surfaces of the engine, as shown in Figure 3.0-1.

3.1 GENERAL DESIGN GUIDELINES

The regeneratively cooled surfaces must be designed and fabricated to minimize engine performance losses. In addition to providing the basic contours, the cooled surfaces must be fabricated and assembled in a way that avoids discontinuities; leading edges must use the minimum radius compatible with reliable structural design.

Because of the research nature of the HRE program, temperatures and pressures will be measured throughout the engine. Consequently, the engine structures must accommodate static pressure taps and metal temperature thermocouples.

The total amount of fuel available to the engine and for cooling of the structure is severely limited by X-15A-2 storage capabilities. Consequently, in cooling the structure, fuel usage in excess of combustion requirements must be minimized. To accomplish this goal, the cooled surfaces must function at maximum metal temperatures and temperature differences compatible with sound structural design.

Engine internal structures and plumbing must be designed to allow space for installing fuel system components, engine controls, instrumentation transducers, and signal conditioning equipment. Because of operating limitations, electronic equipment must be installed in locations having the least severe environment.

To permit the engine to operate over the flight Mach number range from 3 to 8, the inlet spike must be translated to various positions. To conserve coolant prior to and after engine operation, the inlet spike must be translated to a position nearly in contact with the outerbody leading edge. Consequently, it is necessary to have a spike actuation system capable of the desired positioning accuracy, with control provided by the control system computer.

Engine fuel pressurization is provided by a hydrogen turbopump. Therefore, the total pressure drop in the regeneratively cooled surfaces, manifolds, and associated plumbing must be compatible with the pressure output of the turbopump.

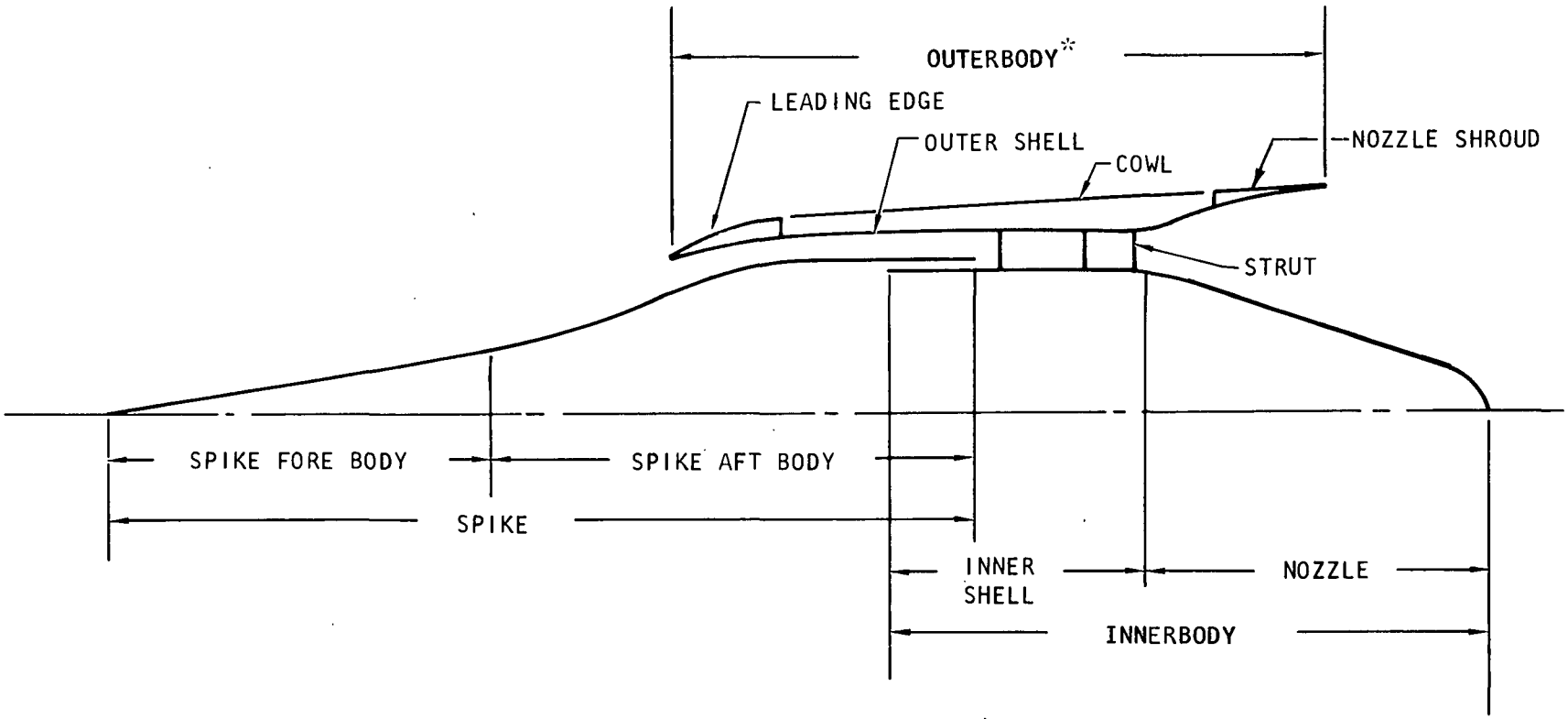

*OUTER BODY = LEADING EDGE + OUTER SHELL + NOZZLE SHROUD + COWL

A-30504

Figure 3.0-1. Cooled Structures Nomenclature

In addition to control of temperatures and temperature differences, the integrity of the coolant structures requires that the flow routes within the engine be matched in such a way as to minimize temperature differences at axial stations for innerbody and outerbody surfaces. This will minimize distortion of the engine internal passages. Axial temperature discontinuities as produced, for example, by the termination of two flow routes that differ greatly in temperature at the same station, are objectionable because of the severe thermal strains that result.

Measurement of engine internal thrust during flight is required. Consequently, external loads (drag and lift) that are transmitted directly to the thrust measuring device must be minimized. Specifically, the engine cowl has drag loads that are of the same order of magnitude as the engine thrust. Mounting of the cowl in such a way as to minimize this external drag load, and thus the uncertainties in calculation of thrust, is therefore required.

A basic engine design requirement is that malfunction of the engine will not endanger the safety of the aircraft or the life of the pilot. Therefore, provision must be made to jettison the engine. Because of probable hydrogen leakage to the engine cavities, the innerbody engine cavity must either be inerted or must be capable of containing an explosive mixture of hot hydrogen and air. To accomplish this, the engine cavity will be vented to near nozzle base pressure and provisions will be made for explosion containment. During ground checkout, the engine cavity will be inerted with nitrogen.

The weight of cooled structures, inlet spike actuation system, internal supporting structures, and plumbing is most of the total engine weight. Although optimization of the structures and structural components for minimum weight is not an objective, the specified weight limitation requires careful consideration of structural weight.

The instrumentation, controls, and fuel subsystems contained in the engine cavity will require servicing prior to and after each test. Consequently, the mechanical assembly of the engine cooled structure components must provide easy access to subsystem components for replacement in the field.

3.2 OPERATIONAL BOUNDARIES

3.2.1 General Design Ground Rules

The maximum dynamic pressure specified for the current phase of the program is 2000 psfa. This compares with the specified dynamic pressure of 2500 psfa, specified for the HRE Phase I program. Consequently, the minimum altitude at Mach 8, during which cooling must be provided, is 85,000 ft, as compared to the Phase I minimum altitude of 81,000 ft. The minimum design altitude for the current program is 88,000 ft. The increased altitude results in a reduction of heat flux throughout the engine, but this reduction is offset in part by an increase in engine contraction ratio from 10 in Phase I to 14.6 in Phase IIA. In summary, the operating envelope for the engine is as follows:

Engine Structural Design - With engine either lit or not lit, dynamic pressure (q) = 2000 psfa

Engine Cooling Design

Normal design, engine lit: q = 1750 psfa, h = 88,000 ft minimum

Emergency design, engine lit: q = 2000 psfa, h = 85,000 ft minimum

For the emergency design, engine lit conditions, all of the pump output pressure is available for coolant pressure drop. The dump valve opens and fuel injection valves close as the aircraft approaches these conditions from the normal operating line.

3.2.2 Engine Operating Cycles

A qualitative definition of the engine operating cycles has been formed for the purpose of providing a basis for analyzing heat transfer transients, evaluating the structural effect of transient temperature differences, establishing general control requirements and typical environmental conditions, and for defining acceptable operating cycles. The types of missions or conditions the engine must survive are as follows:

Case I - Constant M, with aircraft power on, at a constant high q

Case II - Constant M, with aircraft power off, aircraft diving

Case III - Variable M, expected to involve a change in M of 0.5 during 20-sec engine operating cycle

Case IV - Subsonic-supersonic combustion transition at M = 6

Case V - Inlet unstart, with shock expelled

Figure 3.2-1 is a qualitative representation of the critical cases. The common features, typical for all missions, are numbered on the figure and are as follows:

1. Launch to M = 3+, during which the engine structure is assumed to go from a soak at -65°F to a soak at 1140°F. No cooling is required. At the end of this period, the helium purge is performed and coolant flow started through all portions of the cooled structure.

2. Approach to test Mach number, inlet closed (leakage flow only), during which coolant flow is increased to maintain maximum structure temperature (cold surface) at 1140°F.

3. Time for retraction of inlet spike to desired position. The solid lines assume programmed cooling flow; the dashed line assumes controlled cooling flow based on temperature sensing. The approach selected will be a function of control system response and actuating system response. Controlled cooling is preferred.

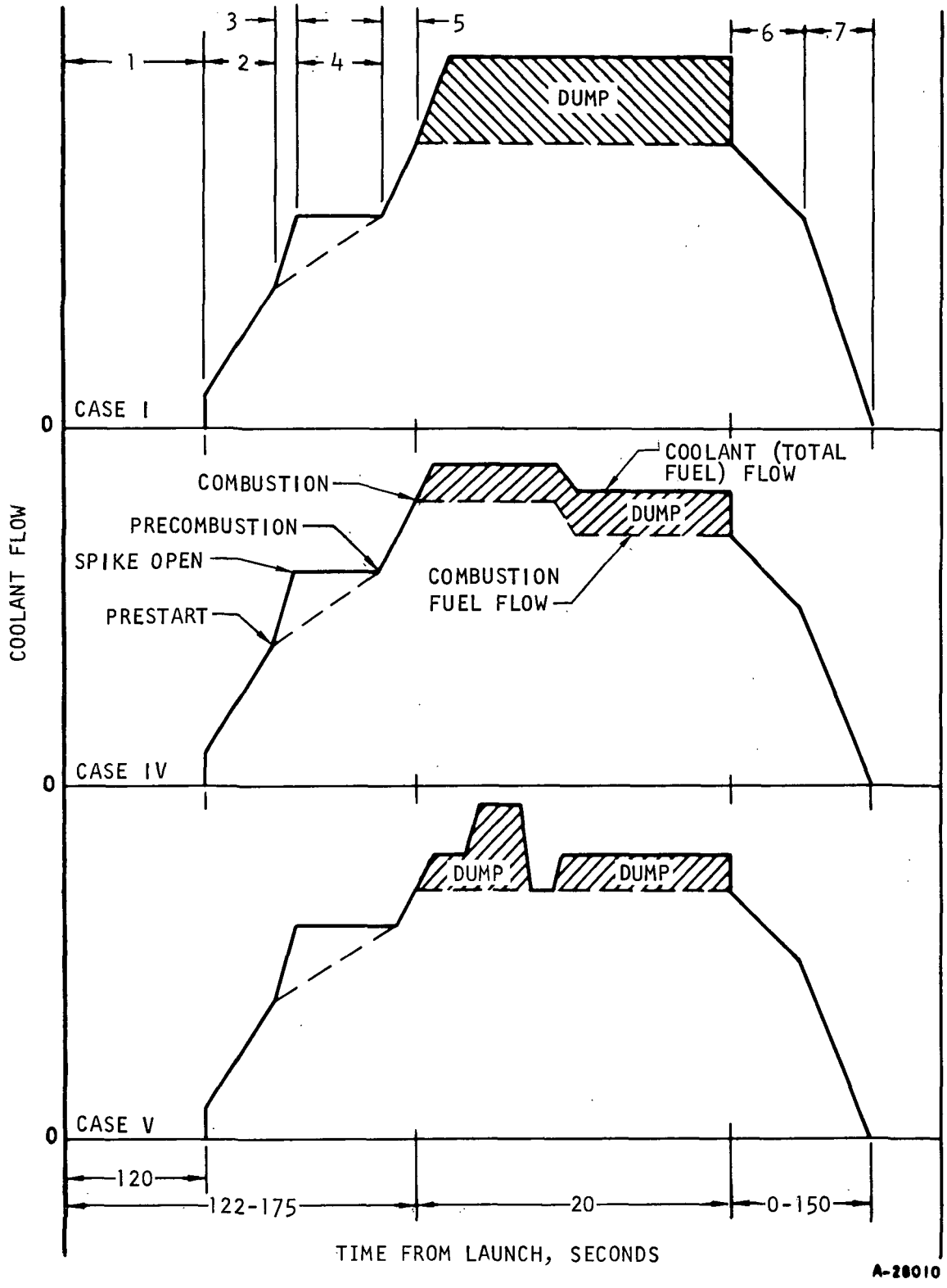

Figure 3.2-1. **Typical Engine Operating Cycles**

4. Inlet spike in starting position, full airflow through the engine, no combustion.

5. Programmed increase in cooling flow to starting combustion equivalence ratio (ϕ). This ϕ will be less than the test ϕ. Combustion ϕ will ramp to test ϕ (not shown).

6. Combustion terminated and inlet spike being extended to closed position.

7. Inlet closed (leakage flow only), deceleration to M = 4 +, with coolant flow decreased to maintain maximum structure temperature at 1140°F. Helium purge.

As combustion starts, the cooling ϕ must be controlled to accommodate increasing heat fluxes. The variations among missions occurring during the combustion phase are as follows:

Case I - Shown in Figure 3.2-1. Cooling ϕ is in excess of combustion ϕ. Combustion ϕ will ramp at beginning and end of test. Ramps of 5-sec duration to and from φ = 1 may be assumed at beginning and end of test.

Case II - Not shown. Represents a gradual change in conditions shown for Case I and will involve less severe transients. Not considered a design point.

Case III - Same comments as Case II, but may become a design point at lower Mach numbers because of potential for increased test time and wider Mach number range.

Case IV - Shown in Figure 3.2-1. Involves a near-step change in gas-side engine conditions during test run.

Case V - Shown in Figure 3.2-1. The general rise in pressure would be expected to cause a step-change type increase in heat flux. Spike will extend and close, then retract to operating position for second attempt at starting. At this point, either normal operation or a second unstart is possible.

4. OVERALL APPROACH

The diverse requirements imposed on the cooled structures require iteration of the cooled structural design with (1) the engine aerodynamic design; (2) the instrumentation, control, and fuel subsystems designs; and (3) the airplane interface design. Internal contraints on cooled structural design are imposed by the close coordination required in thermal design, structural design, mechanical design, and manufacturing. It is generally not possible to treat any one of these areas independently of the others. During Phase I of the program, the basic design concepts for the engine were defined and are basically feasible in terms of the constraints imposed on the design. These concepts and the design data generated during Phase I are being used as the starting point for design of the Phase IIA cooled structures. Component layout drawings of acceptable mechanical design and with acceptable manufacturing features form the initial step in the iteration. These layout drawings have been evaluated to establish the required thermal and structural design features. Based on these inputs, layout drawings are revised to incorporate the required features, followed by substantiation of thermal and structural performance of the revised design.

Although the Phase I design is being used as the starting point of Phase IIA cooled structure design, each of the components is being reviewed with the objective of simplification in terms of mechanical design and manufacturing features. The interfaces between two or more components, in particular, will be reevaluated . The interfaces include engine-to-airplane mounting, outer-shell-to-innerbody mounting by means of the support struts, nozzle-to-inner-shell assembly, inlet spike-to-innerbody assembly, inlet spike actuator-to-inlet spike and innerbody mounting, leading edge-to-outer shell mounting, and cowl-to-outer shell support.

The general approach to cooled structures development places heavy emphasis on fabrication and testing of the full-scale components. A limited number of types of cooled structural elements and models is being fabricated and tested to evaluate the problems which are basic to the overall engine design, or which are sufficiently localized in nature to permit use of subscale evaluation. All significant manufacturing development and evaluation is being accomplished using the full-scale components. The nature of the required manufacturing operations for the components is such that use of subscale components would be expected to lead to only limited information on the adequacy of manufacturing techniques and processes.

4.1 THERMAL DESIGN

The overall thermal design approach is by analyses based on experimental data obtained from tests on similar geometric configurations and heat transfer situations. These experiment-based analyses, in turn, will be verified by experiments where the geometry or fluid conditions, or both, will be like those existing for the flight engine.

Where the discrepancy between calculated and experimental heat flux values is large, steps are being taken to improve the analytical techniques so that the correlation between calculated and experimental results can be improved.

The basic goals of all thermal analyses and designs are (1) limiting temperature and temperature differences to structurally acceptable values, while keeping hydrogen cooling flow equal to or less than hydrogen flow required for combustion, and (2) at the same time maintaining hydrogen pressure drop compatible with cooling jacket pressure containment and pump outlet pressure capabilities. The limiting values being used at present are (1) a maximum gas side metal temperature of 1700°F (2160°R), (2) a maximum primary structure temperature of 1140°F (1600°R), and (3) a hydrogen pump outlet pressure of 1100 psia.

The thermal design procedure involves separate calculation of aerodynamic heating and cooling jacket performance. The aerodynamic heating conditions are calculated (as during Phase I) primarily by use of the computer program HI940. Special aerodynamic heating conditions, such as shock wave/boundary layer interaction, are computed separately. Cooling jacket fin performance is calculated (as in Phase I) by use of computer program HI930. Special conditions, such as pressure and flow distributions for inlet, outlets, and bolted flange/manifolds, require separate calculations. Verification of aerodynamic and cooling jacket heat transfer and pressure drop calculations will be accomplished by actual tests. Specifically, aerodynamic heat transfer calculations will be verified by tests of engine component models, such as the combustor, and with the boilerplate engines. Calculated performance of cooled structures will be verified by full-scale component and some subscale component testing at heat flux levels and distributions comparable to those calculated for the flight engine components. The primary areas requiring verification in the cooled structures performance are flow distribution and associated temperature distribution and its effects on structural performance in terms of life and contour.

4.2 STRUCTURAL DESIGN

The structural design approach utilizes a combination of analytical and experimental methods. Experimental verification of detailed parts, such as short-term burst, creep-rupture, and thermal fatigue tests on sandwich plate-fin elements, will be employed wherever necessary. Generally, the structural tests will be performed on composite structural elements, such as the inlet spike and the innerbody assembly.

The bulk of the HRE structures consists of ring-stiffened orthotropic shell structures of variable thicknesses and contours. The ring stiffeners are also used for coolant flow manifolding and fuel injection rings for the engine combustor section. The structural loadings will produce axisymmetric and asymmetric forces and moments due to static normal pressures, acceleration, vibrational inputs, and aerodynamic flutter and buffeting effects.

Fully operational computer solutions are available to analyze axisymmetric isotropic thin shells of variable thicknesses and contours for stresses due to axisymmetric loads and temperature profiles. In addition, the isotropic shell analysis had been extended to treat orthotropic cylindrical shells with axisymmetric loads. Two MIT finite difference nodal circle solutions (SABOR III and DASHER I), which have been adapted for use on the AiResearch computer system (IBM-360/50), are available for use.

The SABOR III program is applicable for axisymmetric isotropic shells (local departures from ideal isotropy can be treated) that may be subjected to nonsymmetrical static forces. The SABOR III program may also be used to obtain the stiffness and mass matrixes for direct input into the DASHER I program to obtain dynamic response.

It would have required an extensive programming effort to modify the SABOR III and DASHER I programs to treat accurately many of the problems that will be encountered in the HRE. Rather than attempt this approach, a further survey of existing shell programs was carried out, and it was determined that an extremely applicable program had been developed under the auspices of the Analysis Group of the Theoretical Mechanics Branch, Structures Division of the Wright Patterson Air Force Base, Dayton, Ohio. This program is based upon the very recent improvement in matrix shell solutions generated by A. Kalnins (Department of Mechanics, Lehigh University). It solves the general axisymmetric orthotropic thin shell problem for symmetric and nonsymmetric loads due to static as well as dynamic inputs. The program has been successfully adapted for use on the AiResearch computer system. Although the program has been debugged, the final report describing the usability limitations, and methods of data input has not been completed, and will not be released by the Wright Patterson Air Force Base for at least twelve months. Until a program of this magnitude has been completely checked out by trying numerous test cases, a note of caution must be exercised regarding its capabilities. Another important point is the fact that the problem inputs and the data

reduction of the outputs require considerable effort on the part of the user. The existence of the program also does not eliminate or substantially reduce the work needed to generate a sound design; however, it is the objective of careful analysis to discover design inadequacies that would otherwise not be recognized.

The eventual objective of the test program is to verify the actual performance capabilities of the structures as fabricated. Although it will not be possible to predict analytically the influence of realistic fabrication restrictions and limitations on the end product, the initial analysis will identify the serious design problem areas. Results of the test program will be used to assess the extent of the changes required to achieve the structural integrity goals.

4.3 MECHANICAL DESIGN

The guidelines used in mechanical design of the cooled structures components and assembly of the components into the engine require the use of known materials and joining techniques. Standard fasteners and seals are used to the greatest extent possible. Design for brazing is aimed at minimizing the total number of braze cycles to which a given part must be subjected. In some cases, this is done by redesigning the parts to allow use of prebrazed subassemblies, substitution of machined or welded subassemblies, or substitution of bolted interfaces for brazed or welded interfaces. Also, as a general rule, all welding into or close to braze joints is being avoided, although in certain cases, such a procedure may be acceptable.

The mechanical design effort will be supported by experimental verification in selected areas. In particular, selected configurations that present analytical problems and raise questions as to manufacturing feasibility will be fabricated and tested on a subscale basis. The purpose of such tests will be to provide design data and guidance for possible design revision. Currently planned tests, which are in support of mechanical design rather than thermal or structural design, include the following:

Test specimen to evaluate feasibility of bolting the nozzle flange manifold to the inner shell through the removable nozzle cap

Fabrication of a section of the inlet spike near the spike tip to help resolve questions regarding the best manufacturing approach, and hence, the best design for this portion of the inlet spike

Fabrication of the spike-to-innerbody seal to evaluate the adequacy of the design solution

Fabrication of a straight section of the bolted nozzle manifold to verify both the manufacturing aspects and structural integrity of the design solution

Fabrication and evaluation of the various mechanical seals used in the components to verify the adequacy of the design solution

Fabrication of flat panels using the various instrumentation and fuel injector fittings that penetrate the regeneratively cooled surfaces to verify manufacturing feasibility and structural integrity of the design. Tests results will be used to select the final configuration used in the engine.

4.4 MANUFACTURING

The manufacturing approach being used on this program has two aspects: (1) that dealing with the approach to development of manufacturing techniques and processes, and (2) that dealing with the specific manufacturing processes planned for use.

4.4.1 Development Approach

The development of the manufacturing techniques and processes will rely primarily on full-scale components. Except where isolated problems or basic data must be obtained, the use of subscale components represents a duplication of development effort. The compound forming of the shell-face sheets in half-scale, for example, results in working with radii of curvature which are half those encountered in the full-scale part. Use of lighter-gauge material to facilitate forming, on the other hand, is impractical. In addition, the size of the full-scale tooling, the machines required to use this tooling, and the unique problems associated with the forming of large thin wall shells cannot be duplicated in half-scale. As a result, a half-scale compound-curved model of the isentropic surface of the inlet spike is the only subscale component on which fabrication development work is being done. This part is being used to establish forming characteristics, evaluate electrohydraulic forming parameters, and investigate brazing problems.

4.4.2 Fabrication Approach

The most critical area of cooled structures fabircation is in the cooled surface shell face sheets. The starting point for these shells can either be rolled-and-welded-cone sections or flat sheets. The rolled-and-welded cones are bulge-formed, then final-sized, using electrohydraulic forming. Using flat sheets as a starting point, the shells must be deep drawn in about three stages. Final sizing of the shells occurs as for the welded cones. Of the two approaches, the one using the seam-welded cone has been selected. The weld seam is not considered structurally objectionable and the approach involves fewer steps than are required for deep drawing.

To ensure adequate braze fitup, forming accuracy for the shells must be high. Specifically, it is expected that the clearance between shells must be maintained within a tolerance of approximately ±0.001 in. Given this accuracy, the brazing of the fins between the face shape still requires special attention. To ensure sound braze joints, pressure must be exerted on the shells in

such a way as to provide a crushing load on the fins. The methods available for providing this braze fixturing load include the following, as a function of the component being brazed:

Graphite fixtures, with an external piece containing the assembly and an internal piece using expanding segments to exert pressure.

Steel bags placed inside the shell and pressurized to a level sufficient to deform the shell with which the bag is in contact. Containment on the external face sheet may or may not be required with this approach.

Evacuation and backfilling of the space between the two shell face sheets, using atmospheric pressure to provide the load.

Integrity of the shell joining will be experimentally evaluated and adjustments in shell forming tools and brazing procedures and fixtures made to correct problems that appear.

4.4.3 Nondestructive Testing

The critical area in fabrication of the full-scale components involves the shells themselves, as discussed in the two previous paragraphs. For structural integrity of the shells, only very limited areas of unbrazed joint areas are tolerable. These joints are detectable by proof pressure testing at sufficiently high pressure levels. Only in exceptional cases, however, will a defect that is revealed by proof pressure test be repairable. In general, a nondestructive test capable of revealing braze voids is preferable and offers better opportunity for subsequent repair. The two techniques available are radiographic inspection of the entire shell surface and the use of temperature-sensitive paint on one of the face sheets with a heating transient imposed on the other face sheet. These methods will show a braze void; that is, an unbonded joint. Weak joints are not discernable as such. In general, however, the existence of a brazed joint is reasonable assurance that adequate joint strength can be achieved. Verification of the result of radiographic or thermal inspection of the shells will be done by proof-pressure testing.

The repair techniques available for unbonded joints in the shells would generally be the following:

Recycling of the complete shell to a slightly higher temperature than used during the first braze cycle. In this way, remelt and flow of the braze alloy is obtained with the objective of filling the void. Orientation of the shell in the brazing furnace can be used to assist the process.

Removal of a portion of the face sheet in the unbrazed area, addition of filler alloy and closeout using a patch, with the entire shell recycled in the brazing furnace. The applicability of this repair procedure will be a function of the location of the affected shell area in the engine gas stream.

5. ANALYTICAL DESIGN

5.1 SAM WATER-COOLED COWL/PYLON

The Cowl/Pylon of the Structural Assembled Model (SAM) of the HRE is a water-cooled, double-walled structure. The cowl consists of a tapered-truncated cone and a cylindrical section. Leading edge of the pylon is a 30-deg wedge which is attached to a straight section and a closing (box) section.

The pylon outer (hot) wall is 0.090 in. thick, while the thickness of the inner wall is 0.125 in. Coolant passages are 0.1-in.-high straight fins 0.004 in. thick, 10 fins per in. Walls and fins are fabricated from CRES Type 347 stainless steel. Both the pylon and the aft box are brazed.

The cowl is a welded assembly fabricated from CRES Type 321 steel. Steel plugs, 0.1 in. high, welded between the 0.125-in. outer shell and the 0.1875-in.-thick inner shell on a 2.5-in. radius, tie the two shells together and form the coolant passage. Between Stations 41.455 and 44.455, the shell thicknesses are 0.080 in. (outer) 0.12 in. (inner). Welded spacer bars keep the two shells tied together and form the coolant passages in this area.

Mechanical properties of CRES Type 347 and 321 stainless steel were given in Table 5.2-4 and Figure 5.2-10 of Reference 5-1. Stress analysis of the structure was performed using the EASE (Elastic Analysis for Structural Engineers) digital computer program. A combination of triangular shell elements and beams are used in this program to represent the structure in the analysis. An isometric plot of the beams and the shell elements generated during execution of the computer program is shown in Figures 5.1-1 and 5.1-2. The cowl/pylon was represented by 786 shell elements and 88 beam elements. Some of the beam elements are marked with an asterisk on Figure 5.1-1; these are the imaginary beams simulating the aft box.

5.1.1 Loads

The analysis of the structure is based on the assumption that the following loads are acting on the cowl/pylon:

(a) Aerodynamic Loads

Five different aerodynamic load cases were investigated. A description of these load cases, and the magnitude and location of the resultant loads are shown in Figure 5.1-3. Load cases 1 and 2 were used during the design of the flightweight engine, while the other load cases are the results of additional investigations, taking the operating conditions of the wind tunnel into

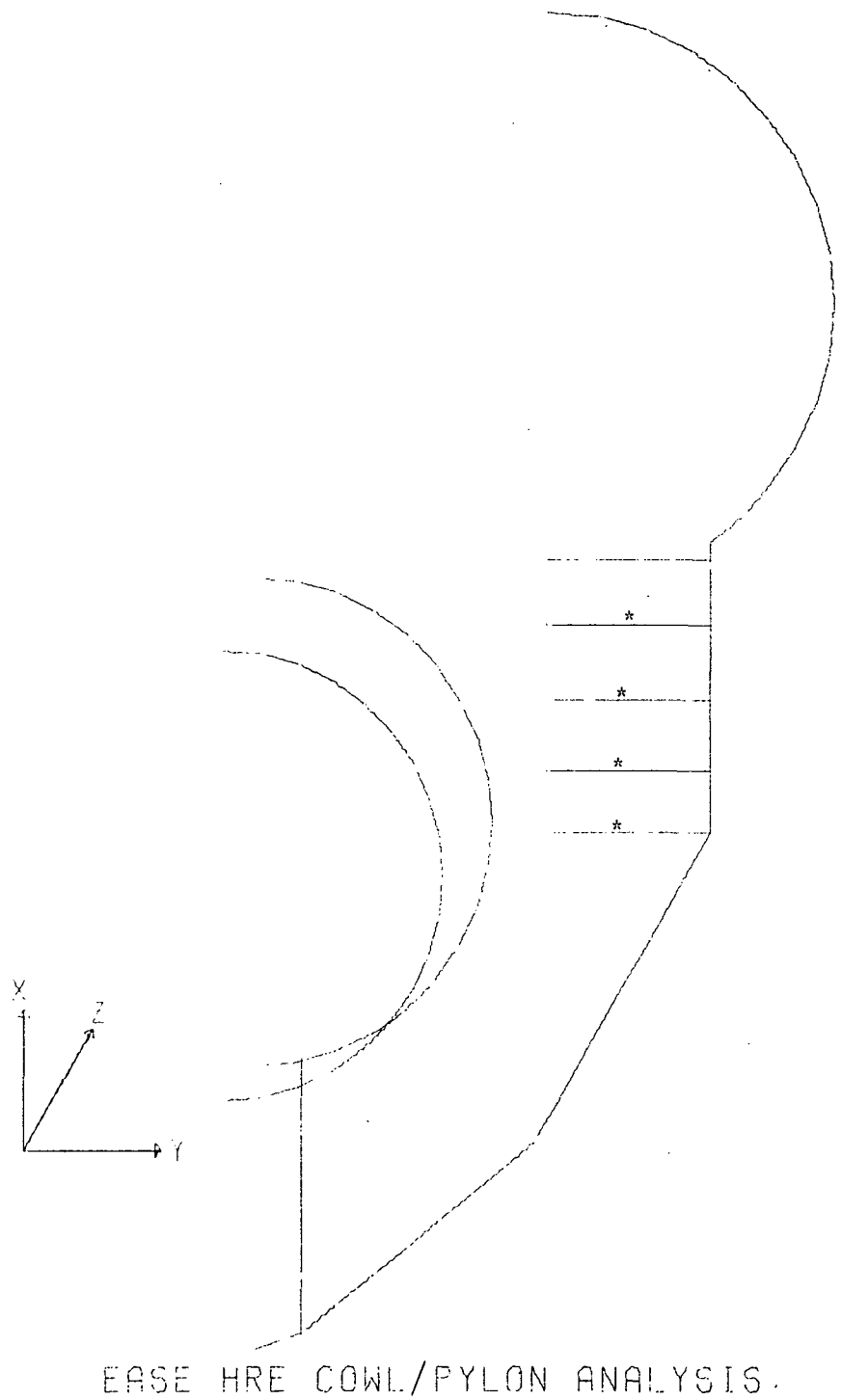

Figure 5.1-1. EASE HRE Cowl/Pylon Analysis

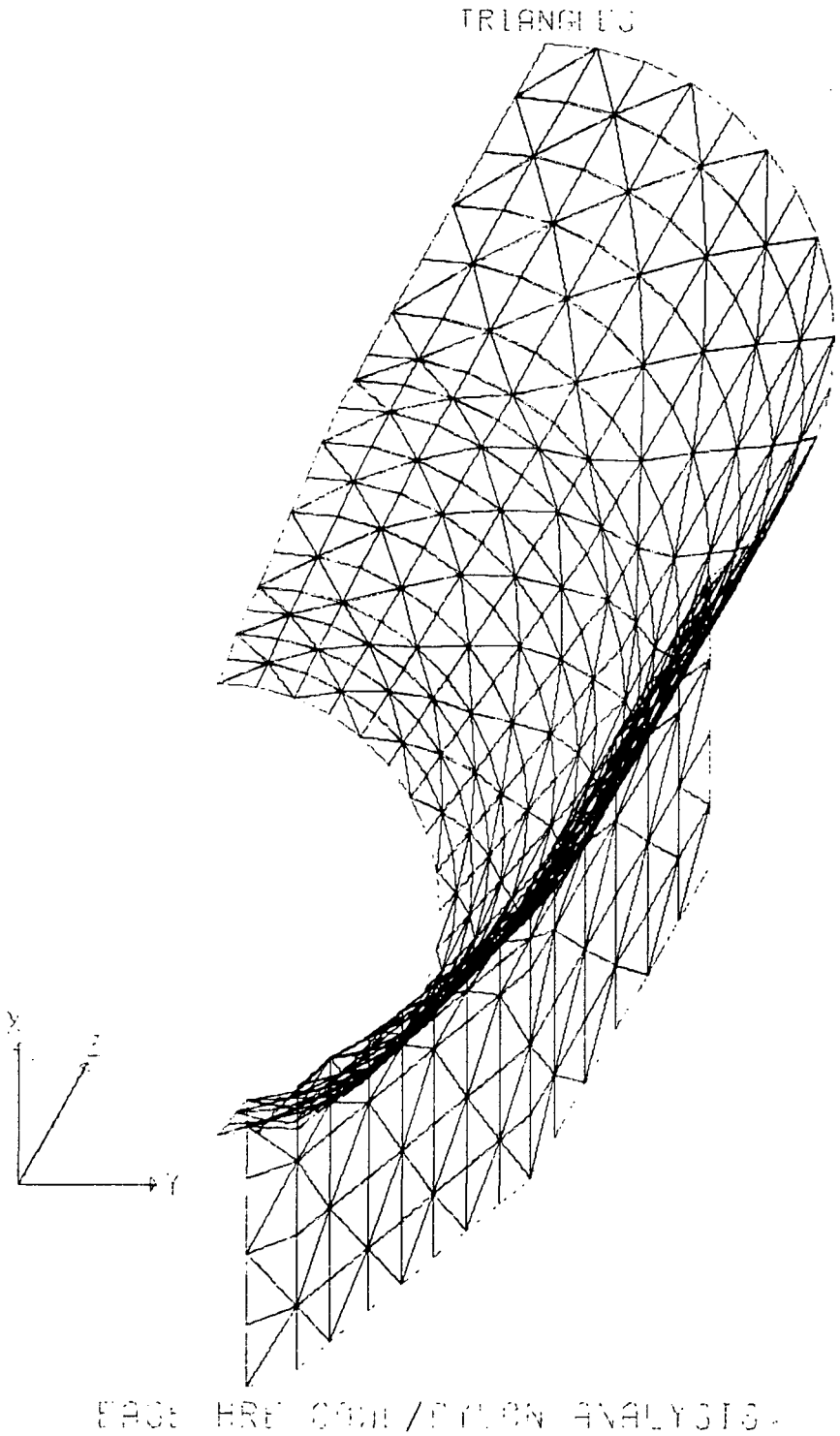

Figure 5.1-2. EASE HRE Cowl/Pylon Analysis

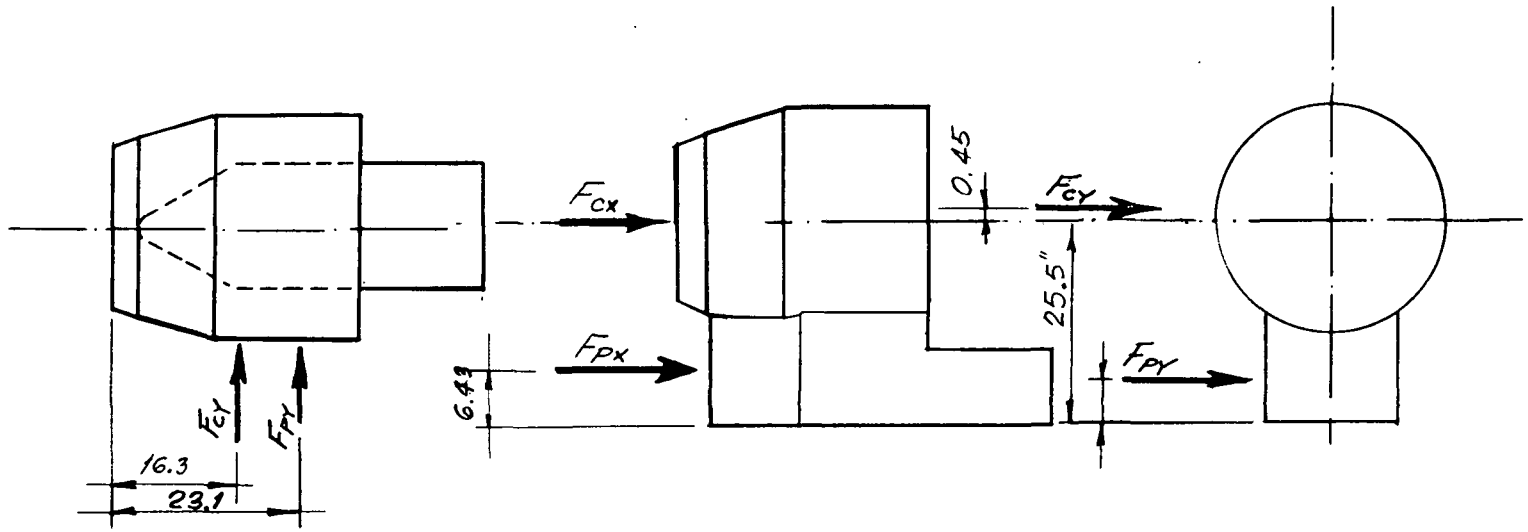

LOAD CASE N°	Description	F_{CX}	F_{PX}	F_{CY}	F_{PY}
1	Symmetrical Inlet Unstart	230	2500	0	0
2	Asymmetic Inlet Unstart	230	2500	0	0
3	Symmetrical Tunnel Unstart	- 1253	- 500	0	0
4	Asymmetrical Tunnel Unstart	230	2500	12100	8017
5	Inlet and Tunnel Started	230	2500	0	0

S-50977

Figure 5.1-3. SAM Cowl/Pylon Aerodynamic Loads

consideration. Load case 4 is based on the assumption that 15 psi is acting on the vertical projected area of the cowl/pylon. Since such a load is of extremely short duration, any analysis considering it as a static load is considered conservative. Pressure during normal operation of the tunnel will not exceed 2.0 psi.

(b) Inertia Loads

The cowl/pylon assembly is assumed to be exposed to 5.0 g loading in either of the x, y, or z direction during transportation, fabrication, and assembly. These loads are applied at room temperature.

Insertion and retraction of the model will result in a maximum 2.0 g inertia load at elevated temperatures. Since the cold wall temperatures will not exceed 285°F at any point, and the yield strength of the material only decreases approximately 9 percent, the 5.0 g inertia load creates more significant stresses.

(c) Thermal loads and coolant pressure

This information was presented earlier in Reference 5-1.

5.1.2 Stress Analysis

The results of the analysis are shown in Table 5.1-1. Only the maximum stresses are shown. The high, but localized, temperature differences across the hot-gas exposed metal will cause substantial plastic deformation, but the calculated maximum cycle life will be above 100.

The cowl/pylon is attached to the HRE suspension frame (wishbone) at four places. Stresses due to the loads transmitted to the suspension frame by the cowl will be well within allowables.

5.2 SAM WATER-COOLED MOUNTING STRUCTURE

The results of a preliminary heat transfer and coolant pressure drop analysis for the water-cooled mounting structure of the SAM (Drawing L980628, attached at end of this report), were reported in Reference 5-1. During this reporting period, refined aerodynamic, heat transfer, coolant pressure drop, and stress analyses were performed. The results are summarized in the following sections. (Some of the results reported in Reference 5-1 have not been changed, but are repeated in this report for convenience.)

5.2.1 Design Gas Conditions

Methane combustion products will be used for testing of the SAM. The gas conditions in the wind tunnel, upstream of the engine, used for heat transfer analysis are $M_\infty = 7.34$, $P_{T_\infty} = 3300$ psia, $T_{T_\infty} = 3600°R$, $H_{T\infty} = 1095.3$

TABLE 5.1-1

SAM COWL/PYLON MAXIMUM STRESS DUE TO PRESSURE AND INERTIA LOADS

	Pressure Loads, psi		5 g Inertia Load		
	2.0 Uniform	15.0 Side	X	Y	Z
Maximum stress, psi	10,500	37,200	10,000	5,040	-16,300
Yield strength at temperature	33,700	36,750	39,500		
Margin of safety	2.11	-0.01	2.95	6.83	1.42

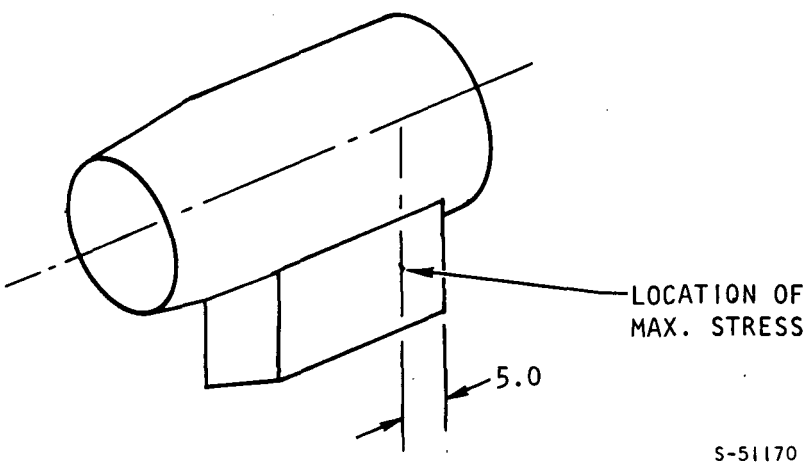

Btu/lb and $\phi = 0.8$. The variations of flow properties along the wedge-shaped mounting structure are shown in Figure 5.2-1. The shock from the mounting structure leading edge sweeps the flat bottom surface of the pylon to produce a line of static pressure differential.

5.2.2 Heat Transfer Analysis

The mounting structure and the flat bottom surface of the pylon are cooled together by a single coolant water flow route as shown in Drawing L-980628 and also schematically shown in Figures 5.2-2 and 5.2-3. Coolant operating conditions are as follows:

Coolant	Water
Flow rate	70 gpm
Inlet pressure	180 psig
Outlet pressure	20 psig
Inlet temperature	80°F
Outlet temperature	165°F
Overall heat load	800 Btu/sec

5.2.2.1 Leading Edge

The leading edge of the wedge-shaped mounting structure is cooled by water flowing through a stainless steel tube of 1.62-in. OD, 0.12-in. wall thickness, and parallel to the leading edge. The gas-stagnation heat transfer coefficient was obtained by the theory of Reference 5-2 and multiplied by an upstream turbulence factor of 1.8. One-dimensional radial heat flow analysis was performed, and the results indicate the following heat transfer conditions at the leading edge:

Stagnation heat flux	165 Btu/sec ft^2
Gas side wall temperature	940°F
Coolant side wall temperature	240°F
Coolant temperature	90°F
Coolant flow velocity	15 ft/sec

The coolant flow velocity of 15 ft/sec at this flow section determines the overall coolant flow rate of 70 gpm for the entire mounting structure.

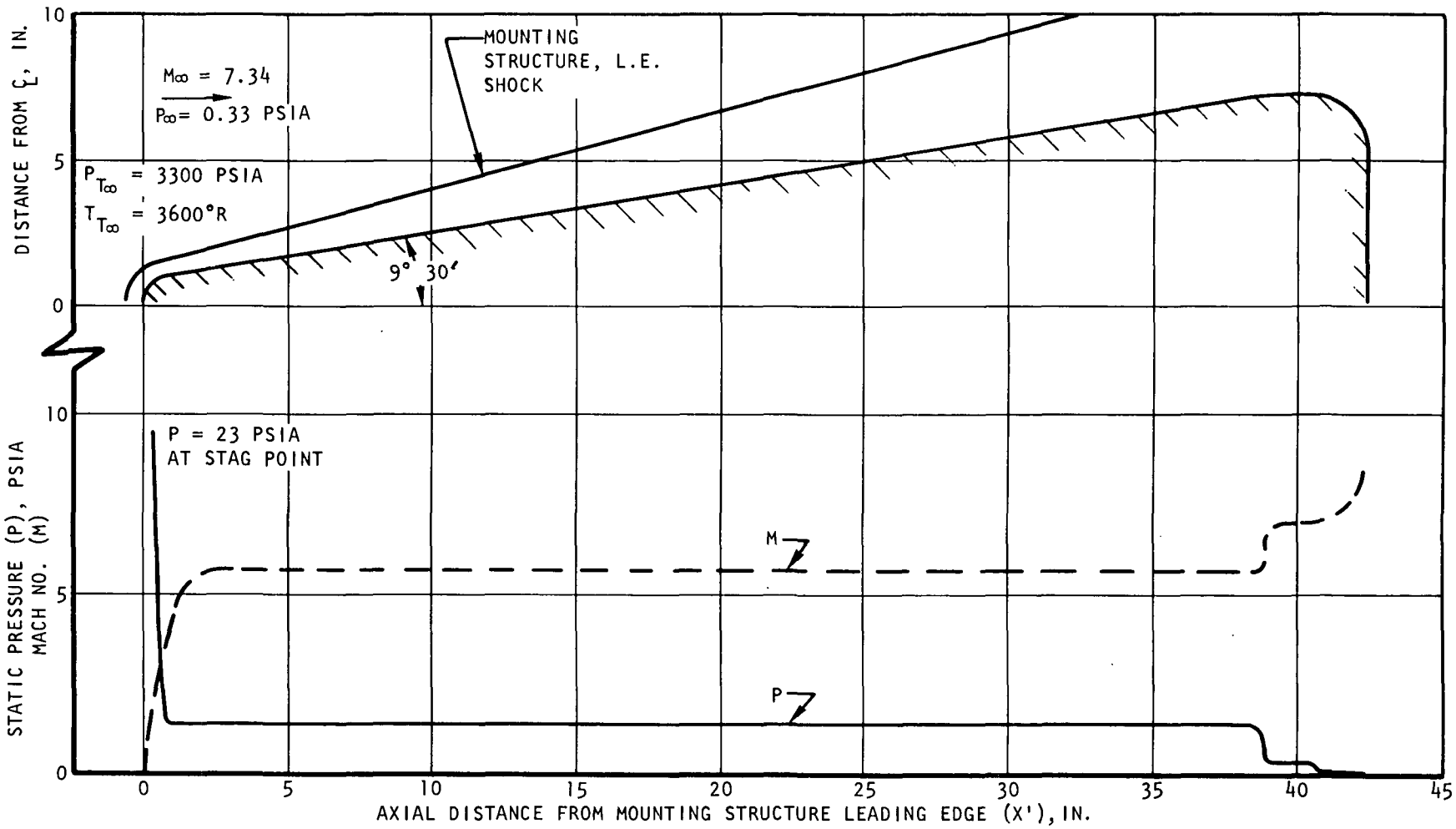

S-51074

Figure 5.2-1. External Flow Properties on Mounting Structure

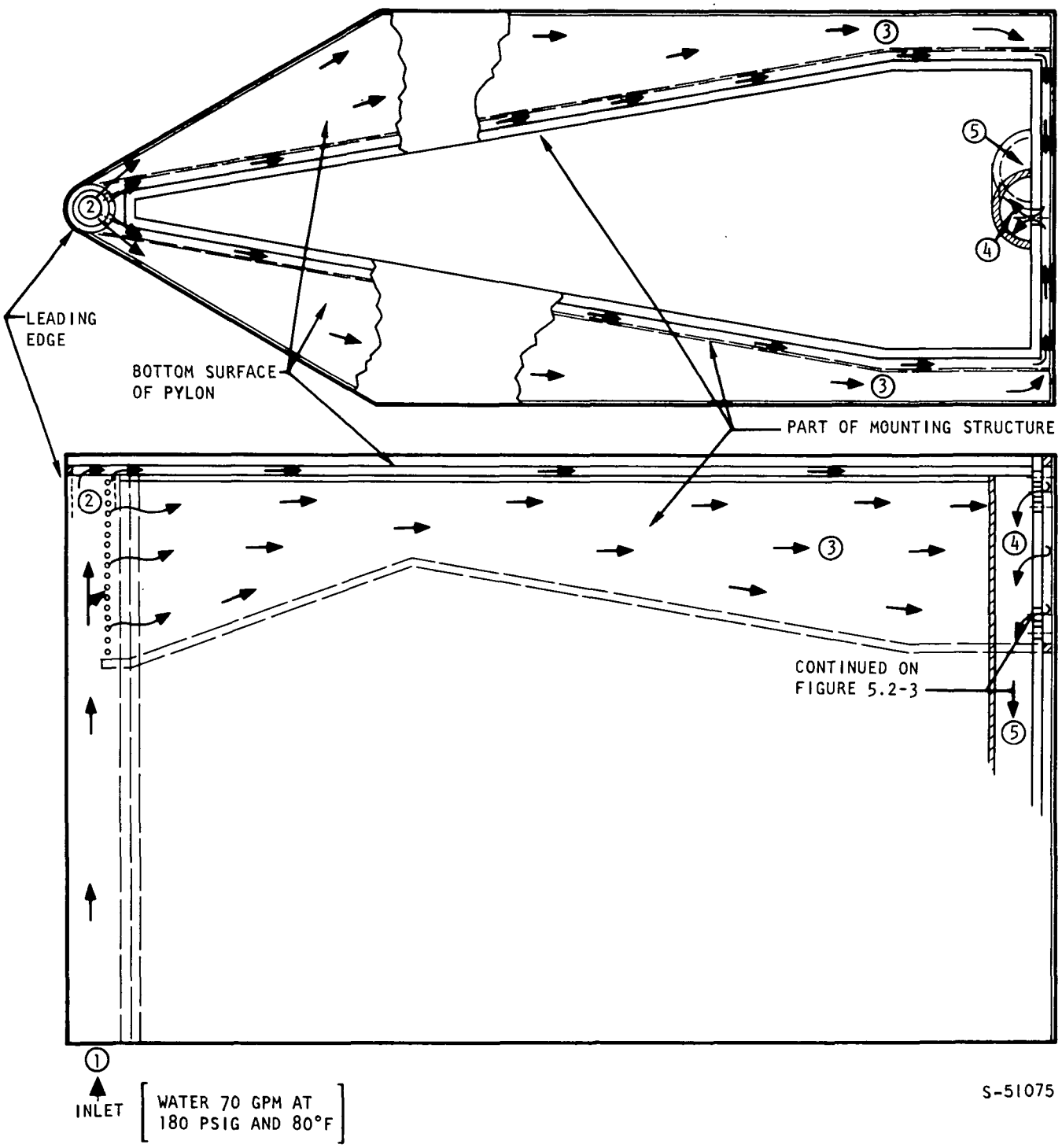

Figure 5.2-2. Cooling of Flat Bottom Surface of Pylon and Part of Mounting Structure (Reference Figure 5.2-3)

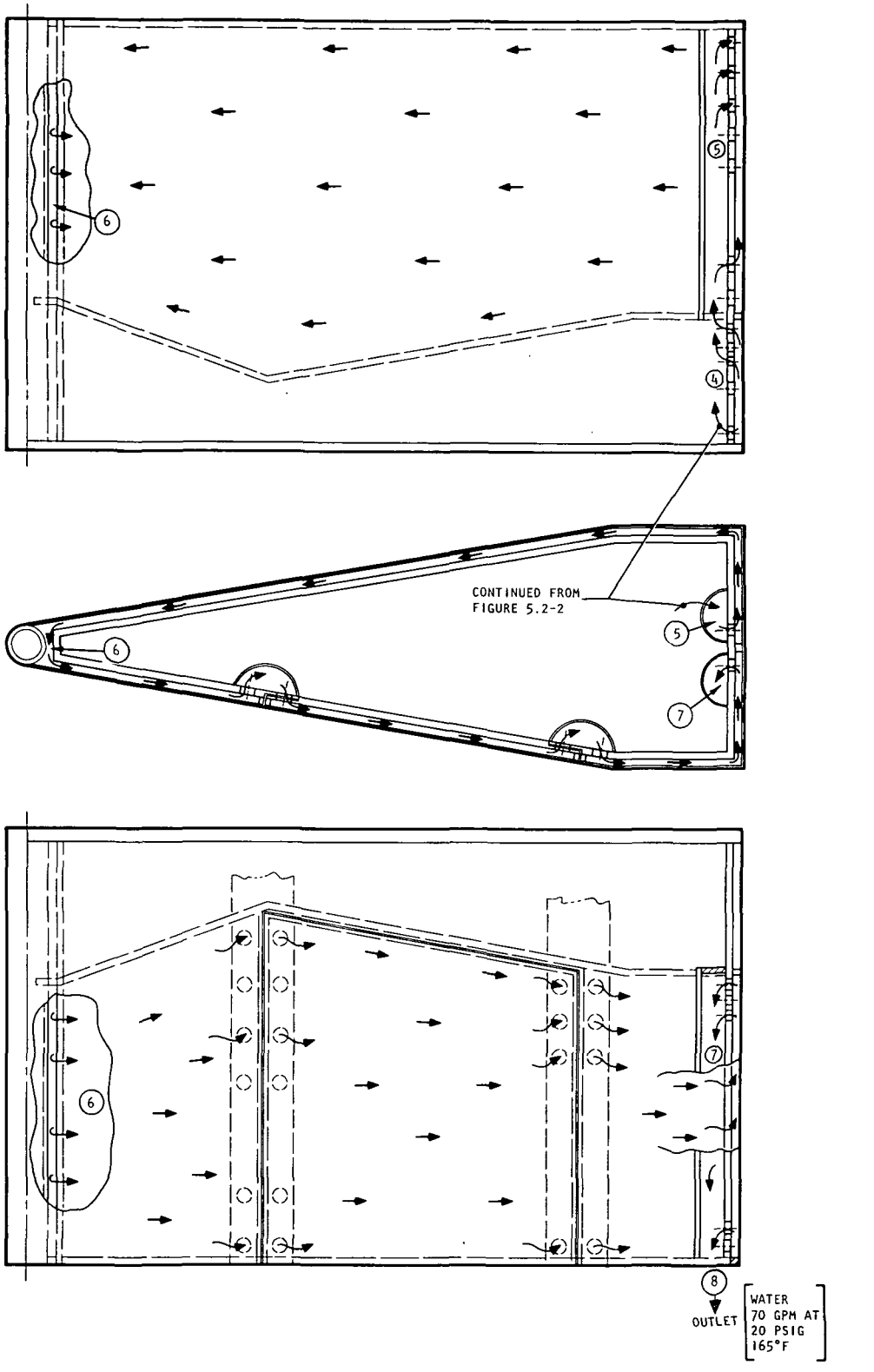

Figure 5.2-3. Cooling of Remaining Part of Mounting Structure (Reference Figure 5.2-2)

5.2.2.2 Side Surfaces of Mounting Structure and Bottom Surface of Pylon

Using the conditions shown in Figure 5.2-1, the heat fluxes on the side surfaces of the mounting structure and on the bottom surface of the pylon were computed and the results are graphically shown in Figures 5.2-4 and 5.2-5. The effects of the shock from the mounting structure leading edge on the pylon bottom surface were taken into consideration. In these figures, the gas side wall temperature used for heat flux calculation is constant at 700°R for convenience; therefore, these curves, when divided by a temperature difference of 3600 - 700 = 2900°R, show the distribution of the gas heat transfer coefficient. The calculated gas side wall temperature is between 630°R and 830°R resulting in a negligible difference between the true heat flux and the quoted heat flux.

Integration of these heat flux curves as well as leading edge heat flux with respect to the heat transfer area gives an overall heat load of 800 Btu/sec. The coolant temperature rise is expected to be 85°F for the design cooling water flow rate of 70 gpm, to result in an outlet water temperature of 165°F for an inlet water temperature of 80°F.

The side surfaces of the mounting structure and the bottom surface of the pylon are cooled by water flowing through the flow channels with a uniform channel height of 0.1 in. The flow channels have 10-fins-per-in., 0.004-in.-thick, CRES 347 brazed between surface sheets for structural reasons. Fins are locally removed at various locations to permit cross-flow for better coolant distribution. The average water velocity in the channel is about 15 ft/sec.

The wall between the hot gas and cooling water is made of 90-mil-thick stainless steel. The wall temperatures can be estimated with the use of the heat fluxes shown in Figures 5.2-4 and 5.2-5, and with the coolant heat transfer coefficient of 1.58 Btu/sec ft^2 °F, which was calculated for the water flow velocity of 15 ft/sec, hydraulic diameter of 0.2 in., and maximum local coolant temperature of 165°F. For example, for a heat flux of 50 Btu/sec ft^2, the coolant side wall temperature will be 165 + (50/1.58) = 197°F and the gas side wall temperature will be 197 + (heat flux) $\times \frac{\text{wall thickness}}{\text{conductivity}}$ = 197 + 50 $\times$ $\frac{9.3/3600}{0.09/12}$ = 342°F.

5.2.3 Coolant Pressure Drop

The coolant pressure drop due to skin friction, area changes, and turns in the flow route of Drawing L-980628 was estimated to be 160 psi for the design water flow rate of 70 gpm. This value excludes pressure drops in the supply and discharge tubes for which only the tube diameters are known. Table 5.2-1 shows sectional pressure drops, with location identified as in Figures 5.2-2 and 5.2-3.

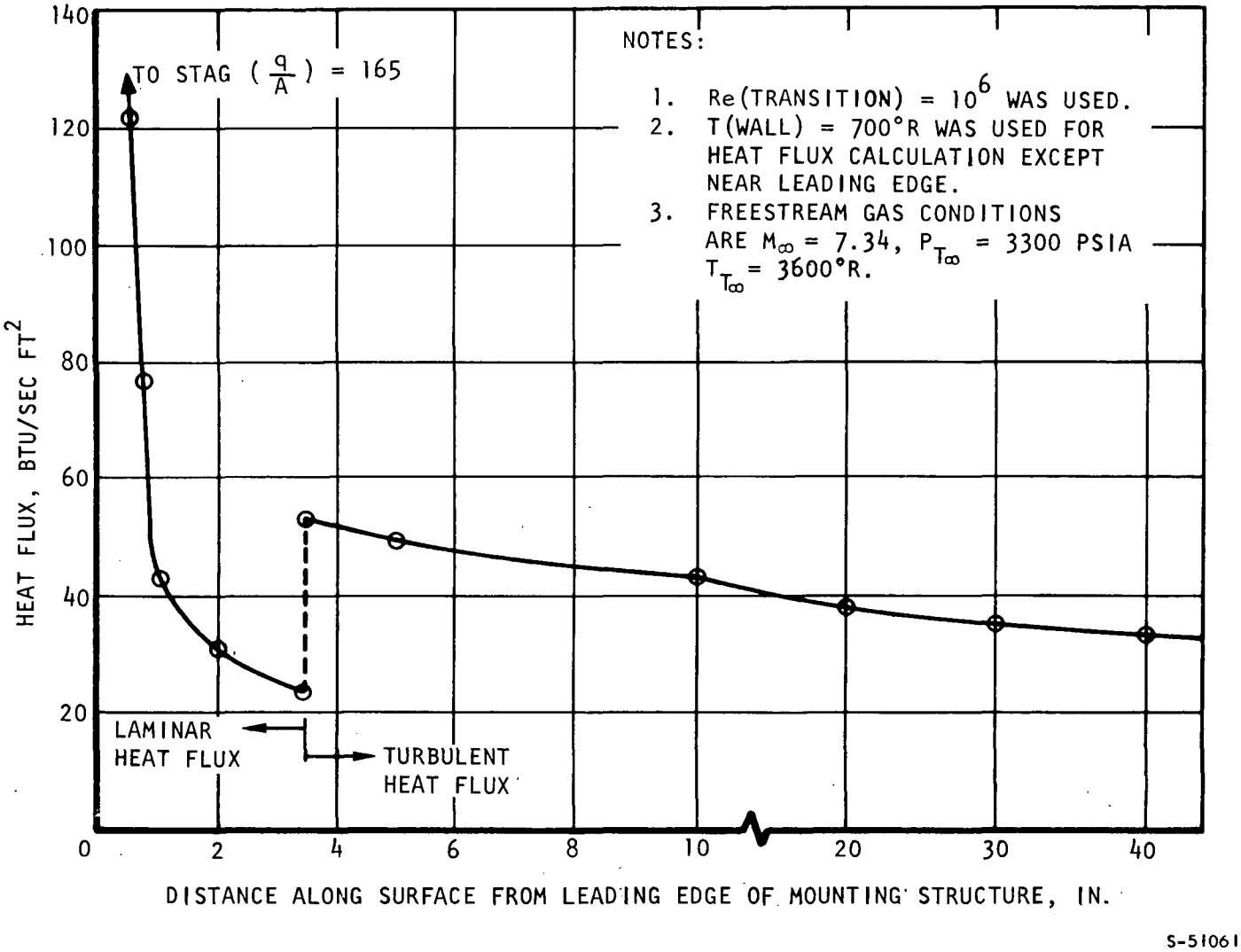

Figure 5.2-4. Heat Flux Along Side Surface of Mounting Structure

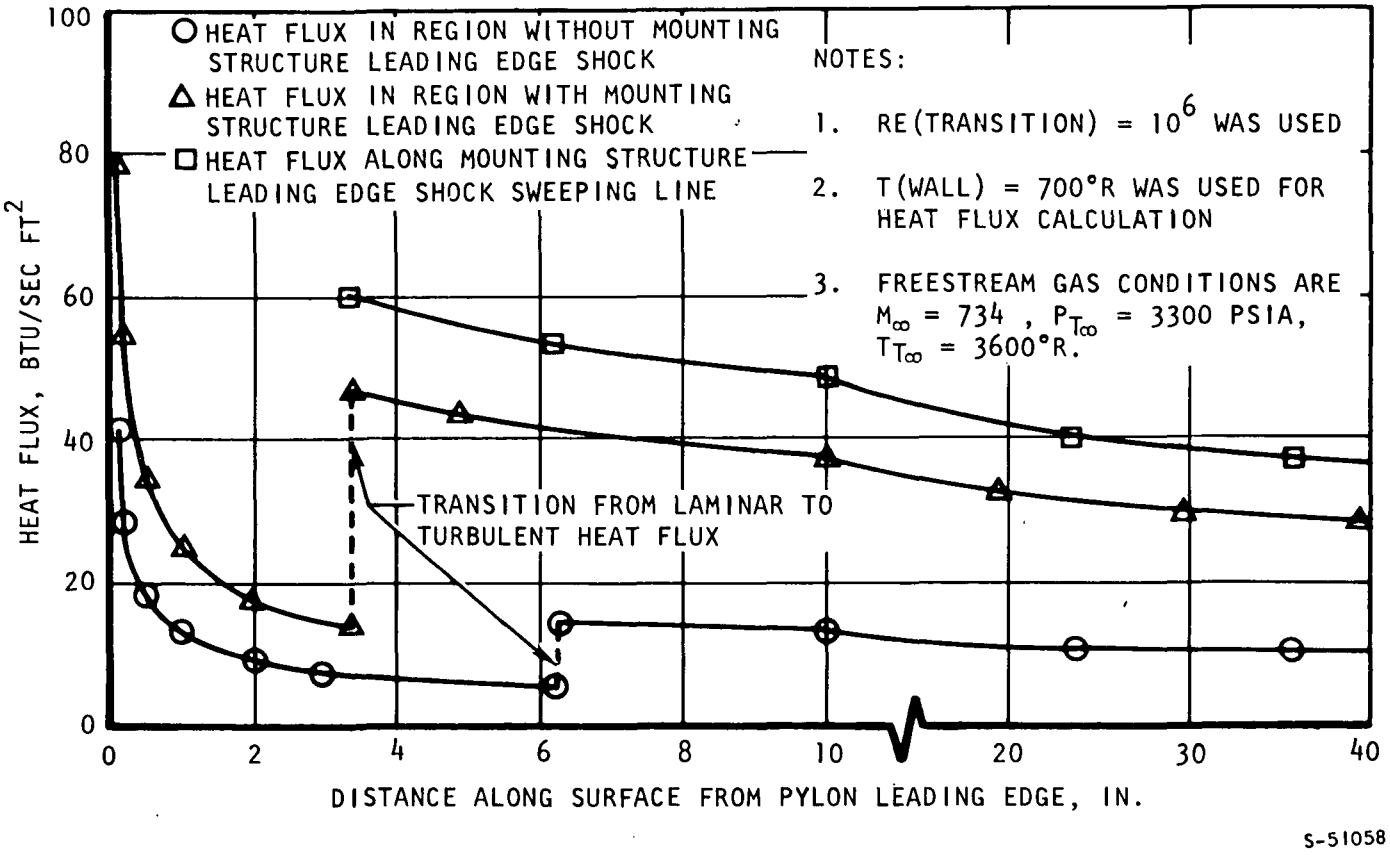

Figure 5.2-5. Heat Flux on Pylon Bottom Surface at Pylon/Mounting Structure Interface with T (WALL) = 700°R

TABLE 5.2-1

SECTIONAL PRESSURE DROPS FOR COOLING SYSTEM OF MOUNTING STRUCTURE L980628

Location From	Location To	ΔP, psi	Items Entered in ΔP Calculation
1	2	3.5	Inlet fitting, friction in leading edge flow
2	3	40.1	Holes from leading edge flow to side panel. 90 degree turn from leading edge flow to pylon bottom panel, skin friction, area changes, cross-flow at pylon mounting structure intersection
3	4	17.5	Skin friction, turns, area changes, holes from rear panel to rear manifold (4)
4	5	2.0	Pressure drops in rear manifolds (4) and (5), transition from manifold (4) to manifold (5)
5	6	36.0	Holes from rear manifold (5). Skin friction, turns, area changes, forward manifold (6)
6	7	54.3	Skin friction, turns, area changes. Two door joints [ΔP (2 door joints) = 18.5 psi], holes to outlet manifold (7)
7	8	4.0	Outlet manifold, outlet fitting

$(\Delta P)_{Total}$ = 157.5 psi ~ 160 psi

Note: Location numbers correspond to those of Figures 5.2-2 and 5.2-3

5.2.4 Structural Analysis

The SAM of the HRE is supported on a 24-in.-high, 19-deg-wedge-shaped structure. This support structure is a double-walled, brazed structure fabricated from type 347 stainless steel. The outer surface, which is exposed to the hot gas flow, is 0.1 in. thick. Coolant passages between the outer surface and the inner wall are formed by 0.1-in.-high plain fins. The inner wall is 0.31 in. thick. An 18-in.-wide opening is provided on one side for access to piping and instrumentation. Figure 5.2-6 shows the basic geometry of the structure. The assembly is anchored to its base by 11 5/8-in.-dia bolts.

5.2.4.1 Loads

The SAM support structure is designed to carry the following loads:

(a) Aerodynamic loads due to four different combinations of inlet- or tunnel-unstart, and during normal operation during testing. These loads are shown on Figure 5.2-7. The leading edge hot-gas side metal temperature will be 940°F, while the coolant-side metal temperature will be 240°F. Metal temperatures of other areas will be considerably lower; 380°F on the hot-gas side and 220° on the coolant side. Side plates of the assembly must be able to withstand 15 psi pressure load.

(b) Insertion and retraction of the SAM into the tunnel will impose a vertical inertia load of 2.0 g on the assembly. The weight of the assembly and the c.g. of each component are shown in Figure 5.2-8. It is assumed that the structure is at elevated temperature as described above.

(c) Loads due to transportation and handling are taken as 5.0 g inertia with the unit at room temperature.

(d) Coolant pressure in the leading edge coolant circuit during operation will be 90 psig maximum, while in the side panels it will be 180 psig. Proof pressure will be 1.5-times operating pressure (135 and 270 psig).

5.2.4.2 Stress Analysis Results

The maximum bending stress due to the combination of aerodynamic load case (d) and the 2.0 g inertia load is 17,952 psi. A maximum allowable stress of 85 percent of the 0.2-percent yield strength, the margin of safety, $M.S. = \frac{0.85\ Fy}{f6} - 1 = 0.7$ (quite high). The deflection of the structure perpendicular to the $\mathbb{C}$ of engine is 0.000296 in., which is entirely acceptable.

Stresses in the leading edge due to pressure containment of the coolant are 1780 psi. Thermal stresses in the side panels will be below the elastic limit, but the leading edge will undergo some plastic deformations. The

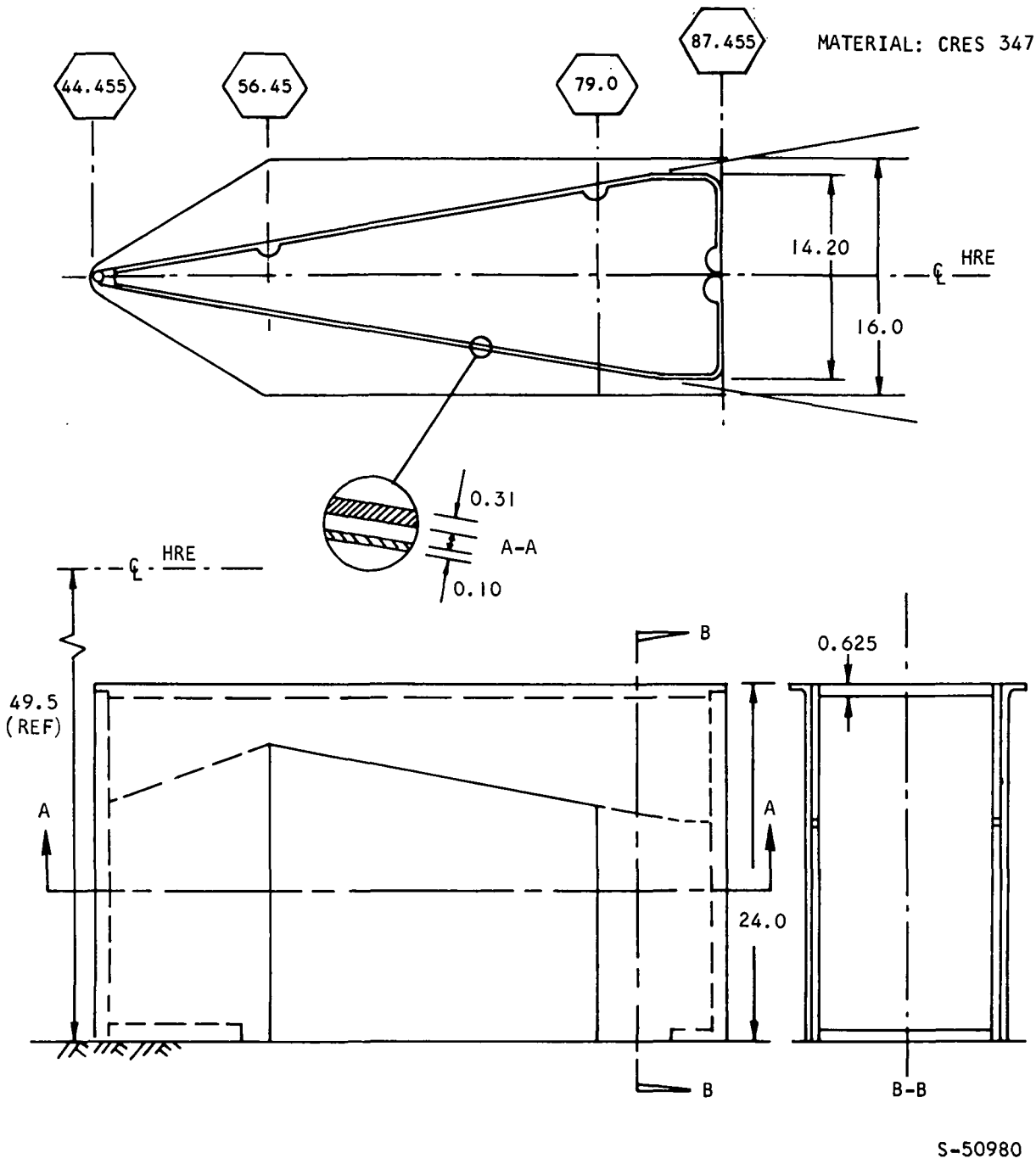

Figure 5.2-6. SAM Support Structure

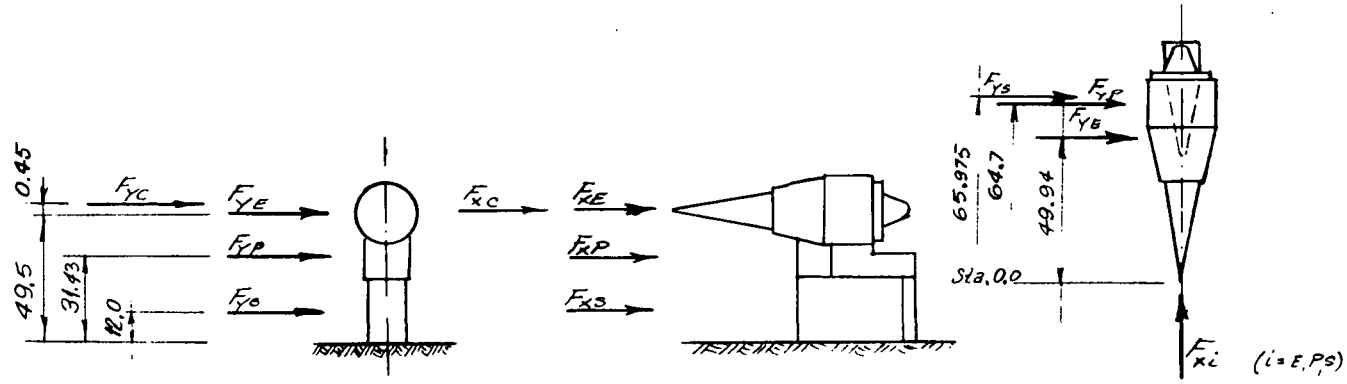

№	LOAD CASE DESCRIPTION	F_{XE}	F_{XC}	F_{XP}	F_{XS}	$F_{YE}+F_{YC}$	F_{YP}	F_{YS}
1	Symmetrical Inlet Unstart	4005	230	2500	1360	0	0	0
2	Asymmetric Inlet Unstart	5350	230	2500	1360	~2000	0	0
3	Symmetrical Tunnel Unstart	-8000	-1253	-500	-3400	0	0	0
4	Asymmetrical Tunnel Unstart	960	230	2500	1360	18860	8017	15615
5	Inlet and Tunnel Started	960	230	2500	1360	0	0	0

S-50978

Figure 5.2-7. SAM Aerodynamic Loads

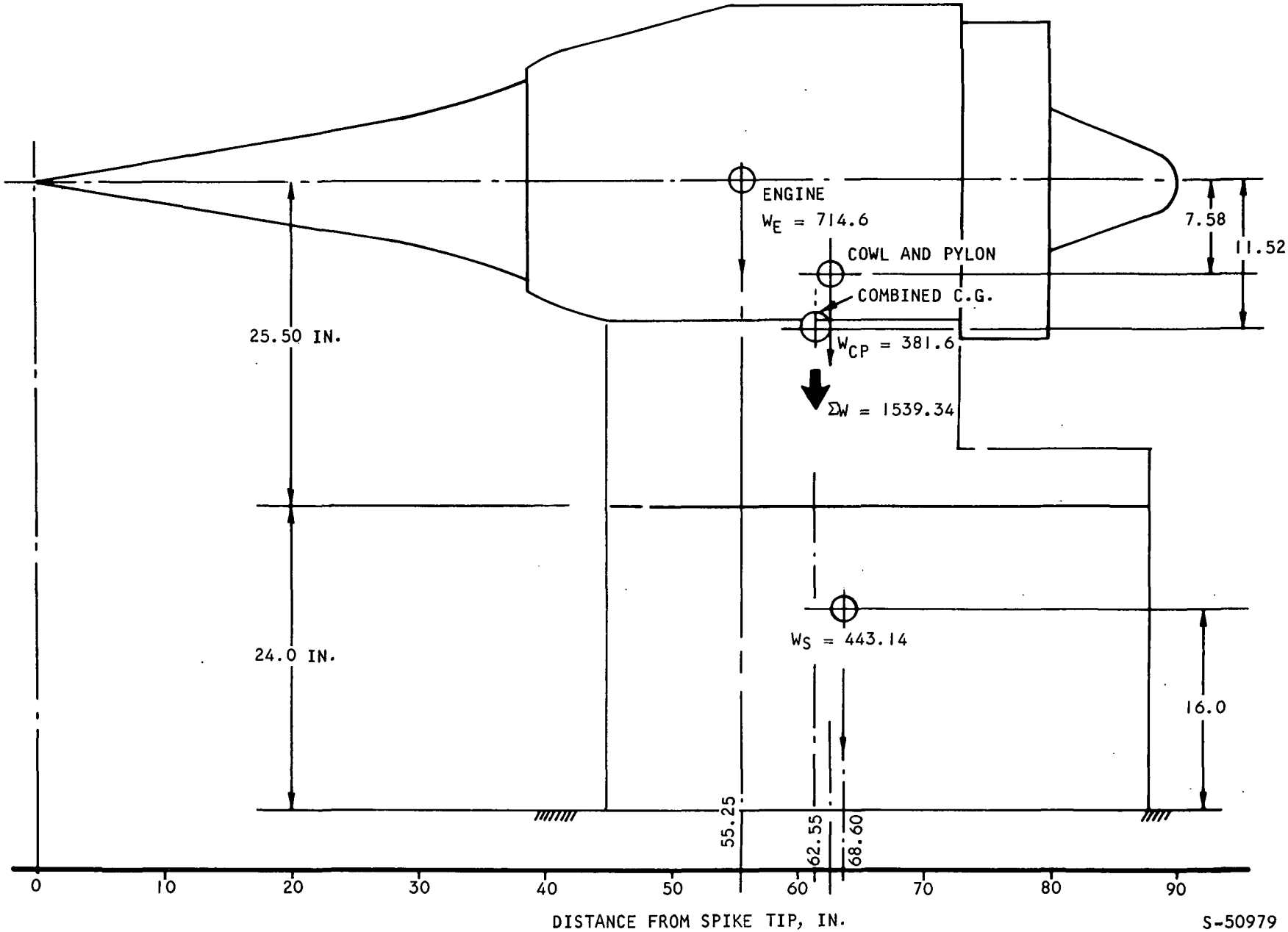

Figure 5.2-8. SAM Weight Distribution, Spike Retracted

expected number of life cycles will exceed 5000. The natural frequency of the support with the model in place is 181 cps, which is well above an expected 27-cps wind tunnel input.

5.3 SAM COOLANT REGULATING VALVES

5.3.1 System Configuration and Requirements

The SAM coolant schematic is presented in Figure 5.3-1 with the pertinent operational parameters. The four coolant regulating valves (CRV's) will each be set to a fixed position prior to SAM test. During operation, the dump plenum pressure will be maintained at 550 psia. If any of the 27 outlet coolant temperature sensors demands more coolant for a particular flow route, the pressure control valve (PCV) and the fuel dump valve (FDV) will be automatically adjusted to increase coolant flow to all flow routes, while maintaining the dump valve plenum pressure at 550 psia. The coolant rate to all routes will increase until the affected temperature control sensor is returned to within its set-point tolerance. The facility supply pressure is 1000 ±100 psia with a maximum hydrogen coolant rate of 1.25 lb/sec at 200°R. The SAM inlet pressure, P_A, in Figure 5.3-1, will be approximately 735 psia for design point conditions of 0.622 lb/sec total coolant flow. An inlet pressure of 735 psia was selected because this pressure is high enough to provide an approximately linear relationship between coolant flow rate and CRV area for all four CRV's, and low enough to allow twice-design-point flow with increase in inlet pressure to 900 psia.

The range of CRV effective areas required for SAM wind tunnel operation are noted in Figure 5.3-1. These effective valve areas are defined as physical free-flow area times flow-discharge coefficient and will be used to select the four CRV's. At the SAM wind tunnel design point of 0.622 lb/sec total engine coolant hydrogen flow, the required effective areas are 0.012 $in.^2$ for CRV 2 (innerbody), 0.023 $in.^2$ for CRV 4 (aft outer shell), 0.038 $in.^2$ for CRV 3 (leading edge and forward outer shell), and 0.048 $in.^2$ for CRV 1 (spike). For the coolant flow rates expected for SAM off-design operation (1/3- to 2-times the design point flow rate) the CRV effective areas range from 0.0043 $in.^2$ (CRV 2 at 1/3-design-flow rate) to 0.080 $in.^2$ (CRV 1 at 2-times the design flow rate). For comparison, at Mach 6.5 local, Mach 8 freesteam, 88,000-ft altitude flight conditions, the CRV 2 effective area is 0.040 $in.^2$ and the CRV 1 effective area is 0.115 $in.^2$ as calculated from data in Reference 5-3, page 5-25.

5.3.2 Flow And Sizing Analysis

Effective CRV areas versus inlet pressure, P_A, are presented in Figures 5.3-2, 5.3-3, and 5.3-4. These curves were calculated for the fixed-design-point flow rate indicated for each flow route, and fixed-dump plenum pressure of 550 psia. The pressure drop for each CRV and the associated flow route are indicated in Figure 5.3-2. The CRV effective areas for Mach 6.5 local,

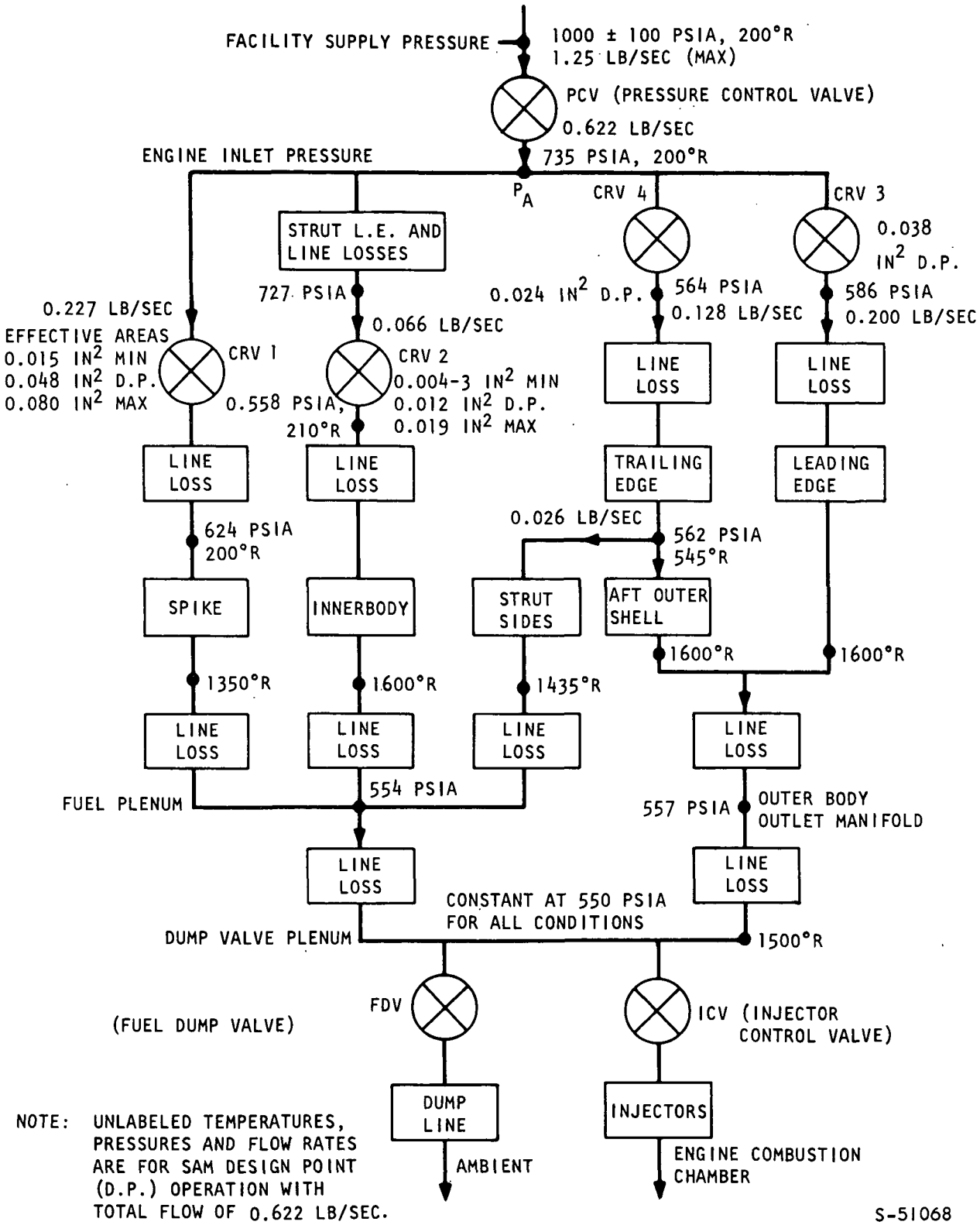

Figure 5.3-1. SAM Hydrogen Coolant Schematic

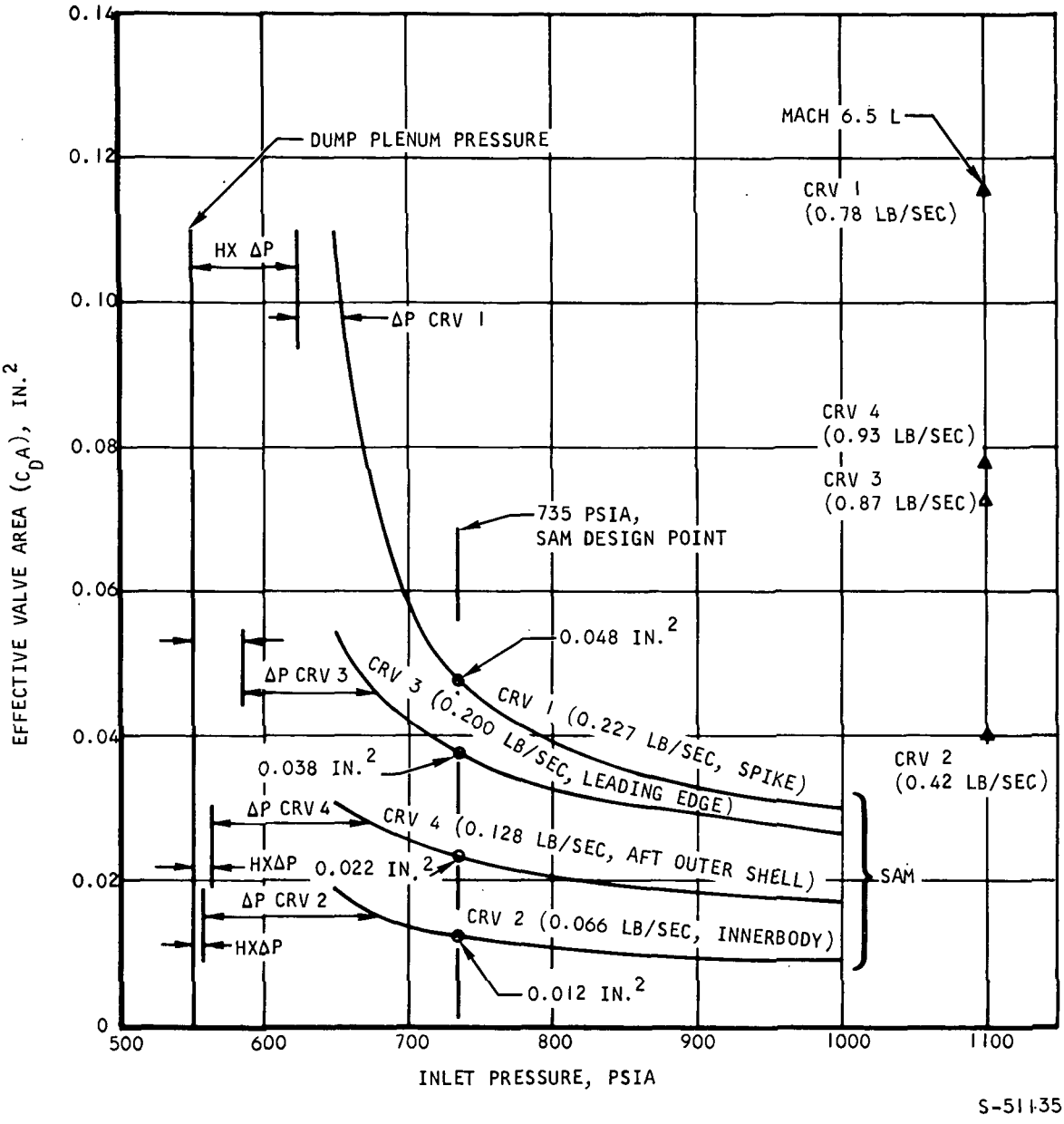

Figure 5.3-2. CRV Effective Areas at SAM Design-Pointed Flow Rate

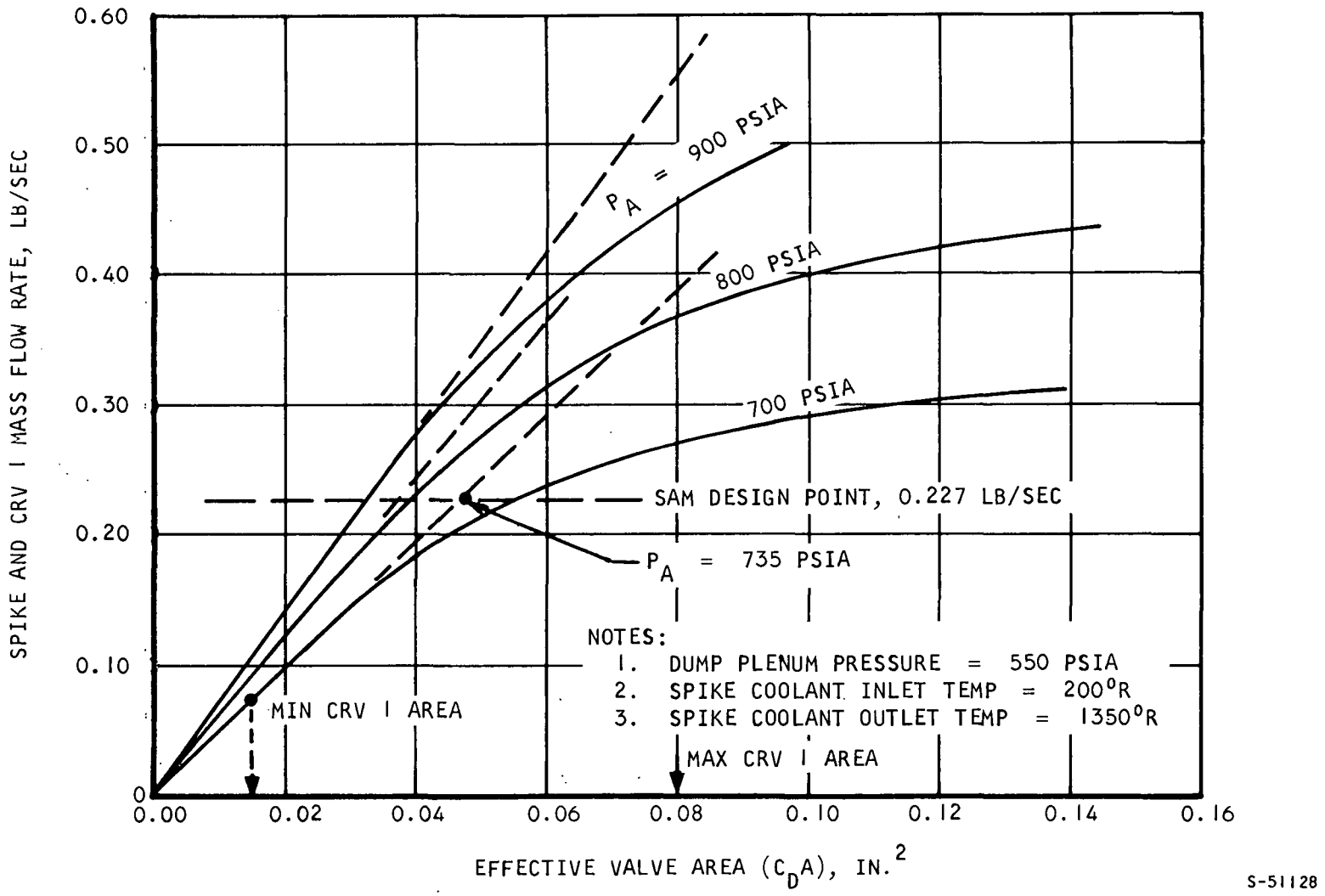

Figure 5.3-3. Spike Coolant Regulating Valve (CRV I) Characteristics

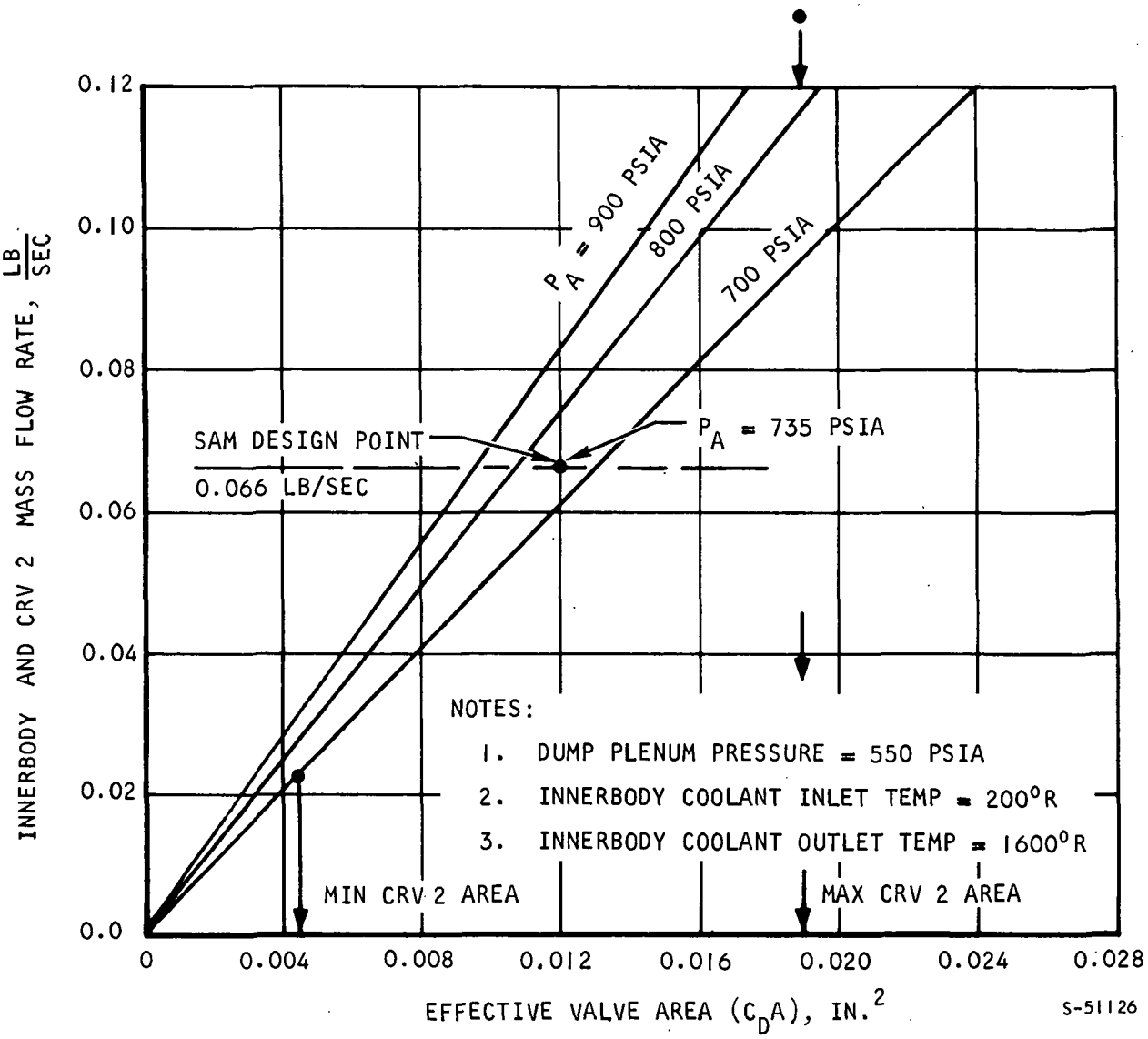

Figure 5.3-4. Innerbody Coolant Regulating Valve (CRV 2) Characteristic

88,000-ft altitude flight conditions are also indicated for comparison. Coolant flow rate versus CRV effective area at inlet pressures of P_A = 700, 800, and 900 psia, and a constant dump plenum pressure of 550 psia are presented in Figures 5.3-3 and 5.3-4, respectively, for CRV 1 (spike flow route) and CRV 2 (innerbody flow route). The range of expected flow rates for SAM operating conditions will vary from 1/3- to 2-times the SAM design point flow rates indicated in Figure 5.3-2. A flow rate of 1/3 of the design flow rate is considered a threshold flow rate. A flow rate of 2-times the design flow rate is approximately the facility maximum of 1.25 lb/sec. Under this range of flow rates, the CRV 1 effective area varies from 0.015 $in.^2$ (1/3 of 0.227 lb/sec or 0.076 lb/sec, 700 psia inlet pressure) to 0.080 $in.^2$ (2 x 0.227 lb/sec, or 0.45 lb/sec in the spike; however, this would require a disproportionately higher CRV 1 effective area. For example, if 800 psia inlet pressure is used, an effective area of 0.16 $in.^2$ is required. This is double the area required at 900 psia. CRV 2 effective area varies from 0.0043 $in.^2$ (1/3 of 0.066 lb/sec, or 0.022 lb/sec, 700 psia inlet pressure) to approximately 0.019 $in.^2$ (2 x 0.066 lb/sec, or 0.132 lb/sec, 900 psia inlet pressure) in Figure 5.3-4. An inlet pressure of 700 psia or lower will be used at the lower flow rates, while an inlet pressure near 900 psia will be used at the higher flow rates.

The ranges of effective areas for CRV 3 and CRV 4, for the leading edge and aft outer shell flow routes, respectively, will be between the reported ranges of effective areas reported for CRV 1 and CRV 2.

5.4 LEADING EDGE THERMAL PERFORMANCE

Thermal performance data for the SAM leading edge was presented in Figure 5.1-8 of Reference 5-1. The hot surface temperature profile from that reference is repeated in Figure 5.4-1 of this report (1.7-mil SAM curve), along with three additional hot surface temperature profiles. The new data results because of further analytical interpretation of References 5-4, 5-5, 5-6, 5-7, and also because of application of a factor for freestream turbulence in the methane-air combustion products that will be used for SAM testing.

The spike-tip-shock impingement on the leading edge has been increased in width from 1.7 to 4 mils and decreased from 18.1- to 15.4-times the heat transfer coefficient for spike-shock-inside-lip aerodynamic conditions. This change in spike-shock impingement characteristics produces a modest 150°F surface temperature increase. Use of a turbulence factor of 1.8 for both the shock impingement and adjacent area on the semi-cylindrical leading edge produced a maximum temperature of 1930°R. This is expected to result in a fatigue life for the leading edge of between 40 and 200 cycles. Use of a turbulence factor of 1.8 is consistent with the turbulence factor of two being used for the strut leading edge design and was measured for subsonic flow with turbulence of from 3 to 11 percent as reported in Reference 5-8. Since the actual turbulence level in the 8-foot Hot Structure Tunnel is not known, the 1.8 turbulence factor is merely indicative of typical results and could have a range from 1.0 to above 1.8.

NOTE: SAM CONDITIONS

1. $\frac{\text{SHOCK OUTSIDE LIP } h_s}{\text{SHOCK INSIDE LIP } h_s} = \frac{0.323}{0.206} = 1.57$
2. HYDROGEN TEMP = 321°R, h_s = 2.15 BTU/SEC °R FT^2
3. METHANE - AIR COMBUSTION PRODUCTS TEMP = 3600°R

MACH 8 CONDITIONS

1. HYDROGEN TEMP = 156°R, h_s = 5.3 BTU/SEC °R FT^2
2. AIR TEMP. = 4650°R

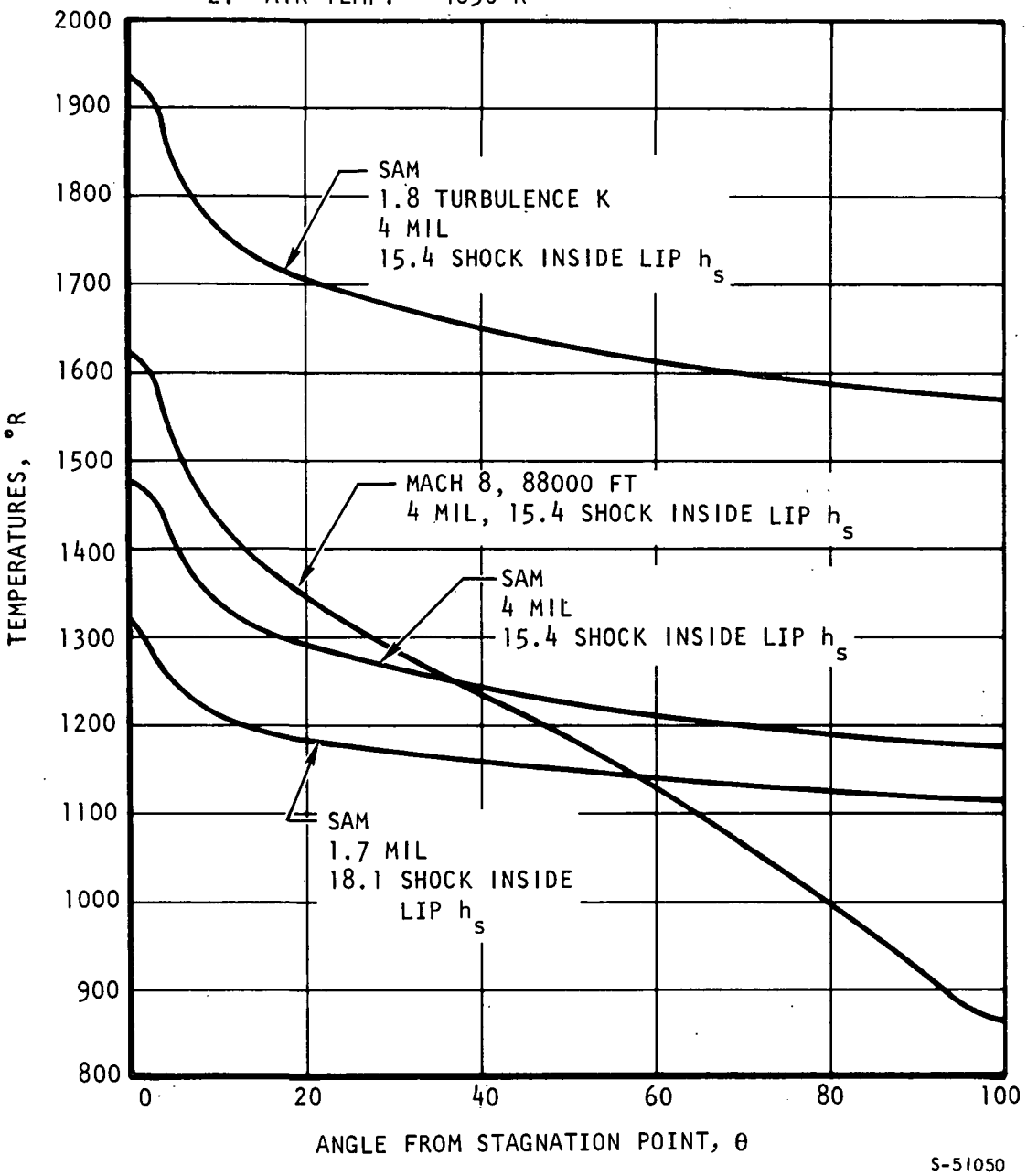

Figure 5.4-1. Leading Edge Hot Surface Temperatures

The hot surface temperature, also shown on Figure 5.4-1, for the 88,000-ft altitude, Mach 8 design point is not expected to be increased by turbulence, since the leading edge is in the freestream.

6. DESIGN EFFORT

The major design effort during the reporting period has involved the preparation of detail and assembly drawings for the water-cooled cowl/plylon and water-cooled mounting structure for use with the SAM in wind tunnel testing. Drawings and a description of the adapters were presented in the previous TDR (Reference 5-1). At that time, the cooling design of the adapters was essentially complete. In the interim, the structural design of the adapters has been completed and the cooling design for the mounting structure reviewed, based on more detailed aerodynamic parameters. In neither case did the results require significant revisions in the basic design as previously described.

6.1 WATER-COOLED COWL/PYLON

The final layout drawing, L-980630, for the water cooled cowl/pylon is attached at the end of this report. The single most significant change made to this layout involved the addition of a seal at the interface between the cowl and the leading edge, Station 41.455. The seal is constructed from a molded section of Teflon that carries a silicone rubber O-ring in one of its grooves. The purpose of this seal is to limit the amount of inerting nitrogen gas flow to the model as a result of leakage through an otherwise large gap at the interface. In general, therefore, the seal is acting to prevent leakage from inside the cowl to outside the cowl, rather than leakage of hot gas into the cowl. Inerting pressures will be at levels in excess of wind tunnel static pressures.

A second change to the cowl/pylon configuration involved the configuration of the pylon leading edge. As originally presented, the leading edge used a double-sandwich surface with flow down one side and up the other. This design has been changed to have only a single-sandwich terminating in a plenum. Considerations of flow-routing and water-pressure drop led to this modification.

6.2 WATER-COOLED MOUNTING STRUCTURE

The final layout drawing, L-980628, of the water-cooled mounting structure is also attached at the end of this report. Changes in this layout relative to the one presented in the previous TDR consist primarily in the addition of structural stiffening of the wedge following detailed stress analysis. In all other respects, the configuration shown in the previous drawing was retained.

7. MANUFACTURING

The manufacturing effort during the reporting period has been entirely devoted to assembly of the full-scale components. Important manufacturing operations, assembly operations, and development problems encountered during these operations have been discussed in previous TDR's for all of the components, and manufacture has now been completed. The following discussion summarizes the general experience for each component on an overall basis.

7.1 INLET SPIKE

The inlet spike is a brazed assembly consisting of three separate, brazed, plate-fin shell assemblies and a sheet metal nose cone. Figure 7.1-1 illustrates the orientation of these components. The subassemblies are step-brazed with a series of precious-metal brazing alloys to form a single integral unit as shown in Figures 7.1-2 and 7.1-3.

7.1.1 Shell Fabrication

The Hastelloy X shells used in the spike were all made from sheet stock, final-sized by Electroshape forming, with the exception of the hot and cold sheets used in the spike tip which were rolled and formed. The large manifolds used in the spike were machined from Hastelloy X forgings.

7.1.2 Basic Shell Assembly Brazing

The basic fin-to-shell braze joint is made with Palniro-4 ($2150^{0}F$) on all of the brazed-shell assemblies. The stacking procedure for all of the shell assemblies was to resistance tack-weld braze alloy foil to the outside of the cold skin, resistance tack-weld fins on top of the braze alloy to the cold skin, and then resistance tack-weld braze alloy foil to the fins on the hot skin side of the fin to provide alloy for the hot skin-to-fin joint.

The integrity of the basic braze joint (fin to shell) was evaluated during a StressCoat proof-pressure test on all brazed assemblies except the spike tips, which were subjected to a pneumatic proof-pressure test. The StressCoat was able to detect any unbrazed areas in the assemblies by cracking at the unsupported areas above the braze voids.

7.1.3 Component Fabrication

The components of the spike were the nose cone, spike tip assembly, fore spike assembly, and aft spike assembly.

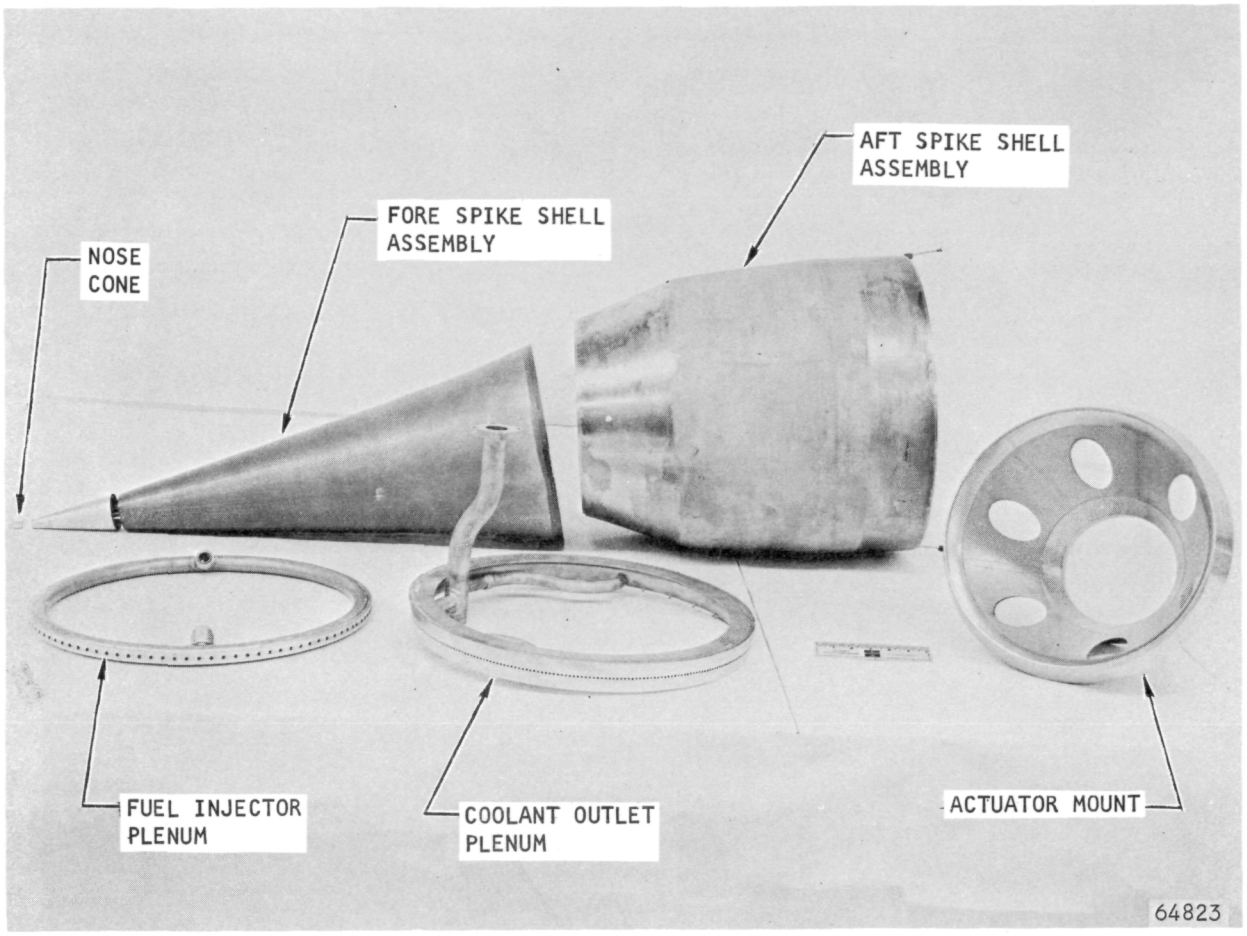

F-11106

Figure 7.1-1. Major Components of Inlet Spike Brazed Assembly

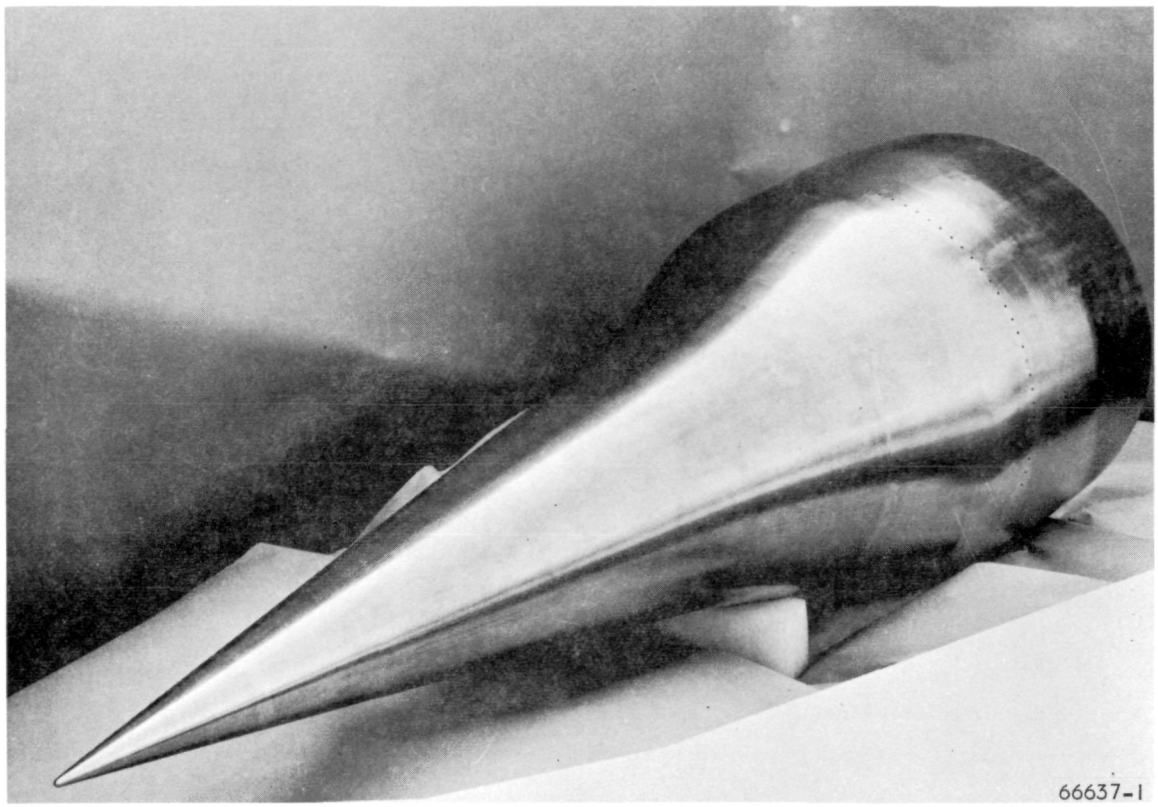

Figure 7.1-2. Inlet Spike Assembly

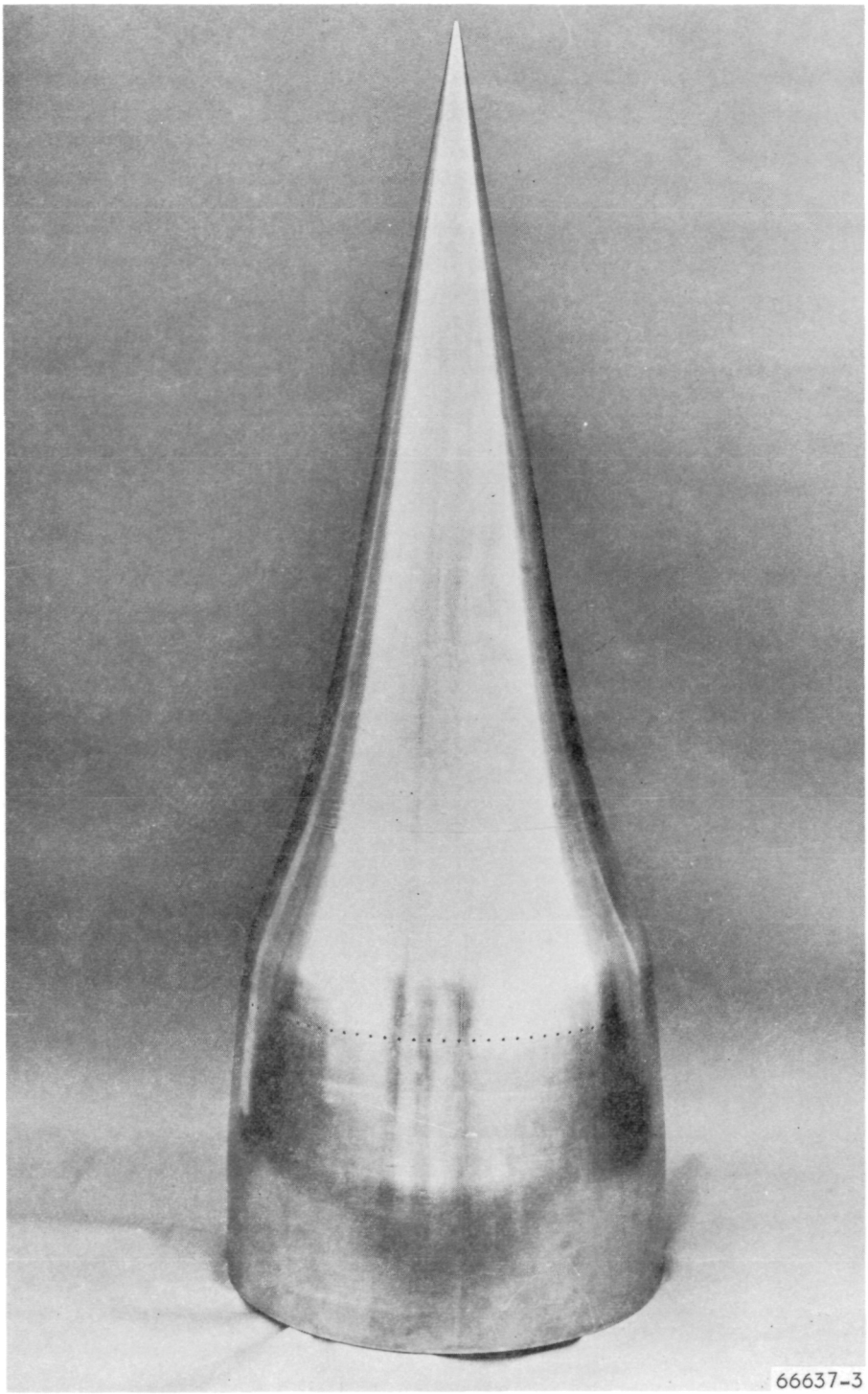

Figure 7.1-3. Inlet Spike Assembly

7.1.3.1 Nose Cone

The nose cone was machined from bar stock with no additional operations prior to assembly.

7.1.3.2 Spike Tip Assembly

After the basic shell assembly was brazed, the single remaining operation on the spike tip was to electrical-discharge-machine holes into the fins, through the cold skin, for coolant flow.

7.1.3.3 Fore Spike Assembly

After the basic shell assembly was brazed, instrumentation insert holes were electrical-discharge-machined through the shell assembly. The dummy headers of the shell assembly were trimmed away to allow cleaning fluid to remove the oil used in the machining operation.

7.1.3.4 Aft Spike Assembly

The holes for the fuel injector inserts were electrical-discharged-machined through the shell assembly slightly undersized to allow for reaming of the holes to the final diameter. The dummy header at the forward end of the shell assembly was removed to allow removal of the oil, used in the machining operation, with cleaning fluid.

7.1.4 Fabrication of Spike Assembly

The spike components were sequentially brazed with the Palniro series of alloys with lower brazing temperatures used in each successive brazing operation. The brazing sequence for fabrication of the spike assembly is tabulated below:

Palniro-1 (2050°F)

(a) Spike Tip

1. Plenum and tip-coolant tube brazed to cold skin of spike tip
2. Cold skin doublers brazed to cold skin of spike tip

(b) Fore Spike Assembly

1. Pressure and temperature inserts brazed into assembly
2. Hot and cold skin doublers brazed to the shell assembly at the forward end

(c) Aft Spike Assembly

1. Brazing done during component fabrication

Palniro-RE (2025°F)

(a) Spike tip and fore spike assembly

1. Nose cone brazed to spike tip

2. Spike tip brazed to fore spike assembly

(b) Aft Spike Assembly

1. Doubler at forward end brazed to cold skin

2. Actuator mounting cone brazed to cold skin

3. Fuel injector plenum brazed to cold skin

4. Coolant outlet plenum brazed to cold skin

5. Control thermocouple inserts brazed to cold skin

Palniro-7 (1970°F)

(a) Joining of forward-brazed assembly and aft spike brazed assembly

Silver Braze- BAg-8

(a) Coolant control thermocouples brazed into inserts

7.1.5 Summary

The two brazing difficulties encountered in the fabrication of the spike assembly were fin-plugging in the 0.050-in.-high fin in the aft spike assembly and voids at the header at the back of the aft spike. The use of stop-off and careful control of the amount and placement of braze alloy, minimizes the problem of fin-plugging. A revision of the header design used on the folded-over fin passage of the aft spike appears desirable in order to insure more reliable brazing at this location.

The electroshape forming of the fore spike hot and cold shells proved to be more difficult than anticipated, due to tearing in the metal at the small diameter. This problem can be largely obviated by having the fore spike assembly begin at Station 8.000 instead of Station 7.000, thus increasing the length of the spike tip hot and cold shells by one inch.

7.2 INNERBODY (INNER SHELL)

The inner shell and nozzle, bolted together, form the innerbody of the engine as shown by Figure 7.2-1. The inner shell, shown by Figures 7.2-2 and 7.2-3, contains, in addition to the coolant manifolds, the mounting pads for the spike actuator, the mounting pads for the struts connecting the inner and outer shell, and two of the three inner rows of fuel injectors. These fuel injectors are not installed in the SAM component.

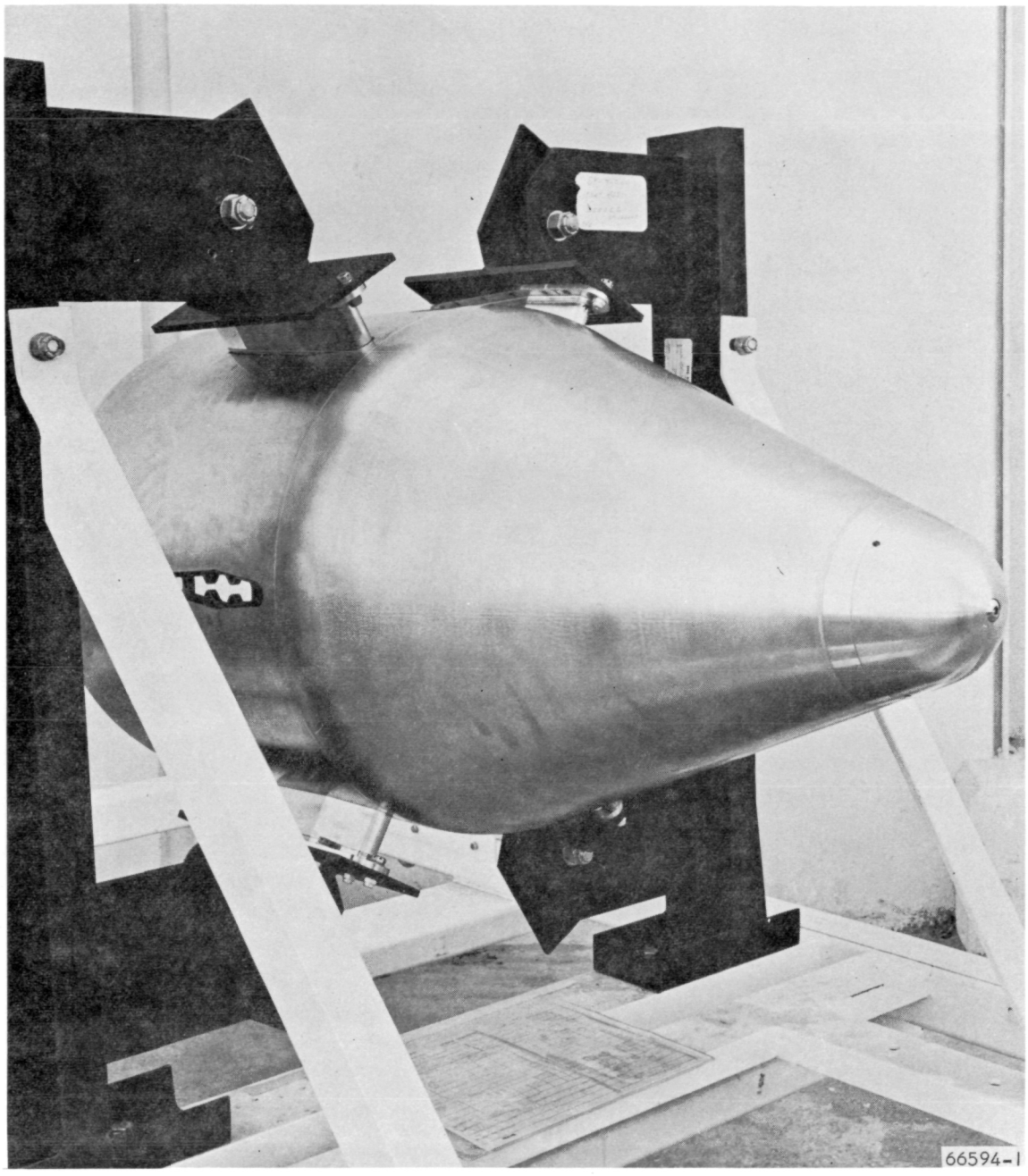

Figure 7.2-1. HRE Innerbody

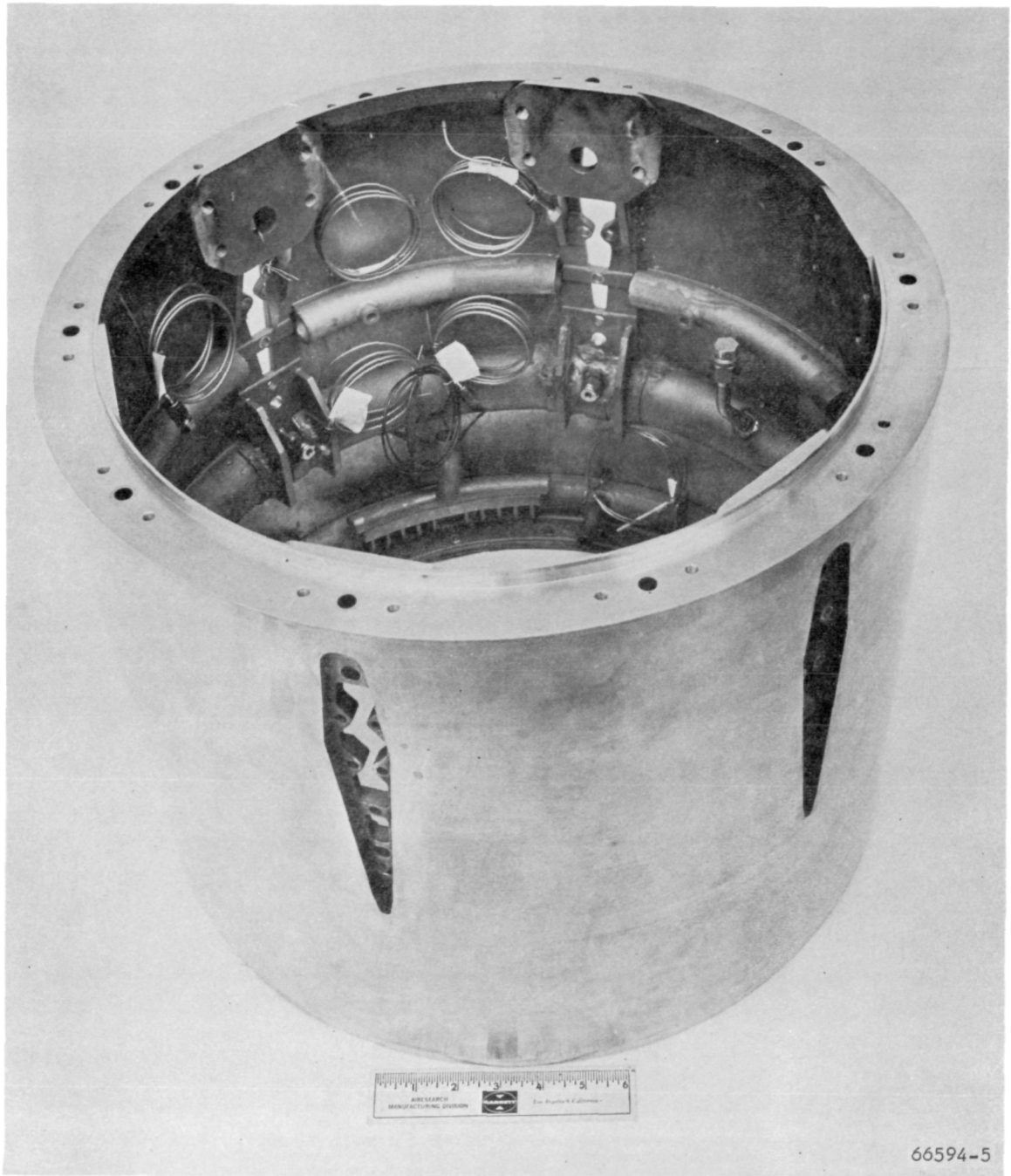

Figure 7.2-2. Inner Shell Assembly - View into Aft End Showing Actuator Mounting Pads, Strut Mounting Pads, and Nozzle Mounting Flange

Figure 7.2-3. Inner Shell Assembly - View of Forward End

The manifolds and mounting pads were all fabricated from Hastelloy X forgings or plate stock, utilizing conventional joining and machining operations. Because of the small clearances (0.001 to 0.005 in.) required for optimum brazing conditions, the final machining of the manifold mating surfaces to the shell was deferred until after the final brazing and pressure testing operations had been completed on the basic shell.

The basic shell assembly, because of its straight-walled, essentially cylindrical shape, was the most simple of all structures to jig, fixture and inspect. The inner skin of the shell was fabricated from 0.063-in.-nominal-thickness, and the outer skin from 0.015-in.-nominal-thickness Hastelloy X. The fins used between the two skins of the structure were 0.050 in. high with 28 convolutions per in.

In addition to the fins between the two skins, six pads of 0.050-in.-thick Hastelloy X were installed. These ultimately became the headers around the strut openings. These pads, accurately machined around the circumference and positioned accurately in the assembly, were brazed in place to the two skins, along with the fins. Then, during subsequent operations, the center of each pad was removed by electron-discharge machining leaving 0.050 in. around the circumference to form the headers. To provide additional coolant flow area around the headers, a groove was cut through the thick inner skin around the major portion of the external header circumference. During final assembly operations, the strut mounting flanges were brazed to the inner skin, covering the grooves. The fabrication sequence of the openings is illustrated by Figure 7.2-4. The grooves around the strut openings proved to be a major fabrication constraint because they provided a opening for braze alloy to flow into the finned passages during brazing of the strut mounting flanges. Use of stop-off to deter the alloy flow, and precautions to ensure good fitup of the flanges to the skin permitted successful fabrication. However, a redesign of the groove, reducing its depth so as not to cut through the inner surface, would result in more reliable manufacture.

Some time after the program had been established, metallagraphic evidence was presented indicating that increased service life of the Hastelloy X skins might be obtained by limiting the maximum brazing temperature to less than 2150°F, the recrystallization temperature of the alloy. This limitation would have prevented use of Palniro-4 braze alloy for the brazing of the skins to fins. Coincident with this evidence a new braze alloy, Paniro-RE, was released with a brazing temperature between that of Palniro-1 and Palniro-7. A review was conducted of the tooling status at the time. The conclusion reached was that the only structure that could practically incorporate the change in brazing sequence was the inner shell assembly. Consequently, the major brazing milestones on this assembly were:

(a) 1st Cycle--Palniro-1. Fins, headers, and strut pads to skins

(b) 2nd Cycle--Palniro-RE. Pressure tap and thermocouple inserts to skins; fuel injectors to skins, (on experimental fabrication and static test models only).

(c) 3rd Cycle--Palniro-7. Manifolds and pads to shell.

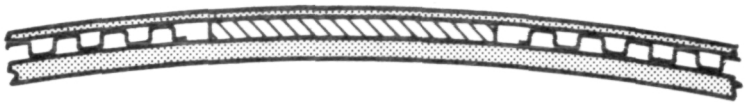

STEP 1. DUMMY HEADER PADS BRAZED TO SKINS

STEP 2. CENTER OF PADS AND GROOVE AROUND CIRCUMFERENCE MACHINED

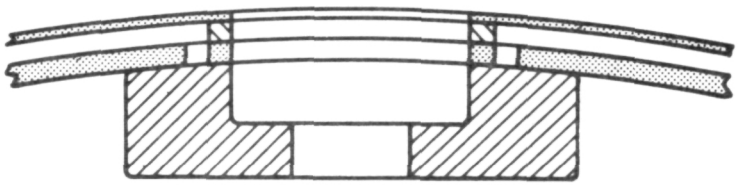

STEP 3. BRAZING OF STRUT MOUNTING FLANGE TO INNER SKIN

S-51063

Figure 7.2-4. Fabrication Sequence - Inner Shell Assembly Strut Openings

In addition to the above cycles, a furnace braze cycle using Nioro alloy was used on the SAM unit to repair leaks in the strut pad and manifold joints that were detected after the third braze cycle.

7.3 INNERBODY (NOZZLE)

This assembly is made up of the finned shell; a flanged crossover manifold at the large end, which bolts to the inner shell assembly; and the closeout rings, brazed to the small end as illustrated by Figures 7.3-1 and 7.3-2. Coolant pressure containment and flow direction at the aft end of the nozzle assembly is achieved by three additional details, bolted or screwed to the brazed and machined nozzle assembly. These are a baffle assembly, Figure 7.3-3, a cover assembly, Figure 7.3-4, and the cap, Figure 7.3-5. The SAM nozzle assembly with these details attached is shown by Figure 7.3-6. Teflon "Omniseals" are used at the flange faces.

The nozzle is the least complex of the components of the engine, in terms of the number of details required for fabrication. However, the geometry of the component created unique fabrication constraints.

The inner cold skin, and outer hot skin of the shell assembly were both fabricated from 0.015-in.-thick Hastelloy X, and the fins were 0.050-in.-tall, 20 convolutions per in. The manifolds and related details were all machined from Hastelloy X forgings.

The braze cycles selected for joining the various subassemblies and final assembly of the nozzle were:

(a) Cycle No. 1--Palniro-4, 2150°F. Shell skins to fins; crossover manifold flange to torus.

(b) Cycle No. 2--Palniro-1, 2050°F. Pressure and thermocouple inserts to crossover manifold.

(c) Cycle No. 3--Palniro-RE, 2000°F. Installation of crossover manifold, small-end rings, thermocouple inserts and pressure tube inserts to shell.

(d) Cycle No. 4--Palniro-7, 1930°F. Pressure tubes and thermocouples to shell.

The nozzle shell, because of its steeply conical shape with the small diameter approximately 28 percent of the large diameter, was particularly critical of setup during the first braze cycle. The first three shells were installed in the furnace for the braze cycle with the small end down. Buckling of the inner shell and blockage of a portion of the fin passages with braze alloy were experienced at the small end. Also, tensile deformations sufficient to rupture the inner skin at the small end was encountered. Two changes in setup were incorporated to ultimately achieve successful braze cycles; (1) the fixture was inverted to permit brazing with the large end of

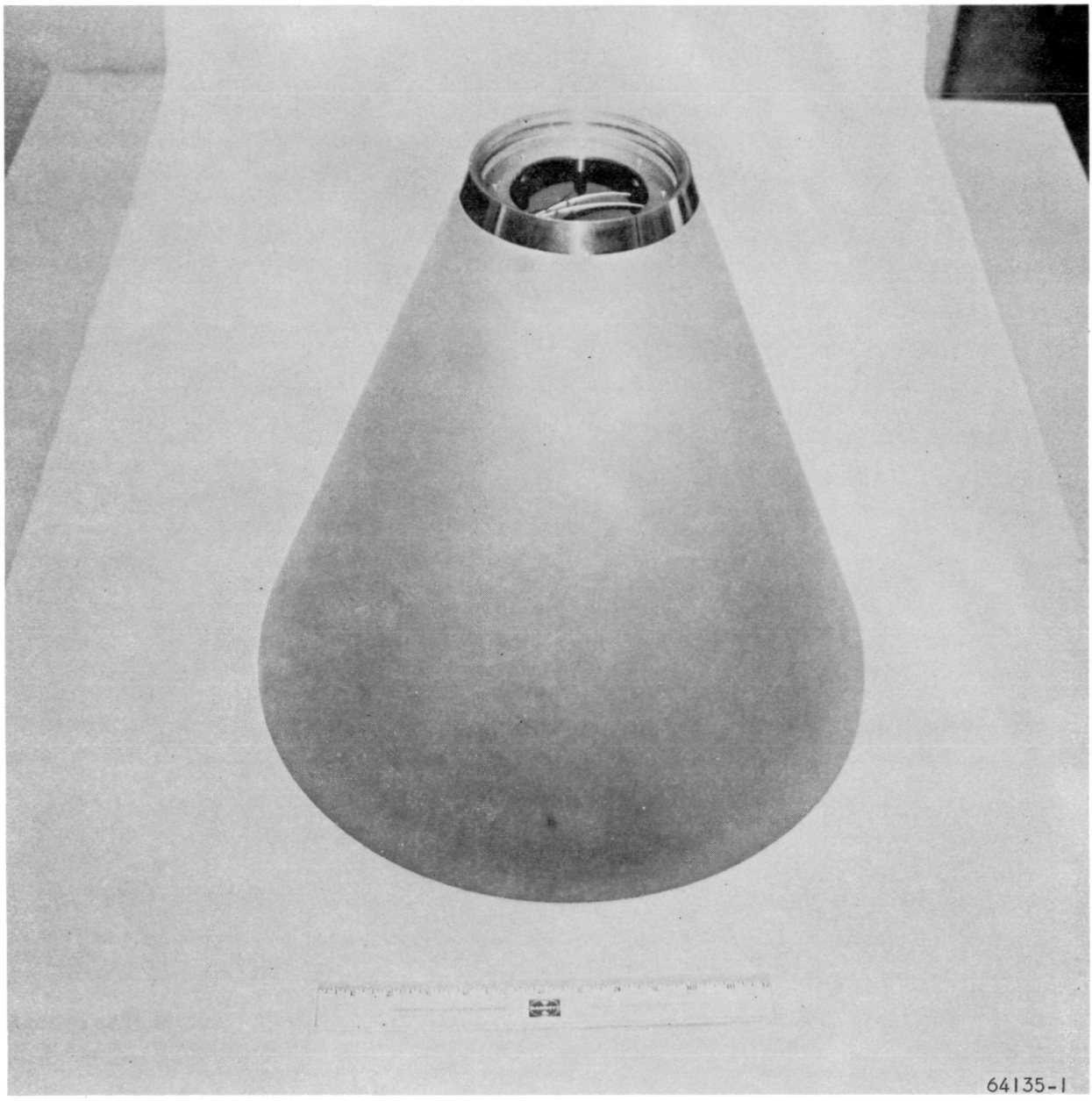

Figure 7.3-1. Aft Nozzle Assembly Viewed from Small (Aft) End

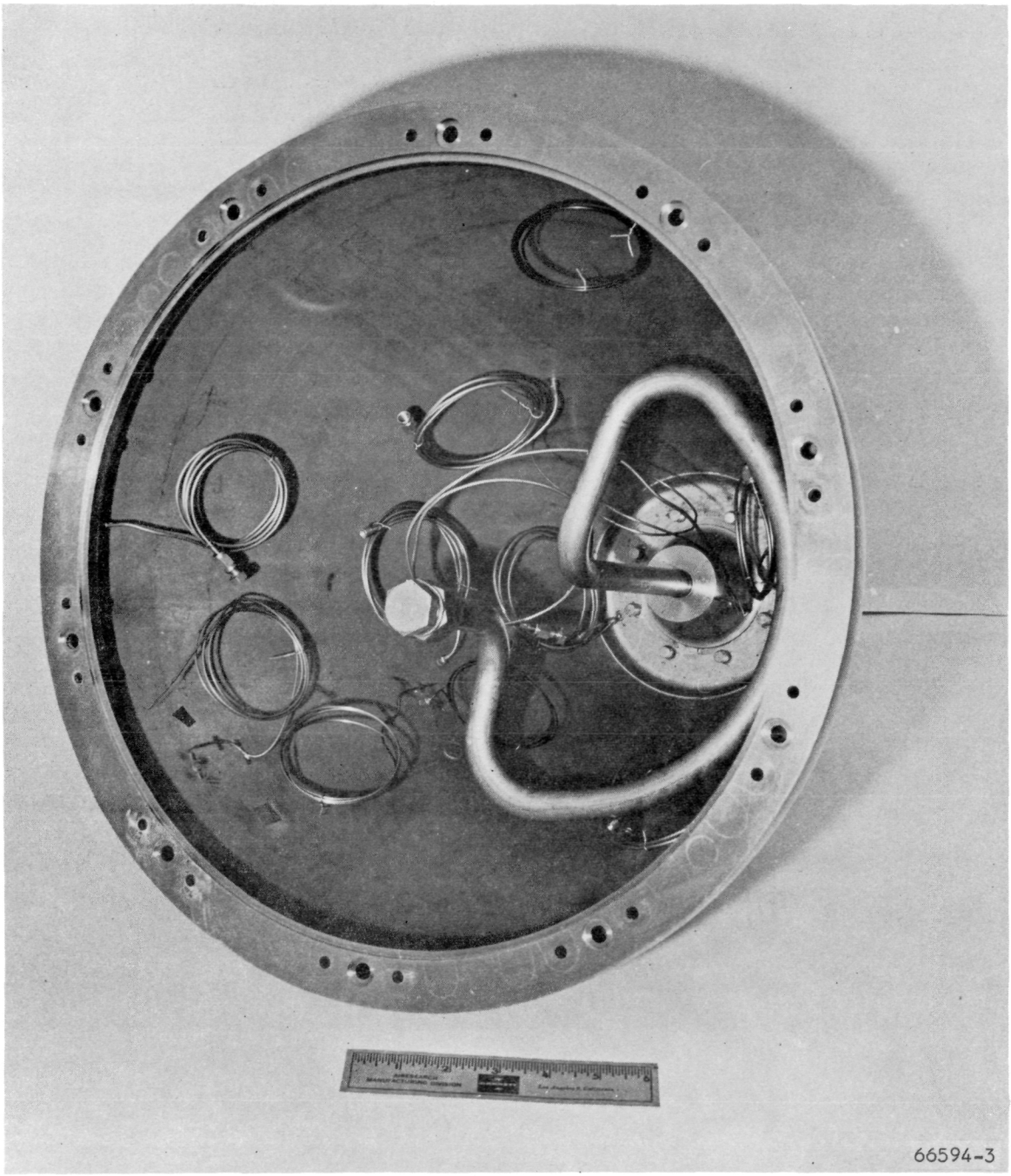

Figure 7.3-2. SAM Nozzle Assembly Viewed from Large (Forward End)

Figure 7.3-3. Nozzle Baffle Assembly

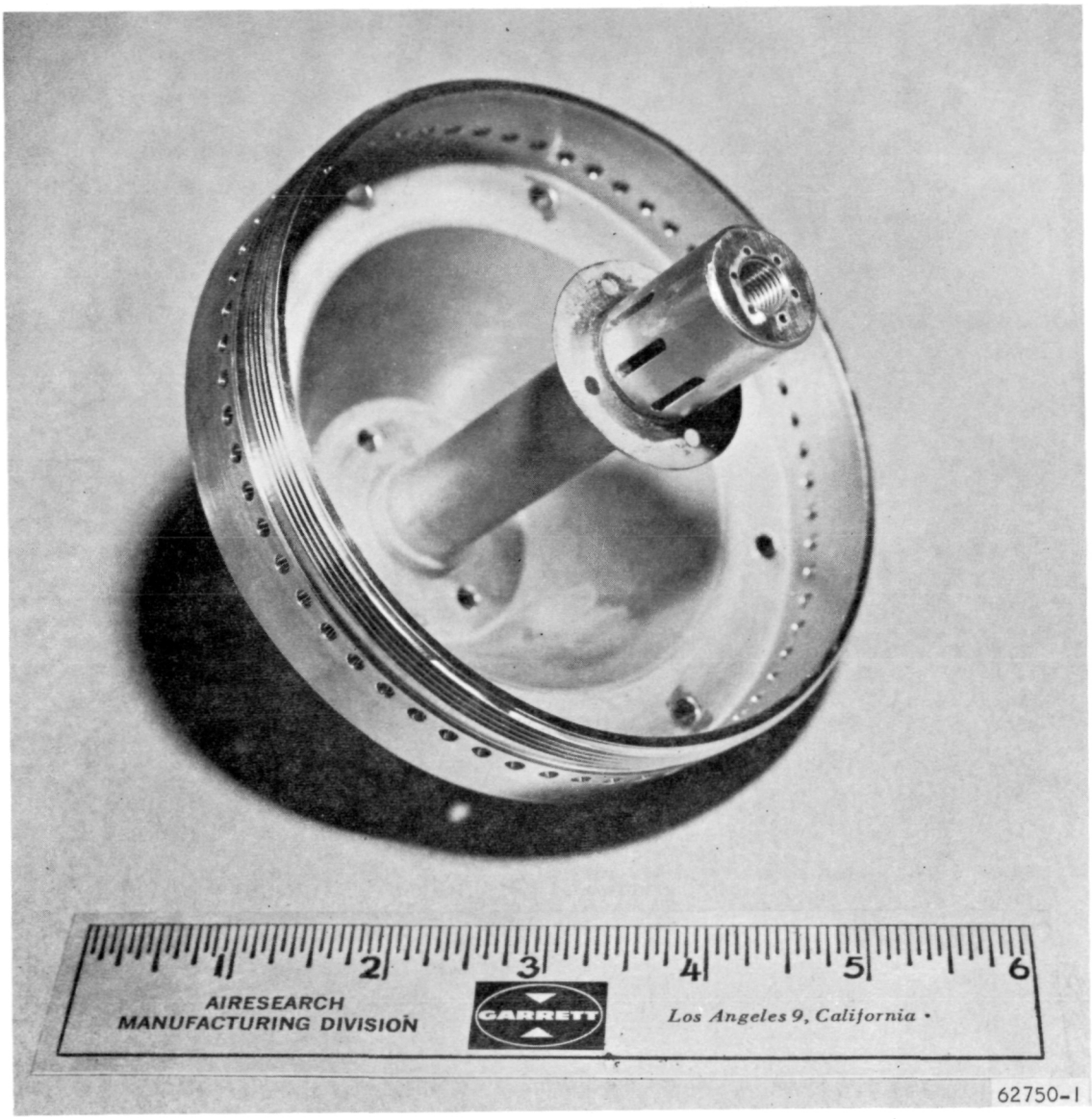

Figure 7.3-4. Nozzle Cover Assembly

F-11099

Figure 7.3-5. Nozzle Cap

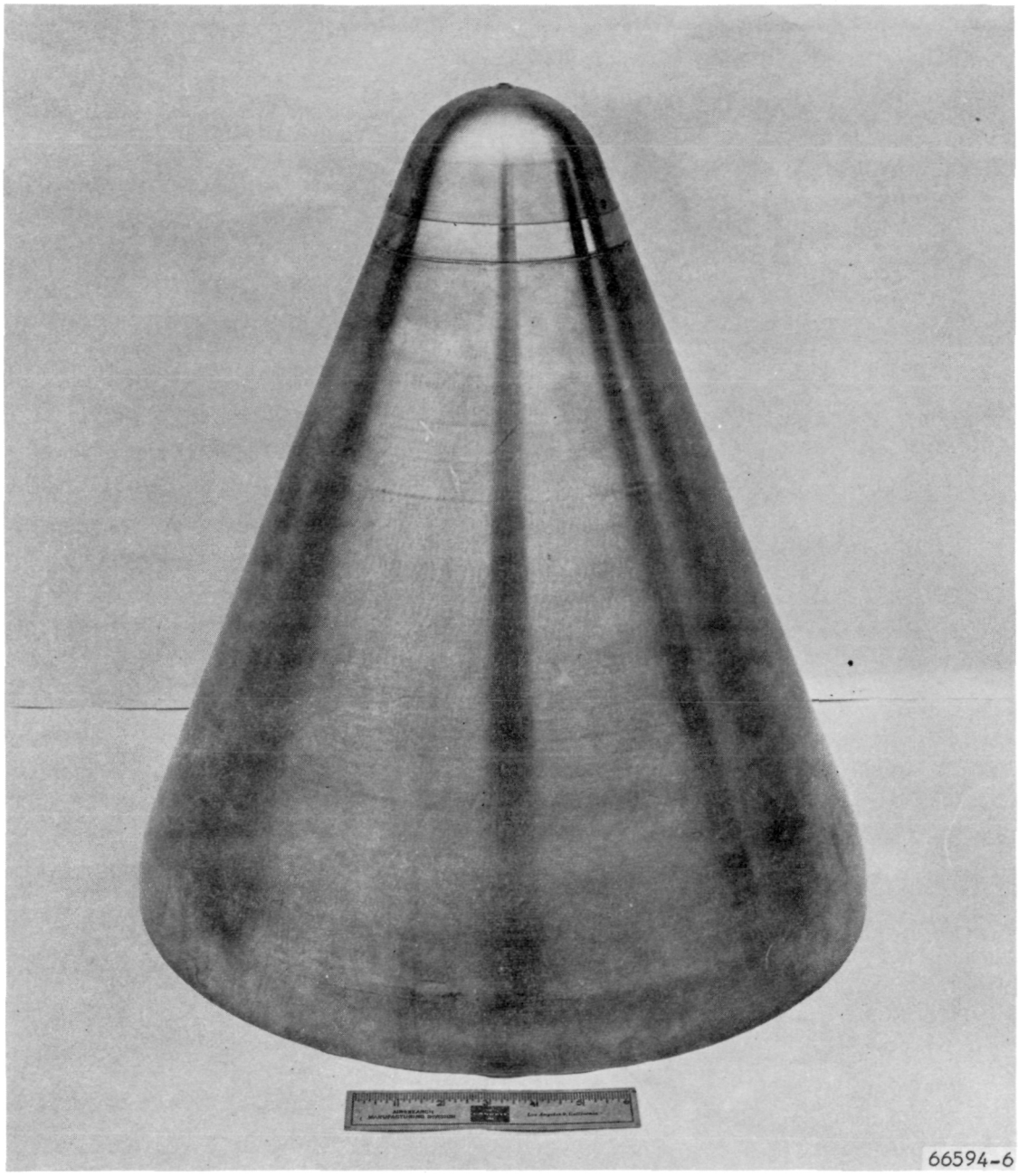

Figure 7.3-6. SAM Nozzle Assembly

the nozzle down. This discouraged the concentration of alloy that might cause fin plugging, and eliminated any tendency for the straight section at the large end to seize prematurely in the graphite/pocket; and (2) the heating cycle was controlled and monitored to restrict the temperature differentials between the inner structure and skin to less than 75°F. This had the effect of approximately doubling the length of the heating cycle, from approximately 4 to 8.3 hr, but eliminated objectionable differential thermal growth.

The control of the temperature of the part (and braze alloy) during the portion of the braze cycle above the solidus temperature of the alloy (2075°F) proved to be extremely critical in limiting the settling of the alloy, and fin plugging. The more rapidly the part could be heated to the liquidus (2140°F and chilled back through the solidus, the less tendency to plug and the more uniform the braze fillets from top to bottom of the structure. This characteristic was evident in all of the fin-skin brazements made.

7.4 LEADING EDGE

The major parts of the leading edge assembly are shown in Figure 7.4-1. Figures 7.4-2 and 7.4-3 show completed parts.

7.4.1 Assembly Sequence

Assembly of these parts occurs in the following sequence, arranged according to the basic braze cycles.

7.4.1.1 Palniro-4 Braze Cycle (2150°F)

(a) Inner shell assembly (shells and fins)

(b) Outer shell assembly (shells and fins)

(c) Tip assembly (shell, inserts, and fins)

Each assembly is individually brazed and proof-pressure tested to 1050 psig after brazing. Pressure testing is performed with StressCoat on the surfaces to permit detection of unbonded areas at stress levels below those that produce yielding in the shells. The tip assembly, at this point, is put aside until required for final assembly.

7.4.1.2 Palniro-1 Braze Cycle (2050°F)

(a) Outlet manifold and instrumentation inserts to inner shell assembly, to form outlet manifold assembly.

(b) Inlet manifold and instrumentation inserts to outer shell assembly, to form inlet manifold assembly.

Each assembly is leak-tested at low pressure (100 psig) following its braze cycle.

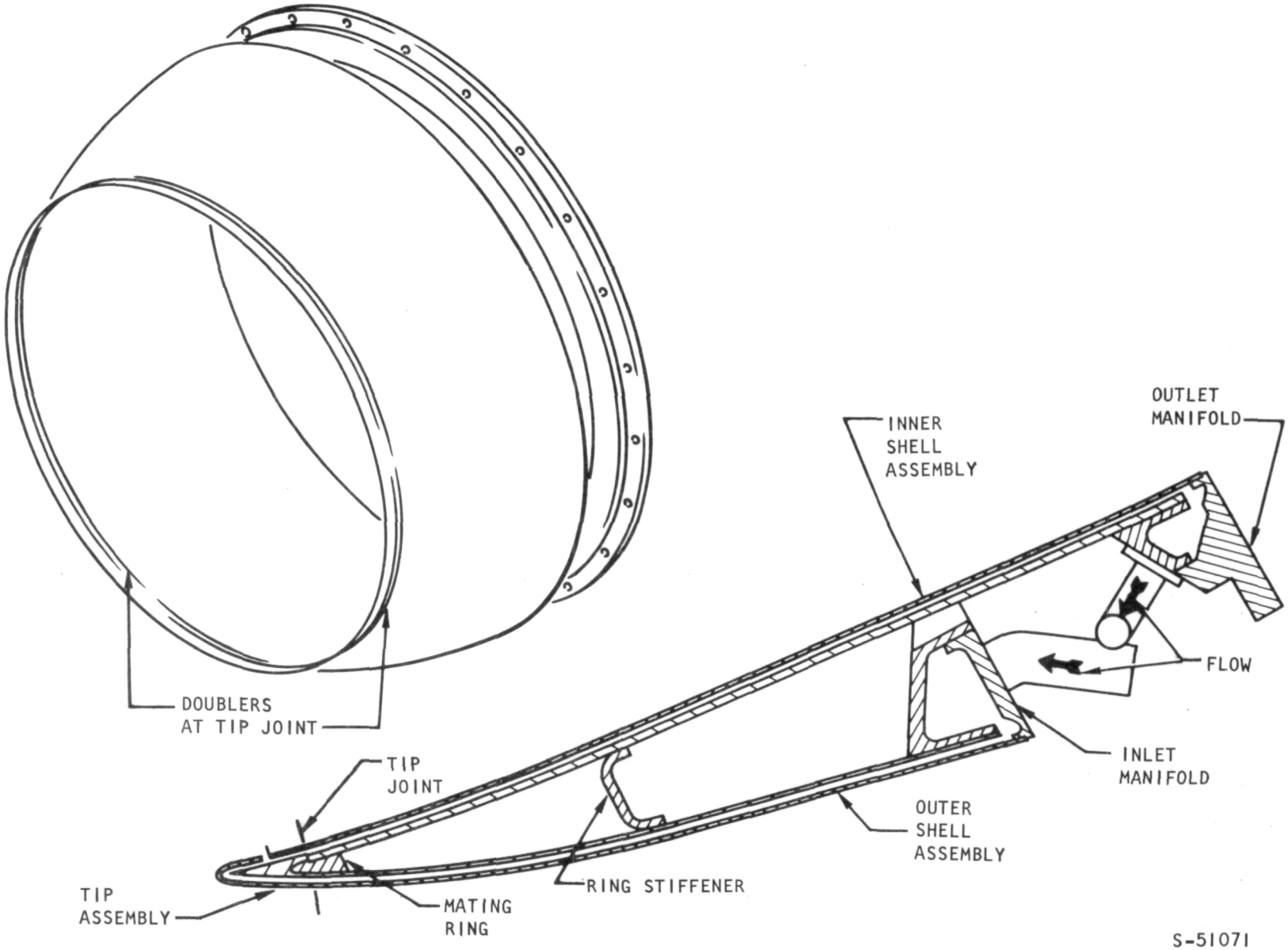

Figure 7.4-1. Leading Edge Assembly

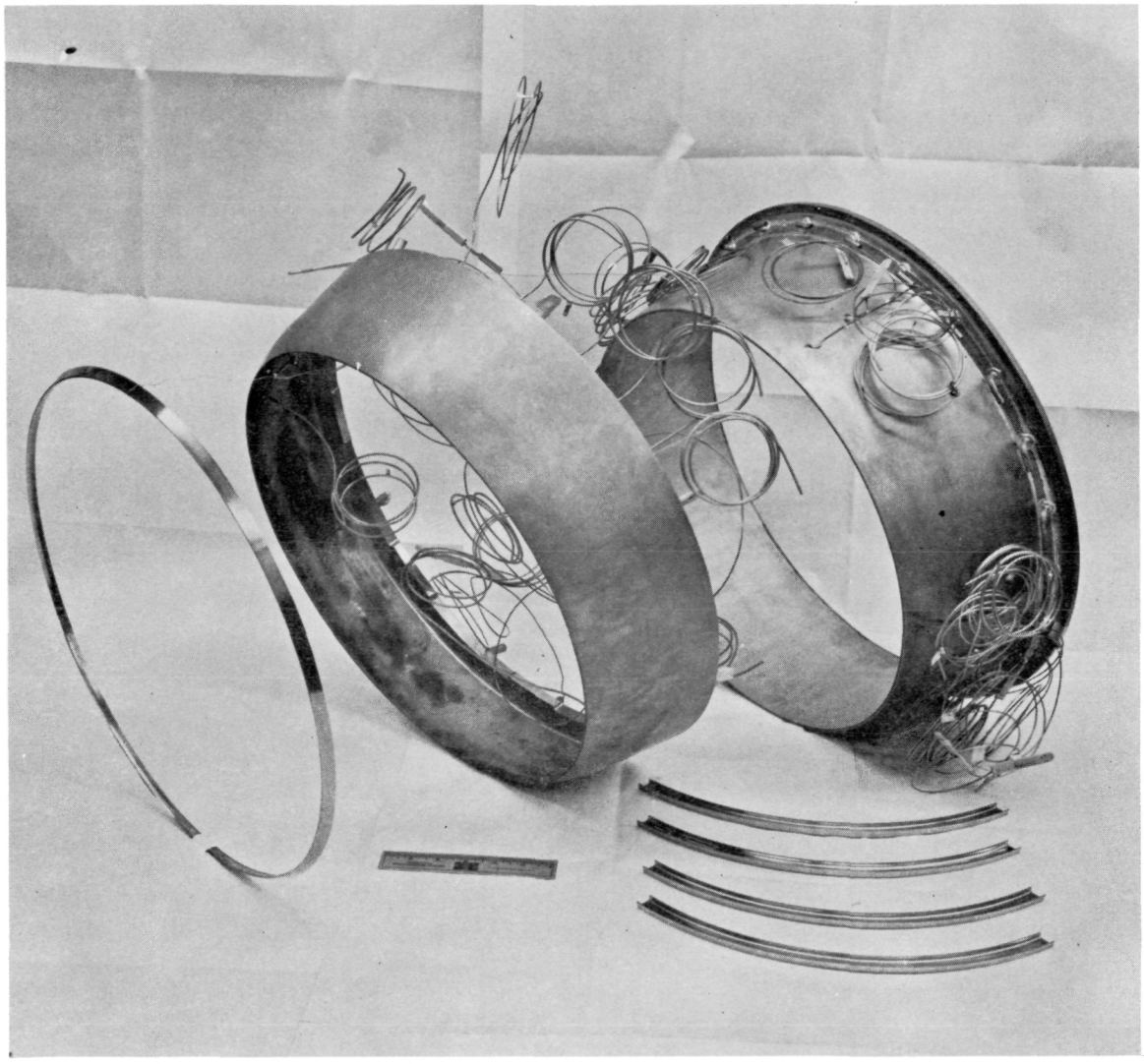

F-11100

Figure 7.4-2. Components of Leading Edge Structural Assembly (Inlet and Outlet Manifold Assemblies, Mating Ring, Ring Stiffener)

Figure 7.4-3. Leading Edge Assembly After Completion of All Brazing Operations

7.4.1.3 Palniro-7 Braze Cycle (1930°F)

This cycle joins the two manifold assemblies, the mating ring, and the stiffening ring into the structural assembly. The joints between the mating ring and the shells are checked for leakage, at essentially zero pressure, in two ways:

(a) With the mating ring down, the cavity above the ring is filled with acetone and the joints inspected for seepage.

(b) With the mating ring up, the cavity below the ring is filled with helium and sniffed, using a mass spectrometer.

7.4.1.4 Nioro Braze Cycle (1850°F)

This cycle joins the tip assembly to the structural assembly to complete the joining operations on the leading edge assembly. Doublers are brazed across both the internal and external tip joints during this cycle. This final assembly is again proof-pressure tested to 1050 psig with StressCoat on the surfaces.

7.4.2 Manufacturing Experience

A review of the manufacturing experience on the leading edge assembly indicates the following:

(a) Shell Assemblies--Brazing of the shells and fins can be accomplished with dimensional repeatibility and sound bonding.

(b) Tip Assemblies--Brazing produced sound joints. For the limited number of parts produced, however, dimensional control was problematical. This is essentially a development problem relating to fixture sizing and loading. Where dimensions were unacceptable, it was possible to resize the part by furnace heating to below the braze temperature with modified fixture dimensions. Dimensional control of the tip is particularly important because of the required fitup with the structural assembly at the mating ring and the differing cone angles on the inside and outside surfaces of the assemblies.

(c) Manifold Assemblies--The principal complication in joining these assemblies was a tendency for fin-plugging at the manifold ends. Subsequently refined techniques for stop-off application would have reduced, if not eliminated, this tendency.

(d) Structural Assemblies--Same comments apply as for the manifold assemblies. Dimensional control was satisfactory for these assemblies.

(e) Final Assemblies--The joining of the tip to the structural assembly posed serious problems in terms of plugging of the tip fins with filler alloy. Application of stop-off to the fins on either side of the joint with an artist's air brush gave good coverage beyond the

immediate joint area. This technique, along with careful limitation of filler alloy quantity, minimized the tendency toward fin-plugging.

7.4.3 Summary

The use of filler alloys of a single system (gold-palladium-nickel) brings with it the potential for alloying and formation of low melting compositions. The penetration of Palniro-1 through a solid Palniro-4 joint, for example, was observed in strut fabrication as well as in experimental samples. The potential for plugging of small passages is, thereby, aggravated. In cases where neither the ductility nor strength of the Palniro series of alloys is important, use of combinations of alloy systems should be considered.

7.5 OUTER SHELL

In terms of the number of detail parts and joints, the outer shell is by far the most complex of the assemblies on the engine. In addition to two separate shell assemblies, it incorporates four tubular ducts, three machined structural support manifolds, two machined plenum assemblies, the six flange pads for strut mounting, and the fuel injectors. These subassemblies are shown in Figure 7.5-1, which shows the completed outer shell assembly.

Fabrication of the manifolds and ducts embodied essentially the full gamut of conventional metal forming, joining, and machining techniques. The two primary support manifolds required four separate circular machined forgings each, in addition to the pads or support lugs. Each of these manifolds was made up of a semi-toroidal ring brazed to an inner cylinder. The close fits required for these braze joints required not only close tolerances (±0.001-in.) but the extra precaution of temperature control of the part during measurement, because of the size of the details and thermal coefficient of expansion. A variation of 10°F temperature in the part represented a change in diameter equal to the total allowable tolerance, 0.002-in. In order to achieve the required 0.001 to 0.005-in. clearance with the shell, all manifolds were final-machined to dimensions taken from the shells after their last preceding braze and test operations.

The braze cycles used for the outer shell assembly were:

(a)	Cycle No. 1--Palniro-4, 2150°F.	Primary shell assembly skin to fin joints Trailing edge shell assembly skin to fin joints Manifold subassembly joining
(b)	Cycle No. 2--Palniro-1, 2050°F.	Primary shell assembly to fuel injectors Trailing edge shell assembly to plenum

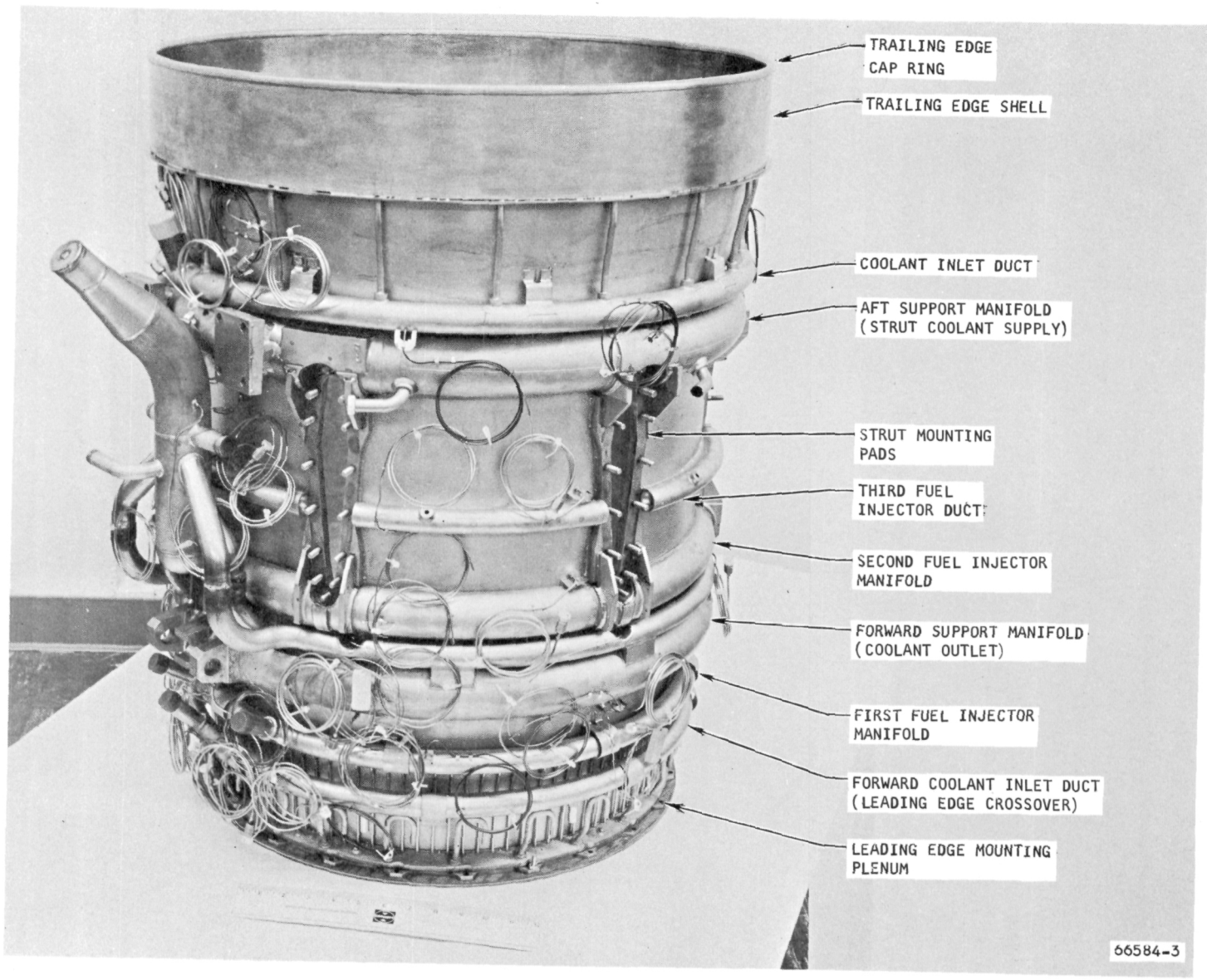

F-11107

Figure 7.5-1. SAM Outer Shell Assembly

(c) Cycle No. 3--Palniro-RE, 2000°F. Primary shell assembly to all manifolds, static pressure sensing tubes, thermocouple inserts, strut mounting pads, leading edge mounting plenum (inner), and trailing edge/primary shell mating ring (inner).

(d) Cycle No. 4--Palniro-7, 1950°F. Primary shell to leading edge mounting plenum (outer), trailing edge cap ring (outer), gussets, doublers and thermocouples.

Experience during brazing of the shells highlighted the special limitations involved in fabrication of this component. The inner (hot) skin, which was welded to the pressurizing insert, is 0.015 in. thick, and much weaker than the insert. The inner skin of the first assembly that was brazed, buckled severly during the brazing cycle because of differential growth resulting from differences in temperature. Incorporation of a strain-absorbing bead in the joint between the inner skin and pressurizing insert, and limitation of the temperature differences between skin and insert to less than 100 deg, permitted successful brazing on the second and third shells. Fin-plugging was avoided during the first braze cycle of the outer shells by limiting the time that the part was in the brazing temperature range.

The third braze cycle using Palniro-RE alloy was the crucial cycle of the outer shell sequence. In addition to the sealing requirements for all of the manifolds and plenums, there was the hazard of fin-plugging by migration of alloy through the slots around each of the strut openings. Application of stop-off in the slots, and extra restraint to maintain minimum clearance between the strut pads and shell, were successful in preventing any plugging except a minor amount in the experimental fabrication model.

7.6 STRUT

Six struts are required to connect the innerbody to the outerbody of the engine and provide passages for all of the service lines between the inside of the innerbody and outside of the engine. The struts use 0.020-in.-high fins formed from 0.004-in. Hastelloy X between the 0.015-in.-thick Hastelloy X skin and the forged Hastelloy X body. Figure 7.6-1 shows the major details used in the fabrication of a typical strut.

Three braze cycles are required for strut assembly:

(a) Cycle No. 1--Palniro-4, 2150°F. Fins to skin and body

(b) Cycle No. 2--Palniro-1, 2050°F. Special fin strip to tip coolant passage

(c) Cycle No. 3--Palniro-7 or AMS 4778. Doublers to skin. Tubes to body

Because of the extremely small fin passages (0.016-in.-tall), the major preoccupation during fabrication is prevention of plugging of the fin passages

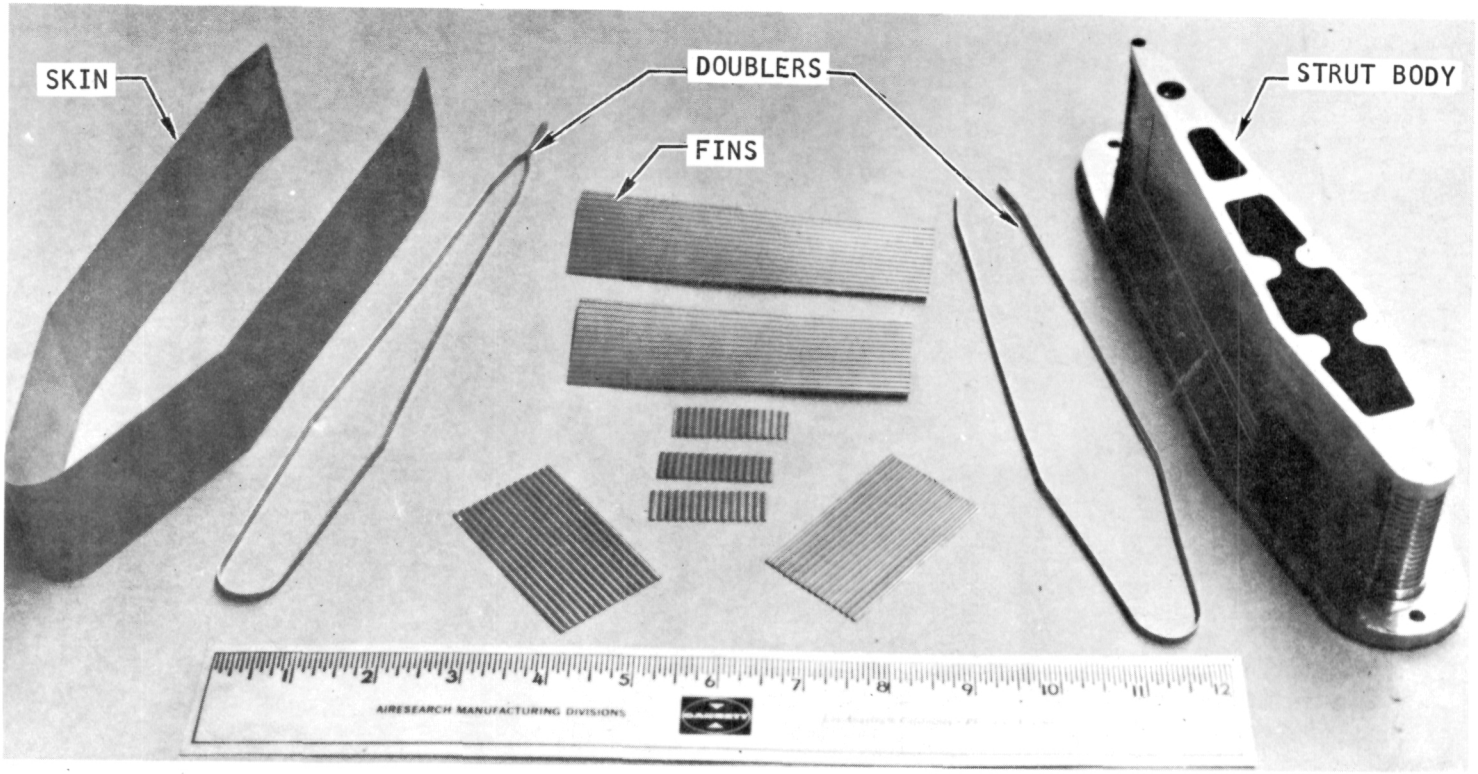

F-9931

Figure 7.6-1. Struts Internal Details

with braze alloy. A quantity (0.001-in.-thick) of alloy pre-placed between the fin sheets and body or skin does not plug fins provided the portion of the braze temperature cycle above the solidus temperature is controlled. However, any excess alloy that is allowed to enter the fin passages in addition to this amount causes plugging. The family of alloys used are sufficiently compatible that interalloying occurs at even the lowest braze temperatures to permit flow of alloys into the passages unless positive provisions are taken to prevent it. "Stop-off" compounds on top of previously brazed joints are proving to be reasonably dependable barriers to flow of alloy through the joints.

7.7 HRE EXPERIMENTAL ASSEMBLY

A preliminary assembly of all of the major components of the HRE was completed and provided fit-and-assembly checks. This work was previously reported (Reference 5-1) and is summarized here for completeness.

Figures 7.7-1, 7.7-2, and 7.7-3 show three views of the assembly on its handling cart. The major components of the assembly are:

(a) Innerbody nozzle, cap, and cover assembly

(b) Innerbody inner shell

(c) Inlet spike

(d) Spike actuation system

(e) Strut bodies

(f) Outer shell assembly

(g) Leading edge assembly

Significant conclusions from this effort were (1) tooling and procedures used in machining of strut cutouts in the inner and outer shells are capable of producing the close tolerances necessary for satisfactory assembly of struts into the shells, and (2) tolerances obtained in the overall assembly resulted in a satisfactory closeout of spike and leading edge, with annular gap variation from 0.035 to 0.048 in. in the latched-actuator position.

7.8 COMPONENT TEST SUMMARY

A summary of the tests performed on the shell assemblies is shown in Table 7.8-1. The final assemblies for the inlet spike, cowl leading edge, outer shell, nozzle, and inner shell are tabulated with their respective shell assembly(ies) for the experimental, static, and SAM units. The components and shell assemblies had no leakage or deformation unless specifically noted in the table. The shell assemblies, as tabulated, are the basic shell assemblies, i.e., shells and fins without any inserts or attachments, tested following the initial braze cycle.

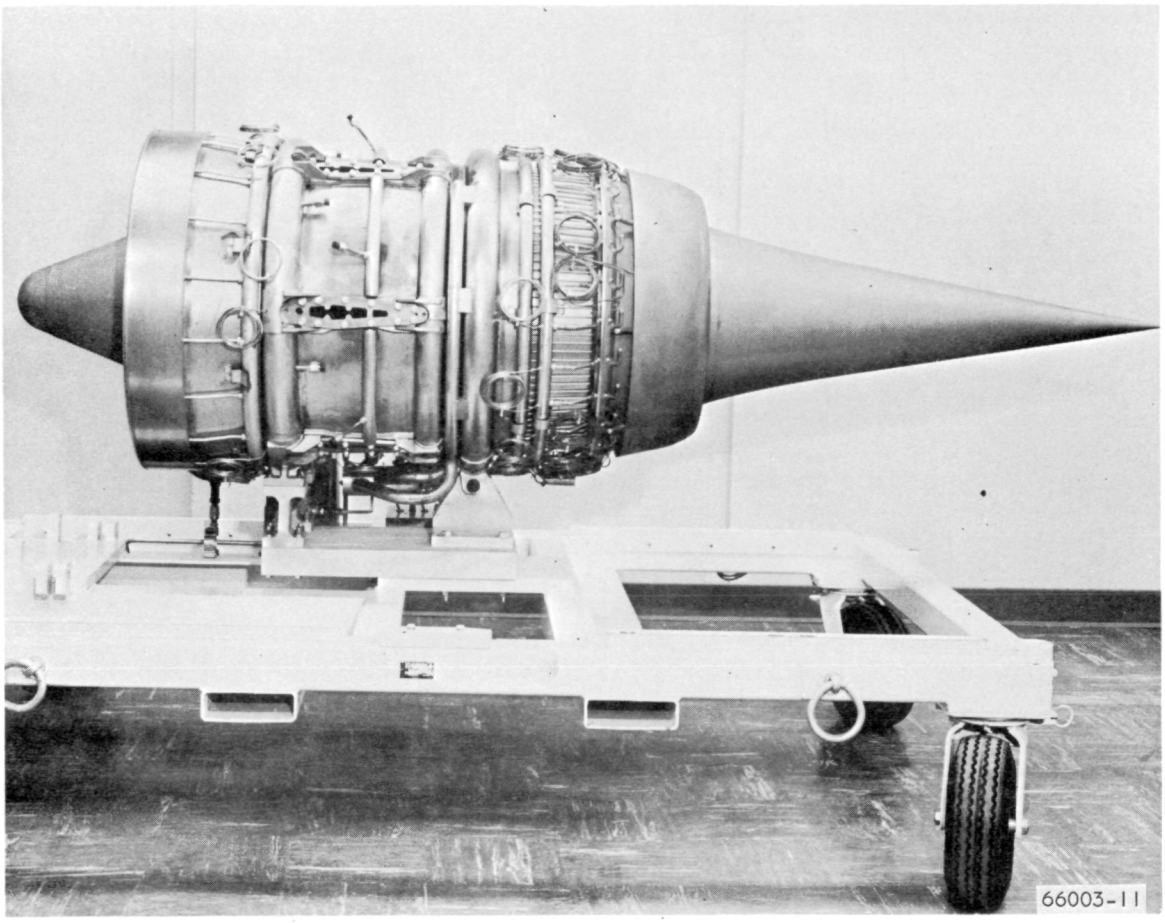

Figure 7.7-1. HRE Experimental Assembly - Engine Profile, Spike Retracted

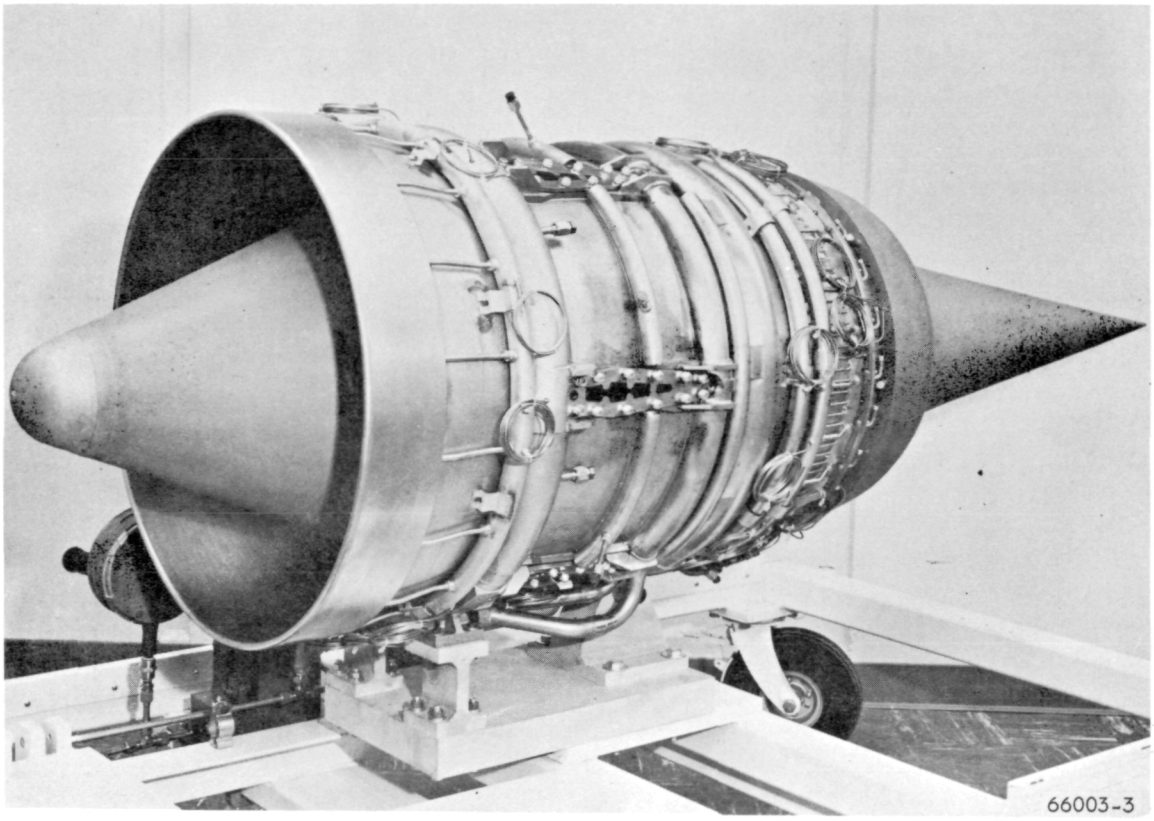

Figure 7.7-2. HRE Experimental Assembly - View Looking Into Aft End

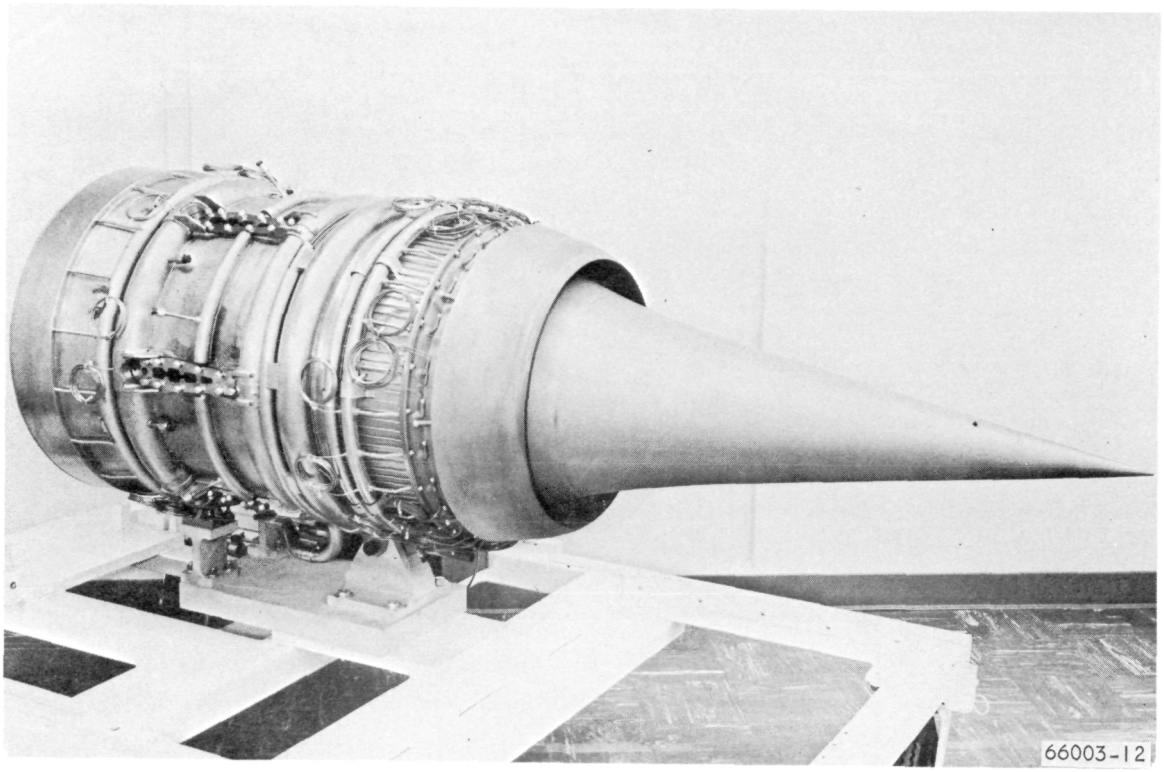

Figure 7.7-3. HRE Experimental Assembly - View Looking Into Forward End, Spike Retracted

Hydrostatic proof-pressure testing is destinguished from leak testing. All units were, in fact checked for leakage during hydrostatic testing. The criterion for acceptability of the SAM final components, however, was that they be bubble-tight when pressurized with gas at the proof pressure and immersed in water for a period of 15 min.

TABLE 7.8-1

COMPONENT TEST SUMMARY

Assy		LEAK TEST*				STRESSCOAT HYDROSTATIC PROOF PRESSURE TEST**				AIR FLOW TEST
		Final Assembly	Shell Assembly 1	Shell Assembly 2	Shell Assembly 3	Final Assembly	Shell Assembly 1	Shell Assembly 2	Shell Assembly 3	Final Assembly
INLET SPIKE	SAM	1050 psig (N_2)	SPIKE TIP 1050 psig (N_2)	FORE SPIKE None	AFT SPIKE None	1050 psig	SPIKE TIP None	FORE SPIKE 1050 psig	AFT SPIKE 1050 psig-yielding after 5 sec	Pressure drop 20% lower than predicted
	STATIC	1050 psig (water)	1050 psig (N_2)	None	None	1050 psig	None	1050 psig	1050 psig	Pressure drop 5% lower than predicted
	EXP	1050 psig (water) Leakage at coolant inlet tube to plenum	1050 psig (N_2)	None	None	600 psig-yielding at repairs on external doubler	None	1050 psig	1050 psig	Pressure drop 23% higher than predicted due to fin blockage
LEADING EDGE	SAM	1050 psig (N_2)	TIP None	INNER SHELL None	OUTER SHELL None	1050 psig	TIP 1200 psig	INNER SHELL 1800 psig	OUTER SHELL 1500 psig	Pressure drop 33% lower than predicted
	STATIC	1050 psig (N_2)	None	None	None	1050 psig-no yielding with doublers brazed on tip assembly	800 psig-evidence of yielding	1800 psig	1500 psig	Pressure drop 15-20% higher than predicted
	EXP	100 psig (air) Leakage between inner and outer shell assemblies	None	None	None	1050 psig	600 psig-evidence of yielding	1800 psig	1500 psig	None
OUTER SHELL	SAM	1050 psig (N_2)	MAIN ASSY 100 psig (air)	TRAILING EDGE 1050 psig (N_2)	None	1050 psig	MAIN ASSY 1050 psig	TRAILING EDGE 1500 psig	None	Forward coolant circuit pressure drop 18% higher than predicted.
	STATIC	No test-unit not completed	100 psig (air)	1050 psig (N_2)	None	No test-unit not completed	2200 psig	1500 psig	None	None - unit not completed
	EXP	825 psig (water)	No test-inner skin buckled during brazing	1050 psig (N_2)	None	825 psig - limited by spalling of StressCoat	No test - inner skin buckled during brazing	1500 psig	None	Forward coolant circuit pressure drop 18% higher than predicted. Aft coolant circuit pressure drop 8% higher than predicted.
NOZZLE	EXP	1050 psig (N_2)	1050 psig (N_2)	None	None	1050 psig	1050 psig	None	None	Pressure drop 18% lower than predicted
	STATIC	1050 psig (N_2)	1050 psig (N_2)	None	None	1050 psig	1050 psig	None	None	Pressure drop 18% lower than predicted
	EXP	1050 psig (N_2)	1050 psig (N_2)	None	None	1050 psig	1050 psig	None	None	None
INNER SHELL	SAM	1050 psig (N_2)	1050 psig (N_2)	None	None	1050 psig	2200 psig	None	None	Pressure drop 16% higher than predicted
	STATIC	1050 psig (N_2)	1050 psig (N_2)	None	None	1050 psig	2200 psig	None	None	Test data not usable because of blockage
	EXP	1050 psig (N_2)	1050 psig (N_2)	None	None	1050 psig	1650 psig	None	None	None

NOTE: *Assembly leakage as noted
**Assembly yielding as noted

8. TESTING

Final results for full-scale strut testing in a wind tunnel, and pressure drop and flow distribution for the full-scale engine components are presented in the following sections. This work completes the scheduled testing on the program.

8.1 FULL-SCALE STRUT

During the reporting period, additional thermal cycle tests were run on two struts. One of these tests was specifically aimed at evaluating the support panels. Data from these tests, as well as an overall summary of the wind tunnel tests of the struts, are included below.

8.1.1 Test Unit Configuration

The two full-scale struts tested were the configuration 1, SN 5, and configuration 2, SN 2, struts. Both test units had oversized doublers brazed onto the strut sides for minimum strut-to-support-panel gap, and Nickel-200 fins brazed into the leading edge coolant circuit. The SN 5 strut had an 0.005-in. coating (80 percent Cr_2C_3 + 20 percent NiCr by volume) sprayed onto the leading edge to minimize erosion, whereas the SN 2 strut had no coating.

Figure 8.1-1 shows the strut, SN 5, prior to testing, and Figures 8.1-2 and 8.1-3 show the strut SN 5 after 102 thermal cycles. Braze alloy plugging in the leading edge is shown in Figure 8.1-4. The coating started spalling after 48 thermal cycles. Figures 8.1-5 and 8.1-6 show the strut SN 2 after 44 thermal cycles. Figures 8.1-7 and 8.1-8 show the top support panel (SK 51509-1, SN 1) after 106 thermal cycles with counterflow hydrogen coolant.

To evaluate support panel flow distribution, thermocouples were attached across the width of both panel cold surfaces, 1.1 in. from the outlet edge, and at one location on each panel centerline, 3.1 in. from the panel outlet edge. Six thermocouple locations on each panel were used for the SN 2 strut testing. The thermocouple locations for the flow distribution profile of the SN 5 strut test are shown in Figures 8.1-9 and 8.1-10 for the SN 2 strut test.

8.1.2 Test Results

A summary of strut and support panel testing in the wind tunnel is shown in Table 8.1-1. The leading edge weight flow ΔT ($W_c \Delta T$), the sidewall weight flow ΔT ($W_s \Delta T$), and the gas total temperature for each cycle are shown in Figures 8.1-11 and 8.1-12 for configuration 2, and configuration 1, SN 5, struts, respectively. These parameters are indicative of the peak-heating environments. The corresponding test conditions for configuration 1, SN 6, strut are shown in

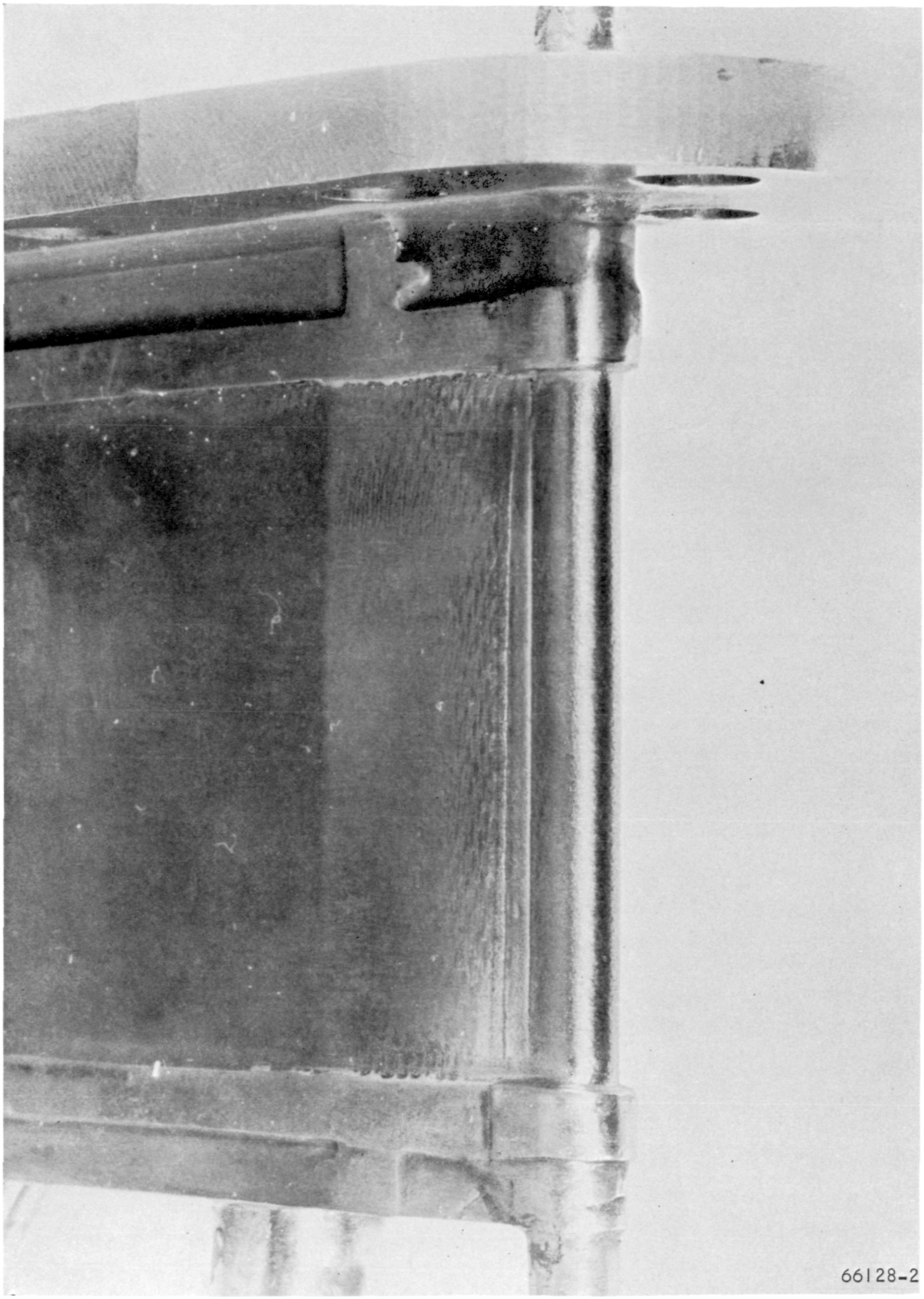

Figure 8.1-1. Strut Configuration No. 1, SN 5 Prior to Thermal Cycling (Coated Leading Edge)

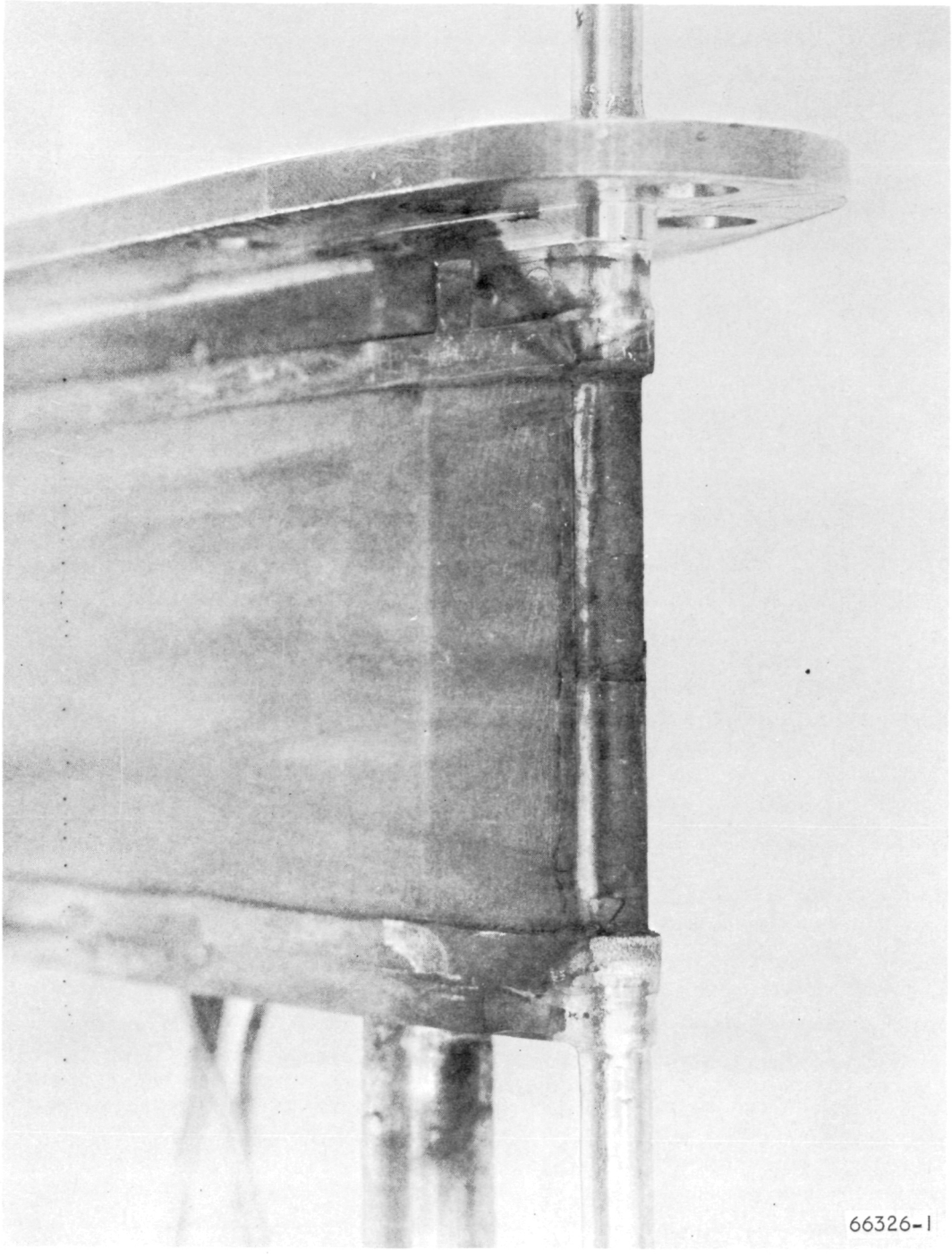

Figure 8.1-2. Strut Configuration No. 1, SN 5 After Thermal Cycle 102 (Coated Leading Edge)

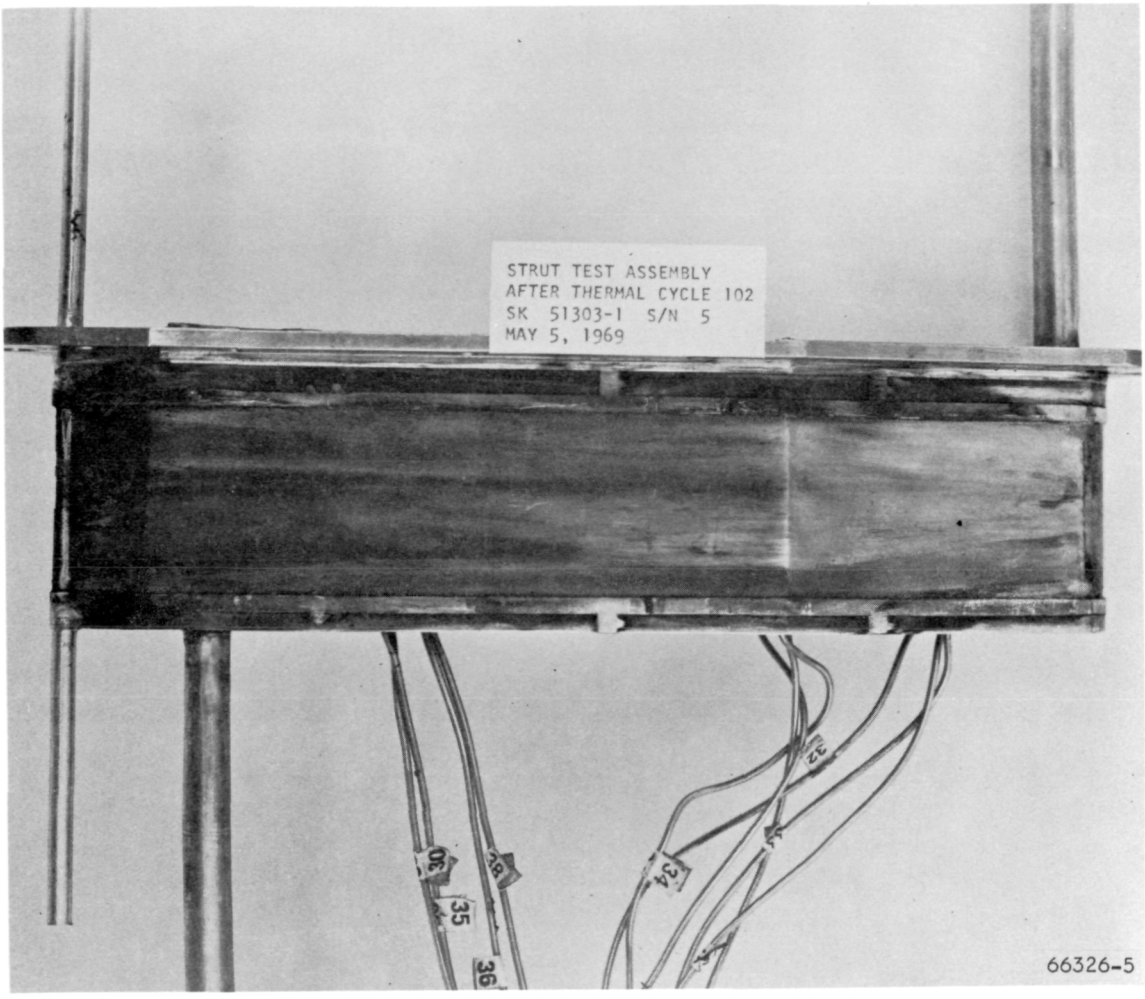

Figure 8.1-3. Strut Configuration No. 1, SN 5 After Thermal Cycle 102

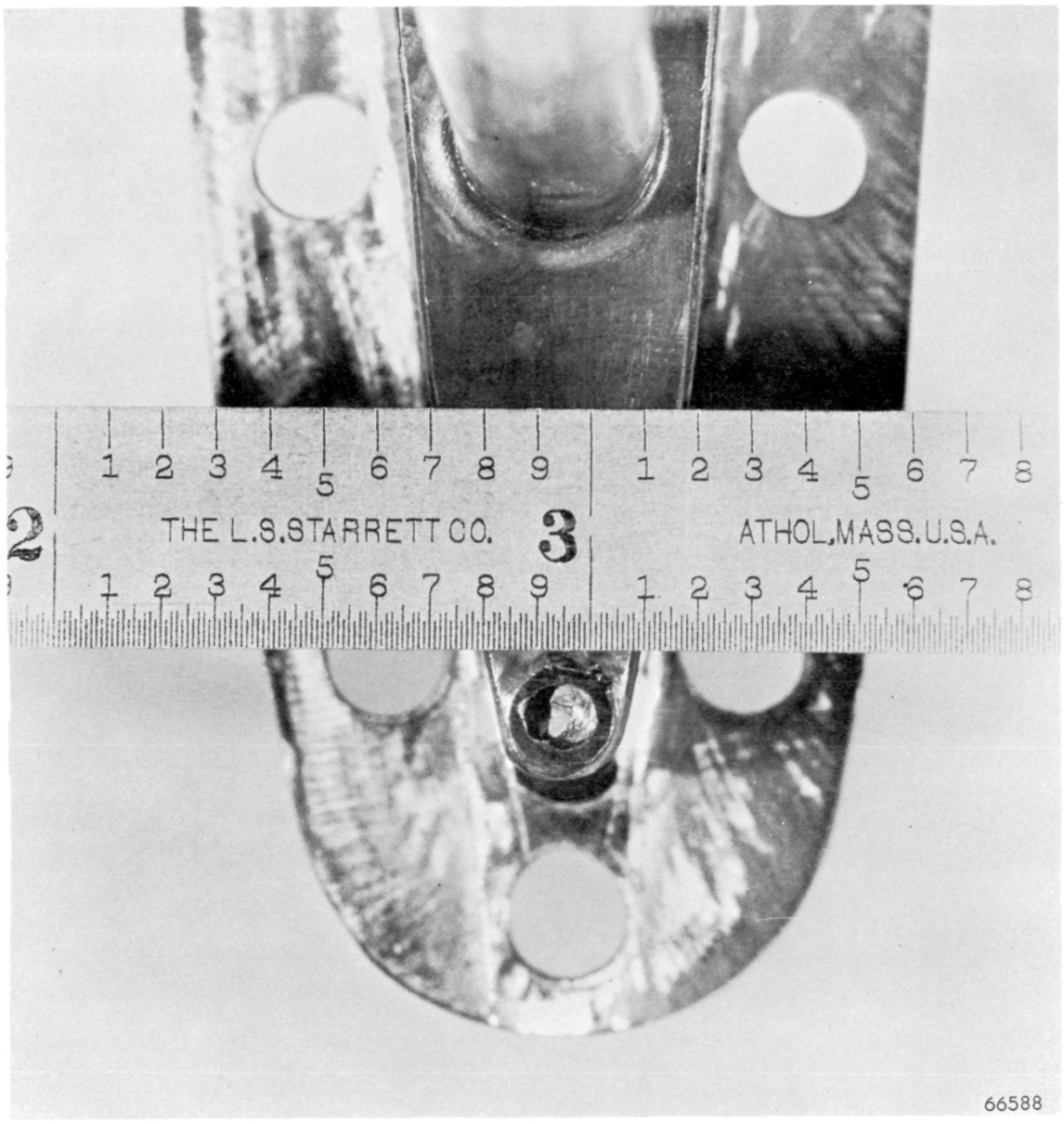

Figure 8.1-4. Strut Configuration No. 1, SN 5 Showing Braze Alloy Plugging in Leading Edge

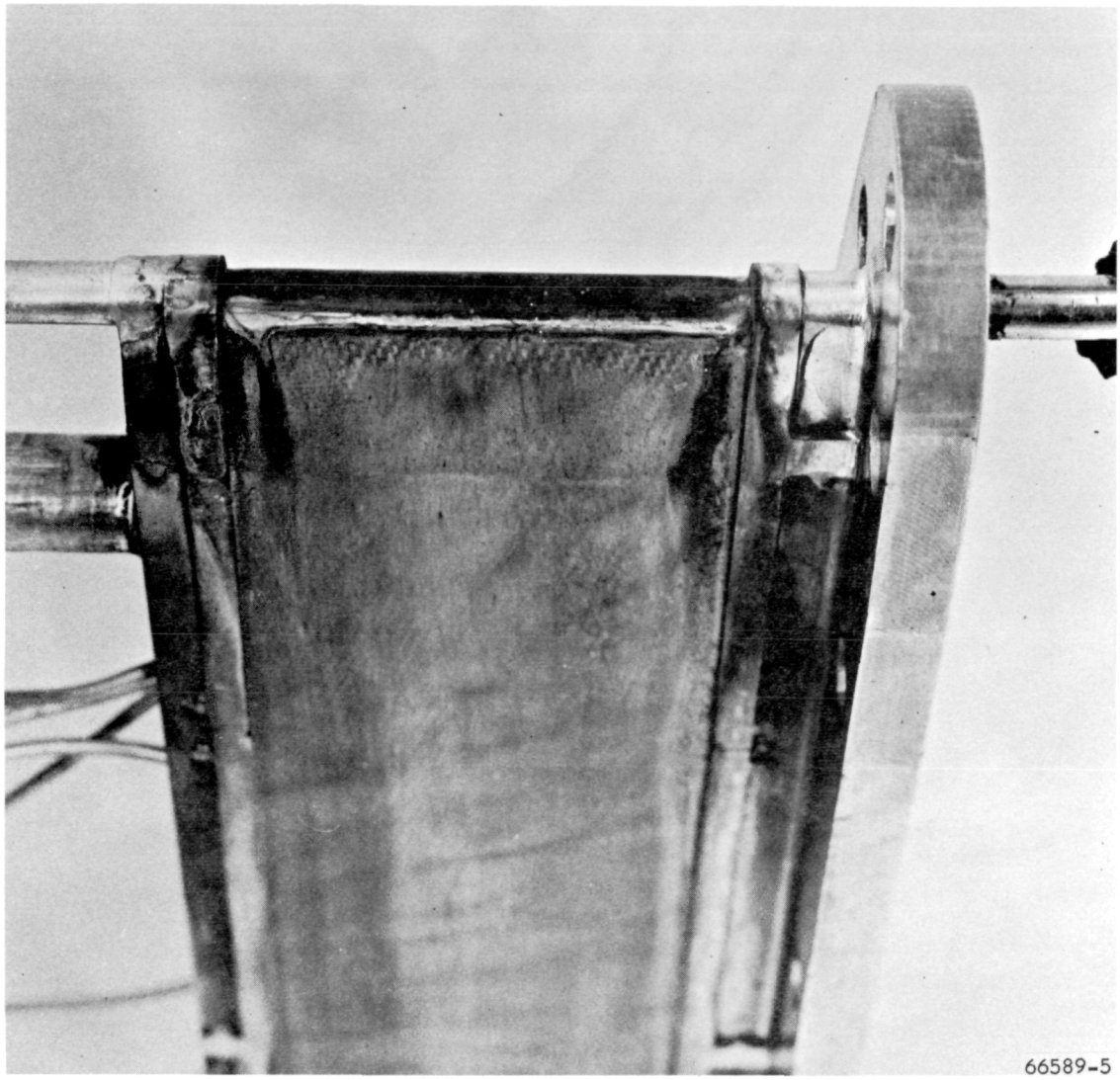

Figure 8.1-5. Strut Configuration No. 2, SN 2 After Thermal Cycle 44

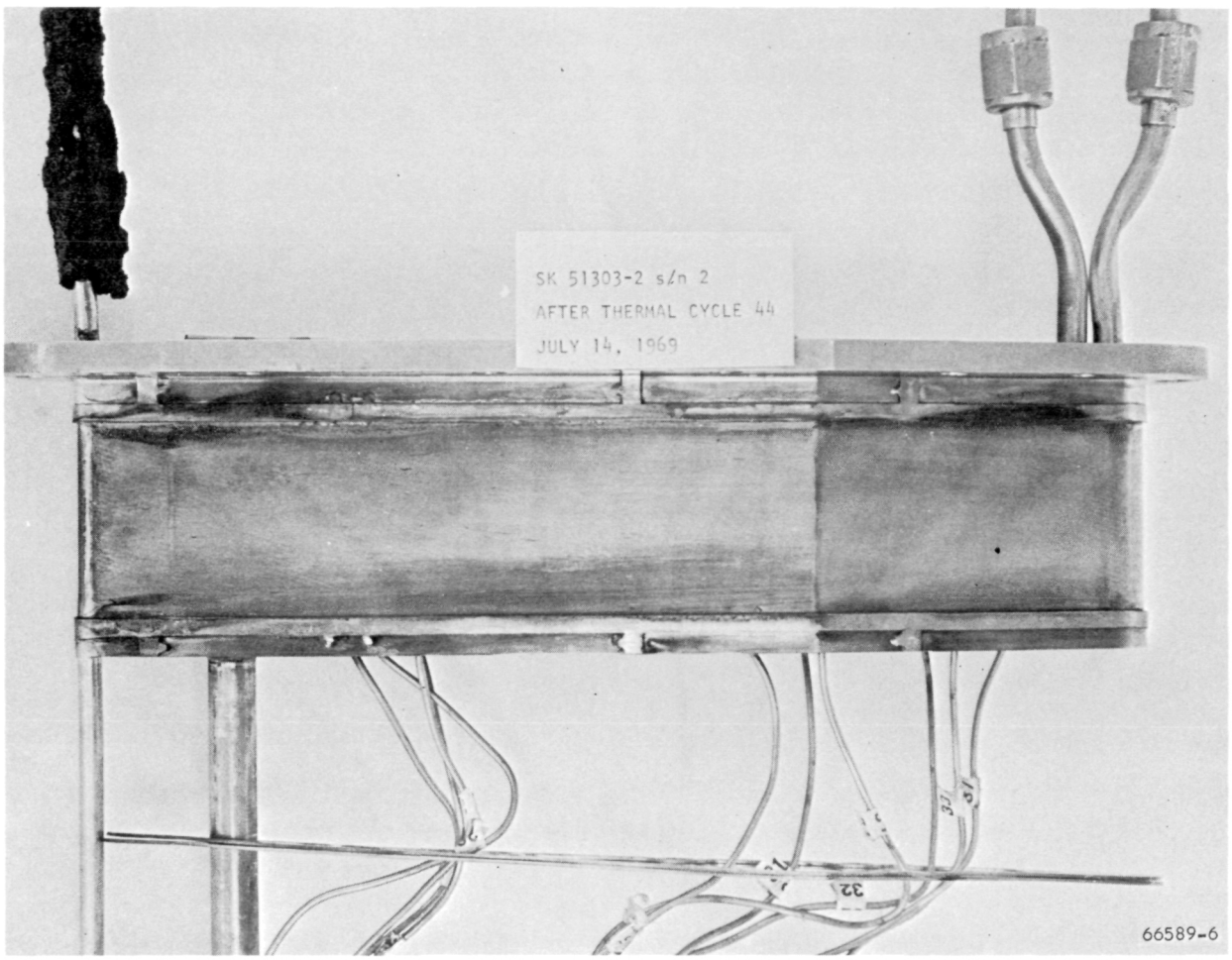

Figure 8.1-6. Strut Configuration No. 2, SN 2 After Thermal Cycle 44

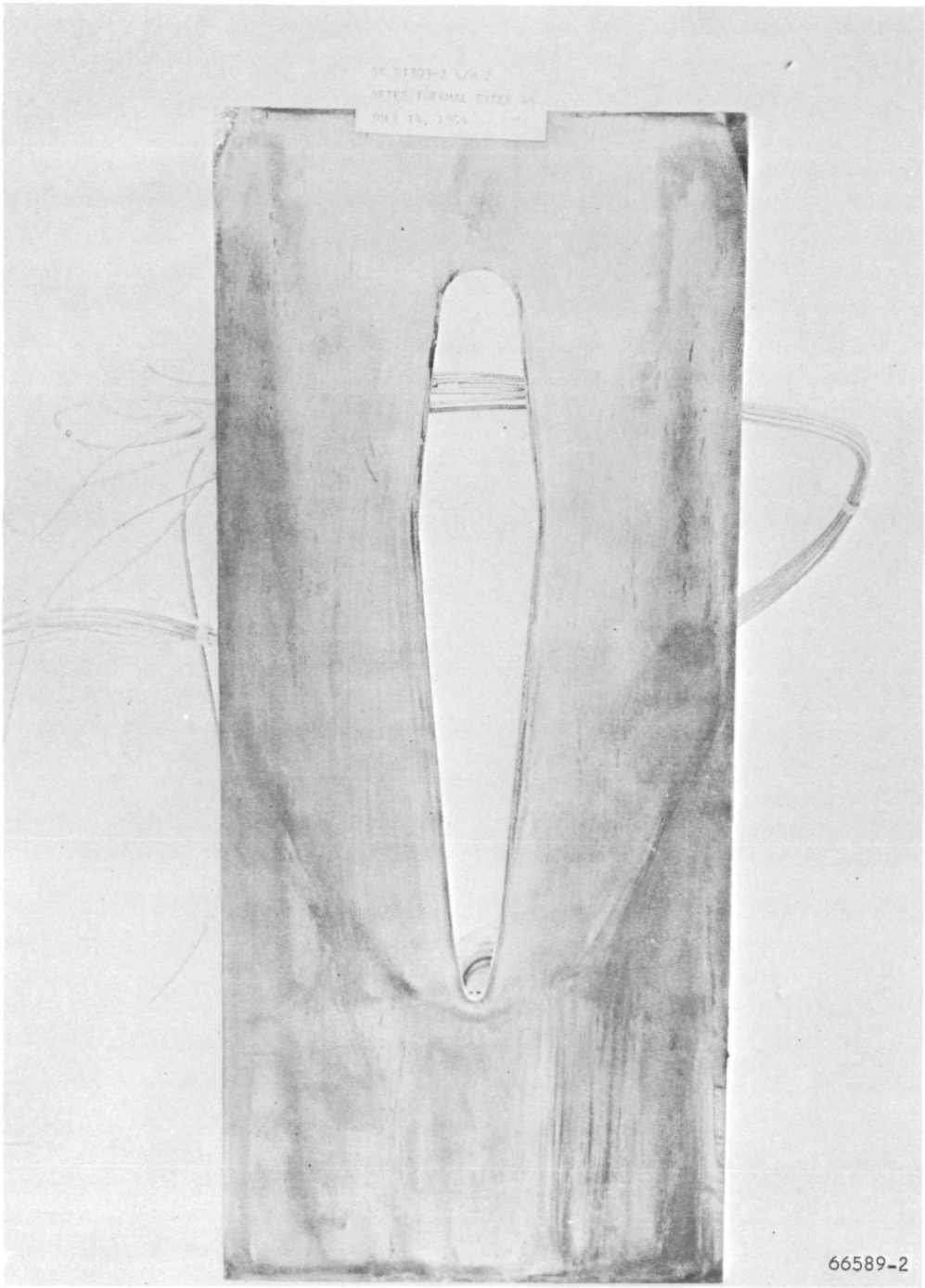

Figure 8.1-7. SK 51509-1 Support Panel After Thermal Cycle 106

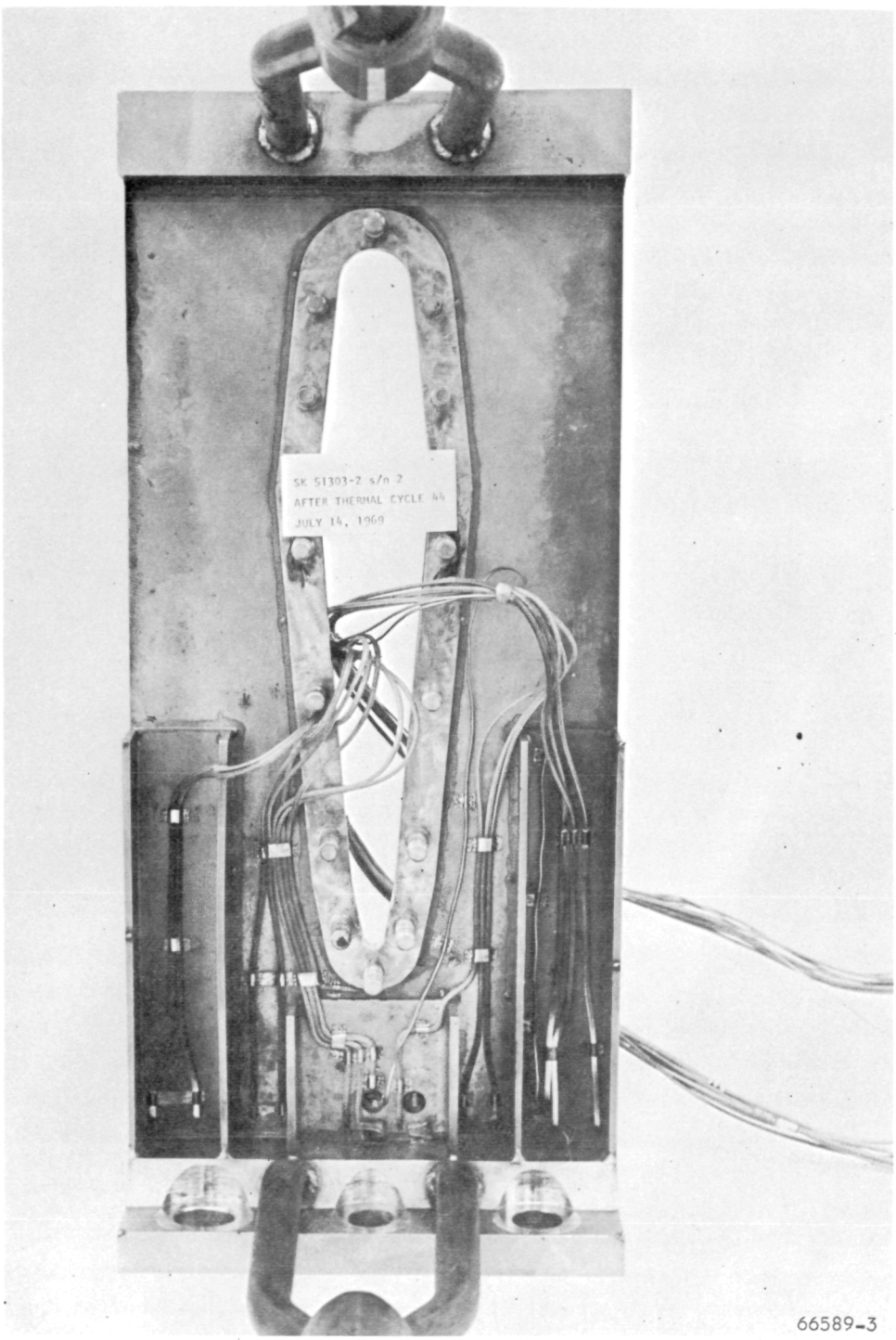

Figure 8.1-8. SK 51509-1 Support Panel After Thermal Cycle 106 Showing Heating Pattern on Edges of Cold Side

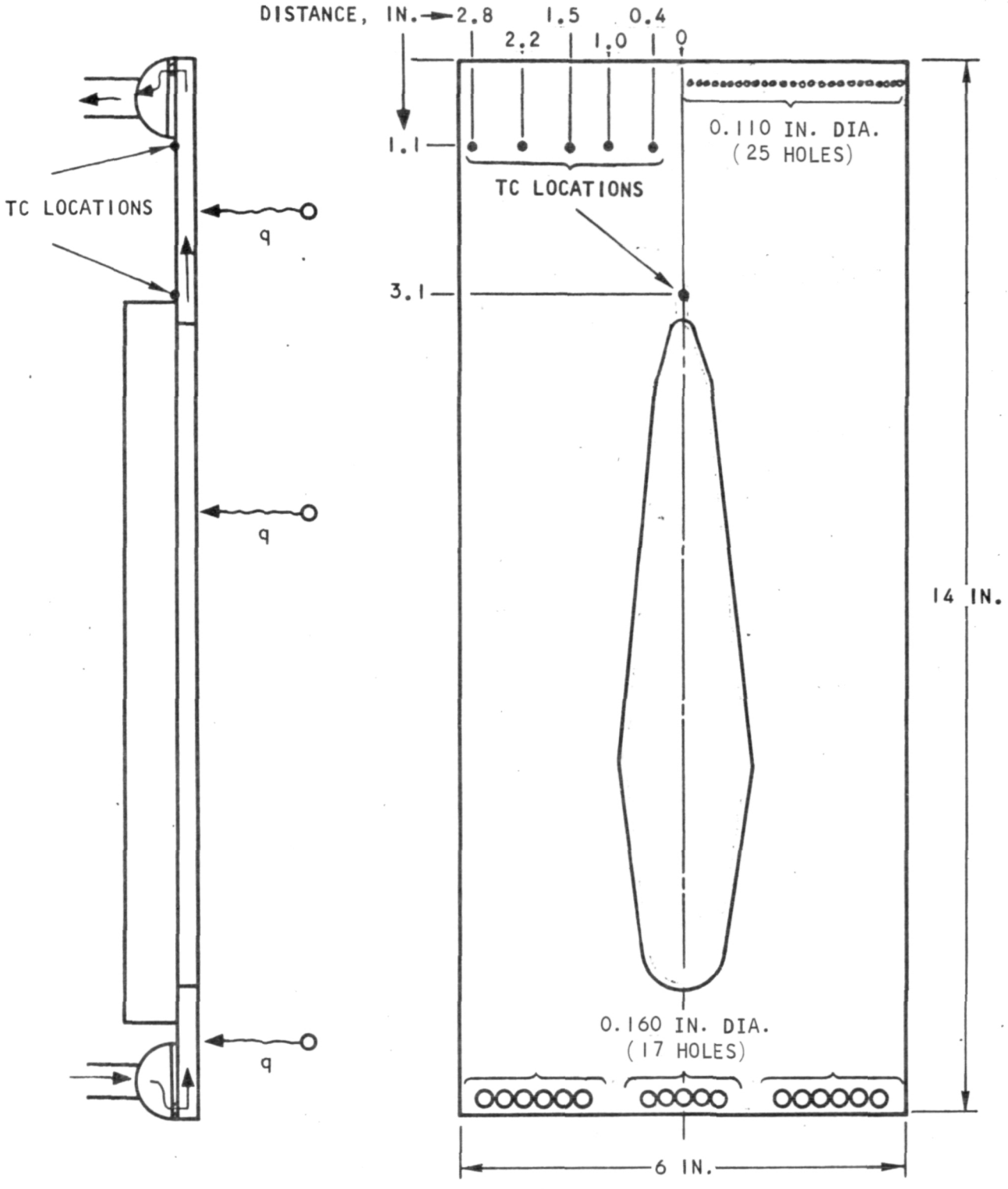

Figure 8.1-9. SK 51322-1 Panel Schematic and Flow Distribution Instrumentation

S-51186

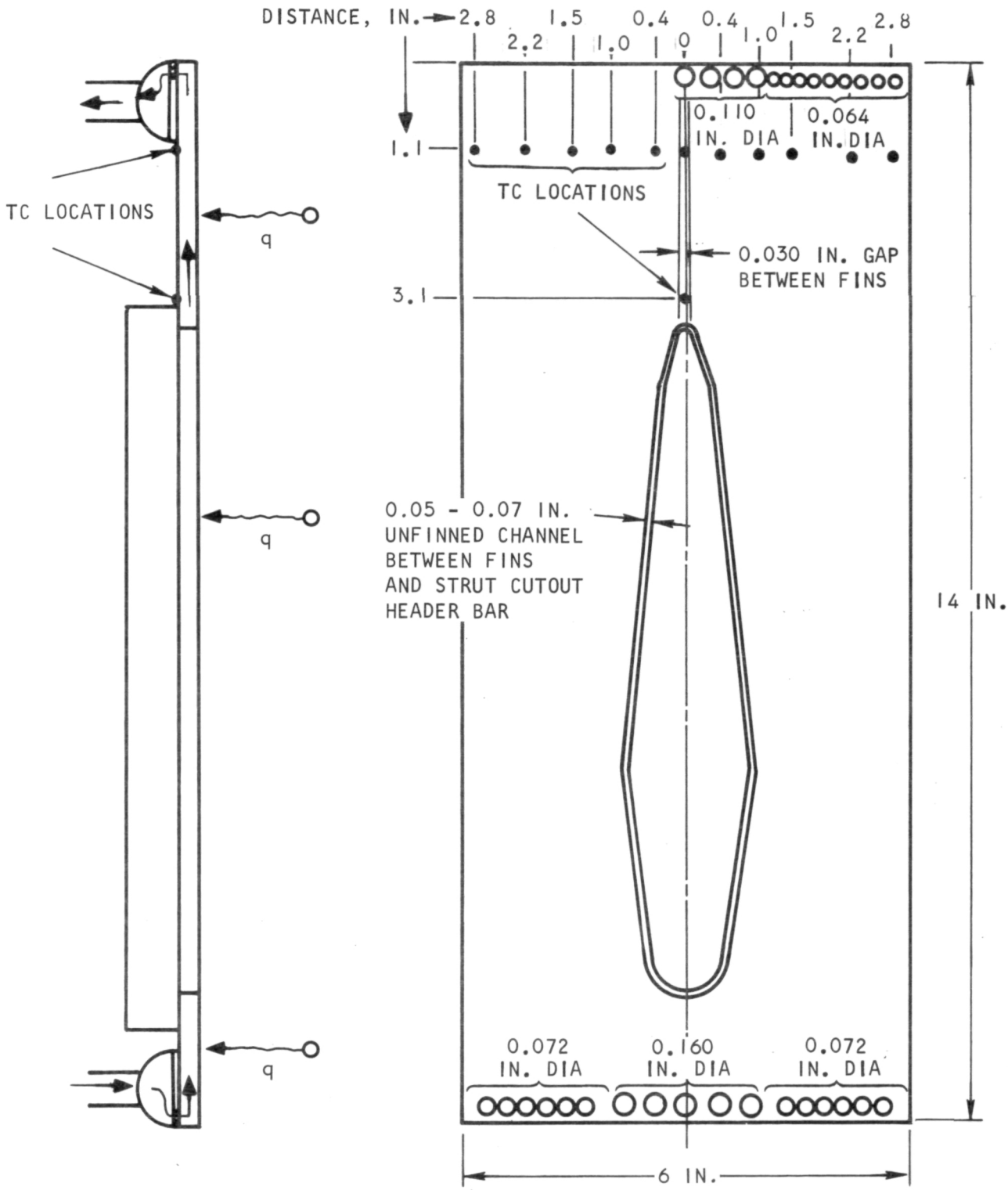

Figure 8.1-10. SK 51509-1 Panel Schematic and Flow Distribution Instrumentation

S-49508

TABLE 8.1-1

SUMMARY OF STRUT AND SUPPORT PANEL TESTING

Type of Test	Hot**** Gas Conditions	Strut Configuration 1			Strut Configur. 2	Support Panels					
		SN 2	SN 5	SN 6	SN 2	-1	-2	-4	-6	-1***	-2***
Thermal Cycling	500-4000°R 270 psia	None	102*	62*	44*	102**	None	62*	None	106*	102** 44*
	500-3700°R 270 psia	None	None	11*	None	None	None	11*	11*	None	None
Steady State	1500-5000°R 180-315 psia	4* 22**	None	14*	1*	4* 22**	4* 22**	14*	14*	1*	1*
Remarks		Leading edge cracking due to accidental loss of coolant	No leaks at 1050 psig proof-pressure test Leading edge coating locally spalled after cycle 48	No leaks at 1050 psig proof-pressure test	No leaks at 1050 psig proof-pressure test	No leaks at 750 psig proof-pressure test	Leak at hot-skin-to-header braze joint	Leak at forward end of strut cut-out at hot-skin-to-header braze joint	Leak at forward end of strut cut-out at hot skin	No leaks at 750 psig proof-pressure test	No leaks at 750 psig proof-pressure test

NOTES:
* Hydrogen-cooled test points
** Water-cooled test points
*** Engine coolant configuration
**** M = 2 upstream of leading edge for all runs

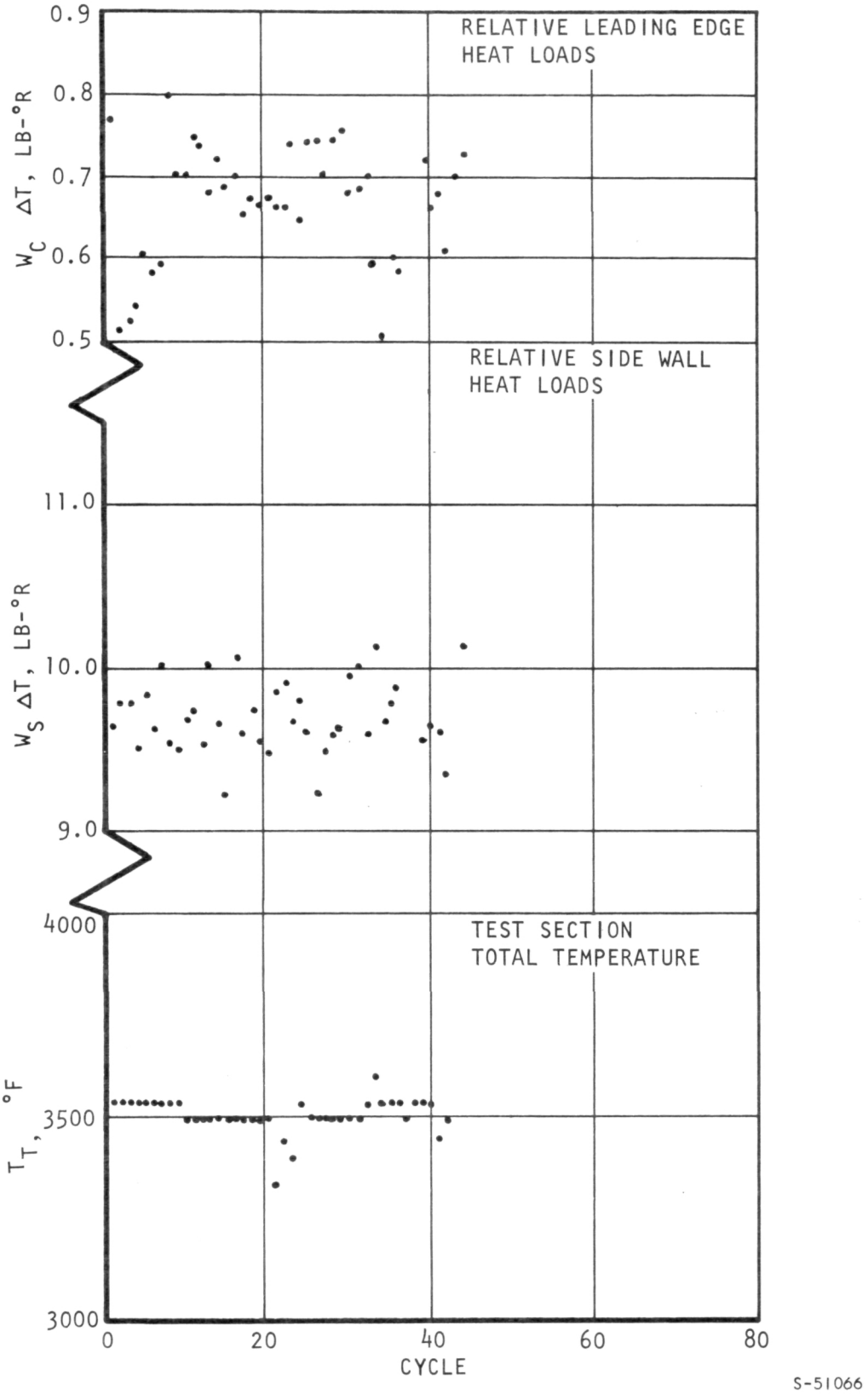

Figure 8.1-11. Configuration 2, SN 2 Strut Thermal Cycle Test Conditions

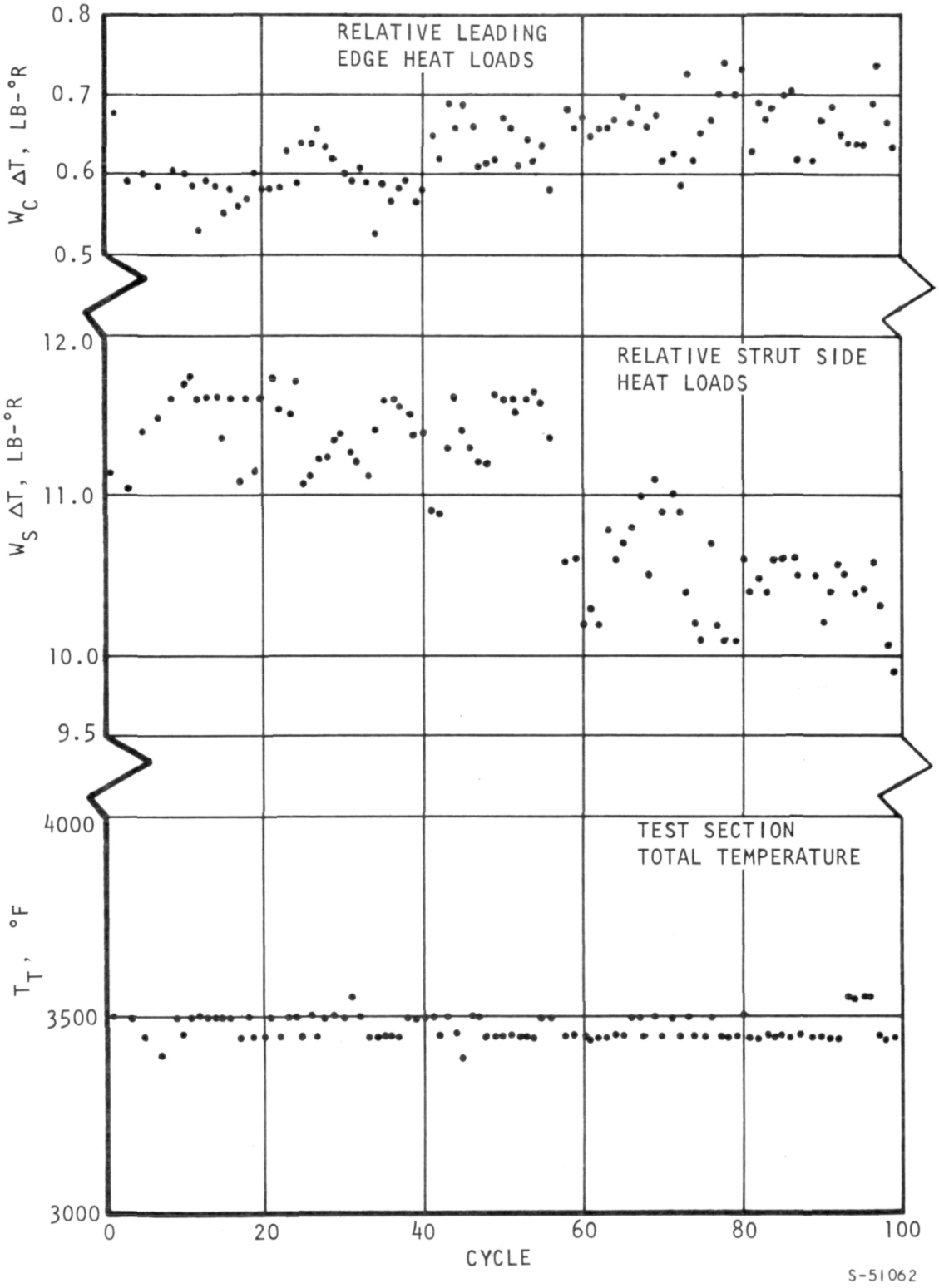

Figure 8.1-12. Configuration 1, SN 5 Strut Thermal Cycle Test Conditions

Figure 8.2-6 of Reference 5-1. Hydrogen at room temperature, which has almost constant specific heat, was used to cool the side wall. Therefore, the measured values provide a direct indication of the test section heating conditions. The $W_s \Delta T$ for the SN 2 test was 9.7 ±0.4 before cycle 57 and was 10.5 ±0.5 after cycle 58. The strut leading edge wall temperature increases with the hot gas total temperature, which increases with the burner hydrogen flow rates. The strut wall temperature vs the burner hydrogen flow rates are shown in Figures 8.1-13, 8.1-14, and 8.1-15, for struts SN 2, SN 5, and SN 6, respectively. The coolant flows were assumed constant at the average test value of 0.045 lb/sec for SN 2 and SN 6 struts, and 0.027 lb/sec for the SN 5 strut.

The stagnation line wall temperature, the hot gas total temperature, and the coolant inlet and exit temperatures for a typical thermal cycle are shown in Figures 8.1-16a and 8.1-16b for struts SN 2 and SN 5, respectively. Shown in Figure 8.1-16b also, is the peak temperature of the strut (excluding the Cr_2C_3 coating) which occurs at a location approximately 30 deg away from the stagnation line. The peak wall temperatures vs the cycle are shown in Figure 8.1-17. The higher wall temperature for SN 5 was the result of the blockage occurred at the leading edge coolant exit. The SN 5 strut, therefore, is not a representative finned model. These test data for this strut are, nevertheless, significant as indicative of conditions at which the strut will survive. As can be observed from Figure 8.1-4, view looking at the exit plane, the right hand passage is completely blocked. However, coolant can still flow from one side of the fin to the opposite side of the fin through the 0.015-in. (estimated) gap between the free edge of the fin and the duct wall. The estimated flow rate in the plugged side was 14 percent of the total leading edge coolant flow, computed based on a choked flow through a gap of 0.015- by 0.25-in. height with a coefficient of discharge of 0.8. The selection of 0.25-in. gap height was made because the region 1/4-in. above the exit plane is through to be the most severe heating region. The coolant in the plugged side increases with increasing distance from the exit plane. The leading edge isotherms for typical peak heating conditions are shown in Figures 8.1-18, 8.1-19, and 8.1-20, for struts SN 2, SN 5, and SN 6 respectively. The latter is a machine plot.

The local heat flux distributions are shown in Figures 8.1-21a, b, and c for struts SN 6, SN 2, and SN 5, respectively. The local heat flux was computed with Lees' distribution theory, a turbulence factor K of 2.5 and a hot gas total temperature of 3800°R for all three struts. The conditions are for cycle 3 of the SN 6 strut. For this cycle, the graphical average heat flux, Figure 8.1-21a, is 625 Btu/ft^2-sec, which is within 9 percent of the measured value of 680 Btu/ft^2-sec.

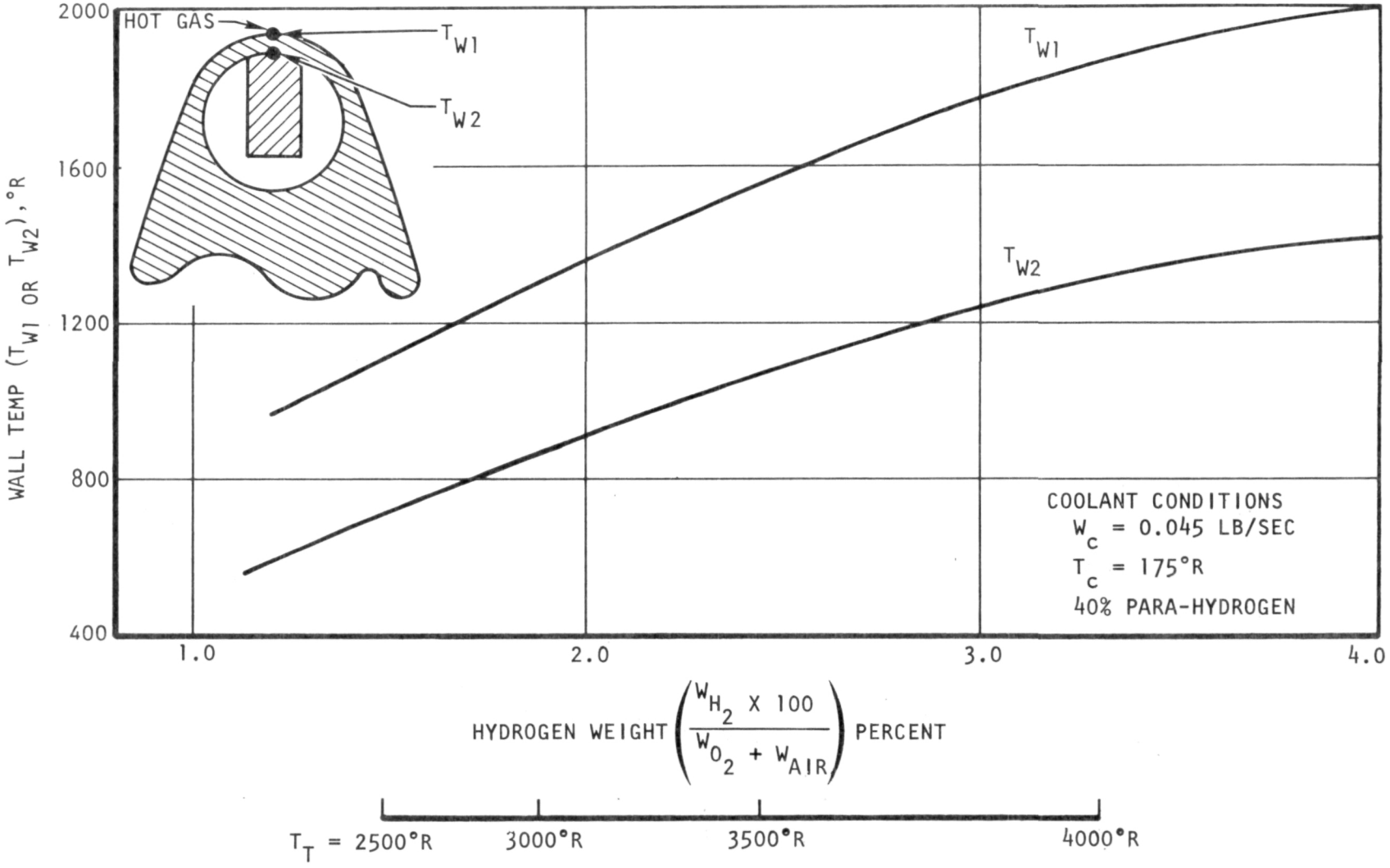

Figure 8.1-13. Configuration 2, SN 2 Strut Leading Edge Temperature vs Burner Hydrogen Flow Rates

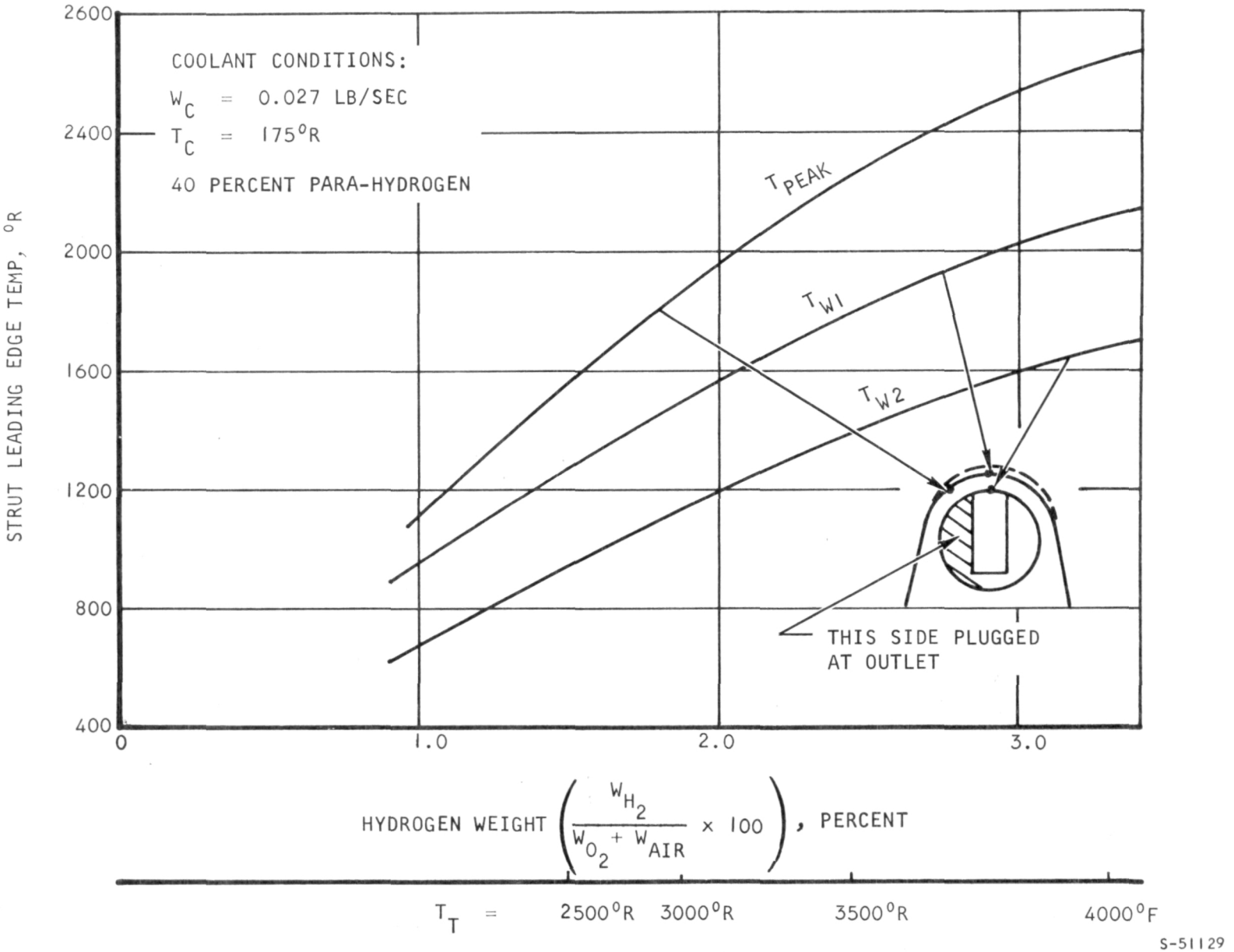

Figure 8.1-14. Configuration 1, SN 5 Strut Leading Edge Temperature vs Burner Hydrogen Flow Rates

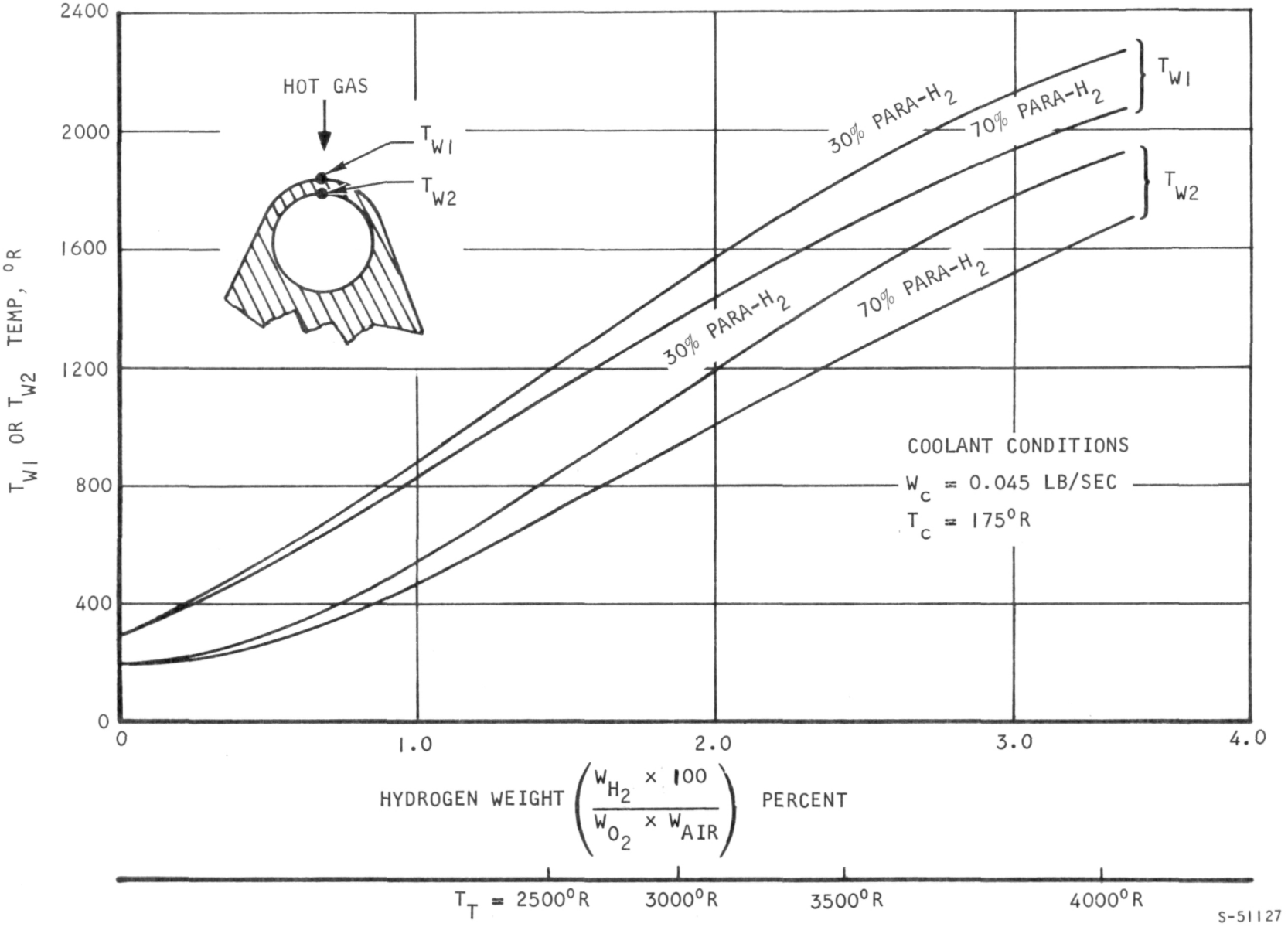

Figure 8.1-15. Configuration 1, SN 6 Strut Leading Edge Temperature vs Burner Hydrogen Flow Rate

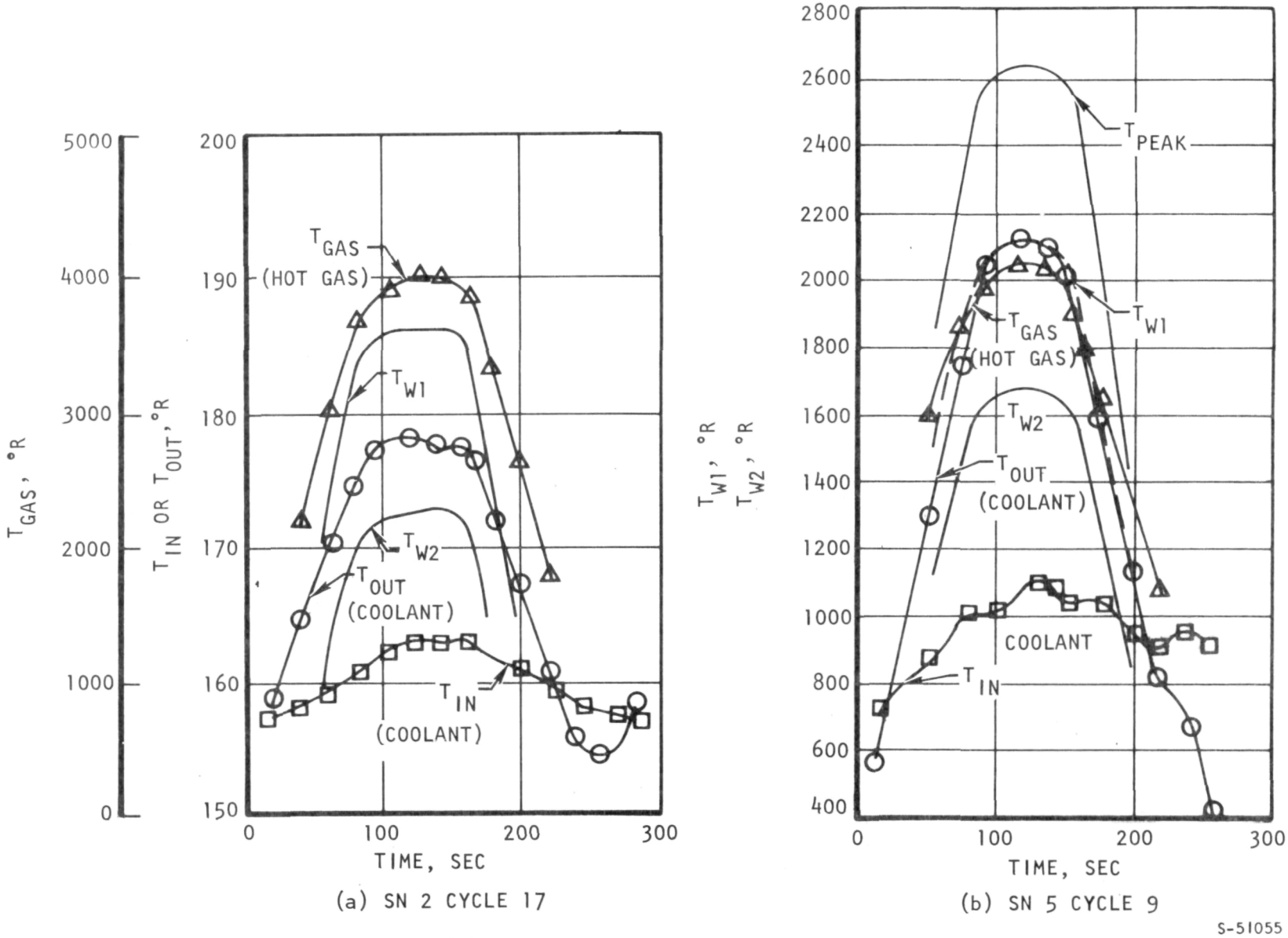

Figure 8.1-16. Typical Thermal Cycle Temperatures

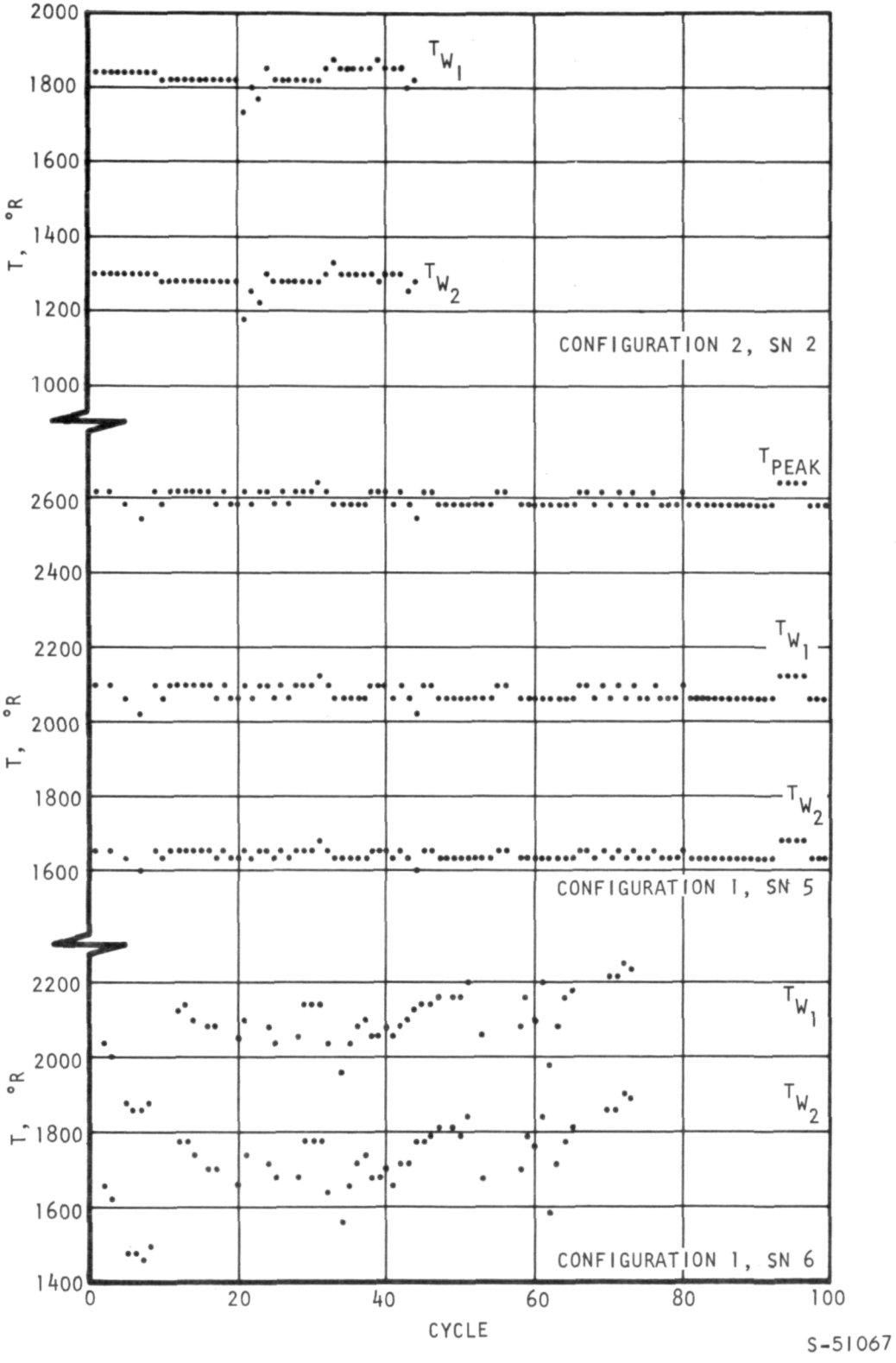

Figure 8.1-17. Wall Temperature vs Cycle

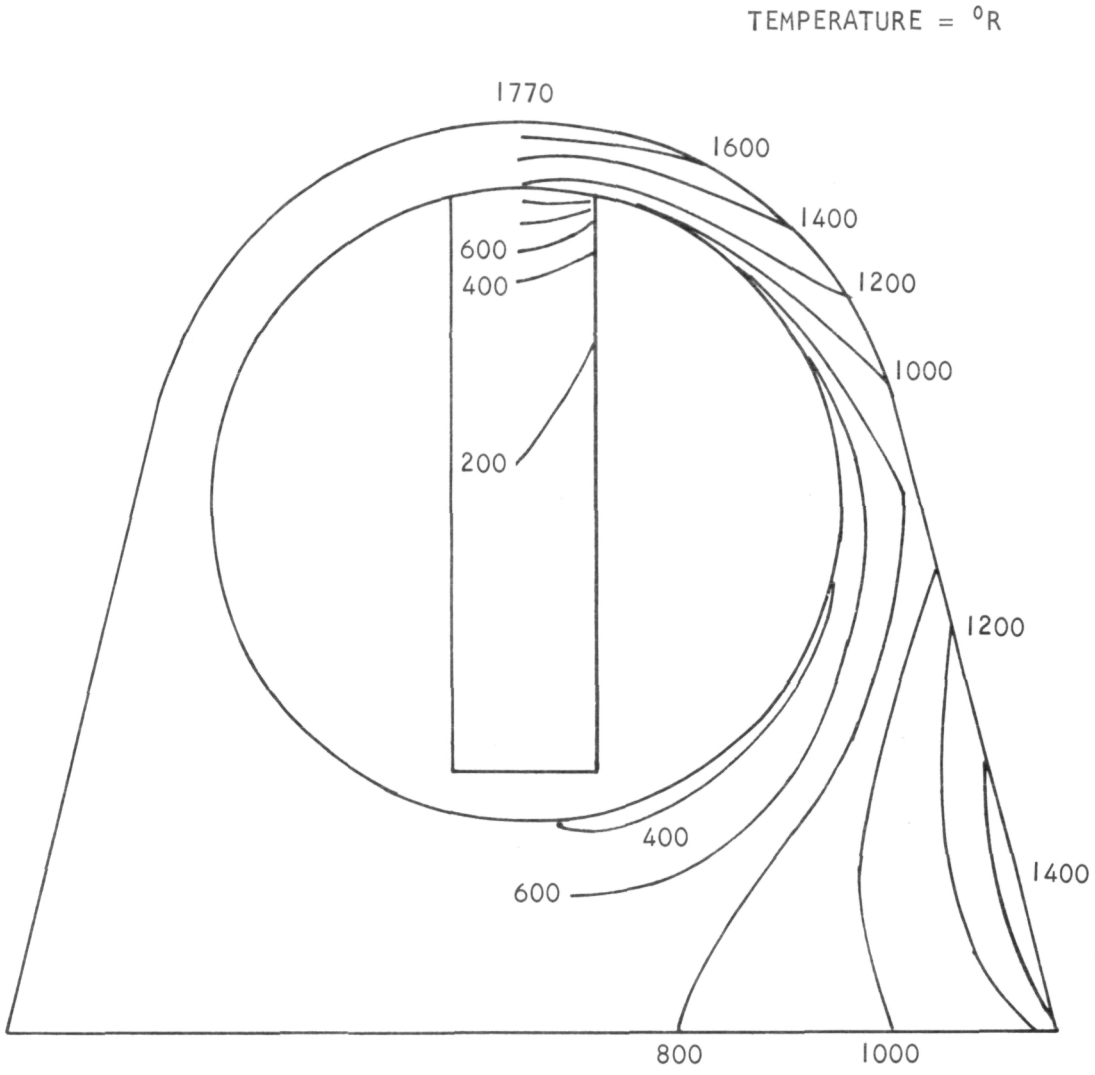

HOT GAS SIDE

$T_T = 3800^0R$

$h_{stag} = 0.69 \frac{BTU}{FT^2\text{-}SEC\text{-}^0R}$

COOLANT CONDITIONS

$W_c = 0.045$ LB/SEC

$T_c = 175^0R$

40 PERCENT PARA-HYDROGEN

S-51123

Figure 8.1-18. Configuration 2, SN 2 Strut Isotherms

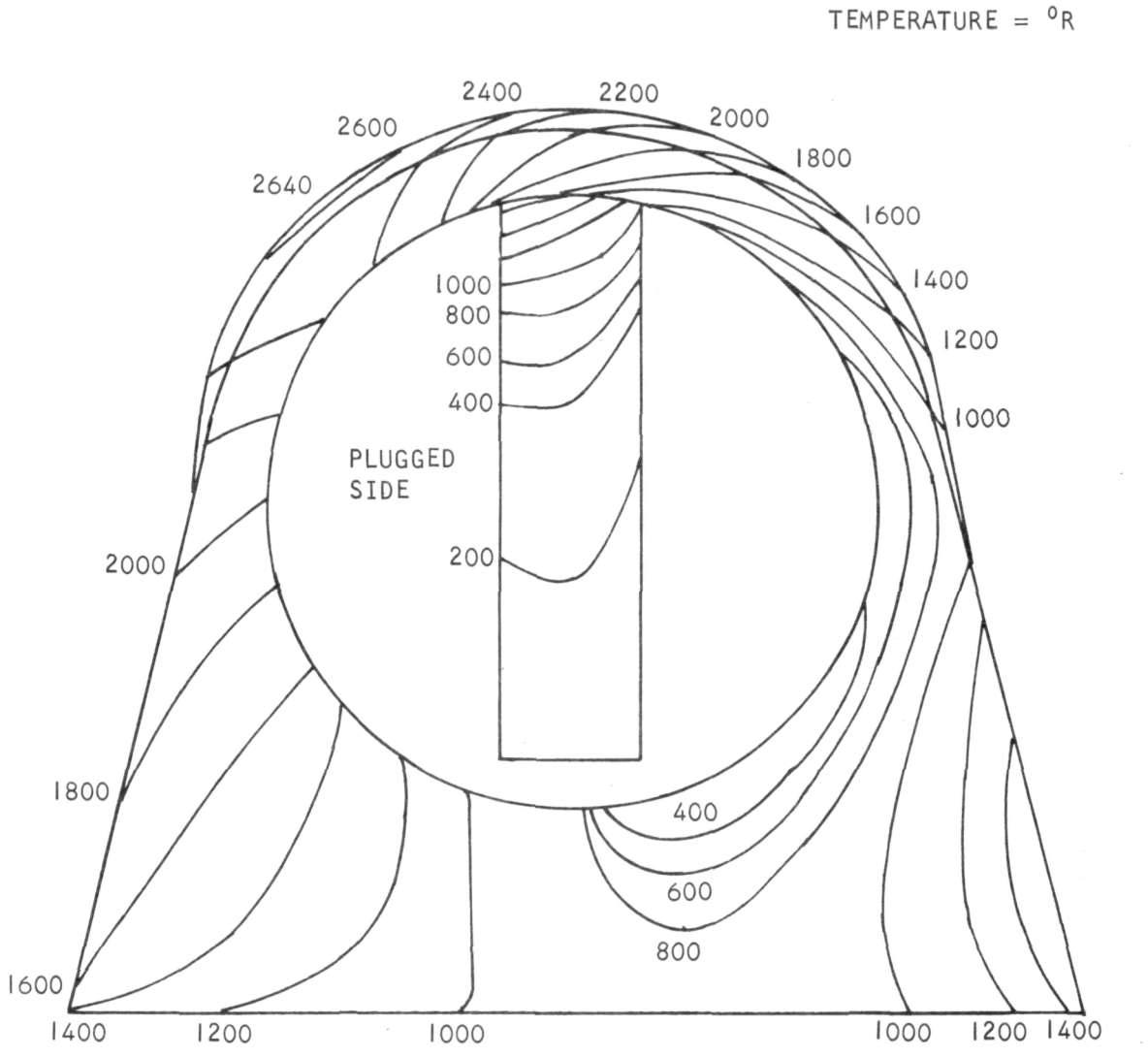

HOT GAS SIDE

$T_T = 3800^0R$

$h_{stag} = 0.69 \frac{BTU}{FT^2\text{-}SEC\text{-}^0R}$

COOLANT CONDITIONS

$W_c = 0.027$ LB/SEC

$T_c = 175^0R$

40 PERCENT PARA-HYDROGEN

Figure 8.1-19. Configuration 1, SN 5 Strut Isotherms

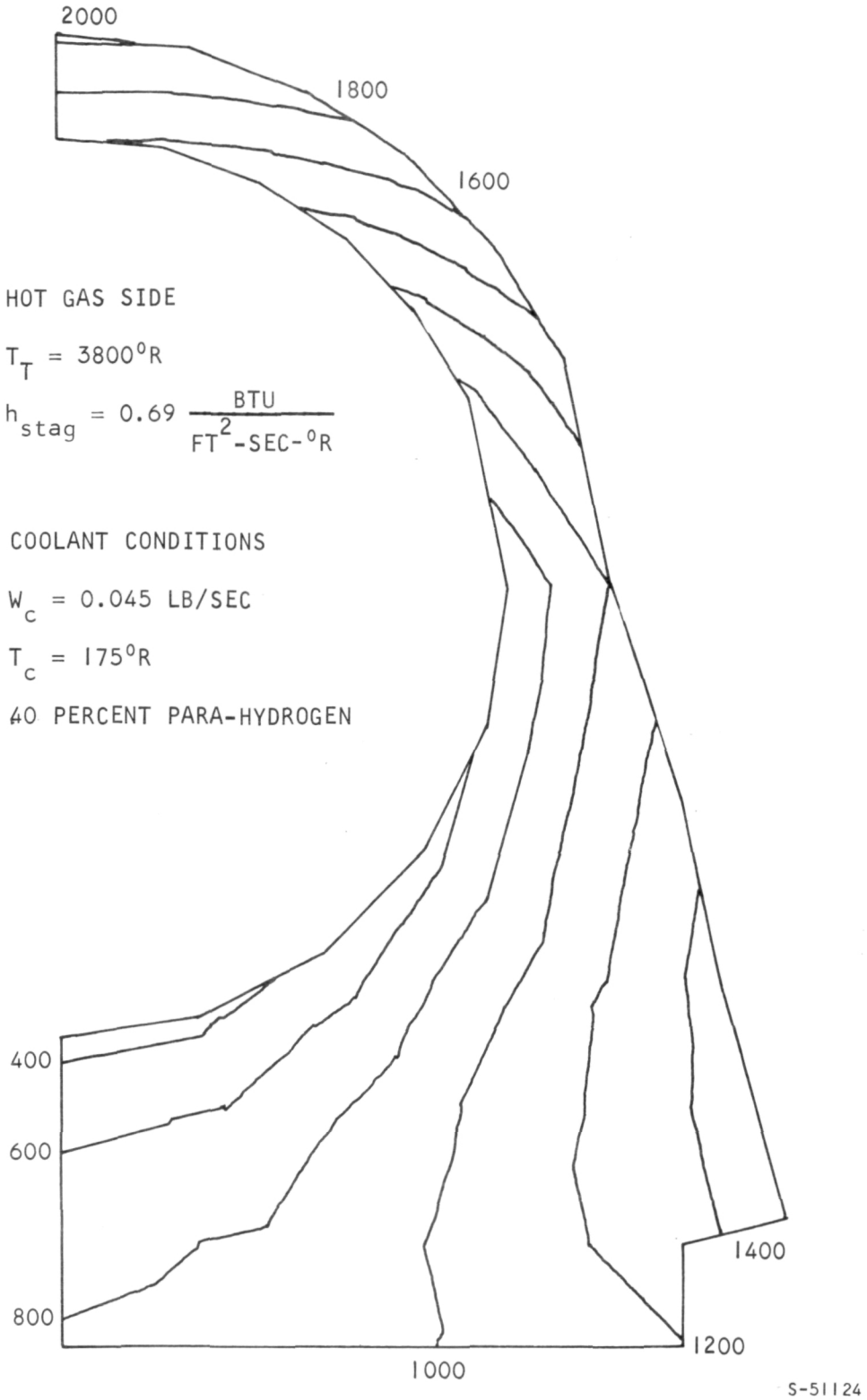

Figure 8.1-20. Configuration 1, SN 6 Strut Isotherms

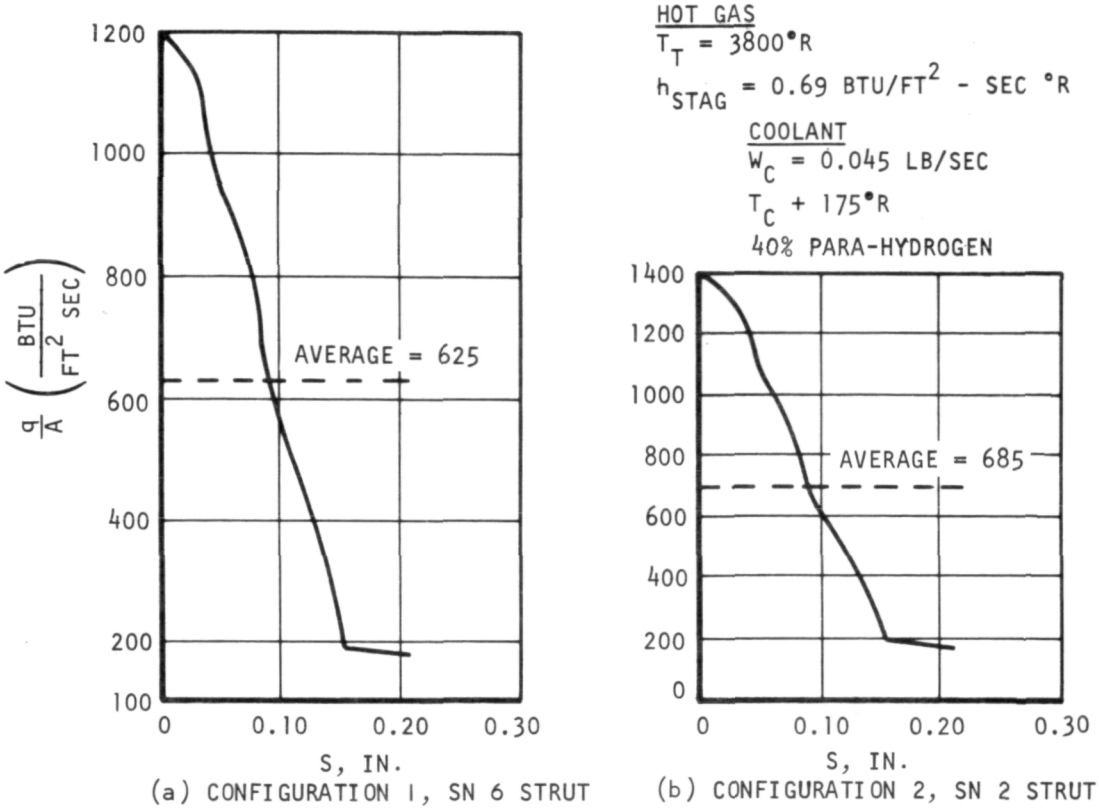

(a) CONFIGURATION 1, SN 6 STRUT

(b) CONFIGURATION 2, SN 2 STRUT

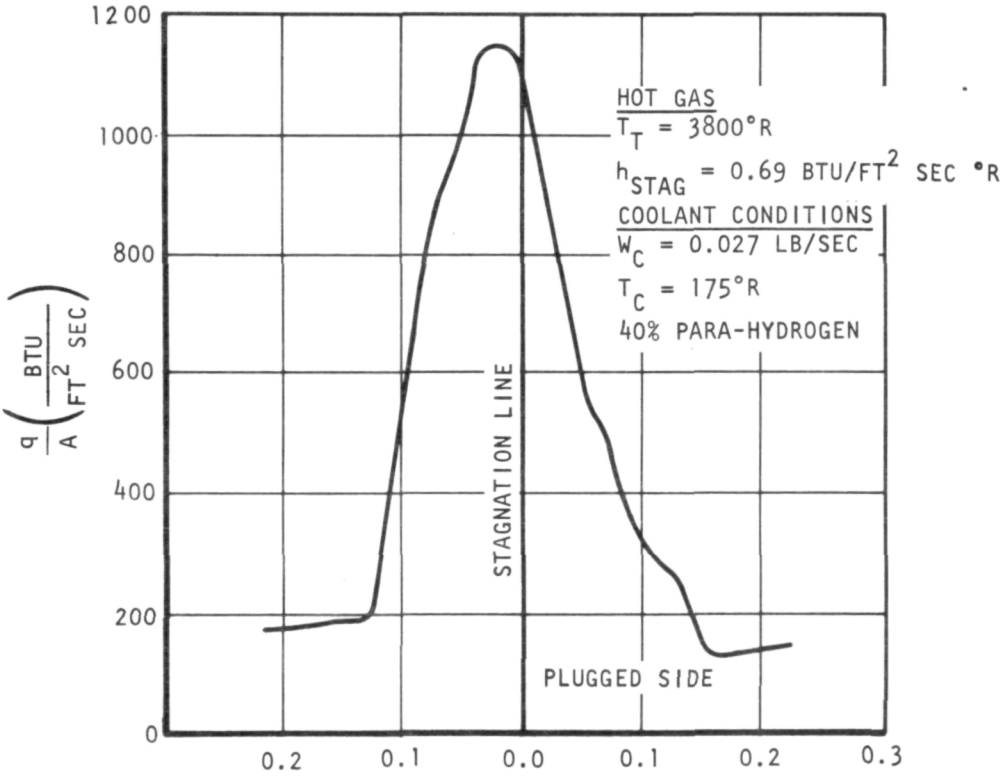

(c) CONFIGURATION 1, SN 5 STRUT

S-51073

Figure 8.1-21. Heat Flux Distribution

8.1.2.1 Heat Transfer

The procedures for strut test data reduction and correlation have been described in Reference 8-1, Section 8.2, for struts without a fin in the leading edge coolant passage. This section presents a refinement in SN 6 data reduction and discusses the data reduction with a fin in the leading edge, struts SN 2, configuration 2, and SN 5, configuration 1. For the SN 6 strut, the coefficients to account for the tangential conduction effects have been revised to agree with the computer results:

$$T_{W1} - T_{W2} = \frac{B_1 \left(\frac{q}{A_1}\right) r_1 \ln \frac{r_1}{r_2}}{k} \qquad (8.1\text{-}1)$$

$$T_{W2} - T_B = \frac{B_2 \left(\frac{q}{A_1}\right)}{h_c} \qquad (8.1\text{-}2)$$

B_1 and B_2, which are given as 0.84 and 1.23, respectively in Reference 8-1 are revised to 0.92 and 1.05, respectively.

For struts with a fin in the leading edge passage, Equation (8.1-2) is not applicable. In order to provide for a technique for hand computation, the leading edge fin geometry is simplified by treating only the shaped area of Figure 8.1-22a. The equivalent system is shown as Figure 8.1-22b. The stagnation line heat flux computed with this model is adjusted to match that of the computer results. The overall heat transfer (U) for Figure 8.1-22b is computed as follows:

$$\frac{1}{U} = \frac{1}{h_o} + \frac{a}{\frac{A_w}{A_1} k} + \frac{1}{\eta_2 \frac{A_t}{A_1} h_c} \qquad (8.1\text{-}3)$$

$$\eta_2 = 1 - \frac{A_f}{A_t}(1 - \eta_f) \qquad (8.1\text{-}4)$$

$$\eta_f = \frac{1}{\ell} \sqrt{\frac{k\delta}{2h}} \qquad (8.1\text{-}5)$$

$$\frac{q}{A_1} = B_3 U (T_T - T_c) \qquad (8.1\text{-}6)$$

where B_3 is 0.945 from computer results.

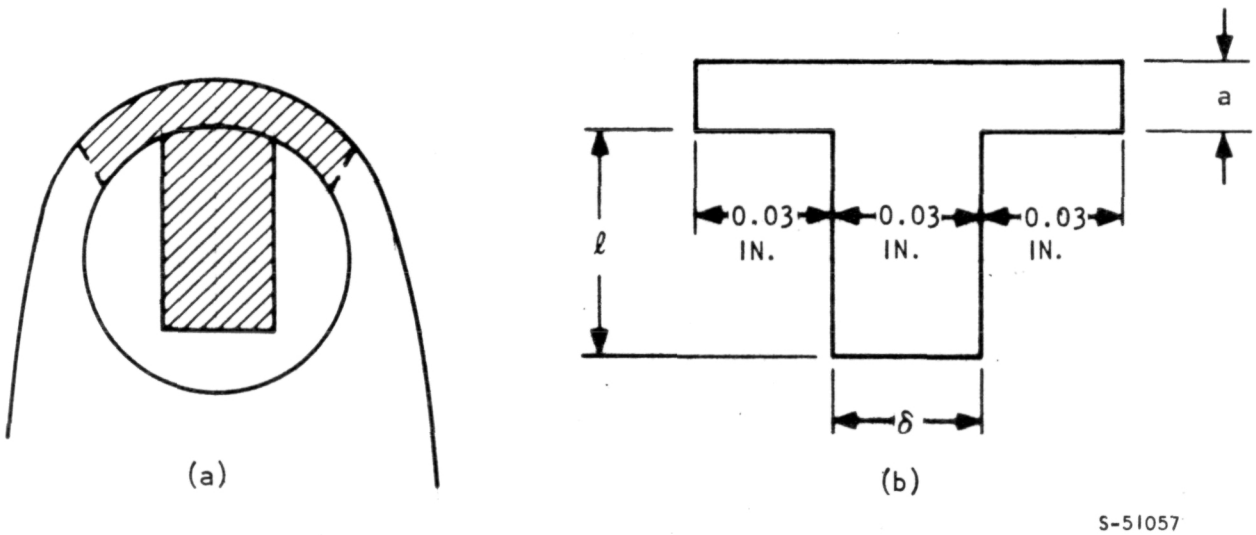

Figure 8.1-22. Simplified Heat Transfer Model for Finned Leading Edge Coolant Passage

This page intentionally left blank for pagination purposes

The leading edge peak temperature for the SN 2, configuration 2, strut is given by:

$$T_{WI} = T_T - \frac{B_3 U}{h_o} (T_T - T_c) \qquad (8.1\text{-}7)$$

$$= T_T - \frac{0.945\,(T_T - T_c)}{1 + \frac{a\,h_o}{\frac{A_w}{A_I} k} + \frac{h_o}{\eta_2 \frac{A_i}{A_I} h_c}}$$

Equations (8.1-6) and (8.1-7) are solved and the results are plotted in Figure 8.1-23 as the stagnation line wall temperature vs the coolant heat loads. The external effective heat transfer area is 0.0041 ft^2. The heat loads shown in Figure 8.1-23 have been raised by 17 percent to account for heating in the strut-support panel gap and heat exchange with the side wall coolant flow.

Properties corresponding to high para-hydrogen concentration were used for all previously reported results due to an incorrect hydrogen calibration of the gas chromatograph. The revised hydrogen compositions for most runs are presented in Figure 8.1-24. The general relation between the para-hydrogen concentration and tank time is shown in Figure 8.1-25. Details of the gas chromatograph measurements are given in Section 8.1.2.2.

The error in heat flux, and the resulting experimental K factor due to erroneous hydrogen composition are illustrated by the SN 6 strut cycling data in Table 8.1-2. For these cycle tests, the calculation assumed the hydrogen was 100 percent para. From Figure 8.1-23 the correct values should have been 33 percent and 42 percent for cycles 3 and 9, respectively.

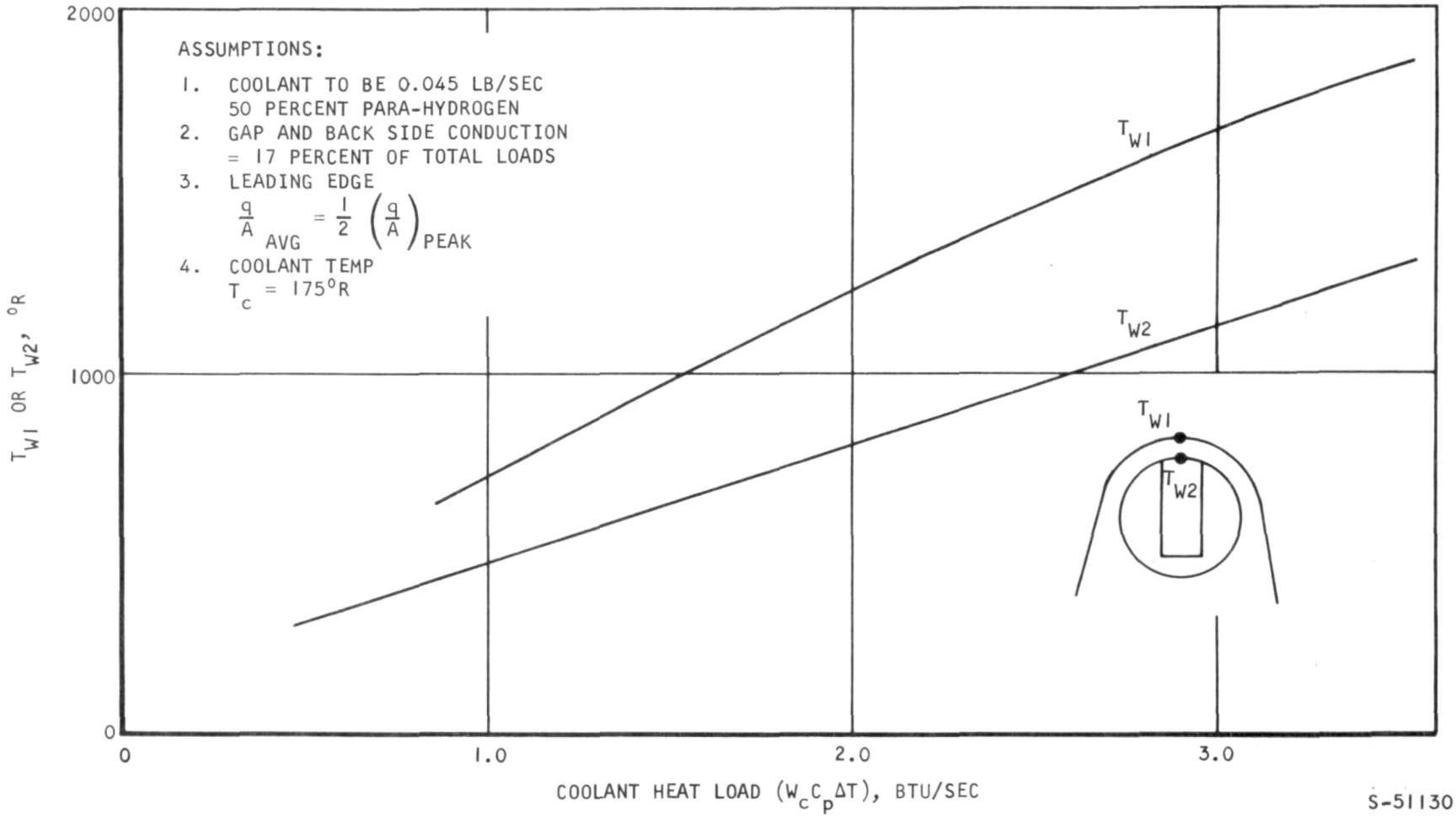

Figure 8.1-23. Configuration 2, SN 2 Strut Wall Temperature vs Heat Load

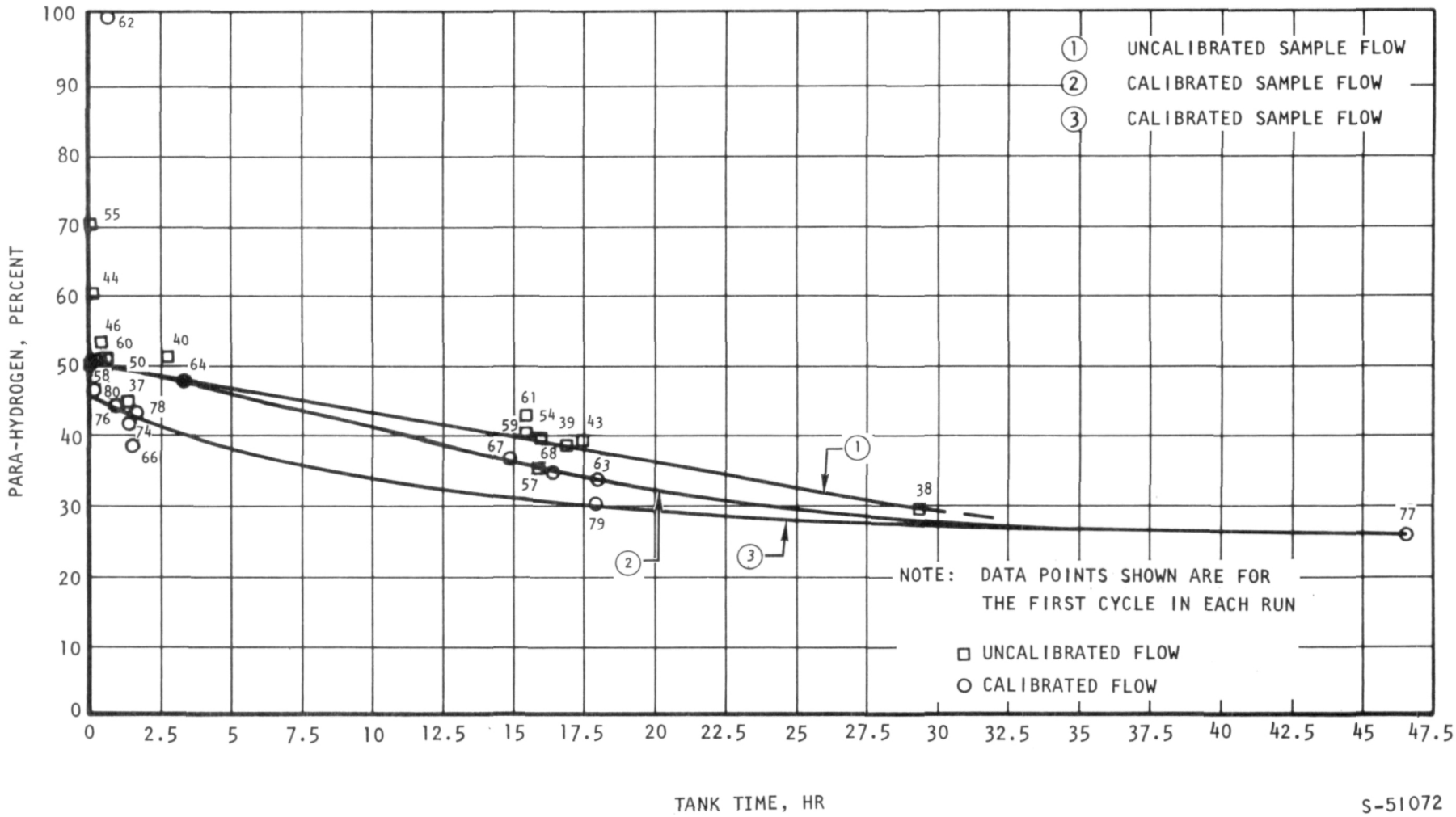

Figure 8.1-24. Para-Hydrogen History

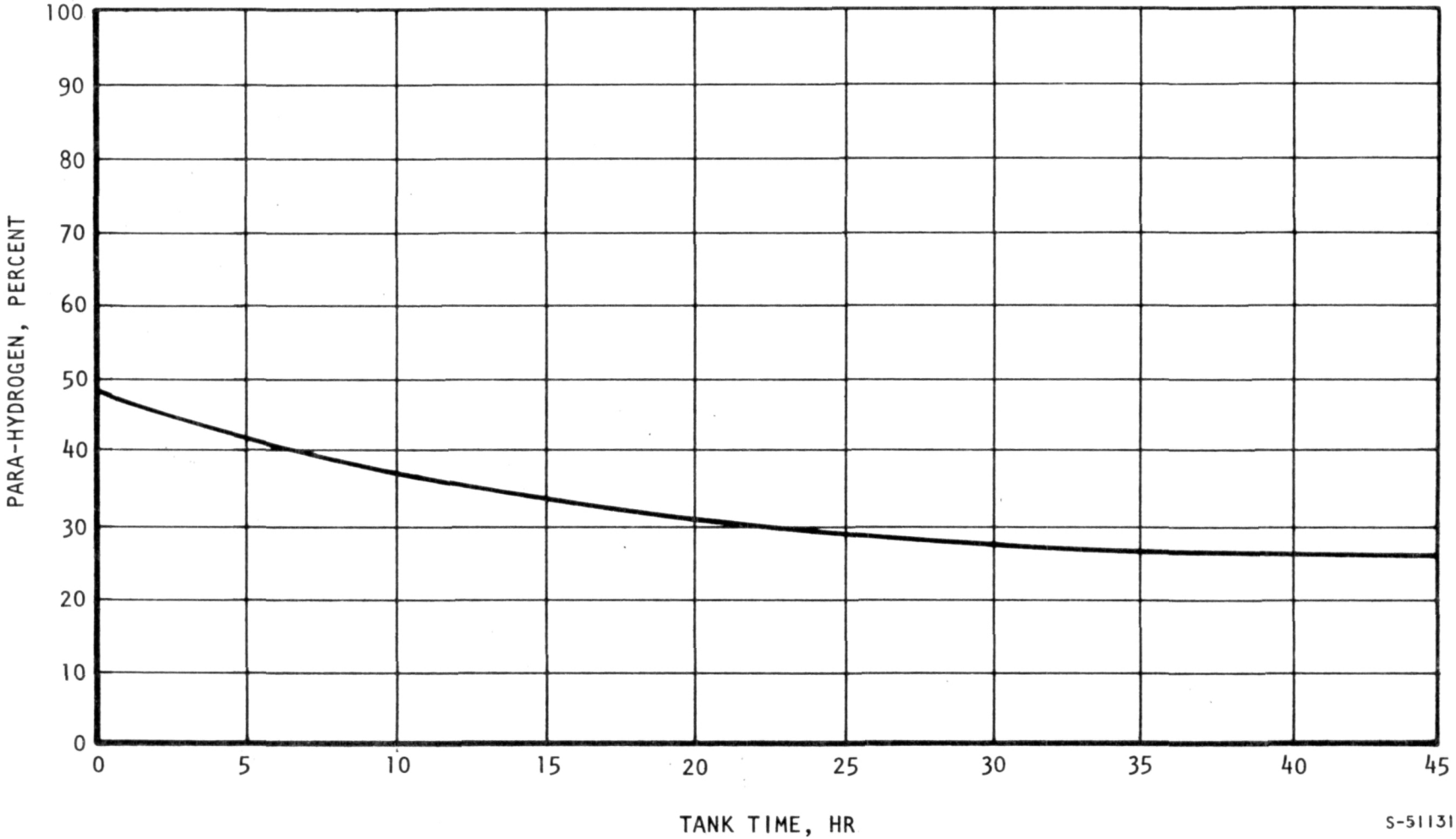

Figure 8.1-25. Para-Hydrogen History

TABLE 8.1-2

ERRORS DUE TO ERRONEOUS HYDROGEN COMPOSITION

	Cycle 3		Cycle 9	
	100% Para	33% Para	100% Para	42% Para
Q/A Btu/ft^2 sec	740	680	650	610
$h_c\left(\frac{T_W}{T_B}\right)^{.57}$ $\frac{Btu}{ft^2\ sec\ {}^0R}$	4.0	2.78	3.82	3.02
K factor	2.0	2.0	2.0	1.96

The net heat flux was 7 to 9 percent too large when properties of 100 percent para-hydrogen were used as opposed to the actual values. However, the resulting turbulence factor K which affects the engine design was changed.

8.1.2.2 Gas Chromatograph Hydrogen Sampling

Gas chromatograph data was obtained during strut testing starting with thermal cycle 12 on the SN 6, configuration 1, strut. The hydrogen sample was taken downstream of the strut leading edge and passed through a heat exchanger before going through a pressure regulator prior to entering the gas chromatograph sampling coil. The reference hydrogen was taken from a standard K-bottle and passed through a catalyst before being passed through the bridge network in the gas chromatograph. The electrical output from the gas chromatograph was recorded on a continuous-reading, one-channel recorder as shown in Figure 8.1-26.

The gas chromatograph sampling system was initially calibrated by taking a gas sample from a liquid hydrogen dewar. Several runs were sampled before it became evident that the original calibration was in error. The gas chromatograph sampling system was then calibrated at the test site using a 51 percent para-hydrogen sample, as a 100 percent para-hydrogen sample was not readily available. The 51 percent para-hydrogen sample was obtained by passing hydrogen from a K-bottle through a catalyst at liquid nitrogen temperatures. The flow rate of the calibration hydrogen gas was limited by the conversion rate of the normal hydrogen as it passed through the catalyst. The succeeding gas chromatograph samples taken during testing were then sampled at the flow rate used for the gas chromatograph calibration. Several calibrations using the 51 percent para-hydrogen technique were performed during and at the end of the test period.

A log of gaseous hydrogen storage tank time was kept in order to obtain a correlation of the percent para-hydrogen as a function of the time the gaseous hydrogen was in the storage tanks. Time zero for computing storage

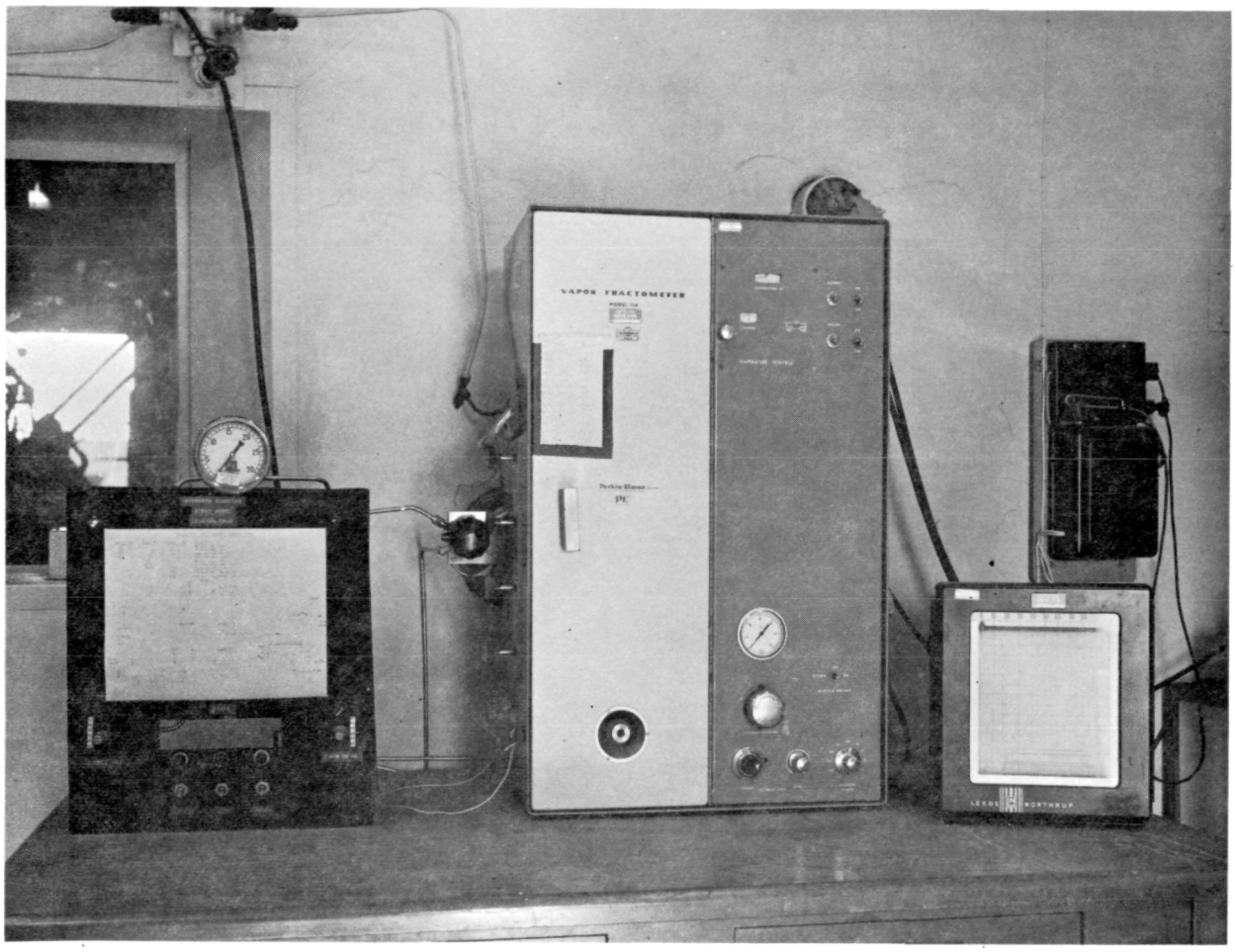

F-11113

Figure 8.1-26. Gas Chromatograph and Continuous Reading Single-Channel Recorder at NATS Laboratory

time began when the liquid hydrogen filling system had completely filled the tanks. Figure 8.1-24 shows the storage time as a function of percent para-hydrogen for the pre-run para-hydrogen readings for three strut test units. For test runs for which no gas chromatograph readings were taken, but tank time was recorded, the relationship between percent para-hydrogen and tank time is shown in Figure 8.1-25.

8.1.2.3 Support Panels Flow Distribution

Thermal cycle tests of the full scale SK 51303-2, SN 2, strut have been performed using an SK 51509-1 top support panel and an SK 51509-2 bottom support panel. These support panels have an internal coolant passage configuration which simulates the design at the strut cutouts of the full-scale inner and outer shells. Hydrogen and cold wall (structural) temperatures as shown in Figure 8.1-27 were used to calculate coolant flow distribution in these panels for a typical thermal cycle. The results are presented in Figure 8.1-28.

Flow distribution test results for the SK 51509-1 top panel were previously reported for SK 51303-1, SN 6, strut thermal cycle test in Section 8 of Reference 5-1 and are reported herein for direct comparison with the SK 51509-2 bottom panel results which have not been previously reported. Flow distribution deduced from the SK 51509-1 top panel test results are essentially unchanged from those reported in Reference 5-1; i.e., the hydrogen coolant mass flux in line with the strut cutout is substantially higher (up to 2-times average panel mass flux in Figure 8.1-28) than the coolant mass flux not in line with the strut cutout (as low as 52 percent of panel average). This flow maldistribution created panel overheating near panel edges. The design objective was a uniform coolant rate distribution across the 6-in. panel width. Coolant flow distribution for the SK 51509-2 bottom panel is better than the top panel. The maximum coolant mass flux was 1.25-times panel average and occurred 0.4 in. from the panel centerline. The minimum coolant mass flux was 80 percent of panel average and occurred near the panel edge.

The coolant maldistribution for both panels can be traced for the most part to braze alloy blockage in the finned passage and misalignment of the slot between fins of inlet. An X-ray photograph of the SK 51509-1 top panel indicates that the slot between fins at the coolant inlet was not aligned with the inlet holes. Instead, the inlet holes were aligned with fins which were blocked with braze alloy near both panel edges. Coolant flow did not enter the panel through the three inlet holes on the left-most panel side and the four inlet holes on the right-most panel side. Coolant in finned passages near the panel edges entered the panel through the center holes and flowed outward through the slot before entering these fins. This more restrictive flow path decreased the coolant rate near panel edges and substantially increased the coolant rate in line with the strut cutout as indicated in Figure 8.1-28.

An X-ray photograph of the SK 51509-2 bottom panel indicates that the inlet holes not in line with the strut cutout were partially blocked by slot misalignment at inlet, and braze alloy blockage of fins adjacent to the slot.

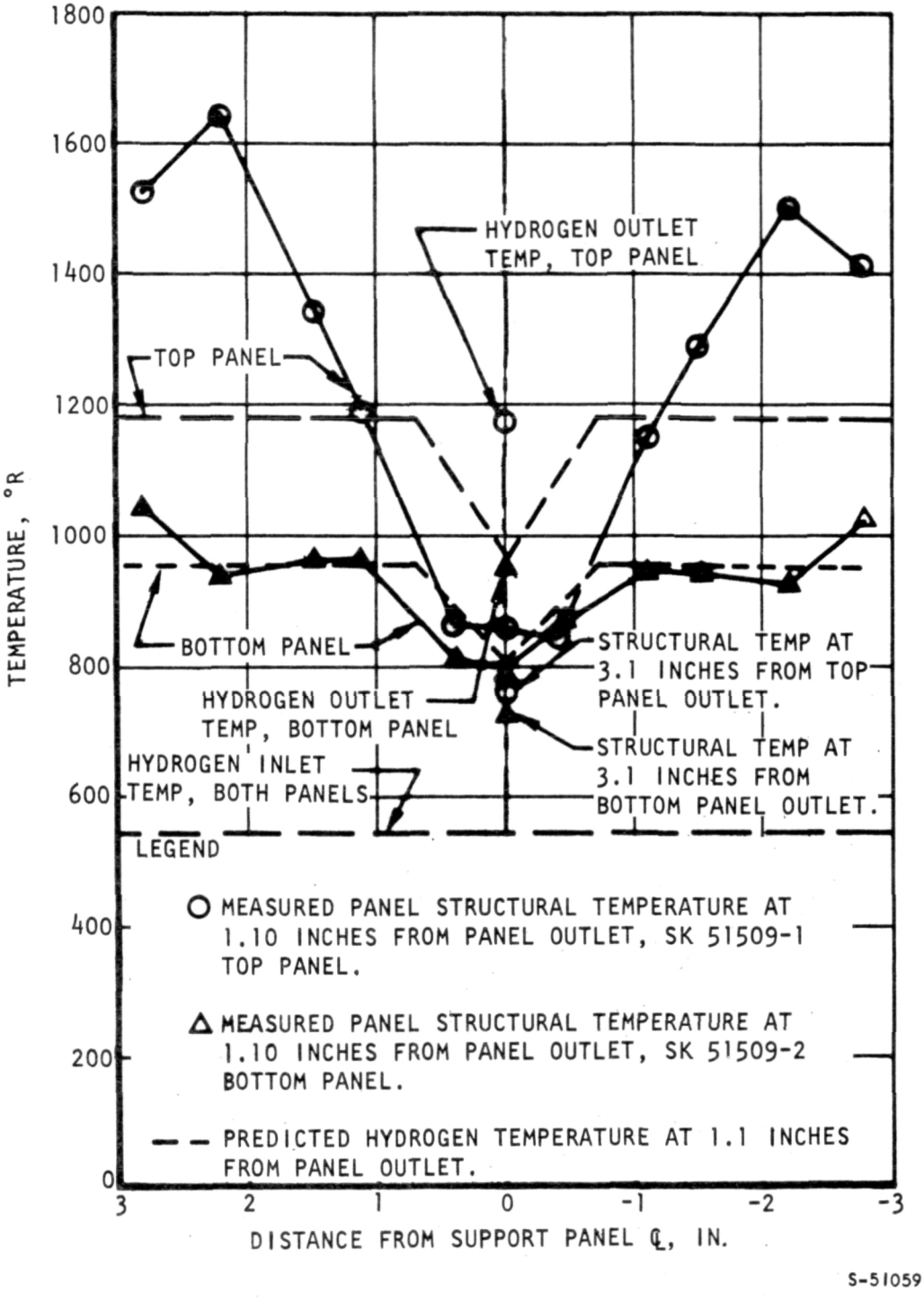

Figure 8-1.27. Support Panel Temperature Distribution for Thermal Cycle 5

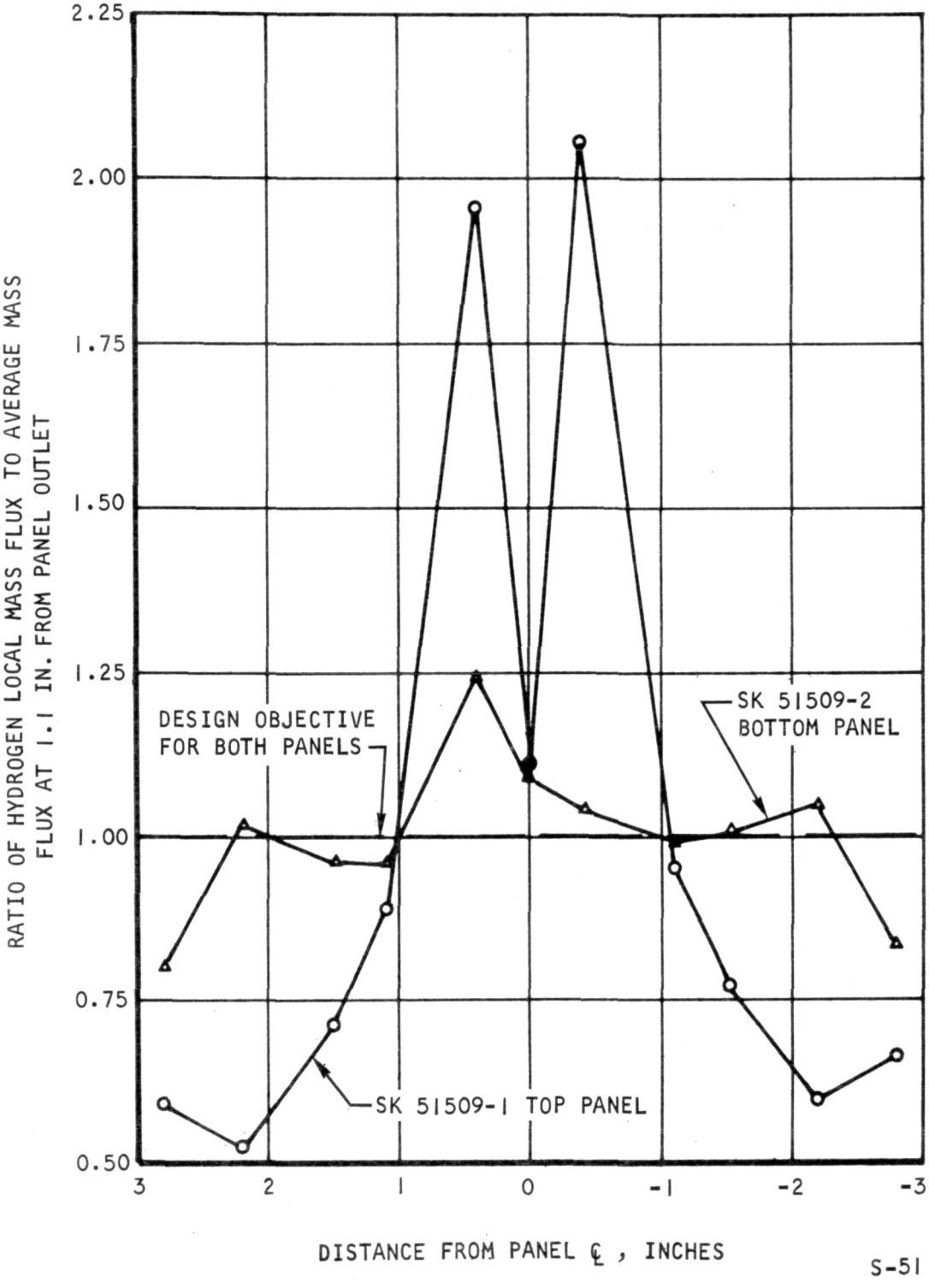

Figure 8.1-28. Support Panels Flow Distribution

This partial blockage created only moderate flow maldistribution as indicated in Figure 8.1-28, where the ratio of local-coolant mass flux to average-panel mass flux varies from 0.80 at panel edges to 1.25 at 0.4 in. from panel centerline. The peak in local mass flux is not symmetrical at 0.4 in. from bottom panel centerline as for the top panel. The local mass flux of the bottom panel is lower at 0.4 in. on the right side because the fins adjacent to the strut cutout on the right side near the strut leading edge are blocked with braze alloy.

In the previous presentation of test results of the SK 51509-1 top panel in Section 8 of Reference 5-1, it was recommended that the inlet and outlet holes should be resized to correct the coolant maldistribution. When the results in Reference 5-1 were reported, panel X-ray photographs were not available, however, at this presentation, X-ray photographs indicate that the absence of braze alloy in the fins, and slot alignment with the inlet holes--not inlet/outlet hole resizing--would correct the maldistribution. At each location of low coolant flow across the width of both panels in Figure 8.1-28, a corresponding location can be found in the X-ray photographs where braze alloy is blocking the passage of coolant flow in the fins. Through coolant flow maldistribution existed in both panels, the SK 51509-1 top panel and the SK 51509-2 bottom panel successfully completed 106 and 44 thermal cycles respectively.

8.1.2.4 Low Cycle Fatigue

The requisite temperature data needed to perform the low cycle thermal fatigue calculations are summarized in the tabular information shown on Figure 8.1-29, where the strut coolant inlet and outlet temperatures are presented. The temperature rise along the strut length is linear, and the strut body will operate at local coolant temperature. Since this temperature rise is gradual and linear, the strut body will be essentially free of thermal stresses, and the differential expansion of the hot surface producing thermal fatigue will be the local difference between the hot surface and the strut body.

In the area of the leading edge, differential expansion has been computed by comparing the local outside wall stagnation temperature, the inside wall temperature at the stagnation line, and the cooling fin temperature to the coolant outlet temperature. The numerical data on Figure 8.1.29 pertains to the cycle thermal testing on specimens SN 2, SN 5, and SN 6, to the SAM test conditions, and finally to the Mach 8 flight conditions.

A thermal fatigue analysis was carried out for each of these thermal conditions. The fatigue performance was based upon Hastelloy X data obtained by AiResearch on the Regeneratively Cooled Panels Program (Contract No. NAS1-5002) and from Nickel-200 data reported in AiResearch Report No. AP-68-4617 during the HRE program.

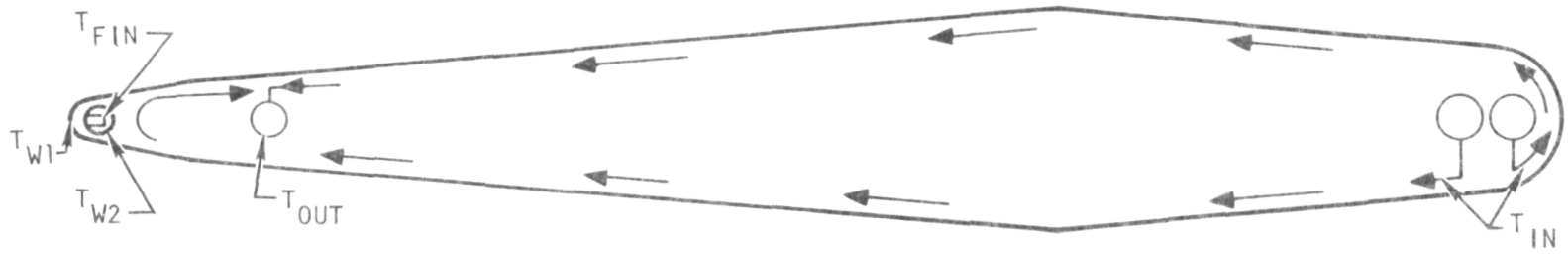

	TEMPERATURES, °R				
	T_{IN}	T_{OUT}	T_{W1}	T_{W2}	T_{FIN}
TEST SPECIMEN SN 2	550	900	1850	1300	200
TEST SPECIMEN SN 5	550	900	2600	2100	200
TEST SPECIMEN SN 6	550	900	2150	1800	NO FIN
TEST COND, SAM	540	1430	1700	1250	200
M = 8 FLIGHT	445	1170	2625	1400	200

S-51054

Figure 8.1-29. Strut Thermal Fatigue Temperatures

8.1.2.4.1 SN 2 Cycle Life

The various temperatures of consequence were:

$$T_{W1} = 1850^{\circ}R\ (1390^{\circ}F)$$

$$T_{W2} = 1300^{\circ}R\ (840^{\circ}F)$$

$$T_{out} = 900^{\circ}R\ (440^{\circ}F)$$

The maximum differential expansion from the strut outlet reference temperature is at the leading edge stagnation line. The differential temperature was

$$\Delta T = 1390^{\circ}F - 440^{\circ}F = 950^{\circ}F$$

The differential expansion due to these two temperature levels was $\alpha\Delta T = 0.0088$ in./in. The plastic strain range corresponding to this total strain amplitude was $\Delta\varepsilon_{pl} = 0.0044$ in./in. From the Hastelloy X low cycle fatigue information, the predicted cycle life would be N = 1650 cycles.

The mean metal temperature at the stagnation line was $1115^{\circ}F$, and the pressure containment stress with 700 psi coolant was

$$\sigma = \frac{p\ r_m}{t} = \frac{(700)(.0725)}{(.015)} = 3350 \text{ psi}$$

At this temperature and stress intensity, creep was not a factor at all. This unit survived a total of 44 actual test cycles.

8.1.2.4.2 SN 5 Cycle Life

This test unit was constructed with a blocked cooling package on one side of the leading edge internal cooling fins. Because of this blockage, the test unit was subjected to extremely severe thermal cycles, and because of this, an excellent measure of cycle life capability was obtained. The pertinent temperatures were

$$T_{W1} = 2610^{\circ}R\ (2150^{\circ}F)$$

$$T_{W2} = 2060^{\circ}R\ (1600^{\circ}F)$$

$$T_{out} = 900^{\circ}R\ (440^{\circ}F)$$

This test unit survived 102 thermal cycles at these conditions with an average time at maximum temperatures of approximately 2 minutes per cycle.

The elapsed time at maximum temperature was approximately 3.5 hr during this test. Based upon a mean metal temperature at the stagnation line of $(2150^{\circ}F + 1800^{\circ}F)/2 = 1825^{\circ}F$, the creep rupture life would have been 50 hr. The creep rupture life fraction was 3.5/50 = .07.

The total applied differential temperature between the strut body at the coolant outlet end was

$$\Delta T = 2150^{\circ}F - 440^{\circ}F = 1710^{\circ}F$$

The differential thermal expansion was .0169 in./in., and the resulting plastic strain range was $\Delta\epsilon_p$ = .0125 in./in. From Hastelloy X fatigue data, the low cycle fatigue life without considering creep was N = 175 cycles. With creep effects included, this would have been

$$N = 175\ (1 - .07) = 163 \text{ cycles.}$$

8.1.2.4.3 SN 6 Cycle Life

This test was subjected to the following pertinent temperatures:

$T_{W1} = 2160^{\circ}R\ (1700^{\circ}F)$

$T_{W2} = 1760^{\circ}R\ (1300^{\circ}F)$

$T_{out} = 900^{\circ}R\ (440^{\circ}F)$

The mean metal temperature at the stagnation line was 1500°F, and the creep rupture life due to pressure containment would have been in excess of 10,000 hr. The total elapsed time of 2.5 hr at maximum temperature, therefore, contributed a negligible amount of creep damage.

The maximum temperature differential during each test cycle occurred at the leading edge stagnation line, and it was

$$\Delta T = 1700^{\circ}F - 440^{\circ}F = 1260^{\circ}F$$

This produced a differential thermal expansion of 0.0120 in./in., and a corresponding plastic strain range of $\Delta\epsilon_p$ = 0.0076 in./in. Based upon 1540°F low cycle fatigue data, the predicted cycle life was 650 cycles.

8.1.2.4.4 SAM Test Conditions

The temperatures for the SAM test unit are shown on Figure 8.1-29. The peak ΔT occurs at the leading edge cooling fin. The predicted temperature levels are

$T_{W1} = 1700^{\circ}R\ (1240^{\circ}F)$

$T_{W2} = 1250^{\circ}R\ (790^{\circ}F)$

$T_{out} = 1430^{\circ}F\ (970^{\circ}F)$

$T_{fin} = 200^{\circ}R\ (-260^{\circ}F)$

Note that the maximum temperature predicted at the leading edge outside stagnation line is virtually identical to the SN 5 outside wall temperature. The inside wall temperature would be considerably lower, while the coolant outlet temperature would be somewhat higher than the SN 5 test conditions. In summary, the Mach 8 flight thermal fatigue conditions are somewhat more moderate than those which occurred during the testing of SN 5.

The average wall temperature at the stagnation line would be approximately $1540^{\circ}F$, which would produce a stress rupture life of 1000 hr due to the pressure containment of coolant at 700 psi internal pressure. The required engine design life of 10 hr would correspond to a creep rupture damage fraction of 0.01.

The differential temperature between the strut leading edge outside stagnation line and the coolant outlet would be

$$\Delta T = 2165^{\circ}F - 710^{\circ}F = 1455^{\circ}F$$

This would produce a thermal differential expansion of 0.0150 in./in., and a plastic strain range of 0.0106 in./in. Based upon $1540^{\circ}F$ thermal fatigue data, the predicted cycle life would be N = 380 cycles without regard to creep. Accounting for the creep rupture life fraction damage of 0.01, the predicted life at Mach 8 flight would be

$$N = 380 (1 - .01) = 376 \text{ cycles.}$$

8.1.3 Conclusions

The test conditions on all three strut specimens were more severe than those that will be encountered during the SAM test program. The most informative test sequence occurred with SN 5, where the test conditions were somewhat in excess of the predicted Mach 8 flight conditions. The successful achievement of 102 test cycles without failure compares favorably with the predicted life of 163 cycles for these conditions. More importantly, since the Mach 8 flight considerations should produce slightly lower thermal expansion and average metal temperature at the stagnation line than the SN 5 conditions, the SN 5 test is a good demonstration of strut adequacy for 100 operating cycles and 10 hr operating time.

8.2 COMPONENT PRESSURE DROP AND FLOW DISTRIBUTION

8.2.1 Spike Air-Pressure-Drop Test Results

Pressure drop tests using room temperature air in the coolant passages and in the injector manifold of the SAM spike have been performed. A photograph of the test setup is shown in Figure 8.2-1 and a schematic indicating pressure tap locations is shown in Figure 8.2-2. Pressure drop test results are presented in Figures 8.2-3 (coolant passages) and 8.2-4 (injector manifold inlet ducting) as the product of static pressure drop and average density,

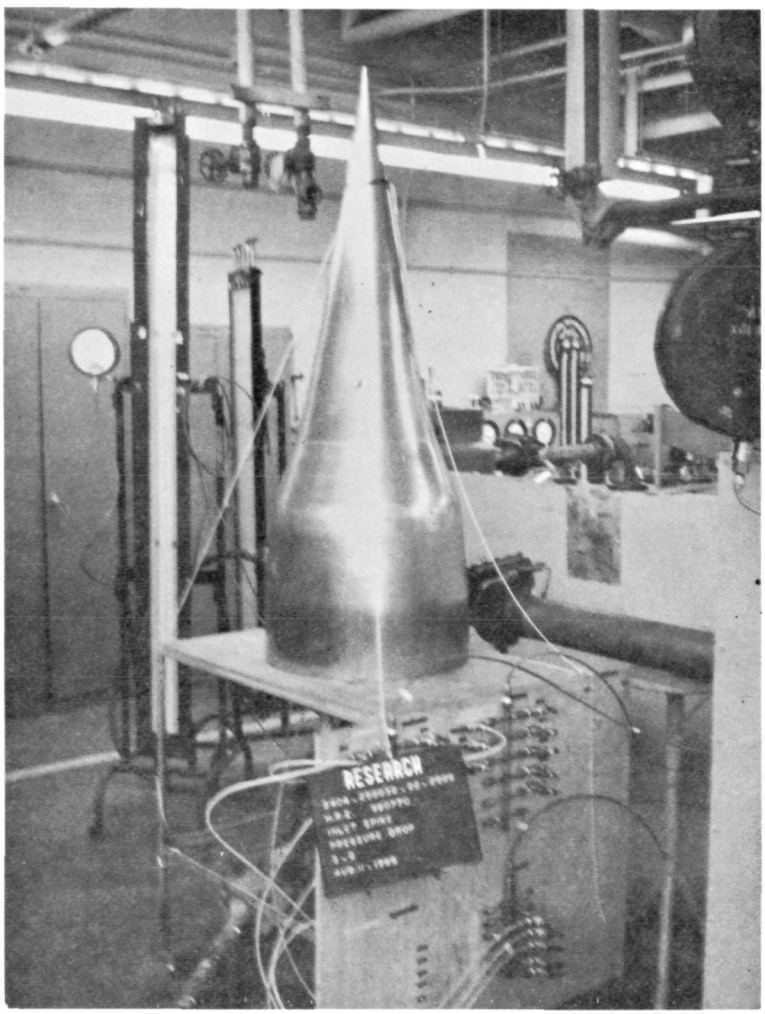

F-11146

Figure 8-2.1. SAM Spike Air-Pressure-Drop Test Setup

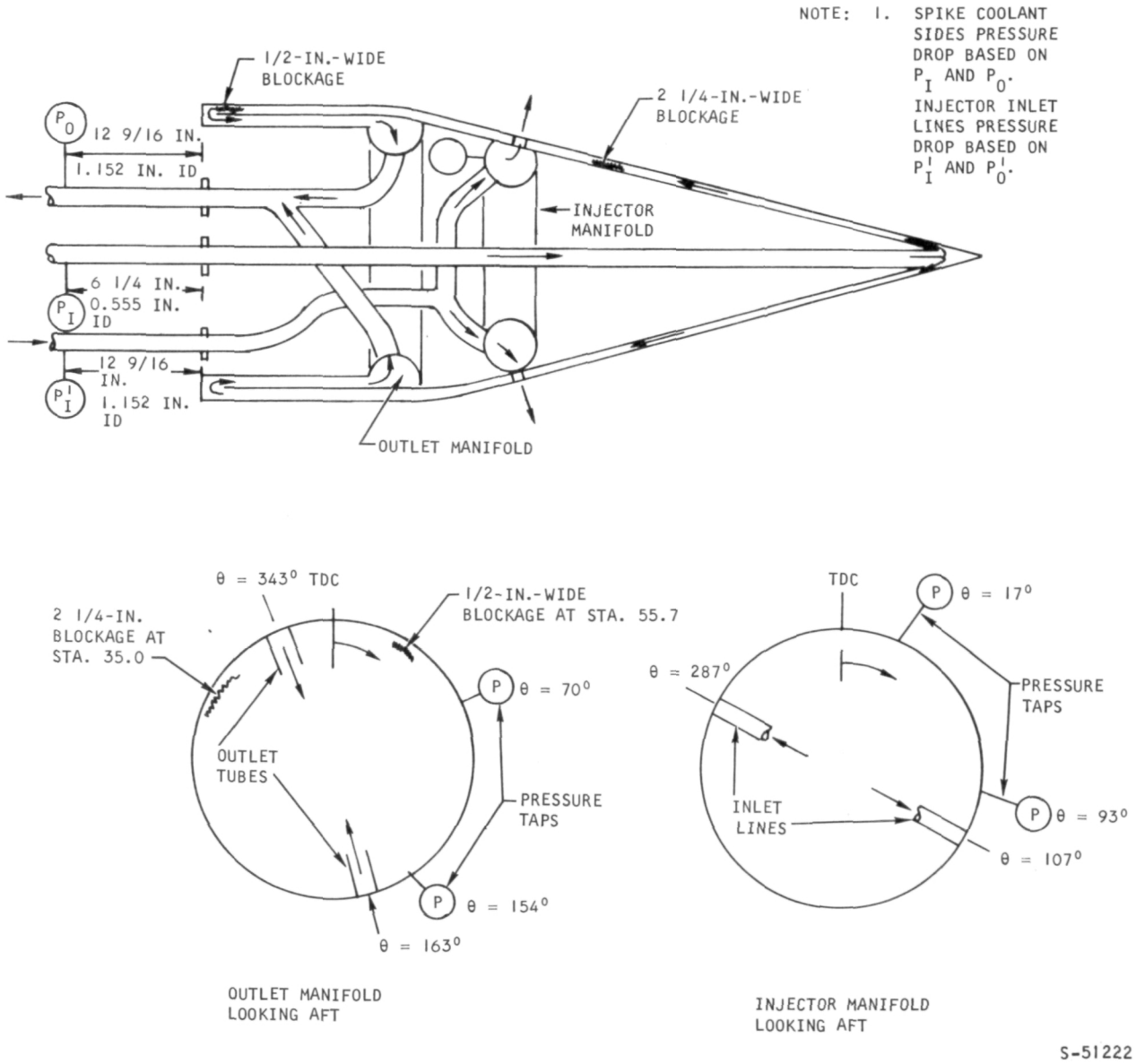

Figure 8.2-2. SAM Spike Air-Pressure-Drop Test Setup

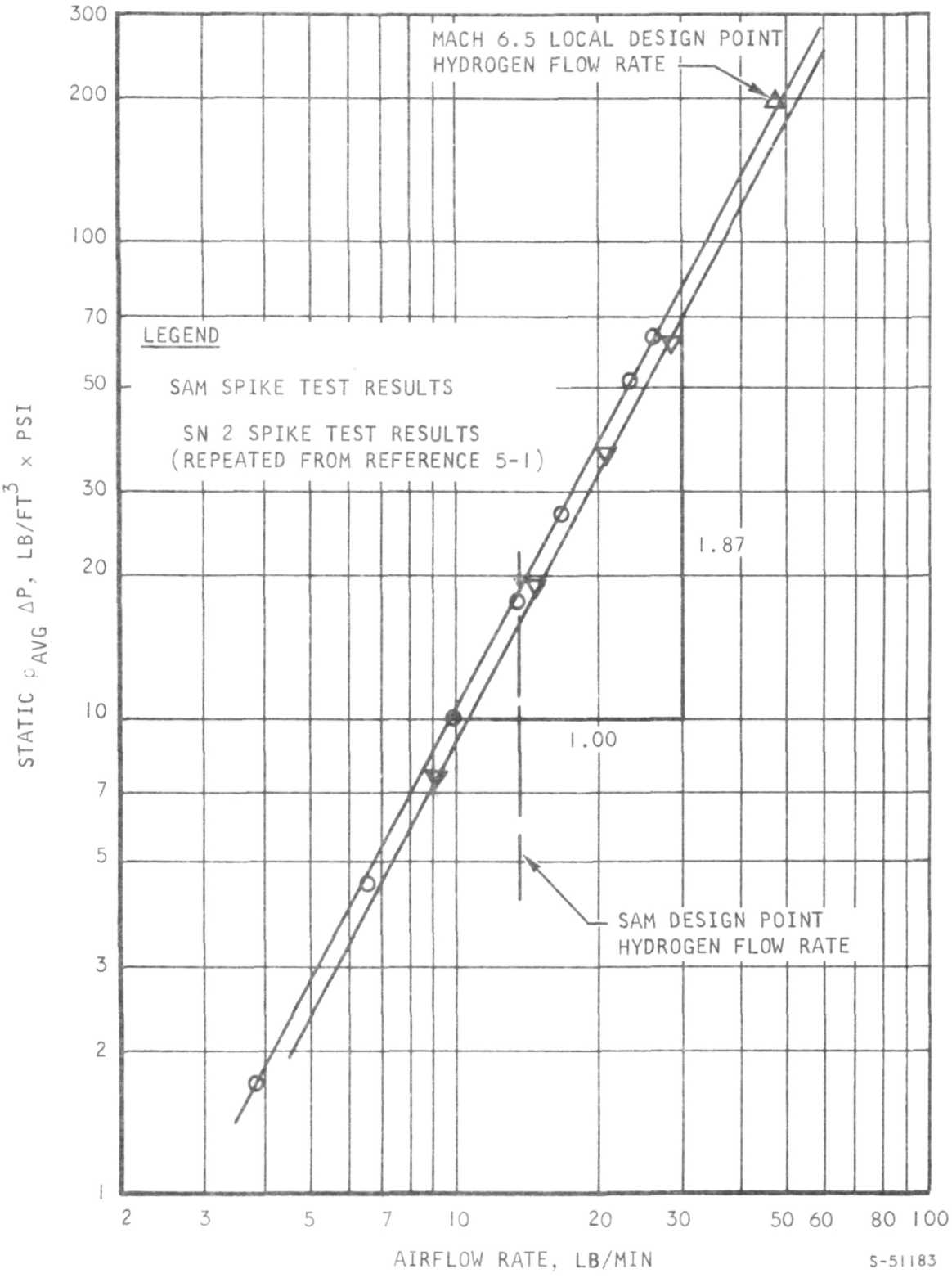

Figure 8.2-3. SAM Spike Air-Pressure-Drop Test Results

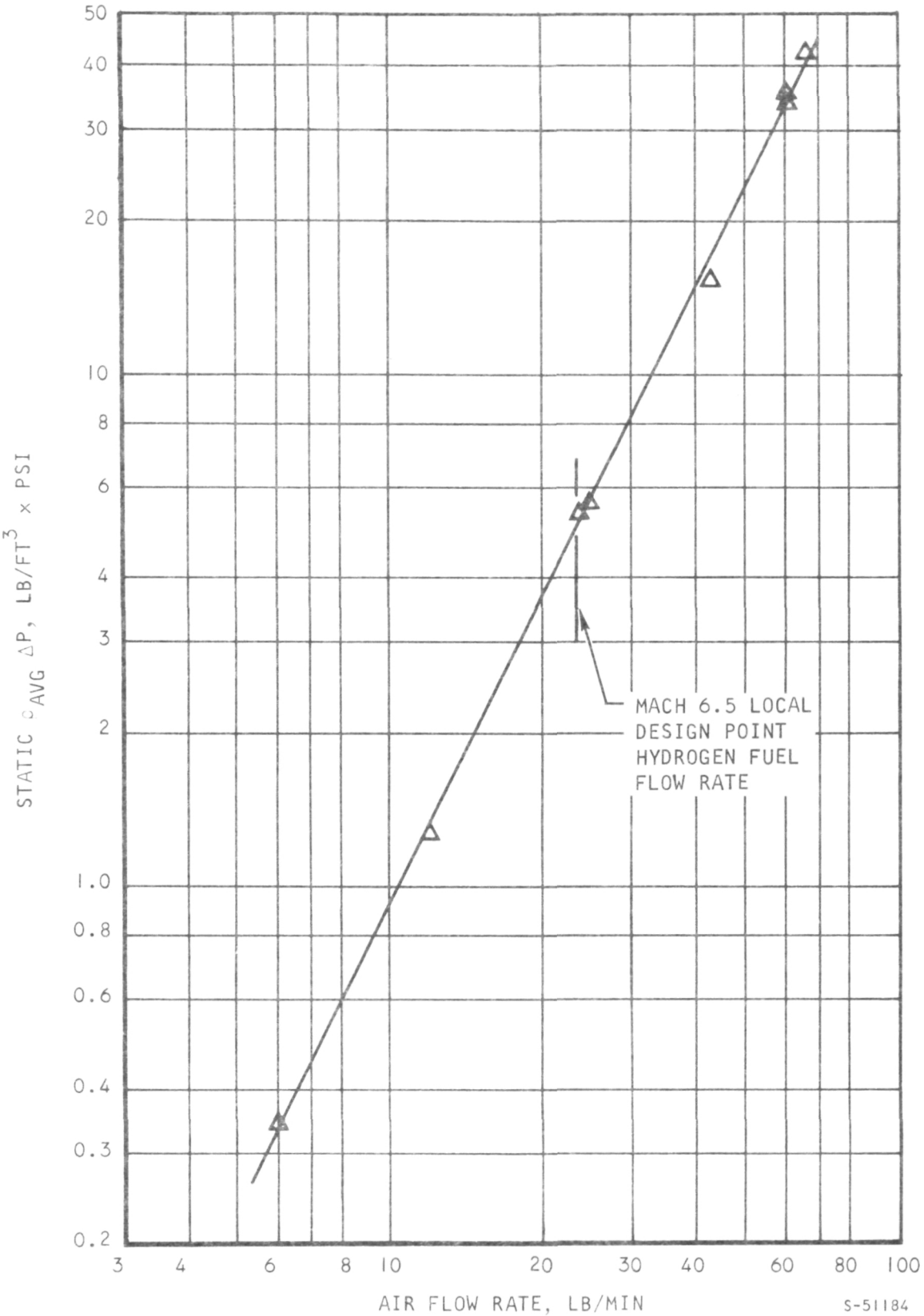

Figure 8.2-4. SAM Spike Injector Manifold Inlet Lines Pressure-Drop-Test Results

versus airflow rate. The predicted value for hydrogen flow at Mach 6.5 local, 88000-ft-altitude flight conditions and the SN 2 spike test results (repeated from Reference 5-1), are included for comparison.

Results indicate that the test pressure drop for the SAM spike assembly (inlet line to outlet line indicated in Figure 8.2-2) is 20 percent lower than predicted and 14 percent lower than test data for the SN 2 spike assembly.

Two pressure taps placed 84 deg apart in the SAM spike outlet manifold, indicated a manifold static pressure differential that was within 15 percent of predictions for uniform flow distribution. This is expected to produce an acceptable local flow rate increase of not more than 0.5 percent above average at 1300°F and 590 psia hydrogen outlet manifold conditions.

Pressure drop results for the injector manifold inlet ducting are presented in Figure 8.2-4. The calculated range of discharge coefficients for the injectors (97 injectors of 0.100-in. diameter, sharp-edged and a length-to-diameter ratio of 1.55) were from 0.869 to 0.877 for choked-flow and with pressure ratios (manifold to ambient) from 4.5 to 4.9. The discharge coefficient was calculated from test measurements and the following relation for choked air flow:

$$C_D = \frac{(W/A)}{\left(\frac{0.532\ P_o}{\sqrt{T_o}}\right)}$$

where W = air flow rate through injectors, lb/sec

A = physical injectors area of 0.765 $in.^2$

P_o = manifold total pressure, psia

T_o = total temperature, 532°R for the tests

A calculation was performed, based on injector circuit test results, to determine the pressure downstream of the fuel control valve required to supply both 0.19 and 0.38 lb/sec of hydrogen at 1600°R to the injectors. A flow rate of .19 lb/sec is the required fuel flow through the spike injectors at the Mach 8 (freestream and local), 88,000-ft-altitude flight condition, and 0.38 lb/sec is required for Mach 8 (Mach 6.5 local) 88,000-ft-altitude conditions. Calculations indicate that the required pressure is 164 psia for 0.19 lb/sec and 328 psia for 0.38 lb/sec. These pressures are both compatible with the fuel plenum pressure which will be maintained at 525 psia.

8.2.2 Strut-Sides Air-Pressure-Drop Test Results

Pressure drop tests using room temperature air in the side coolant passages of the struts have been performed. A photograph of the test setup is shown in Figure 8.2-5. These struts have a single 1/2-in.-dia inlet tube providing coolant to the strut sides. Results are presented in Figure 8.2-6 as the product of static pressure drop and density at average temperature and pressure vs airflow rate. The engine system requirement is included for comparison in Figure 8.2-6. The engine system requirement is determined from the available pressure drop from the outer shell to the fuel plenum and the required hydrogen flow rate as indicated in Figure 8.2-6, and does not represent the pressure-drop characteristic of any air-tested strut. Because the pressure-drop characteristics for the tested struts are lower than the requirement, the strut-sides coolant-passages circuit will be orificed so that the effective strut-sides pressure-drop characteristic will match the requirement. In the data reduction, a velocity head based on the 0.312-in.-inside-diameter outlet tube was subtracted from the overall pressure drop to account for the dump loss to atmospheric pressure.

8.2.3 Innerbody

Pressure-drop tests using room temperature air in the coolant passages of two nozzle assemblies and one inner shell assembly have been performed. One nozzle assembly, (SN 2), was individually tested with air exhausting to ambient pressure through the bolted flange/manifold orifices. Another nozzle assembly (SN 3, SAM) was attached to an inner shell assembly (SN 3, SAM) and tested with air, exhausting to ambient pressure through the six inner shell outlet tubes. The test setup is shown in Figures 8.2-7 and 8.2-8 with the nozzle connected to the inner shell. Pressure-drop results are presented in Figures 8.2-9 and 8.2-10, as the product of static pressure drop and density at average temperature and pressure, versus airflow rate. Predicted results for hydrogen flow are included for comparison. Because several static pressure taps were provided along the flow path in the nozzle and inner shell assemblies (see Figure 8.2-6), a pressure-drop breakdown of the nozzle and inner shell components could be made. Results of this breakdown are presented in Table 8.2-I along with predicted results for hydrogen flow at Mach 6.5 local, 88,000-ft-altitude flight conditions.

The overall innerbody test pressure drops for both nozzles are approximately equal and about 9 percent lower than predicted, primarily because test pressure drops in the inlet tube and nozzle cap, nozzle cap orifices, bolted flange/manifold orifices, and inner shell outlet tubes were from 31 to 52 percent lower than predicted, as shown in Table 8.2-I. These overpredictions, however, were offset by underpredictions of test pressure drop in the nozzle fins by 42 percent, and in the inner shell fins by 16 percent.

X-ray photographs of the two nozzle assemblies and the inner shell assembly indicated essentially clear coolant passages. This is confirmed by the closeness of test results between the two nozzle assemblies.

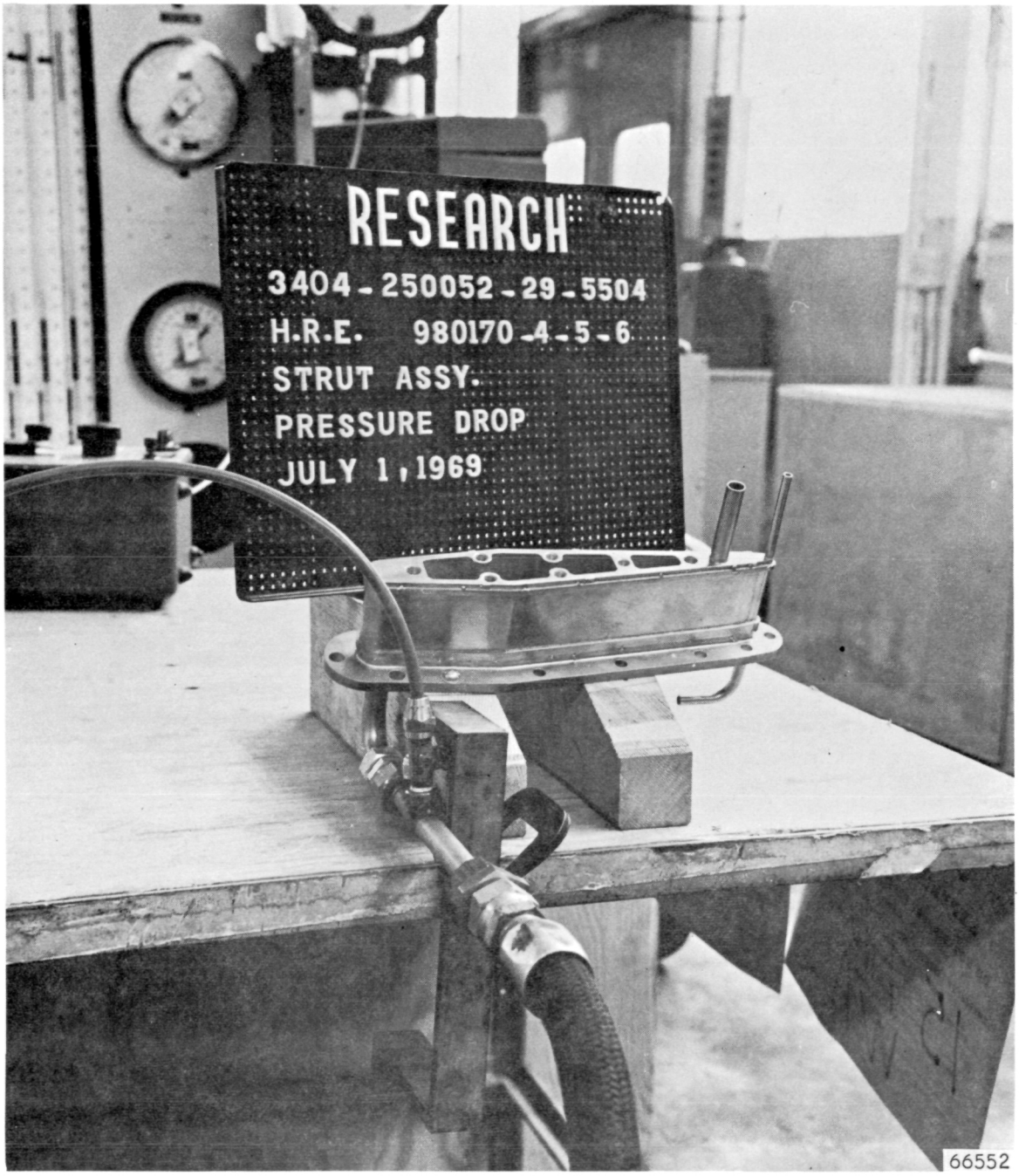

Figure 8.2-5. Strut Sides Air-Pressure-Drop Test Setup

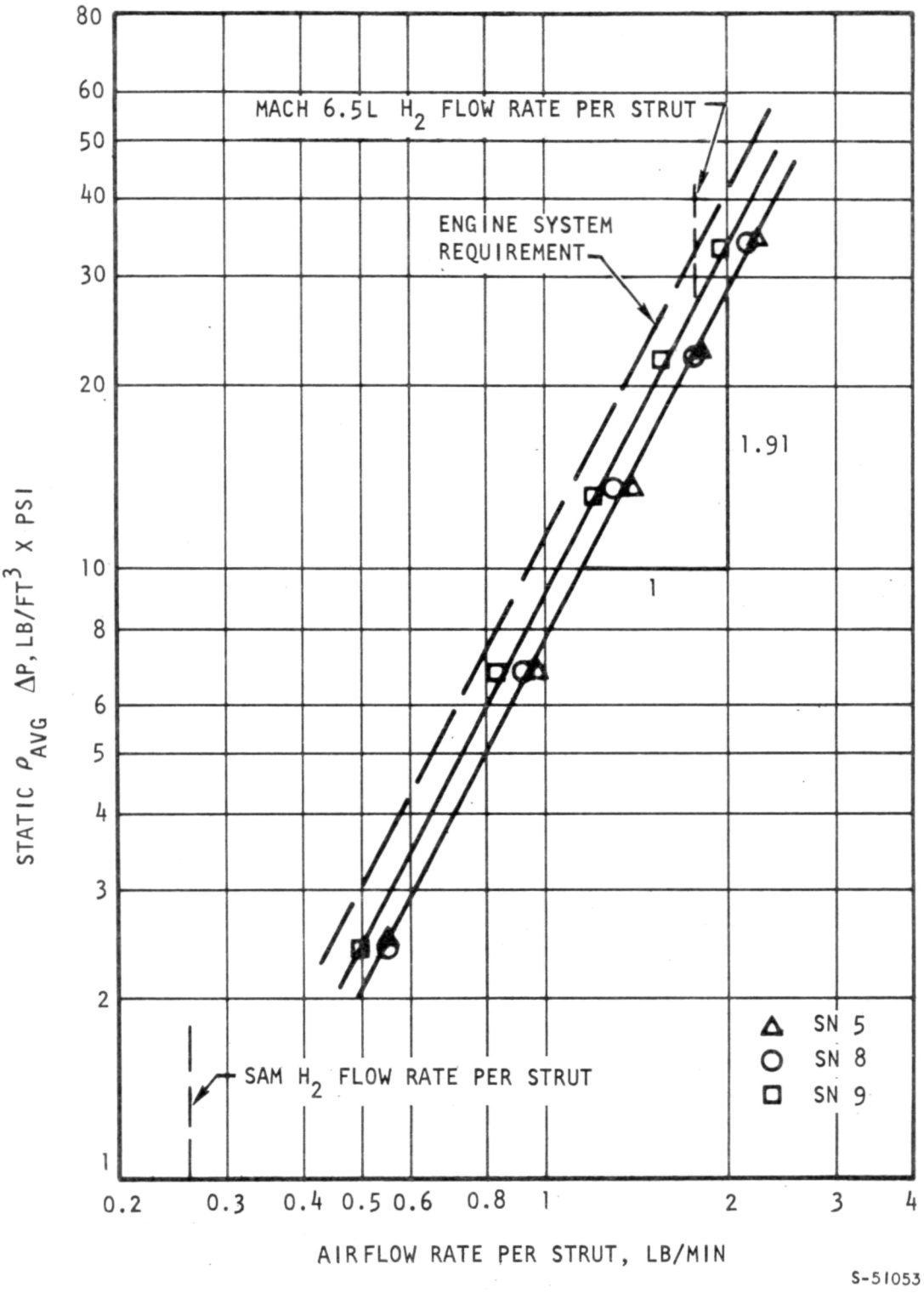

Figure 8-2-6. Strut Sides Air-Pressure-Drop Test Results

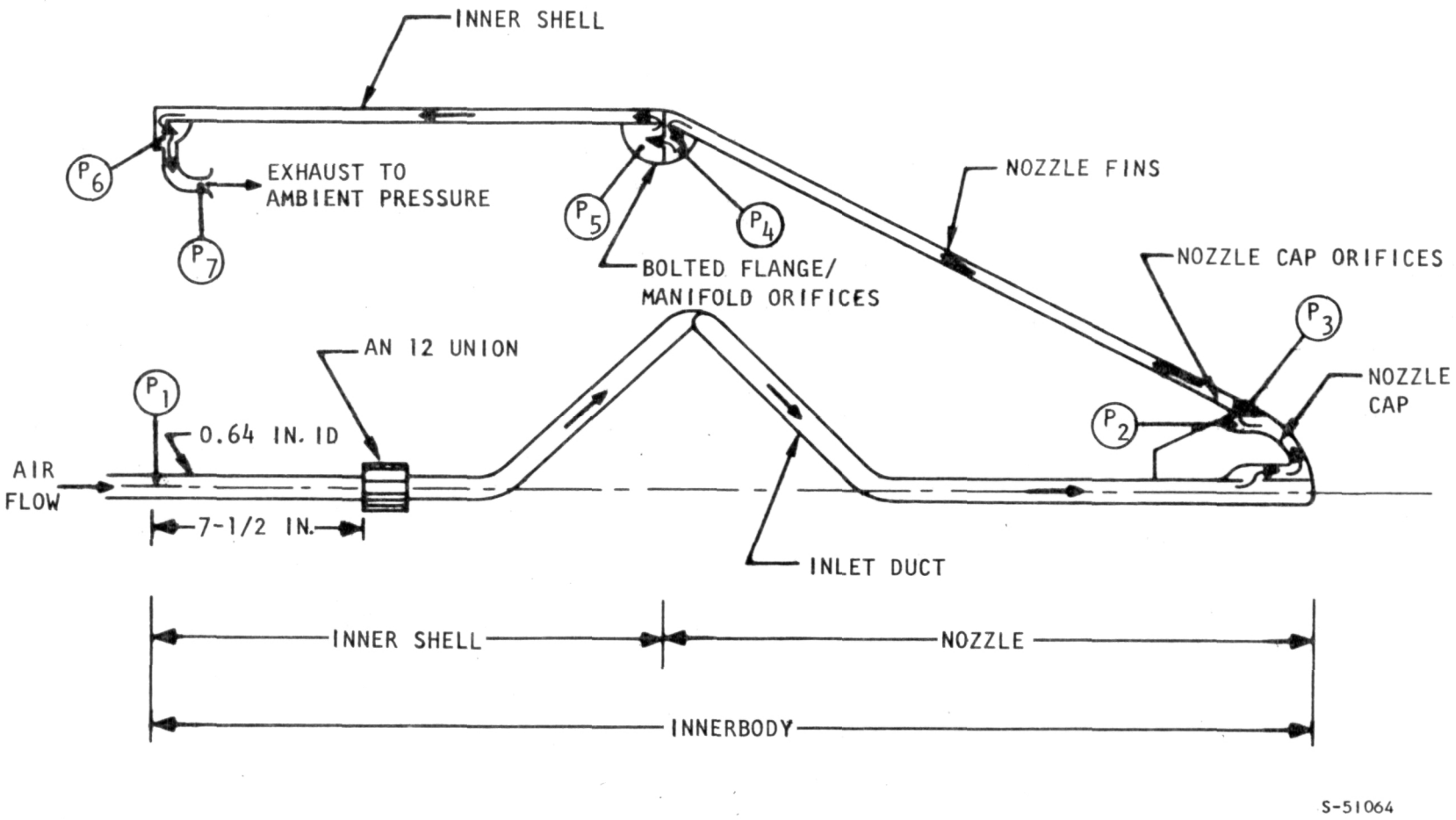

Figure 8.2-7. Nozzle and Inner Shell Air-Pressure-Drop Test Setup

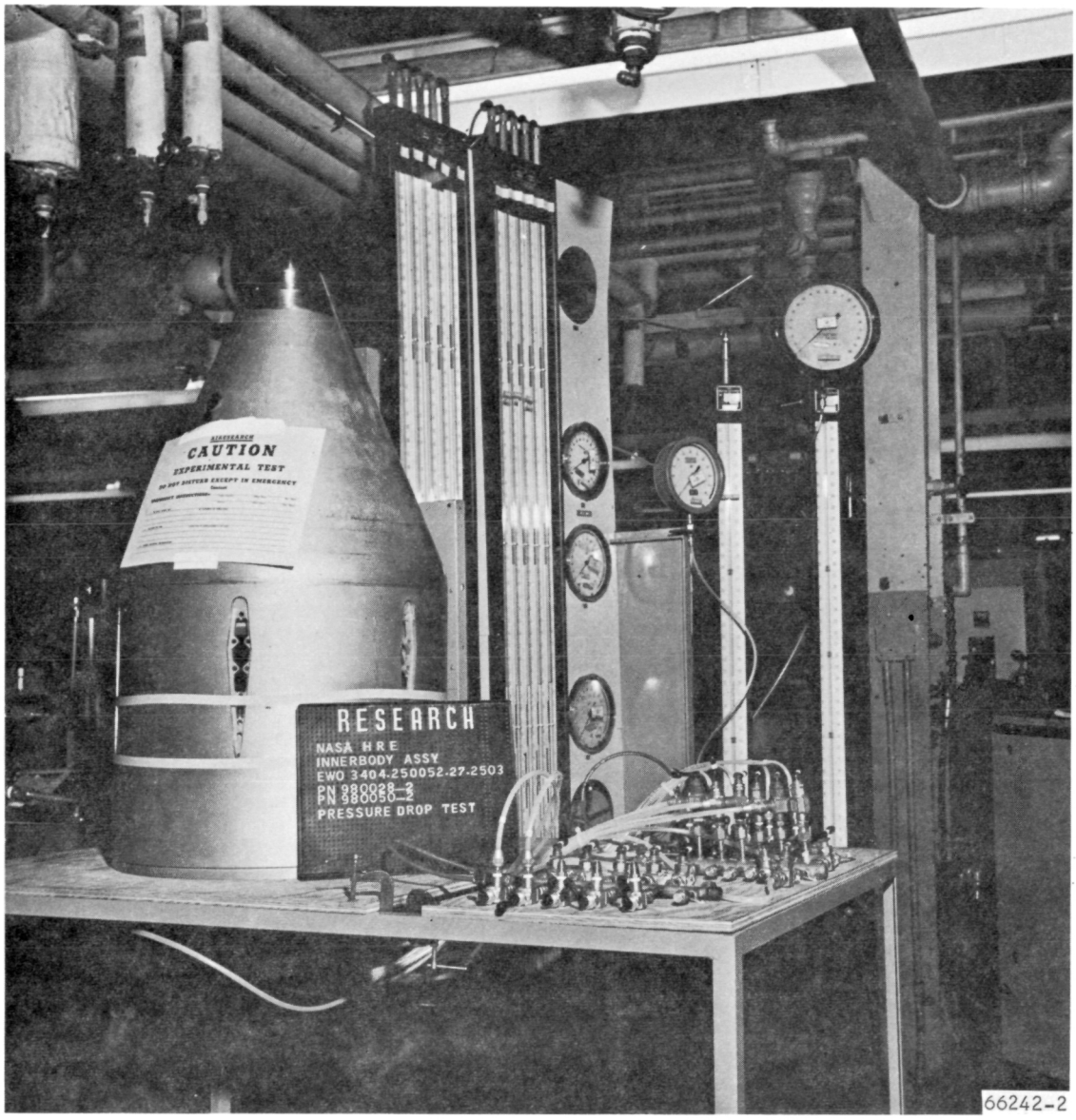

Figure 8.2-8. Innerbody Air-Pressure-Drop Test Setup

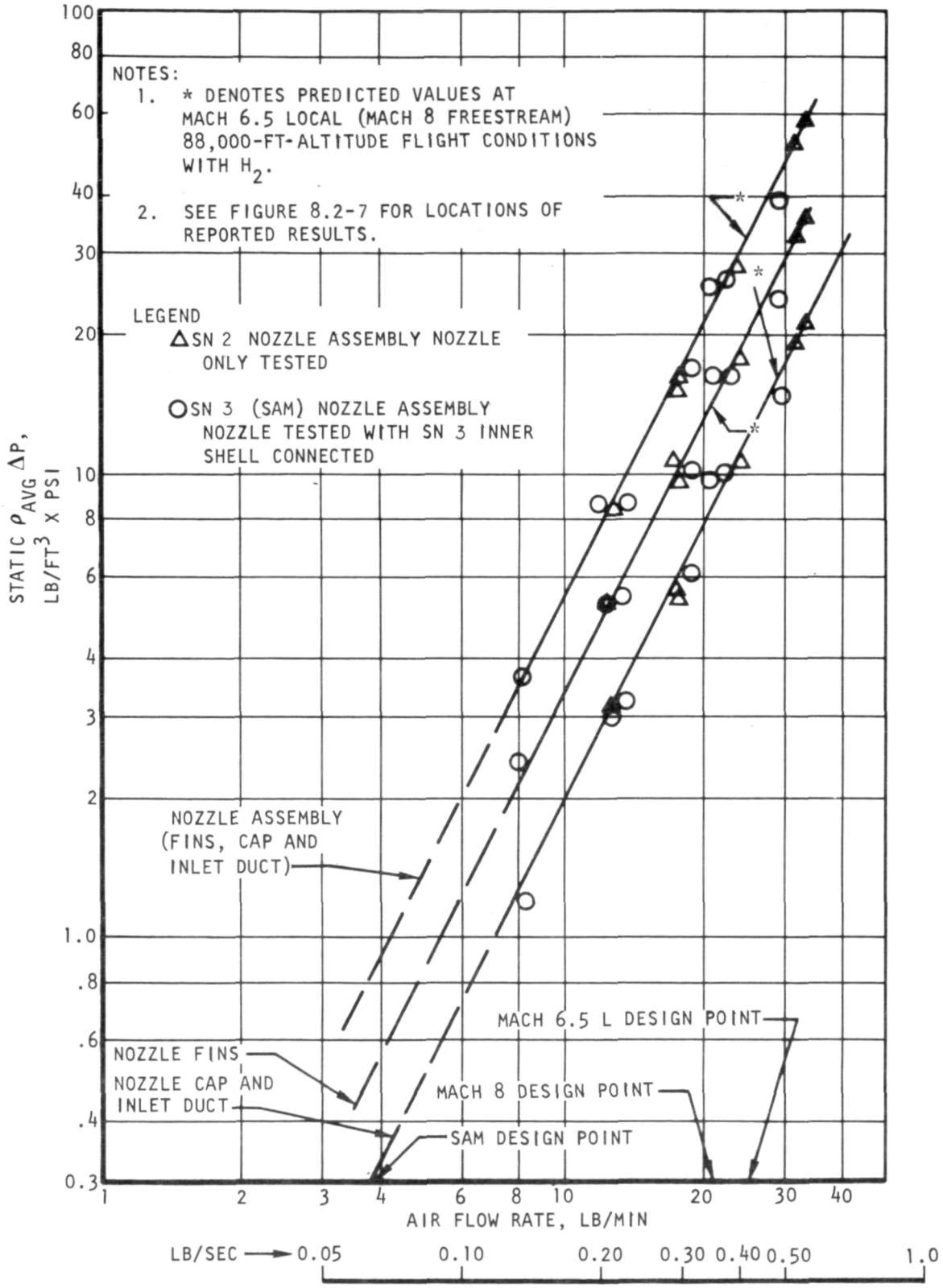

S-51070

Figure 8.2-9. Nozzle Air-Pressure-Drop Test Results

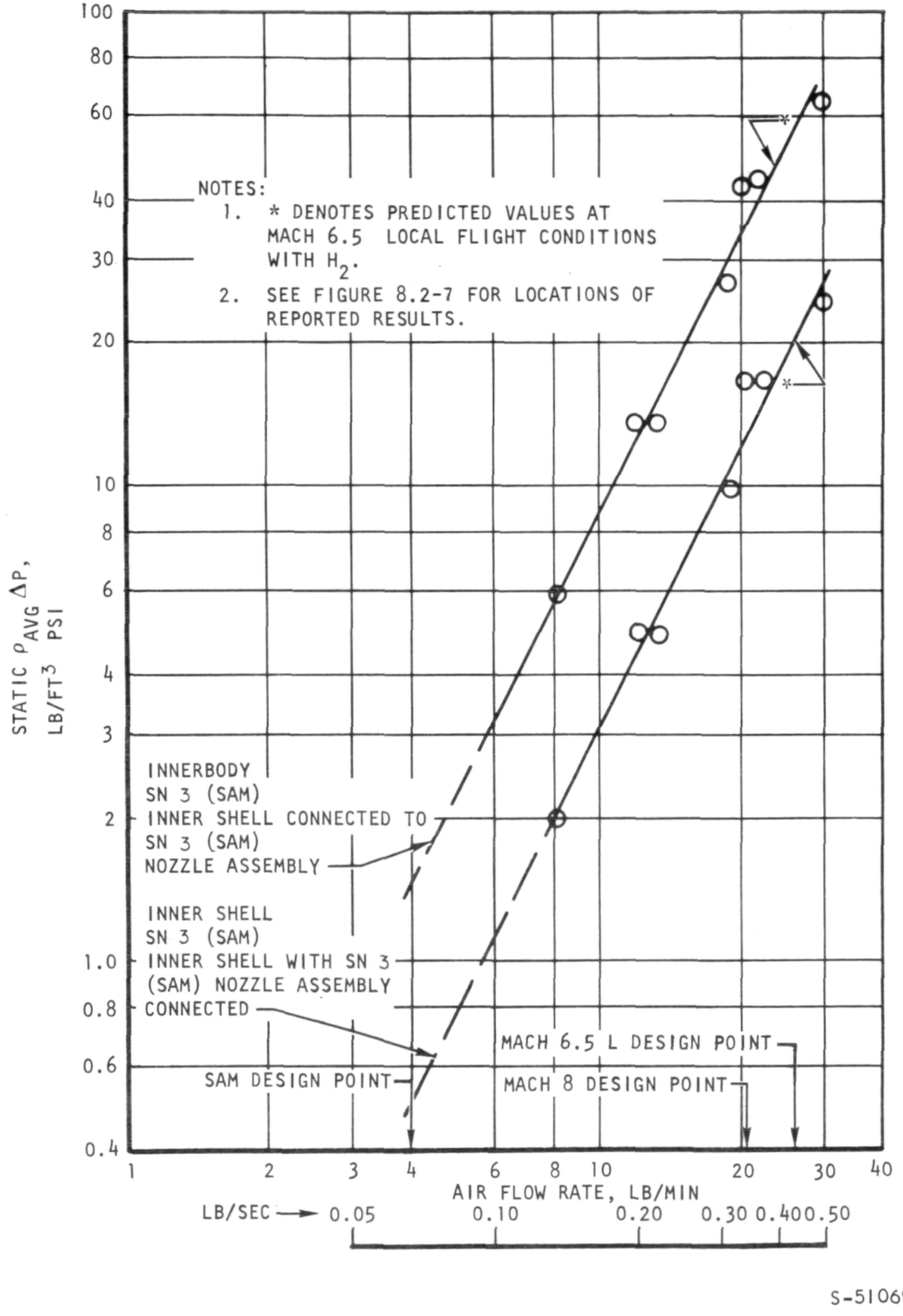

Figure 8.2-10. Innerbody and Inner Shell Air-Pressure-Drop Test Results

TABLE 8.2-1

SUMMARY AND COMPARISON OF RESULTS FOR INNERBODY AIR-PRESSURE-DROP TESTS

Item	Component	Pressure Location in Figure 8.2-7		Mach 6.5L Flow Rate		Test $\rho\Delta P$ / Predicted $\rho\Delta P$	Test Velocity Head Loss Coefficient, K	Predicted Velocity Head Loss Coefficient, K	Comments
		Upstream	Downstream	Test $\rho\Delta P$ at 0.42 lb/sec (25.2 lb/min) with Air, $lb/ft^3 \times psi$	Predicted $\rho\Delta P$ at 0.42 lb/sec (25.2 lb/min) with H_2, $lb/ft^3 \times psi$				
1	Nozzle Cap and Inlet Duct	P_1	P_3	12.5	26.1	0.48	-	-	$\rho\Delta P$ curve in Figure 8.2-9
2	Nozzle Cap Orifices	P_2	P_3	1.3	2.1	0.61	1.7	2.8	60 orifices at 0.125 in. dia
3	Nozzle Fins	P_3	P_4	21.0	14.8	1.42	-	-	$\rho\Delta P$ curve in Figure 8.2-9
4	Nozzle (Sum of ① and ③)	P_1	P_4	33.5	40.9	0.82	-	-	$\rho\Delta P$ curve in Figure 8.2-9
5	Bolted Flange/Manifold Orifices	P_4	P_5	0.8	1.2	0.63	1.8	2.8	10 orifices at 0.35 in. dia
6	Inner Shell	P_5	P_6	19.2	16.6	1.16	-	-	$\rho\Delta P$ curve in Figure 8.2-10
7	Inner Shell Outlet Tubes	P_6	P_7*	0.6	0.9	0.67	1.5	2.2	6 tubes at 0.491 in. dia
8	Innerbody (Sum of ④, ⑤, ⑥, and ⑦)	P_1	P_7*	54.1	59.6	0.91	-	-	$\rho\Delta P$ curve in Figure 8.2-10

*P_7 was not measured directly, but was calculated by adding one velocity head to the ambient pressure

8.2.4 Leading Edge Air-Pressure-Drop and Flow-Distribution Test Results

8.2.4.1 Summary

Pressure drop and flow distribution tests using room air in the coolant passages of the SN 2 and SN 3 (SAM) leading edge assemblies have been performed. The test setup is shown in Figure 8.2-11. Airflow entered the inlet manifold through eight flexible hoses and exhausted to ambient pressure through the 24 crossover tubes. Test results are presented in Figure 8.2-12 as the product of static pressure drop and average density, versus airflow rate. The predicted value of hydrogen flow at Mach 6.5 local, 88,000-ft-altitude flight condition is included for comparison.

Results indicate that the test-pressure drop (inlet manifold to outlet manifold) for the SN 2 assembly, as tested, is approximately 40 percent higher than predicted; however, when the test data is corrected to account for the presence of blocked finned passages, the pressure drop is about 15 to 20 percent above prediction. The data reduction process is discussed below. The test pressure drop for the SN 3 (SAM) assembly is 33 percent lower than prediction.

Several static pressure taps were installed in the inlet and outlet manifolds of the SN 2 assembly in an attampt to measure coolant-passage flow distribution. However, the presence of braze-alloy blockages in the finned passages obscured the outlet manifold pressure distribution and the resulting fin-passage flow distribution. Flow distribution tests on the SN 3 (SAM) assembly were performed by indirectly measuring the outlet manifold pressure distribution. Results presented in Figure 8.2-13 indicate that the ratio of local-maximum to local-minimum flow rate is an acceptable 1.033. The corresponding predicted value is 1.016.

8.2.4.2 Discussion

X-ray photographs of the SN 2 assembly indicated the presence of braze alloy blockage at three locations around the leading edge circumference and adjacent to the leading edge inlet manifold. Braze alloy at two of the three locations appeared to partially block the flow passages. At the third location, a 5.4-in. fin-passage width of 67.8-in. leading edge circumference was thought to be completely blocked. These X-ray observations were confirmed by the test results, which showed an SN 2 assembly pressure drop that was approximately 40 percent higher than predicted, and a circumferential pressure difference in the outlet manifold as high as 19 psi. The minimum outlet manifold pressure was in line with the blockage, and the maximum occurred at 180 deg from the blockage.

The 5.4-in.-wide fin blockage represents about 8 percent of the 67.8-in. leading edge circumference at the inlet manifold. To compare directly the pressure drop of the unblocked passages of the SN 2 assembly with the prediction for an unblocked leading edge assembly, the measured airflow rates were increased by 8 percent and plotted in Figure 8.2-12 against the average density/pressure-drop product obtained from the test data. This adjusted data

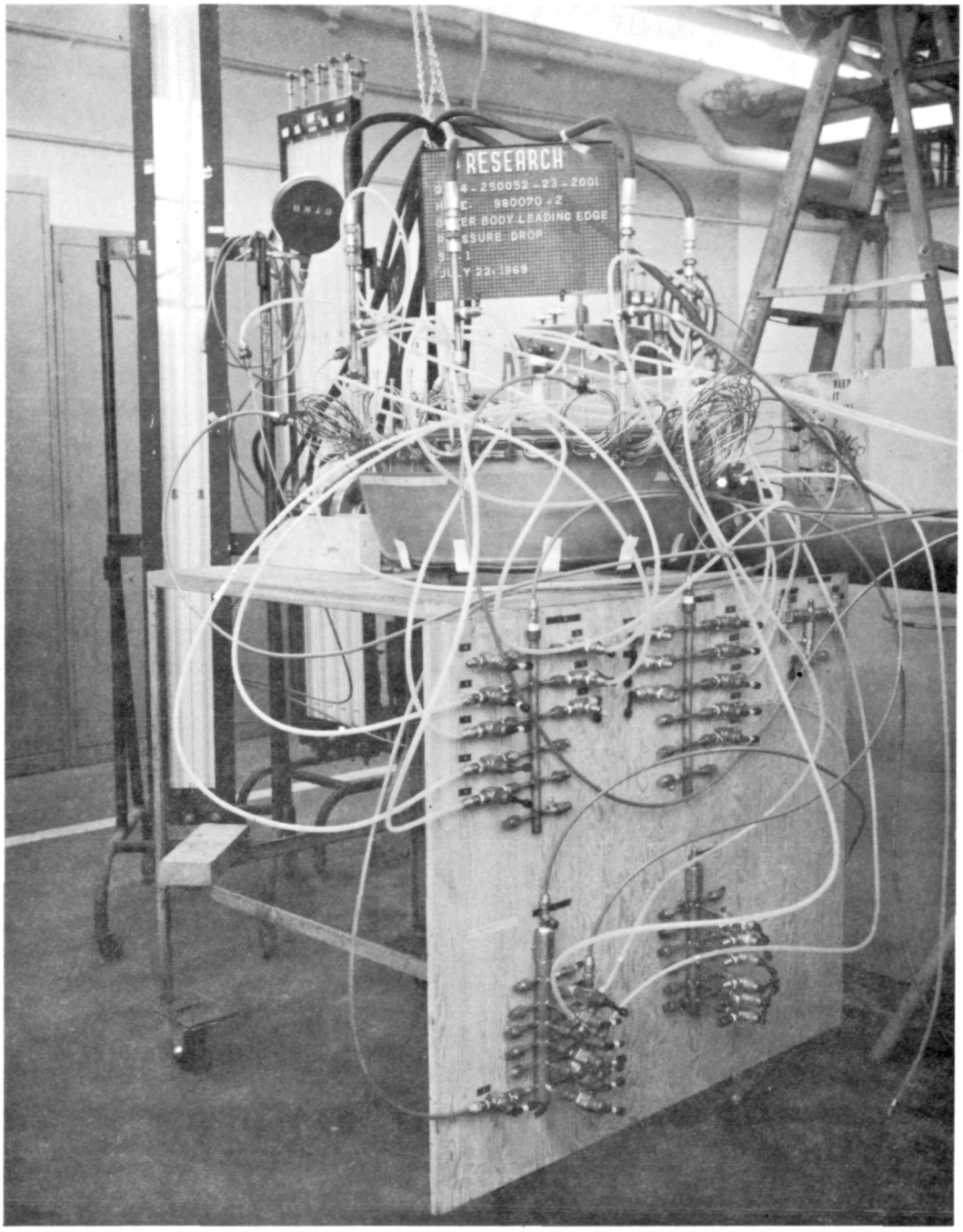

F-11115

Figure 8.2-11. Leading Edge Air-Pressure-Drop Test Setup

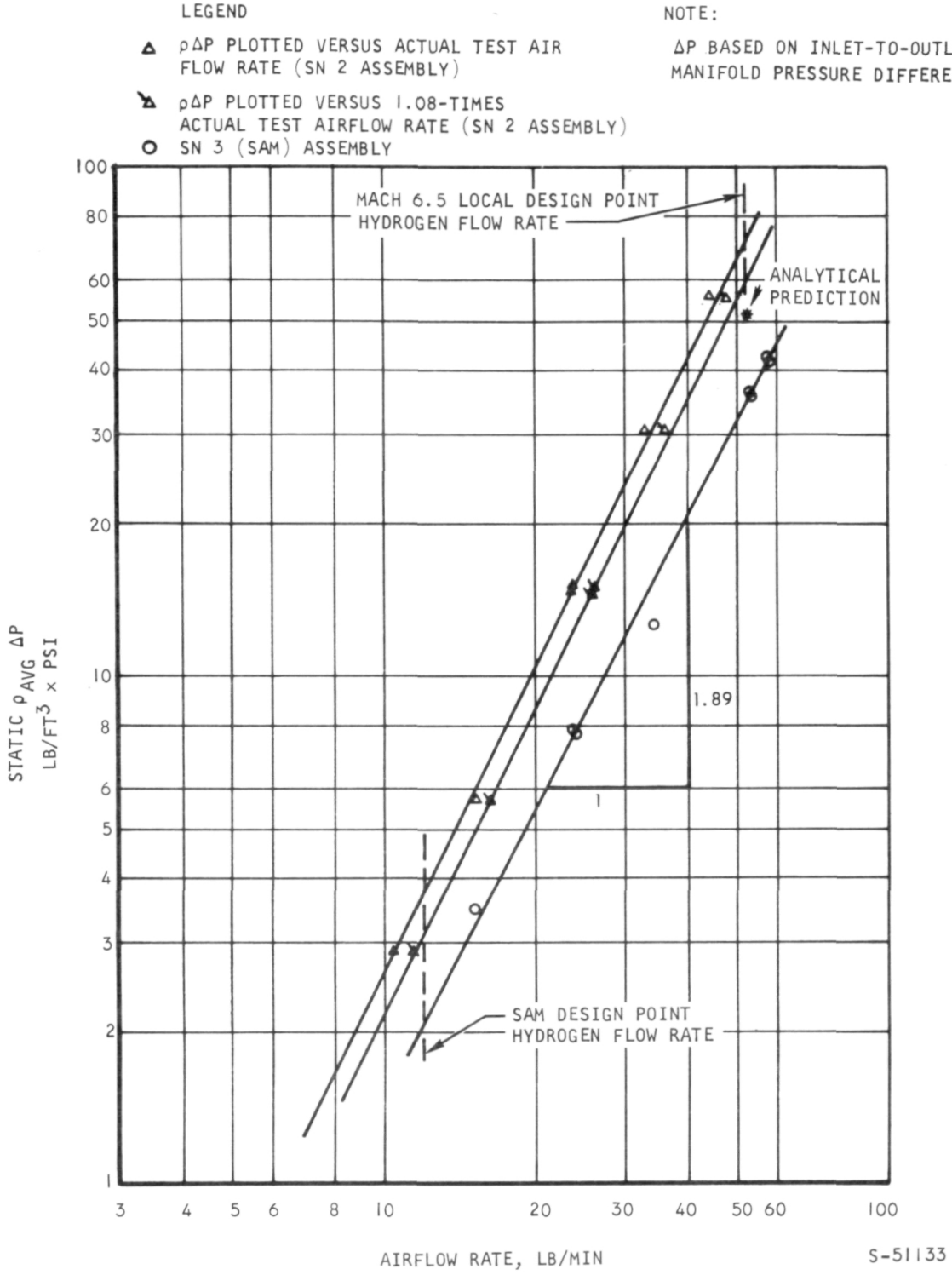

Figure 8.2-12. Leading Edge Air-Pressure Drop Test Results

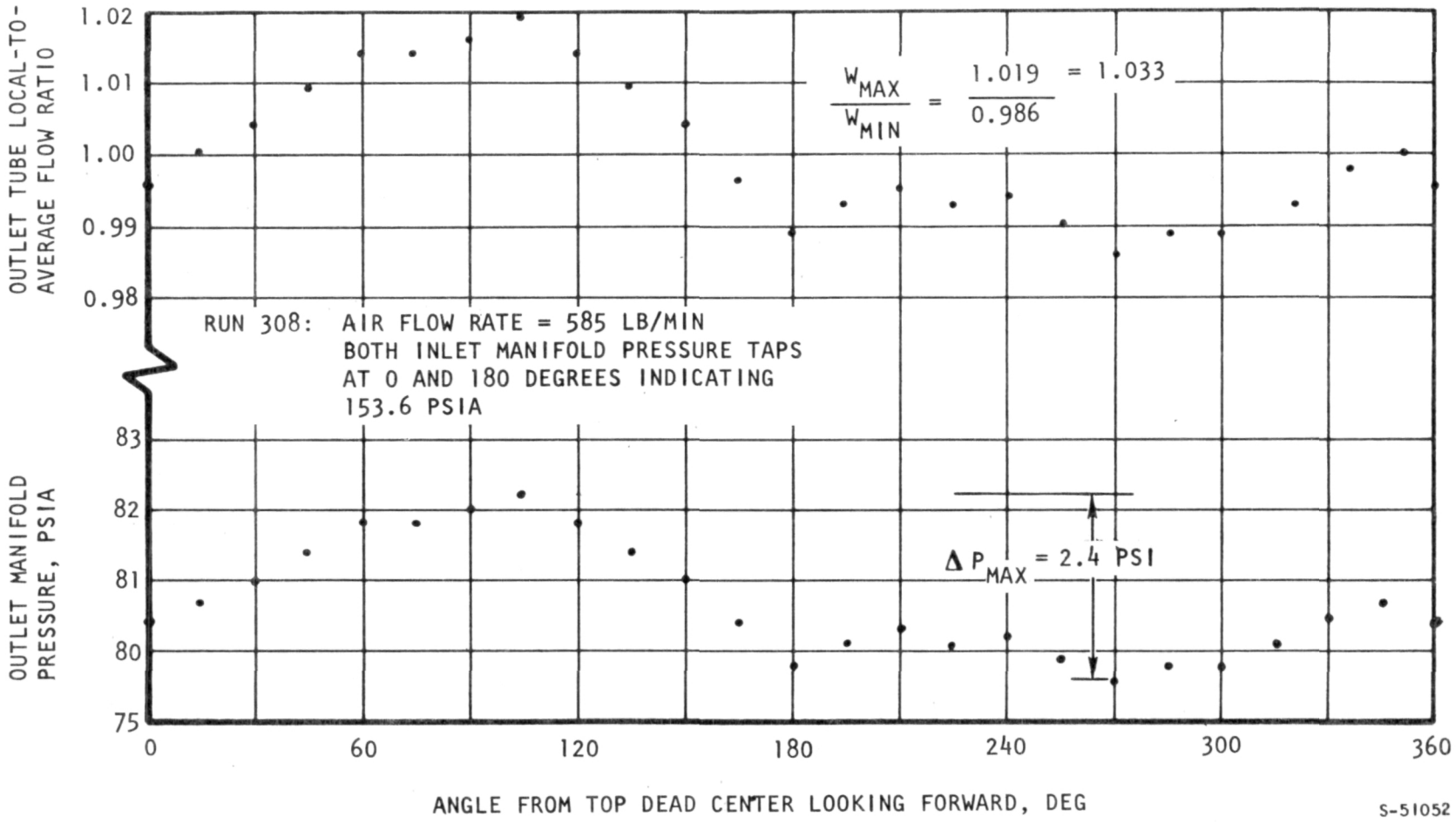

Figure 8.2-13. SAM Leading Edge Flow Distribution and Outlet Manifold Pressure

is still 15 to 20 percent above prediction and probably caused by the partially blocked fin passages and uncertainties in the prediction.

X-ray photographs of the SN 3 (SAM) assembly indicated very little braze alloy blockage of the finned passages. These observations were confirmed by the pressure drop data which was 33 percent lower than the predicted value, and 50 percent lower than SN 2 assembly test pressure drop.

The flow distribution of the SN 3 (SAM) assembly was determined, even though not originally scheduled in the test plan because of the lack of flow distribution data from the partially plugged SN 2 assembly. The two static pressure taps in the outlet manifold were insufficient to measure flow distribution; instead, flow distribution was measured by indirectly measuring the outlet manifold pressure. For one of the test runs with a steady state airflow of 58.5 lb/min flowing through the assembly, one end of a neoprene hose was connected to one of the 24 crossover tubes, with the other end connected to a pressure gage. After the pressure was recorded, the hose was removed and connected to the next crossover tube and the pressure was again recorded. This was continued for all 24 crossover tubes. It was observed that the airflow rate did not change when any of the crossover tubes was connected to the pressure gage. Also, the air exhaust to ambient pressure through the crossover tubes was choked, because the nominal of the 24 recorded pressures was 84 psia. It is noted that when each pressure was recorded, air was exhausting through 23 tubes. To find the equivalent manifold pressure with air exhausting through 24 tubes, the recorded absolute pressures were multiplied by 23/24, since for constant choked flow the supply manifold pressure is inversely proportional to the flow area. These equivalent manifold pressures are plotted in Figure 8.2-13. The flow distribution in the choked outlet tubes was then found by ratioing the local manifold pressure at each crossover tube to the average manifold pressure. This is also presented in Figure 8.2-13

The indicated local-maximum to local-minimum-flow ratio is 1.033 in the crossover tubes. This ratio would exist in the leading edge fin core if no crossflow in the manifold occurred. However, because there is a static pressure difference around the outlet manifold circumference (2.4 psi maximum) some crossflow will occur and will create a local-maximum- to local-minimum-flow ratio greater than 1.033 in the core. The predicted ratio for the leading edge core is 1.016. To assure that the section of least flow is adequately cooled during SAM wind tunnel testing, the hydrogen coolant rate should be at least 1.7 percent (half of 0.033) higher than the predicted value of 0.20 lb/sec.

8.2.5 Outer Shell

8.2.5.1 Summary

Pressure drop and flow distribution tests, using room temperature air in the coolant passages and injectors of outer shell assemblies, have been performed. Two outer shell assemblies were tested. For the first assembly, SN 1, air pressure drop and flow distribution tests were performed on both

the forward and aft outer shell coolant flow passages, with and without simulated strut sides coolant flow. For the second assembly, SN 2 (SAM), air pressure drop tests were performed on the aft outer shell coolant flow passages only, with and without simulated strut sides coolant flow. In addition, air pressure drop tests were performed on the injectors of the SN 2 assembly.

Pressure drop results from the aft outer shell coolant passages of both assemblies are very close and practically indistinguishable within the band of data scatter obtained. When compared to the Mach 6.5 local prediction, aft outer shell test data is 8 percent higher. Pressure drop results for the forward outer shell coolant passages of the SN 1 assembly are 18 percent higher than predicted. Simulating strut sides coolant flow appeared to have no effect on the pressure drop results of the aft outer shell. A simulated strut-sides flow rate of from 17.3 to 21.4 percent of the aft outer shell inlet flow rate was maintained for 15 test runs on the two outer shell assemblies. The flight engine design requires 20 percent for adequate strut sides cooling. The SN 1 forward outer shell coolant maldistribution, W_{max}/W_{min}, is 1.005, as calculated from manifold pressure distributions. The ratio of coolant flow, maximum to minimum, for the aft outer shell is less than 1.005. Both of these are acceptable.

The test setup is shown schematically in Figure 8.2-14 and photographically in Figure 8.2-15. Pressure drop data reduced to the product of static pressure drop and density at average temperature and pressure versus airflow rate are presented in Figure 8.2-16 for the forward outer shell coolant passages (SN 1 assembly only), and in Figure 8.2-17 for the aft outer shell coolant passages (both assemblies). Predicted results for hydrogen coolant at Mach 6.5 local, 88,000-ft-altitude flight conditions are included for comparison in these figures. Static pressure distributions in the SN 1 assembly manifolds are presented in Figure 8.2-18 with predicted values for the given test condition. Pressure drop results for the SN 2 assembly injectors are presented in Figure 8.2-19.

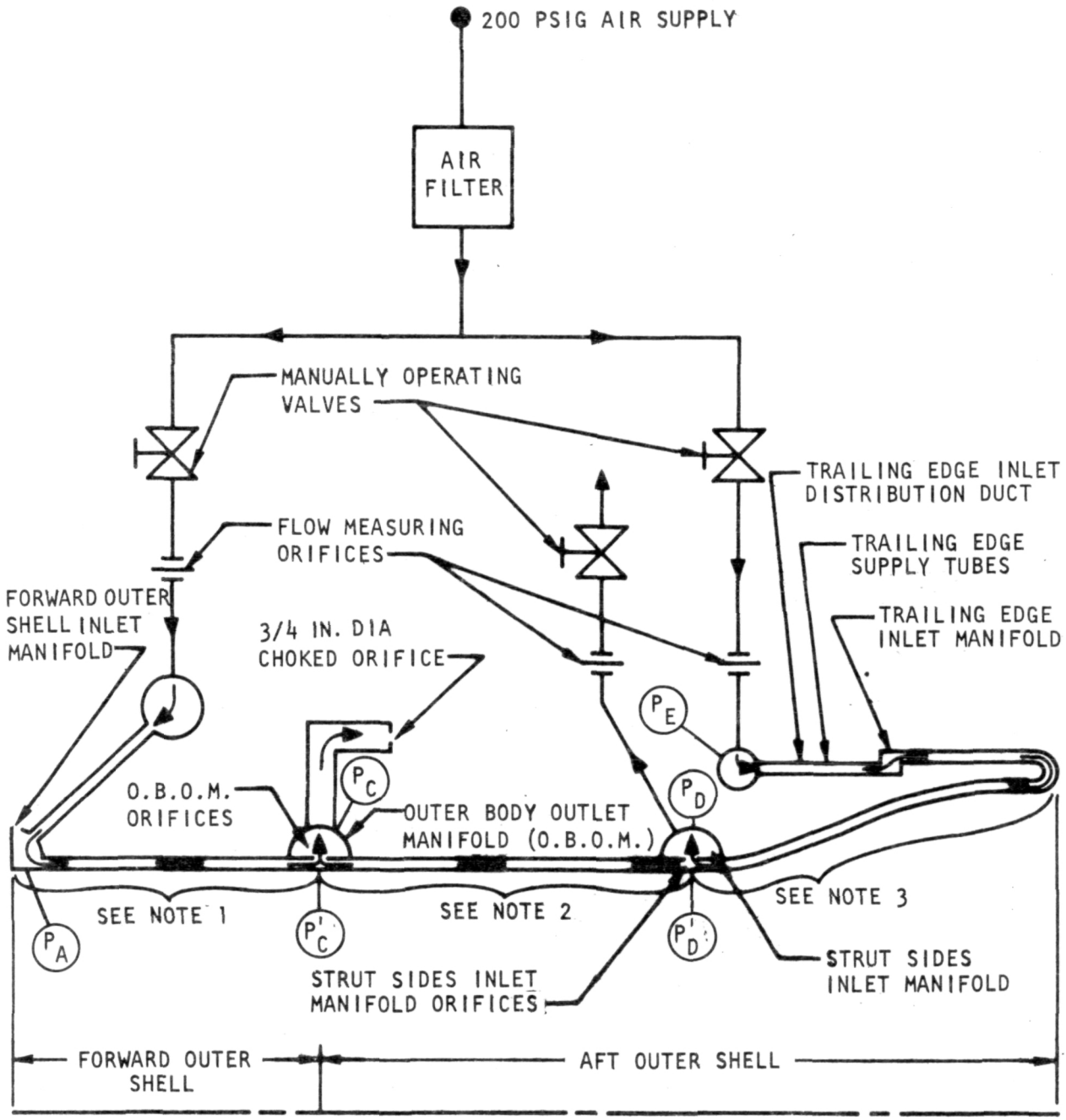

NOTES:

1. P△P FOR THIS ROUTE BASED ON PRESSURES P_A AND P'_C
2. P△P FOR THIS ROUTE BASED ON PRESSURES P_D AND P'_C
3. P△P FOR THIS ROUTE BASED ON PRESSURES P_E AND P'_D

S-51060

Figure 8.2-14. Outer Shell Assembly Air-Pressure-Drop Test Setup

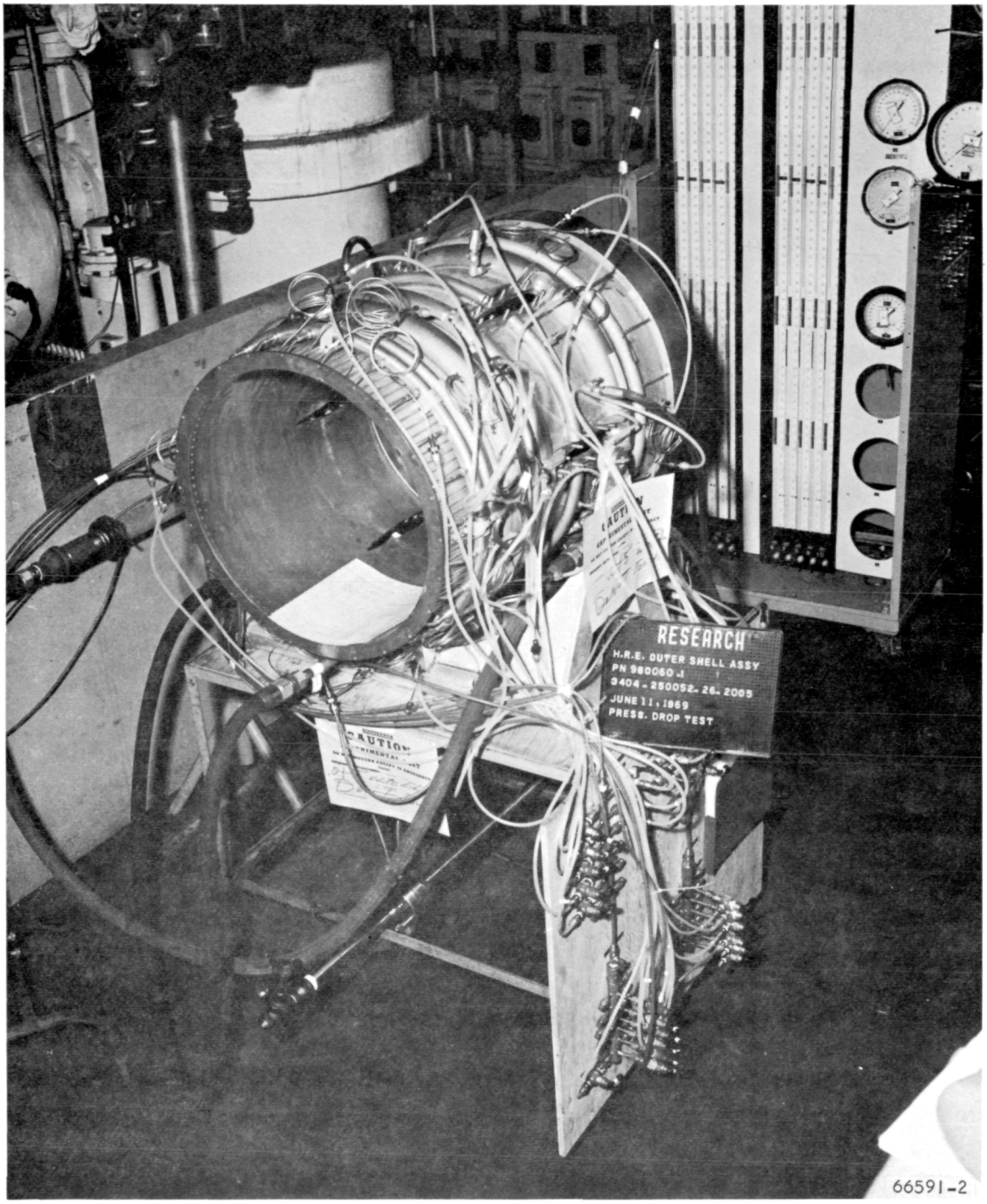

Figure 8.2-15. Outer Shell Assembly Air-Pressure-Drop Test Setup

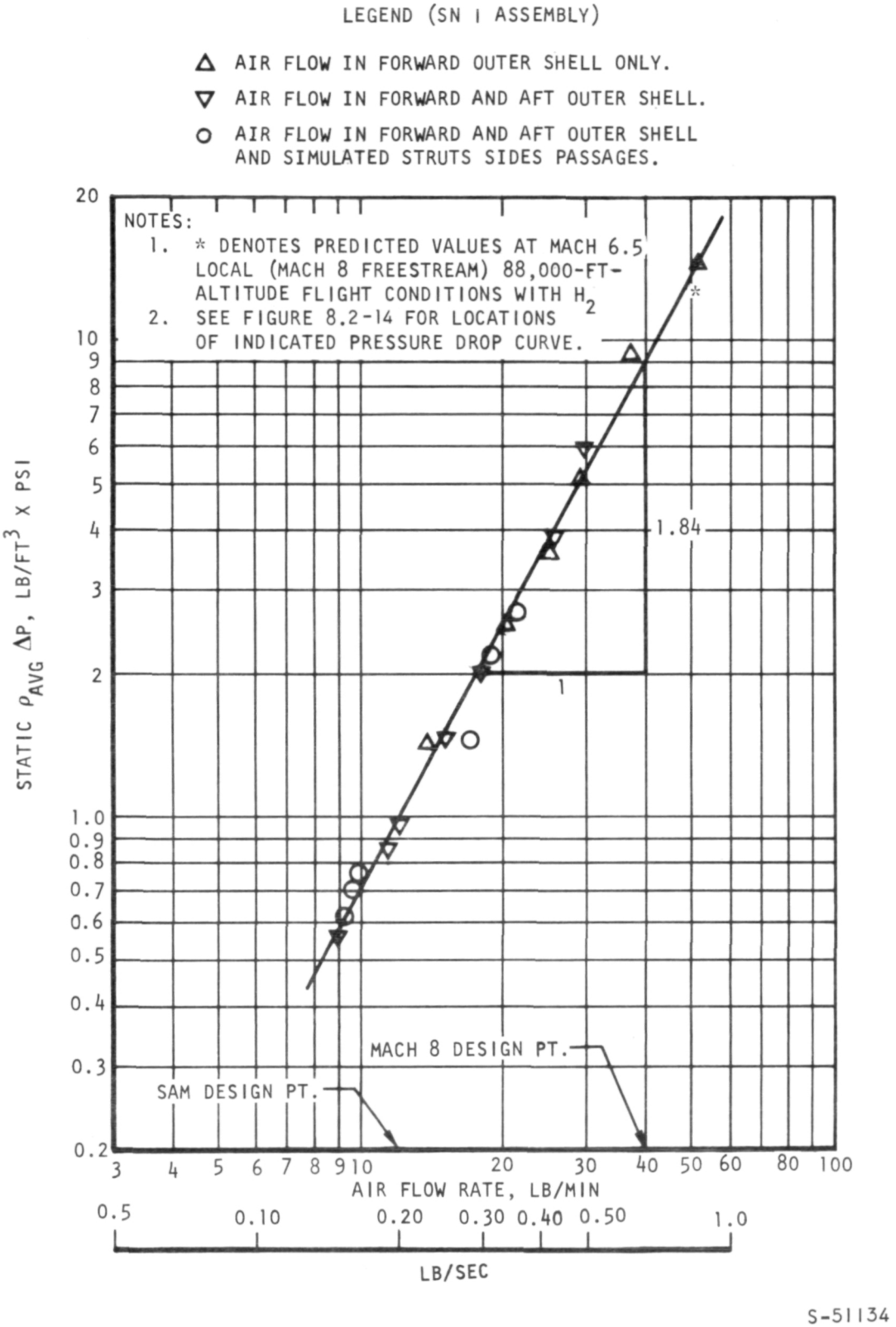

Figure 8.2-16. SN 1 Forward Outer Shell Air-Pressure-Drop Test Results

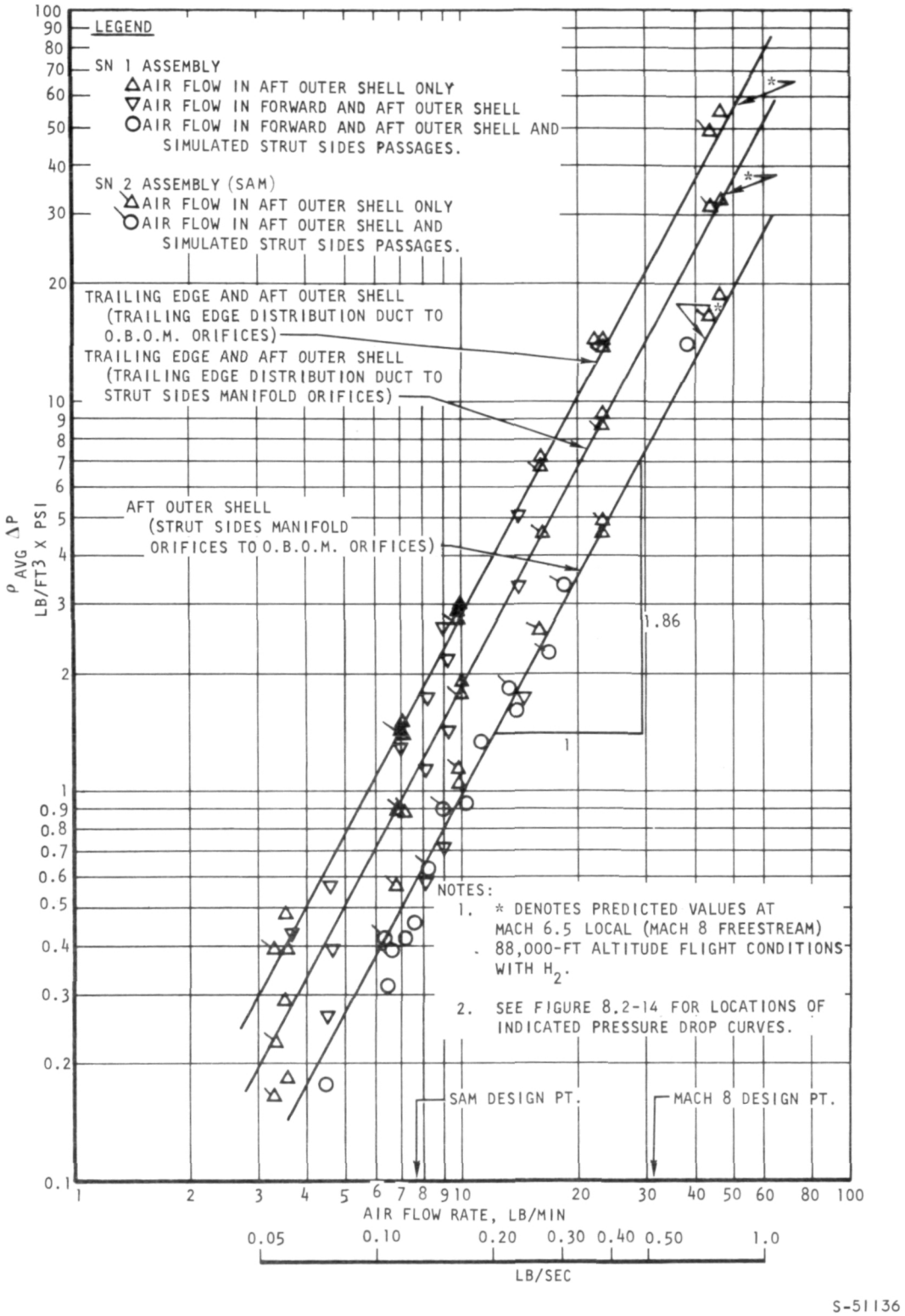

Figure 8.2-17. Aft Outer Shell Air-Pressure-Drop Test Results

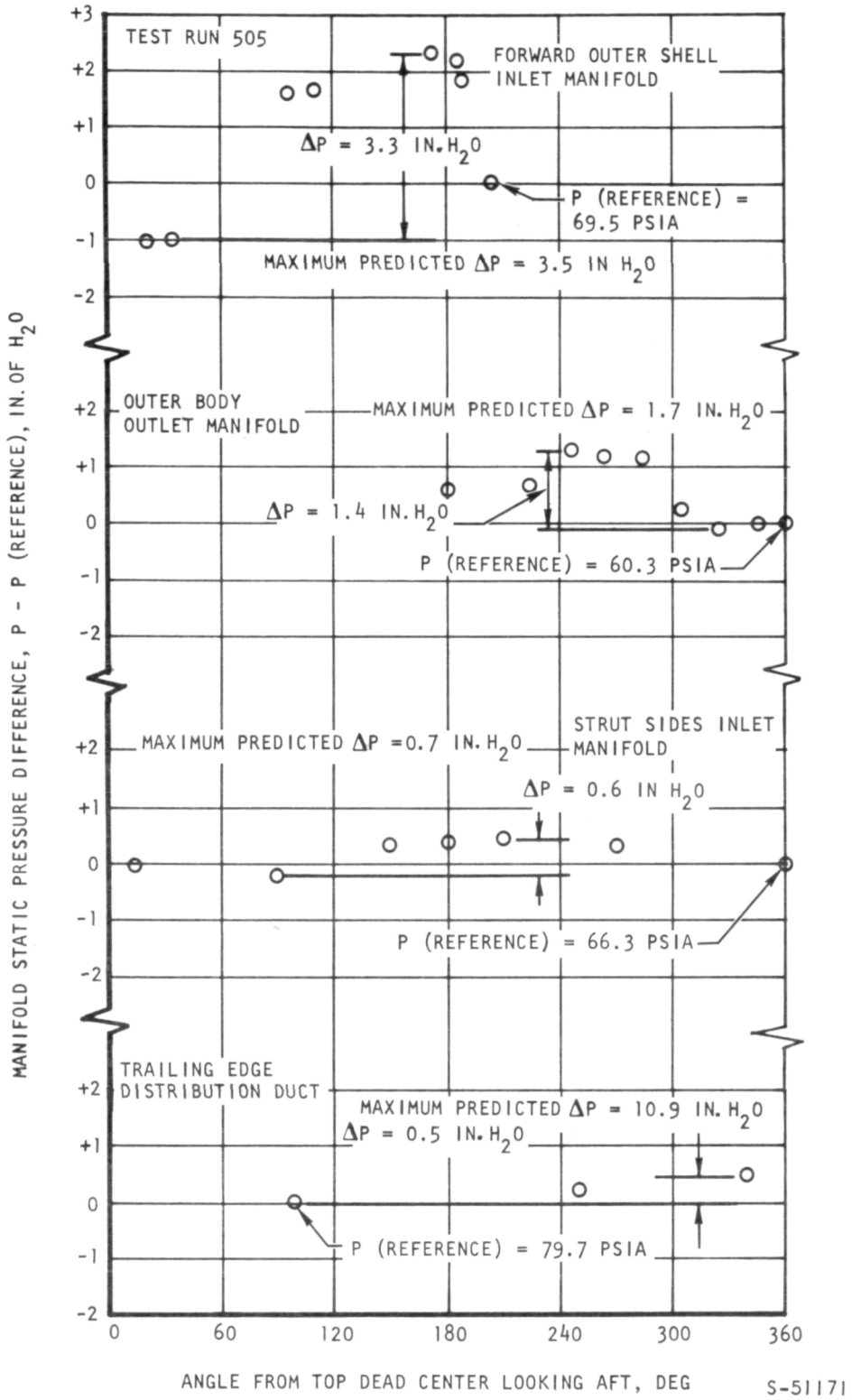

Figure 8.2-18. SN 1 Outer Shell Manifolds Pressure Distributions

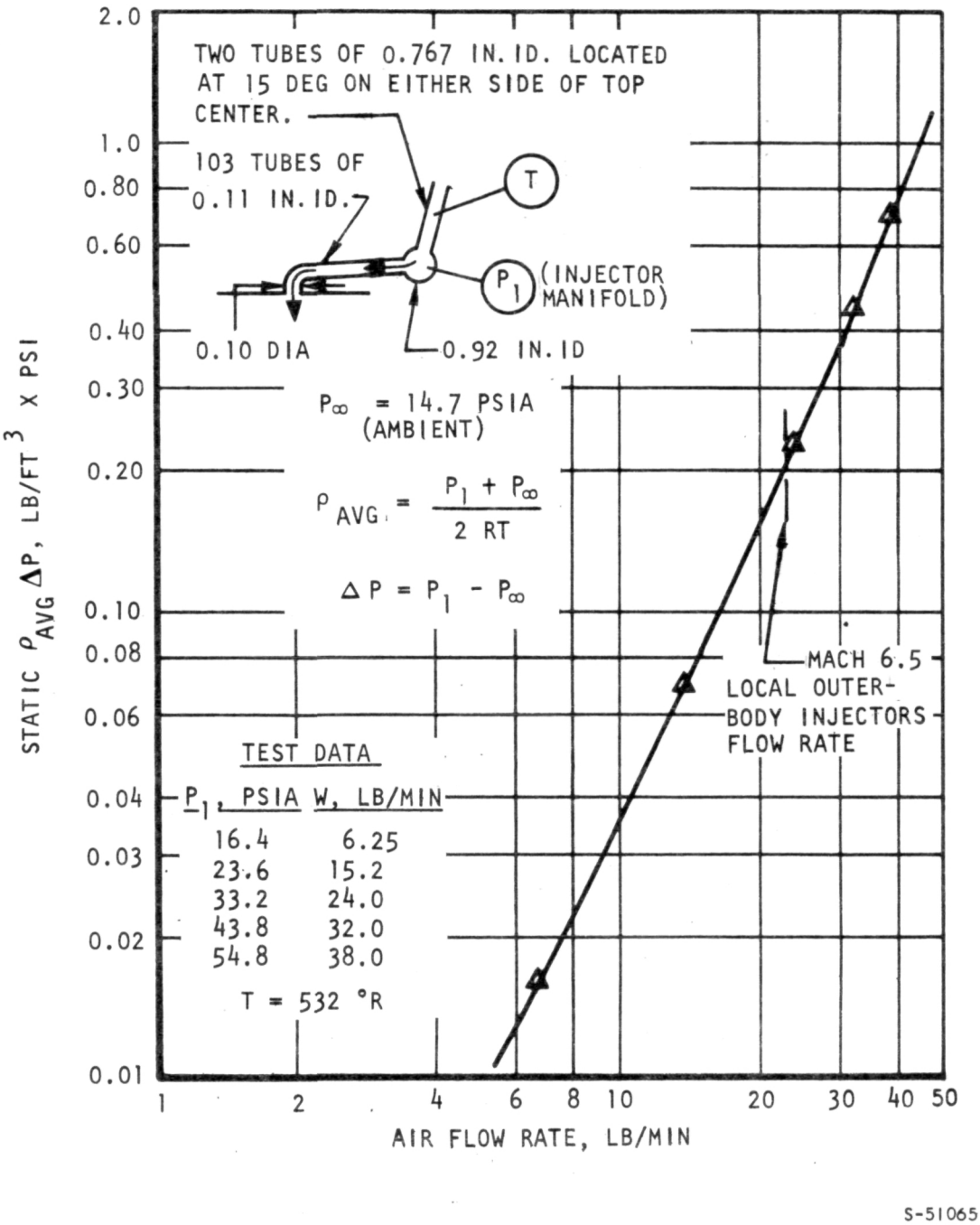

Figure 8.2-19. SN 2 (SAM) Outer Shell Injectors Air-Pressure-Drop Test Results

8.2.5.2 Discussion of Results

Ratios of the average density/static-pressure-drop product between test and Mach 6.5 local prediction for the outer shell coolant passages are summarized in the table below. The test-average density/static-pressure-drop product in these ratios was obtained by interpolating the curves at the Mach 6.5 local coolant flow rates in Figures 8.2-16 and 8.2-17. The curves in Figure 8.2-17 are the interpretation of the test data for both outer shell assemblies.

Flow Rate	$\rho\Delta P_{test}/\rho\Delta P_{predict}$
Forward outer shell	1.18
Aft outer shell (trailing edge distribution duct to strut manifold orifices)	1.22
Aft outer shell (strut manifold orifices to outerbody outlet manifold orifices)	0.95
Overall aft outer shell (trailing edge distribution duct to outerbody outlet manifold orifices)	1.08

Pressure drop test results for the forward and aft outer shells presented in Figures 8.2-16 and 8.2-17 were calculated by using the pressure in the fins just upstream of the outerbody outlet manifold orifices, rather than the measured pressure in the outerbody outlet manifold. This was done because the pressure in the outerbody outlet manifold is dependent on the sum of the forward and aft outer shell flow rates, and would result in errors of up to 5 percent if used to correlate data for either the forward or aft outer shell routes individually. The pressure in the fins just upstream of the outerbody outlet manifold orifices was found by adding the pressure drop through the orifices to the measured outlet manifold pressure. The velocity head loss for these orifices (108 holes at 0.108 in. dia) was experimentally determined by flowing air in the forward outer shell only, with the aft outer shell capped off, and measuring the pressure in the strut-sides-inlet manifold, the pressure in the outerbody outlet manifold and the airflow rate. Because the pressurized air in the aft outer shell was stagnant, the pressure in the strut-sides-inlet manifold was essentially equal to the pressure in the fins, just upstream of the outerbody outlet manifold orifices. Results indicate that the velocity head loss for these orifices is approximately 3. A value of 2.8 was used in the predictions.

The velocity head loss for the trailing edge supply tubes (18 tubes at 0.194 in. ID) was experimentally determined for the SN 2 assembly because a pressure tap was located in the trailing edge distribution duct and the

trailing edge inlet manifold. There were no trailing edge inlet manifold pressure taps in the SN 1 assembly. Results indicate that the velocity head loss for these tubes (contraction, friction and expansion) is 4.3. A corresponding value of 2.2 was used in the predictions.

Part of the outer shell testing consisted of simulating strut-sides coolant flow. This was done by connecting the six strut-sides supply tubes on the strut sides coolant manifold to a common line that had a flow measuring orifice and a valve in it. Air in this common line exhausted to atmospheric pressure downstream of the valve. The valve was manually adjusted during a calibration test to provide 20 percent of the aft outer shell inlet flow to the simulated strut-sides coolant circuit and then left intact for subsequent test runs. A 20 percent strut-sides hydrogen flow is used in the flight engine design. For subsequent test runs, the simulated strut-sides airflow rate varied from 17.4 to 21.4 percent of the aft outer shell inlet flow. These deviations from 20 percent were caused by different combinations of aft outer shell downstream pressure in the outerbody outlet manifold with respect to the constant atmospheric pressure at the outlet of the simulated strut-sides flow circuit. Pressure drop results for the aft outer shell (strut-sides coolant-manifold orifices to outerbody outlet-manifold orifices appear to be unaffected by the simulated strut-sides coolant flow when the flow rate in this part of the aft outer shell is adjusted in the data reduction for the simulated strut-sides flow rate.

A 3/4-in.-dia orifice was attached to the outer shell assembly outlet. This was done to provide a high back pressure in the outerbody outlet manifold so that choking occurred at this orifice and not in the coolant passages, particularly in the outerbody outlet manifold orifices. Choking was eliminated so that the air-pressure-drop data can be applied directly to hydrogen cooled-passage flow conditions which are not choked. The outlet orifice, which was exposed to atmospheric pressure on the downstream side, was choked for most test runs.

Differential pressures relative to a reference static pressure were measured in the forward outer shell inlet manifold, the trailing edge distribution duct, the strut-sides-inlet manifold, and the outerbody-outlet manifold of the SN 1 assembly. Pressure distribution results plotted in Figure 8.2-18 indicate that the maximum circumferential pressure difference for all manifolds is 3.3 in. of H_2O (0.10 psi) and occurs in the forward outer shell inlet manifold. The predicted circumferential pressure difference for this manifold is 3.5 in. of H_2O with test conditions of 21.3 lb/min in the forward outer shell, 16.8 lb/min entering the trailing edge, and 3.1 lb/min in the simulated strut-sides circuit. The 3.3 in. of H_2O manifold pressure difference indicates that the flow maldistribution parameter, W_{max}/W_{min} for the forward outer shell is 1.005. The flow maldistribution parameter for the aft outer shell, based on the recorded manifold pressure distribution, is less than 1.005.

X-ray photographs of the outer two shell assemblies were examined, and indicated relatively small amounts of braze alloy blockage of finned passages in the SN 1 assembly. These blockages did not affect the test results.

8.3 INLET SPIKE ACTUATOR

The previous TDR, Reference 5-1, presented results of the tests on the two inlet spike actuators fabricated on the program. Following completion of the endurance testing, the actuator used in this test was disassembled and inspected. The results of the inspection were reported, but photographs of the various parts were not available at time of publication. These photographs are presented in this report and discussed briefly below:

Figure 8.3-1--The assembly of the inlet spike actuation system prior to endurance testing is shown in this photograph. The external cylinder and the six mounting legs constitute the structural housing; the forward portion of the slide assembly, attached to the actuator rod end, appears at the right of the photograph, and the hydraulic accumulator at the left. The servovalve is visible at the bottom, between mounting legs.

Figure 8.3-2--This is a view of the hydraulic actuator, showing the rod-end assembly at the left, and the universal assembly at the right. The rod end attaches to the structural slide assembly, and the universal assembly is ridigly mounted to the structural housing. The LVDT (linear variable differential transformer) is mounted to the side of the actuator cylinder. The hydraulic manifold fittings and inlet and outlet tubes are at the top right.

Figure 8.3-3--The Fabroid journal bearing is shown installed in the structural housing following the endurance test. Debris from the bearing is visible on the housing walls. Although the bearings experienced considerable wear during the test, their performance remained satisfactory throughout the test.

Figure 8.3-4--The Fabroid journal bearing in the slide assembly. The same comments apply as for Figure 8.3-3.

Figure 8.3-5--The actuator piston assembly is shown. After the endurance test, this assembly showed no unacceptable signs of wear except for the locking mechanism.

Figure 8.3-6--The actuator locking cams showed considerable wear at the conclusion of the endurance test. Metallic particles found in the actuator and shown in the photograph were traced to the locking cams. Before use of the actuator in the SAM, redesign of the locking cams and of the cam seats in the actuator cylinder will be undertaken to remedy this problem.

Figure 8.3-7--Following endurance testing, the Fabroid used in the actuator rod end was found to have become extruded. Substitution of a conventional, all-metallic spherical bearing in the rod end will satisfactorily solve this problem and be used in the SAM actuator.

Figure 8.3-8--The universal pin was deformed at the conclusion of endurance testing. This pin will be strengthened by increasing its diameter before use of the actuator in the SAM.

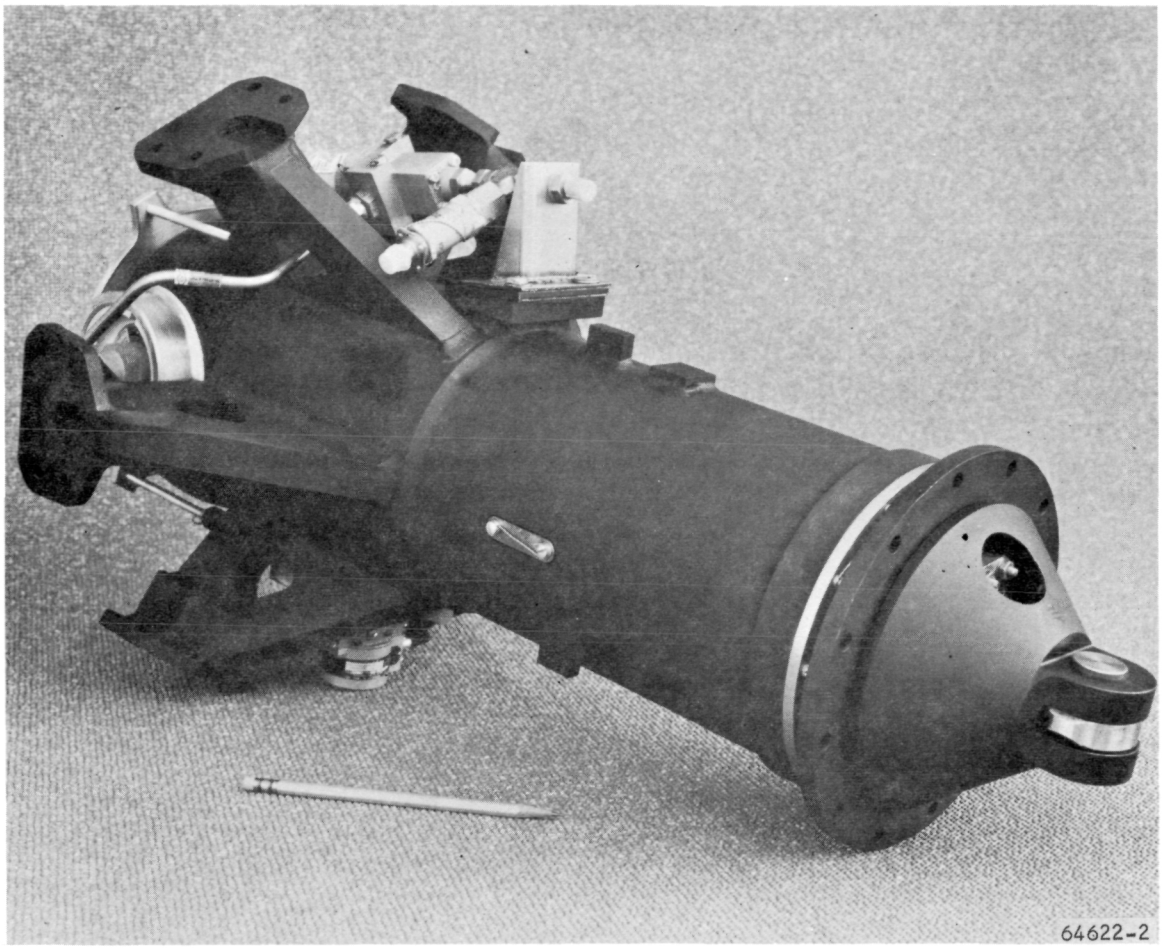

Figure 8.3-1. Inlet Spike Actuation System Assembly

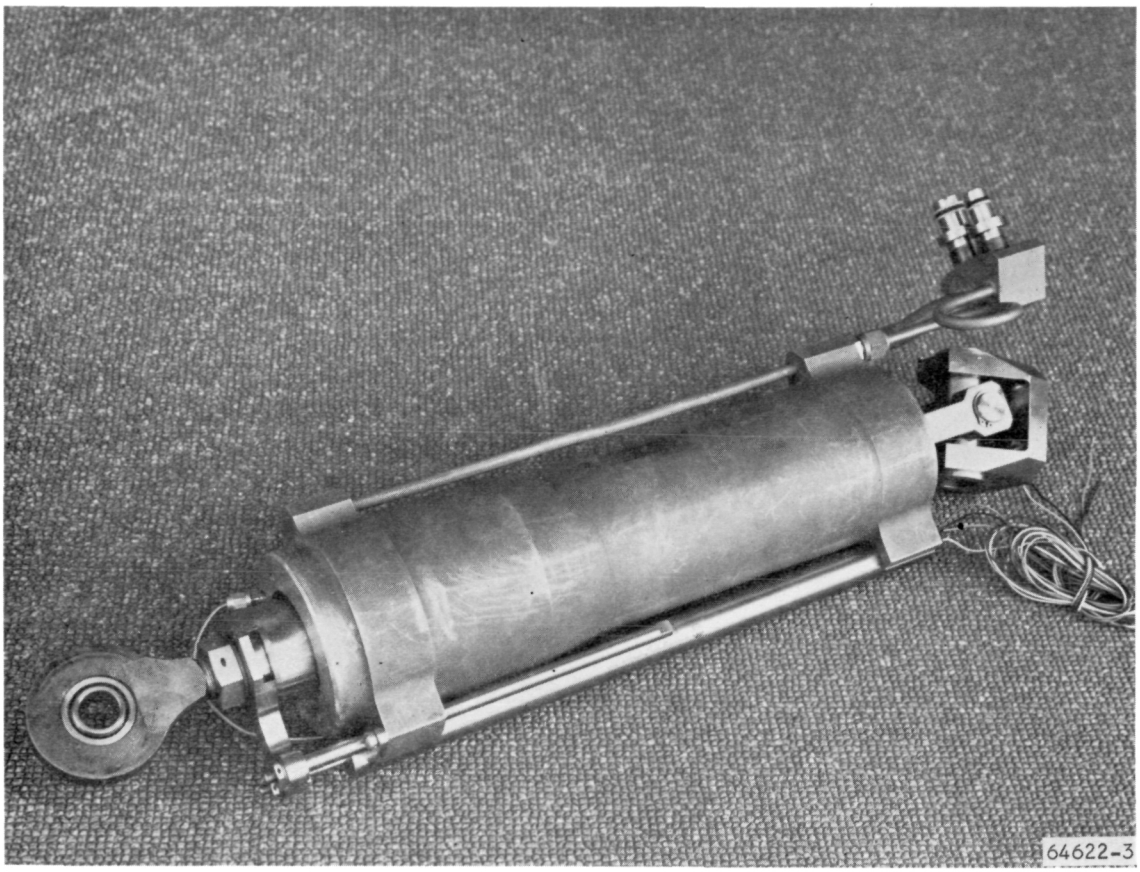

Figure 8.3-2. Hydraulic Actuator for Inlet Spike Actuation System Assembly

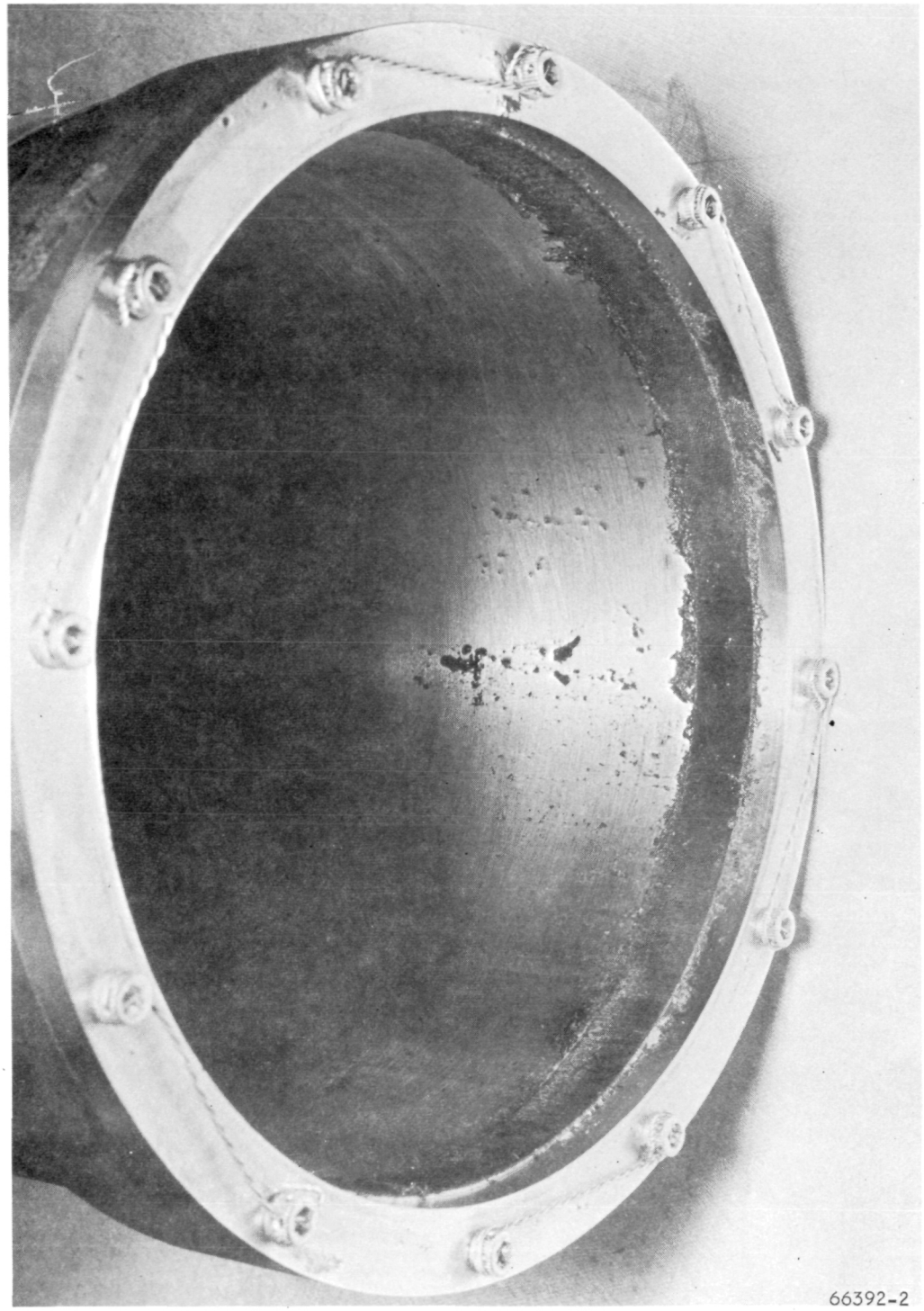

Figure 8.3-3. Fabroid Journal Bearing in Structural Housing After Endurance Test

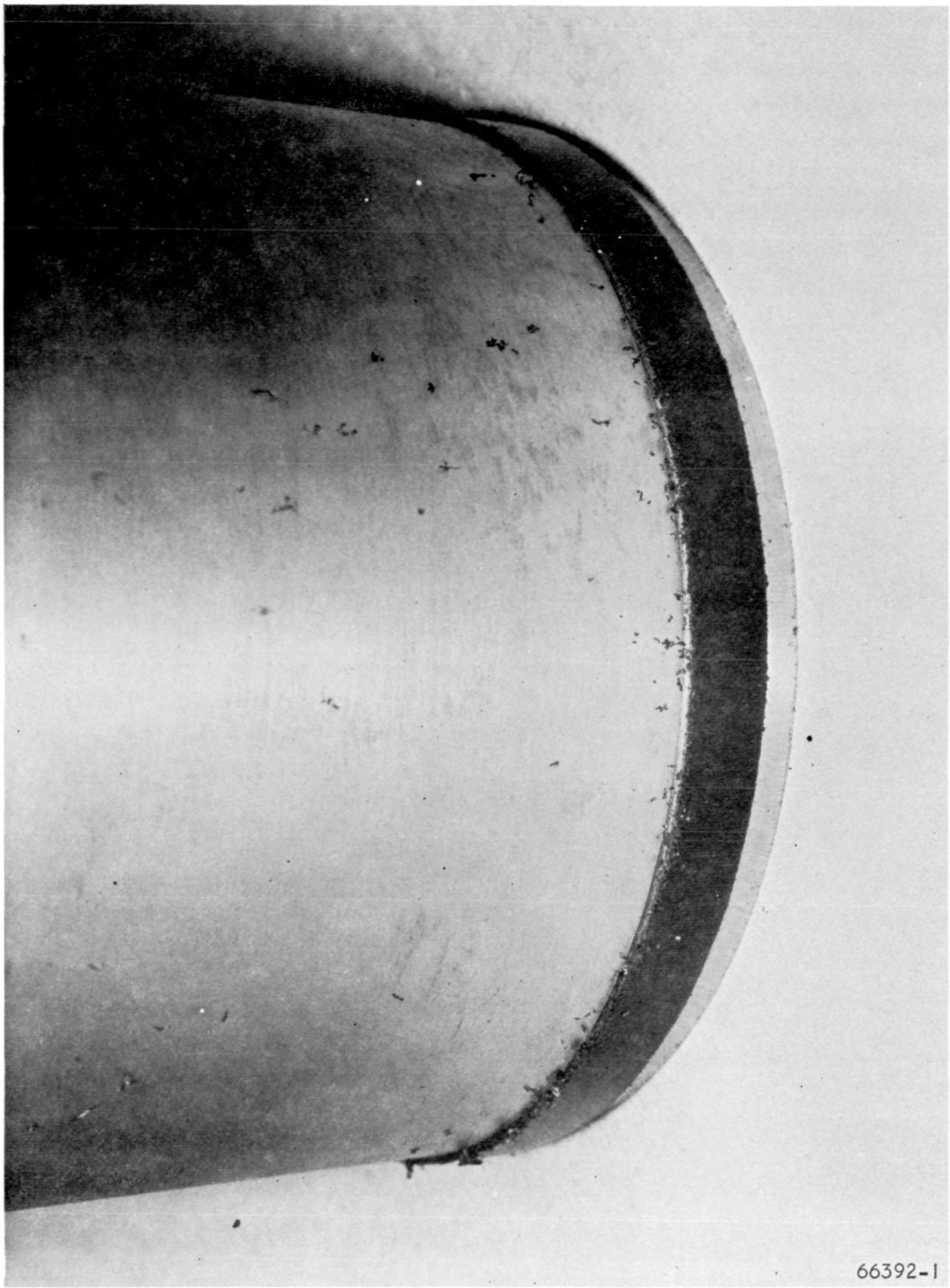

Figure 8.3-4. Fabroid Journal Bearing in Slide Assembly After Endurance Test

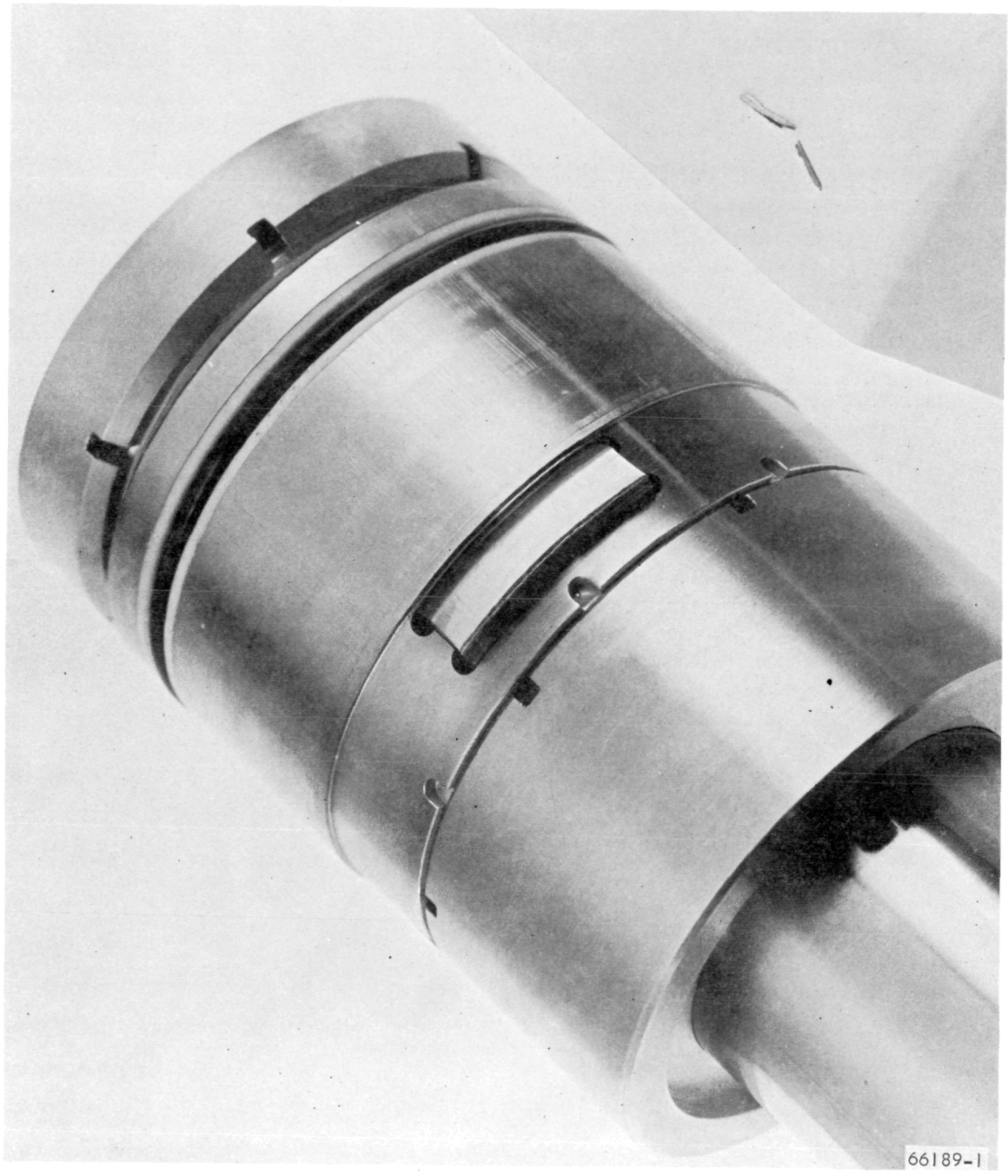

Figure 8.3-5. Actuator Piston Assembly After Endurance Test

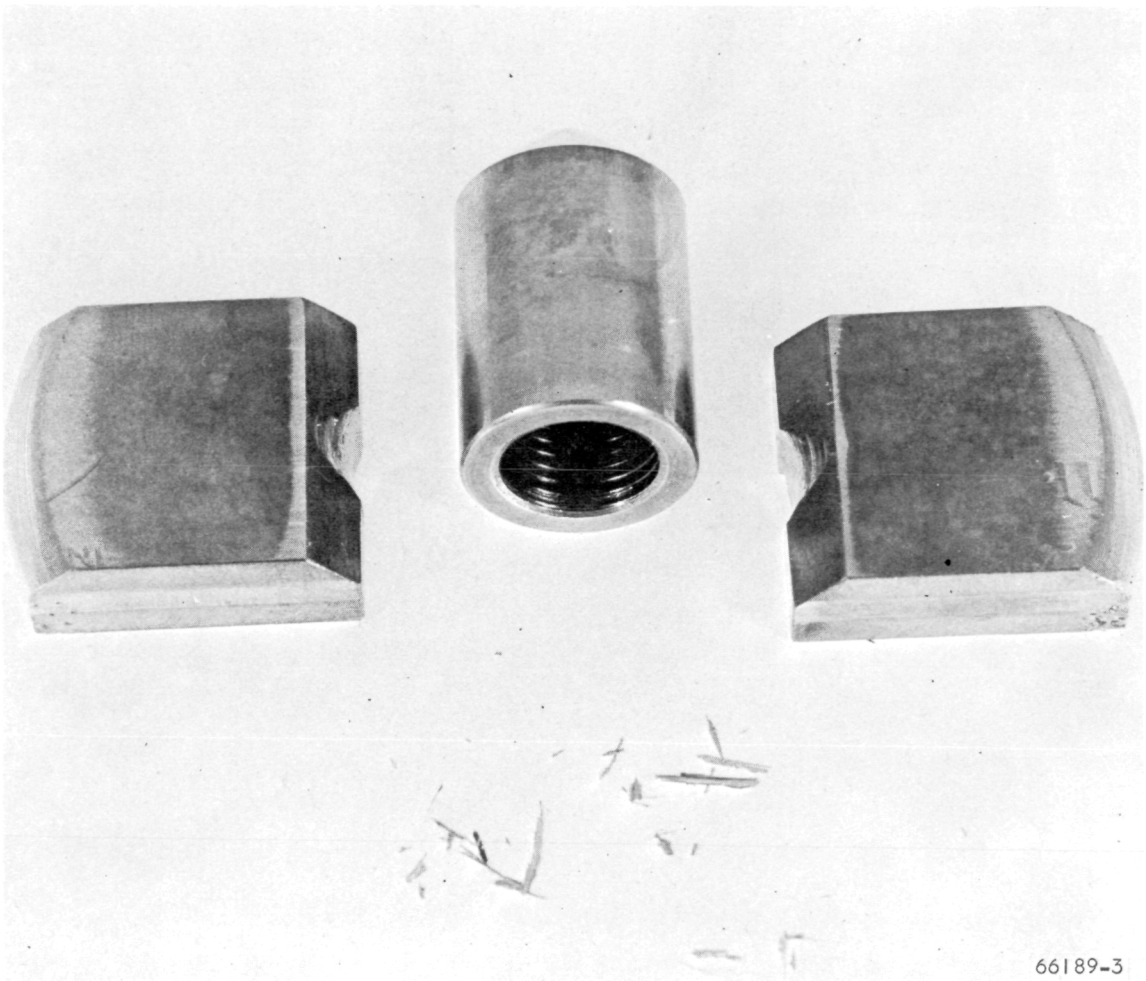

Figure 8.3-6. Actuator Locking Cams and Piston After Endurance Test

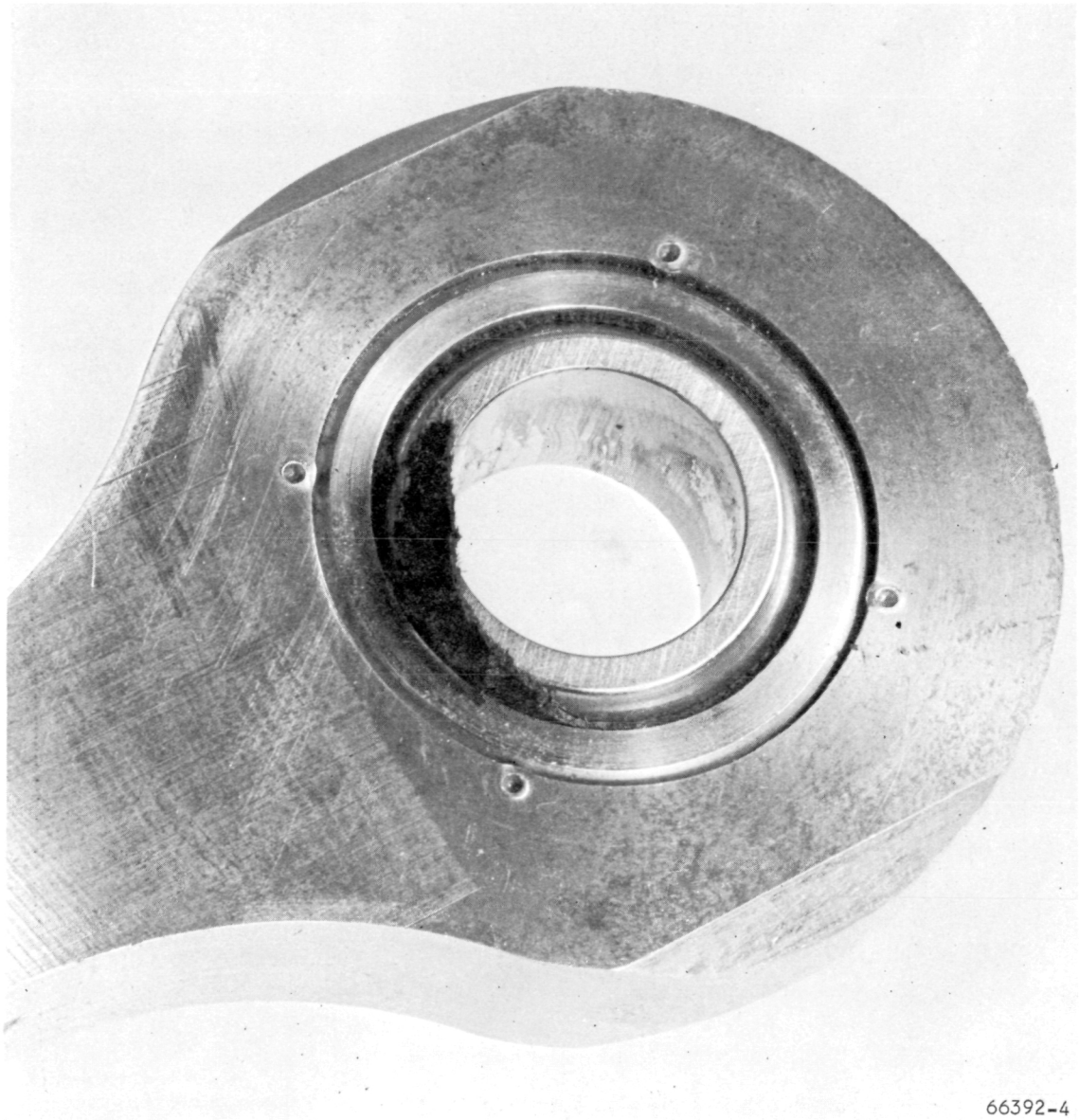

66392-4

Figure 8.3-7. Actuator Rod-End Assembly After Endurance Test Showing Extruded Fabroid

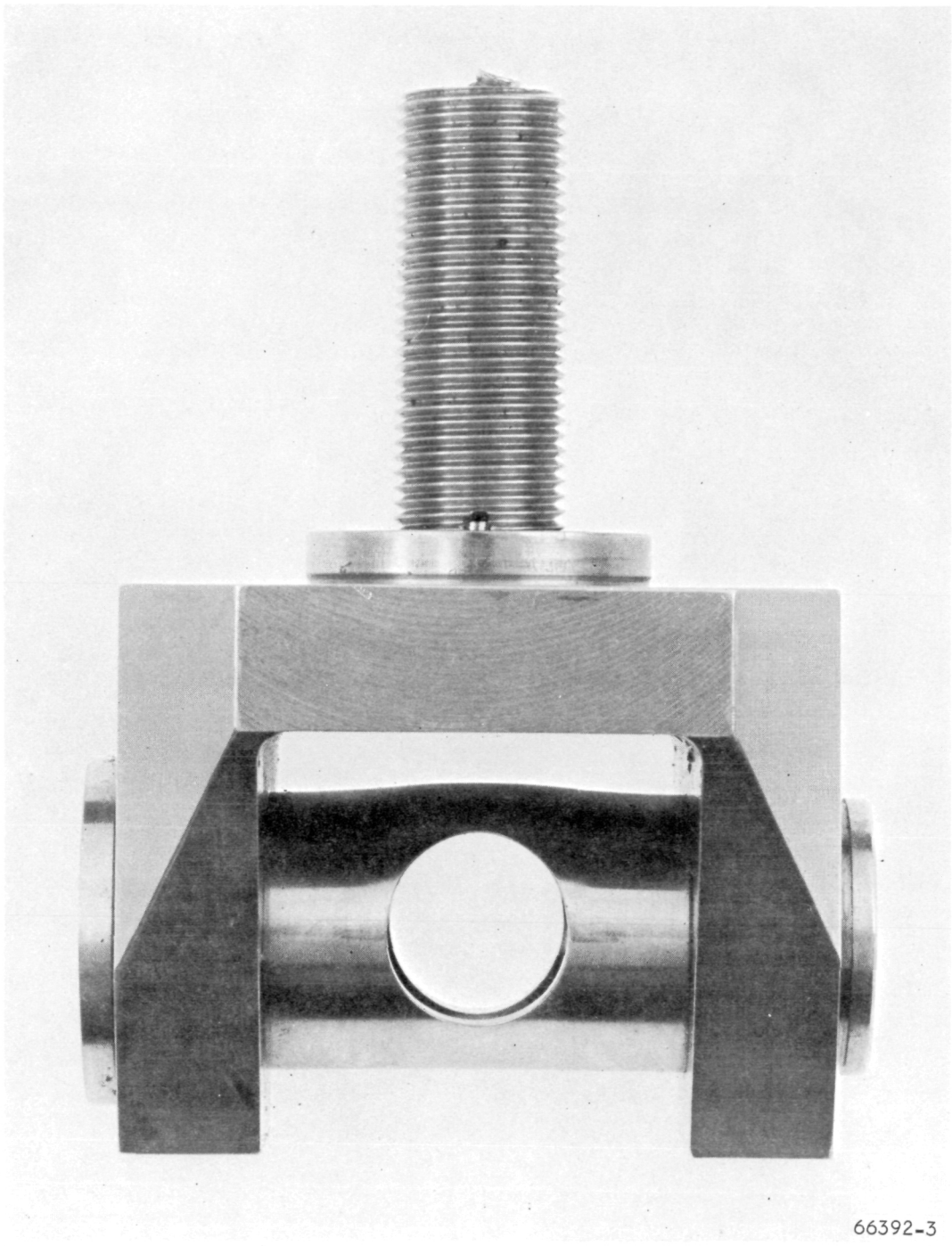

Figure 8.3-8. Actuator Universal Hub and Pin After Endurance Test Showing Deformation of Pin

9. FUTURE ACTION

Scheduled activities for the next reporting period will consist of the following:

(a) Formal design review of the SAM wind tunnel configuration.

(b) Release of assembly and detail drawings of the SAM and its water-cooled mounting structure and cowl/pylon.

(c) Placement of purchase orders for long-lead time parts and raw material.

REFERENCES

5-1 Engineering Staff, Hypersonic Research Engine Project - Phase IIA, Structures and Cooling Development, Ninth Interm Technical Data Report, Data Item 55-7.09, AiResearch Report No. AP-69-5075, 3 June 1969.

5-2 Fay, J. A. and F. R. Riddell, "Theory of Stagnation Point Heat Transfer in Dissociated Air", Journal of Aeronautical Sciences, Vol. 25, No. 2, February 1958.

5-3 Engineering Staff, Hypersonic Research Engine Project - Phase IIA, Structures and Cooling Development, Fifth Interim Technical Data Report, Data Item, 55-7.05, AiResearch Report No. AP-68-3754, 12 May 1968.

5-4 Edney, B. E. "Effects of Shock Impingement on the Heat Transfer Around Blunt Bodies", AIAA Journal, Vol. 6, No. 1, January 1968.

5-5 Hiers, Robert S. and Wm. J. Loubsky, "Effects of Shock-Wave Impingement on the Heat Transfer on a Cylindrical Leading Edge", NASA IN D-3859, 1957.

5-6 Teterin, M. P., "Investigation of a Supersonic Gas Flow and Heat Transfer in the Region of an Incident Shock Wave on a Cylinder", NASA TT F-11, 795.

5-7 Bushnell, Dennis M., "Effects of Shock Impingement and Other Factors on Leading Edge Heat Transfer", NASA TN D-4543 1968.

5-8 Kestin, J., "The Effect of Freestream Turbulence on Heat Transfer Rates" Advances in Heat Transfer, Chapter 1, by T. F. Irvine and J. P. Hortnett, Academic Press, 1966.

8-1 Engineering Staff, Hypersonic Research Engine Project - Phase IIA, Structures and Cooling Development, Eight Interim Technical Data Report, Data Item 55-7.08, AiResearch Report No. AP-69-4759, 27 February 1969.

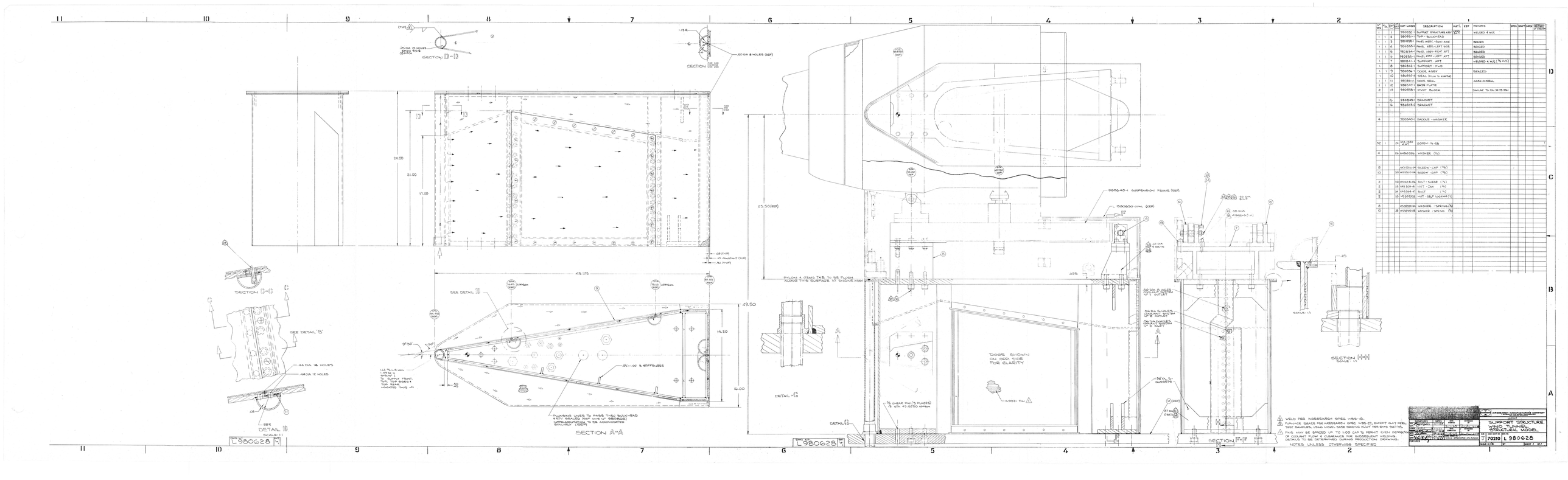
SECTION C-C
SECTION D-D
SECTION E-E
SECTION F-F
SECTION A-A
SECTION H-H
DETAIL B
DETAIL G
DETAIL J
SEE DETAIL 'B'
SEE DETAIL 'D'
.44 DIA 14 HOLES
.44 DIA 12 HOLES
.60 DIA 8 HOLES (REF)
.50 DIA 13 HOLES EACH SIDE STATION
PLUMBING LINES TO PASS THRU BULKHEAD & BE BRAZED (NOT SHN W/ 980808)
INSULATION TO BE ASSOCIATED SEPARATELY (REF)
DOOR SHOWN ON OPP. SIDE FOR CLARITY
980540-1 SUSPENSION TRUNK (REF)
980550 COIL (REF)
34.00
21.00
17.20
25.50(REF)
49.50
14.20
6.00
43.375
9.50
.425
.68
.88
.40 (TYP)
.10 CHAMFER (TYP)
.50 (TYP)
.75
.25
.50
.38
.19
SCALE: 1/2
SCALE: 1/8
SCALE: 1/4
SCALE: 1/1
SCALE: 1/3
SCALE: 1/16
SCALE: 1/12
SCALE: 1/10
SCALE: 1/5
SCALE: 1/15
SCALE: 1/20
SCALE: 1/30
SCALE: 1/40
SCALE: 1/50
SCALE: 1/60
SCALE: 1/80
SCALE: 1/100
SCALE: 1/120
SCALE: 1/160
SCALE: 1/200
SCALE: 1/240
SCALE: 1/320
SCALE: 1/400
SCALE: 1/480
SCALE: 1/640
SCALE: 1/800
SCALE: 1/960
SCALE: 1/1200
SCALE: 1/1600
SCALE: 1/2000
SCALE: 1/2400
SCALE: 1/3200
SCALE: 1/4000
SCALE: 1/4800
SCALE: 1/6400
SCALE: 1/8000
SCALE: 1/9600
SCALE: 1/12000
SCALE: 1/16000
SCALE: 1/20000
SCALE: 1/24000
SCALE: 1/32000
SCALE: 1/40000
SCALE: 1/48000
SCALE: 1/64000
SCALE: 1/80000
SCALE: 1/96000
SCALE: 1/120000
SCALE: 1/160000
SCALE: 1/200000
SCALE: 1/240000
SCALE: 1/320000
SCALE: 1/400000
SCALE: 1/480000
SCALE: 1/640000
SCALE: 1/800000
SCALE: 1/960000
SCALE: 1/1200000
SCALE: 1/1600000
SCALE: 1/2000000
SCALE: 1/2400000
SCALE: 1/3200000
SCALE: 1/4000000
SCALE: 1/4800000
SCALE: 1/6400000
SCALE: 1/8000000
SCALE: 1/9600000
SCALE: 1/12000000
SCALE: 1/16000000
SCALE: 1/20000000
SCALE: 1/24000000
SCALE: 1/32000000
SCALE: 1/40000000
SCALE: 1/48000000
SCALE: 1/64000000
SCALE: 1/80000000
SCALE: 1/96000000
SCALE: 1/120000000
SCALE: 1/160000000
SCALE: 1/200000000
SCALE: 1/240000000
SCALE: 1/320000000
SCALE: 1/400000000
SCALE: 1/480000000
SCALE: 1/640000000
SCALE: 1/800000000
SCALE: 1/960000000
SCALE: 1/1200000000
SCALE: 1/1600000000
SCALE: 1/2000000000
SCALE: 1/2400000000
SCALE: 1/3200000000
SCALE: 1/4000000000
SCALE: 1/4800000000
SCALE: 1/6400000000
SCALE: 1/8000000000
SCALE: 1/9600000000
SCALE: 1/12000000000
SCALE: 1/16000000000
SCALE: 1/20000000000
SCALE: 1/24000000000
SCALE: 1/32000000000
SCALE: 1/40000000000
SCALE: 1/48000000000
SCALE: 1/64000000000
SCALE: 1/80000000000
SCALE: 1/96000000000
SCALE: 1/120000000000
SCALE: 1/160000000000
SCALE: 1/200000000000
SCALE: 1/240000000000
SCALE: 1/320000000000
SCALE: 1/400000000000
SCALE: 1/480000000000
SCALE: 1/640000000000
SCALE: 1/800000000000
SCALE: 1/960000000000
SCALE: 1/1200000000000
SCALE: 1/1600000000000
SCALE: 1/2000000000000
SCALE: 1/2400000000000
SCALE: 1/3200000000000
SCALE: 1/4000000000000
SCALE: 1/4800000000000
SCALE: 1/6400000000000
SCALE: 1/8000000000000
SCALE: 1/9600000000000
SCALE: 1/12000000000000
SCALE: 1/16000000000000
SCALE: 1/20000000000000
SCALE: 1/24000000000000
SCALE: 1/32000000000000
SCALE: 1/40000000000000
SCALE: 1/48000000000000
SCALE: 1/64000000000000
SCALE: 1/80000000000000
SCALE: 1/96000000000000
SCALE: 1/120000000000000
SCALE: 1/160000000000000
SCALE: 1/200000000000000
SCALE: 1/240000000000000
SCALE: 1/320000000000000
SCALE: 1/400000000000000
SCALE: 1/480000000000000
SCALE: 1/640000000000000
SCALE: 1/800000000000000
SCALE: 1/960000000000000
SCALE: 1/1200000000000000
SCALE: 1/1600000000000000
SCALE: 1/2000000000000000
SCALE: 1/2400000000000000
SCALE: 1/3200000000000000
SCALE: 1/4000000000000000
SCALE: 1/4800000000000000
SCALE: 1/6400000000000000
SCALE: 1/8000000000000000
SCALE: 1/9600000000000000
SCALE: 1/12000000000000000
SCALE: 1/16000000000000000
SCALE: 1/20000000000000000
SCALE: 1/24000000000000000
SCALE: 1/32000000000000000
SCALE: 1/40000000000000000
SCALE: 1/48000000000000000
SCALE: 1/64000000000000000
SCALE: 1/80000000000000000
SCALE: 1/96000000000000000
SCALE: 1/120000000000000000
SCALE: 1/160000000000000000
SCALE: 1/200000000000000000
SCALE: 1/240000000000000000
SCALE: 1/320000000000000000
SCALE: 1/400000000000000000
SCALE: 1/480000000000000000
SCALE: 1/640000000000000000
SCALE: 1/800000000000000000
SCALE: 1/960000000000000000
SCALE: 1/1200000000000000000
SCALE: 1/1600000000000000000
SCALE: 1/2000000000000000000
SCALE: 1/2400000000000000000
SCALE: 1/3200000000000000000
SCALE: 1/4000000000000000000
SCALE: 1/4800000000000000000
SCALE: 1/6400000000000000000
SCALE: 1/8000000000000000000
SCALE: 1/9600000000000000000
SCALE: 1/12000000000000000000
SCALE: 1/16000000000000000000
SCALE: 1/20000000000000000000
SCALE: 1/24000000000000000000
SCALE: 1/32000000000000000000
SCALE: 1/40000000000000000000
SCALE: 1/48000000000000000000
SCALE: 1/64000000000000000000
SCALE: 1/80000000000000000000
SCALE: 1/96000000000000000000
SCALE: 1/120000000000000000000
SCALE: 1/160000000000000000000
SCALE: 1/200000000000000000000
SCALE: 1/240000000000000000000
SCALE: 1/320000000000000000000
SCALE: 1/400000000000000000000
SCALE: 1/480000000000000000000
SCALE: 1/640000000000000000000
SCALE: 1/800000000000000000000
SCALE: 1/960000000000000000000
SCALE: 1/1200000000000000000000
SCALE: 1/1600000000000000000000
SCALE: 1/2000000000000000000000
SCALE: 1/2400000000000000000000
SCALE: 1/3200000000000000000000
SCALE: 1/4000000000000000000000
SCALE: 1/4800000000000000000000
SCALE: 1/6400000000000000000000
SCALE: 1/8000000000000000000000
SCALE: 1/9600000000000000000000
SCALE: 1/12000000000000000000000
SCALE: 1/16000000000000000000000
SCALE: 1/20000000000000000000000
SCALE: 1/24000000000000000000000
SCALE: 1/32000000000000000000000
SCALE: 1/40000000000000000000000
SCALE: 1/48000000000000000000000
SCALE: 1/64000000000000000000000
SCALE: 1/80000000000000000000000
SCALE: 1/96000000000000000000000
SCALE: 1/120000000000000000000000
SCALE: 1/160000000000000000000000
SCALE: 1/200000000000000000000000
SCALE: 1/240000000000000000000000
SCALE: 1/320000000000000000000000
SCALE: 1/400000000000000000000000
SCALE: 1/480000000000000000000000
SCALE: 1/640000000000000000000000
SCALE: 1/800000000000000000000000
SCALE: 1/960000000000000000000000
SCALE: 1/1200000000000000000000000
SCALE: 1/1600000000000000000000000
SCALE: 1/2000000000000000000000000
SCALE: 1/2400000000000000000000000
SCALE: 1/3200000000000000000000000
SCALE: 1/4000000000000000000000000
SCALE: 1/4800000000000000000000000
SCALE: 1/6400000000000000000000000
SCALE: 1/8000000000000000000000000
SCALE: 1/9600000000000000000000000
SCALE: 1/12000000000000000000000000
SCALE: 1/16000000000000000000000000
SCALE: 1/20000000000000000000000000
SCALE: 1/24000000000000000000000000
SCALE: 1/32000000000000000000000000
SCALE: 1/40000000000000000000000000
SCALE: 1/48000000000000000000000000
SCALE: 1/64000000000000000000000000
SCALE: 1/80000000000000000000000000
SCALE: 1/96000000000000000000000000
SCALE: 1/120000000000000000000000000
SCALE: 1/160000000000000000000000000
SCALE: 1/200000000000000000000000000
SCALE: 1/240000000000000000000000000
SCALE: 1/320000000000000000000000000
SCALE: 1/400000000000000000000000000
SCALE: 1/480000000000000000000000000
SCALE: 1/640000000000000000000000000
SCALE: 1/800000000000000000000000000
SCALE: 1/960000000000000000000000000
SCALE: 1/1200000000000000000000000000
SCALE: 1/1600000000000000000000000000
SCALE: 1/2000000000000000000000000000
SCALE: 1/2400000000000000000000000000
SCALE: 1/3200000000000000000000000000
SCALE: 1/4000000000000000000000000000
SCALE: 1/4800000000000000000000000000
SCALE: 1/6400000000000000000000000000
SCALE: 1/8000000000000000000000000000
SCALE: 1/9600000000000000000000000000
SCALE: 1/12000000000000000000000000000
SCALE: 1/16000000000000000000000000000
SCALE: 1/20000000000000000000000000000
SCALE: 1/24000000000000000000000000000
SCALE: 1/32000000000000000000000000000
SCALE: 1/40000000000000000000000000000
SCALE: 1/48000000000000000000000000000
SCALE: 1/64000000000000000000000000000
SCALE: 1/80000000000000000000000000000
SCALE: 1/96000000000000000000000000000
SCALE: 1/120000000000000000000000000000
SCALE: 1/160000000000000000000000000000
SCALE: 1/200000000000000000000000000000
SCALE: 1/240000000000000000000000000000
SCALE: 1/320000000000000000000000000000
SCALE: 1/400000000000000000000000000000
SCALE: 1/480000000000000000000000000000
SCALE: 1/640000000000000000000000000000
SCALE: 1/800000000000000000000000000000
SCALE: 1/960000000000000000000000000000
SCALE: 1/1200000000000000000000000000000
SCALE: 1/1600000000000000000000000000000
SCALE: 1/2000000000000000000000000000000
SCALE: 1/2400000000000000000000000000000
SCALE: 1/3200000000000000000000000000000
SCALE: 1/4000000000000000000000000000000
SCALE: 1/4800000000000000000000000000000
SCALE: 1/6400000000000000000000000000000
SCALE: 1/8000000000000000000000000000000
SCALE: 1/9600000000000000000000000000000
SCALE: 1/12000000000000000000000000000000
SCALE: 1/16000000000000000000000000000000
SCALE: 1/20000000000000000000000000000000
SCALE: 1/24000000000000000000000000000000
SCALE: 1/32000000000000000000000000000000
SCALE: 1/40000000000000000000000000000000
SCALE: 1/48000000000000000000000000000000
SCALE: 1/64000000000000000000000000000000
SCALE: 1/80000000000000000000000000000000
SCALE: 1/96000000000000000000000000000000
SCALE: 1/120000000000000000000000000000000
SCALE: 1/160000000000000000000000000000000
SCALE: 1/200000000000000000000000000000000
SCALE: 1/240000000000000000000000000000000
SCALE: 1/320000000000000000000000000000000
SCALE: 1/400000000000000000000000000000000
SCALE: 1/480000000000000000000000000000000
SCALE: 1/640000000000000000000000000000000
SCALE: 1/800000000000000000000000000000000
SCALE: 1/960000000000000000000000000000000
SCALE: 1/1200000000000000000000000000000000
SCALE: 1/1600000000000000000000000000000000
SCALE: 1/2000000000000000000000000000000000
SCALE: 1/2400000000000000000000000000000000
SCALE: 1/3200000000000000000000000000000000
SCALE: 1/4000000000000000000000000000000000
SCALE: 1/4800000000000000000000000000000000
SCALE: 1/6400000000000000000000000000000000
SCALE: 1/8000000000000000000000000000000000
SCALE: 1/9600000000000000000000000000000000
SCALE: 1/12000000000000000000000000000000000
SCALE: 1/16000000000000000000000000000000000
SCALE: 1/20000000000000000000000000000000000
SCALE: 1/24000000000000000000000000000000000
SCALE: 1/32000000000000000000000000000000000
SCALE: 1/40000000000000000000000000000000000
SCALE: 1/48000000000000000000000000000000000
SCALE: 1/64000000000000000000000000000000000
SCALE: 1/80000000000000000000000000000000000
SCALE: 1/96000000000000000000000000000000000
SCALE: 1/120000000000000000000000000000000000
SCALE: 1/160000000000000000000000000000000000
SCALE: 1/200000000000000000000000000000000000
SCALE: 1/240000000000000000000000000000000000
SCALE: 1/320000000000000000000000000000000000
SCALE: 1/400000000000000000000000000000000000
SCALE: 1/480000000000000000000000000000000000
SCALE: 1/640000000000000000000000000000000000
SCALE: 1/800000000000000000000000000000000000
SCALE: 1/960000000000000000000000000000000000
SCALE: 1/1200000000000000000000000000000000000
SCALE: 1/1600000000000000000000000000000000000
SCALE: 1/2000000000000000000000000000000000000
SCALE: 1/2400000000000000000000000000000000000
SCALE: 1/3200000000000000000000000000000000000
SCALE: 1/4000000000000000000000000000000000000
SCALE: 1/4800000000000000000000000000000000000
SCALE: 1/6400000000000000000000000000000000000
SCALE: 1/8000000000000000000000000000000000000
SCALE: 1/9600000000000000000000000000000000000
SCALE: 1/12000000000000000000000000000000000000
SCALE: 1/16000000000000000000000000000000000000
SCALE: 1/20000000000000000000000000000000000000
SCALE: 1/24000000000000000000000000000000000000
SCALE: 1/32000000000000000000000000000000000000
SCALE: 1/40000000000000000000000000000000000000
SCALE: 1/48000000000000000000000000000000000000
SCALE: 1/64000000000000000000000000000000000000
SCALE: 1/80000000000000000000000000000000000000
SCALE: 1/96000000000000000000000000000000000000
SCALE: 1/120000000000000000000000000000000000000
SCALE: 1/160000000000000000000000000000000000000
SCALE: 1/200000000000000000000000000000000000000
SCALE: 1/240000000000000000000000000000000000000
SCALE: 1/320000000000000000000000000000000000000
SCALE: 1/400000000000000000000000000000000000000
SCALE: 1/480000000000000000000000000000000000000
SCALE: 1/640000000000000000000000000000000000000
SCALE: 1/800000000000000000000000000000000000000
SCALE: 1/960000000000000000000000000000000000000
SCALE: 1/1200000000000000000000000000000000000000
SCALE: 1/1600000000000000000000000000000000000000
SCALE: 1/2000000000000000000000000000000000000000
SCALE: 1/2400000000000000000000000000000000000000
SCALE: 1/3200000000000000000000000000000000000000
SCALE: 1/4000000000000000000000000000000000000000
SCALE: 1/4800000000000000000000000000000000000000
SCALE: 1/6400000000000000000000000000000000000000
SCALE: 1/8000000000000000000000000000000000000000
SCALE: 1/9600000000000000000000000000000000000000
SCALE: 1/12000000000000000000000000000000000000000
SCALE: 1/16000000000000000000000000000000000000000
SCALE: 1/20000000000000000000000000000000000000000
SCALE: 1/24000000000000000000000000000000000000000
SCALE: 1/32000000000000000000000000000000000000000
SCALE: 1/40000000000000000000000000000000000000000
SCALE: 1/48000000000000000000000000000000000000000
SCALE: 1/64000000000000000000000000000000000000000
SCALE: 1/80000000000000000000000000000000000000000
SCALE: 1/96000000000000000000000000000000000000000
SCALE: 1/120000000000000000000000000000000000000000
SCALE: 1/160000000000000000000000000000000000000000
SCALE: 1/200000000000000000000000000000000000000000
SCALE: 1/240000000000000000000000000000000000000000
SCALE: 1/320000000000000000000000000000000000000000
SCALE: 1/400000000000000000000000000000000000000000
SCALE: 1/480000000000000000000000000000000000000000
SCALE: 1/640000000000000000000000000000000000000000
SCALE: 1/800000000000000000000000000000000000000000
SCALE: 1/960000000000000000000000000000000000000000
SCALE: 1/1200000000000000000000000000000000000000000
SCALE: 1/1600000000000000000000000000000000000000000
SCALE: 1/2000000000000000000000000000000000000000000
SCALE: 1/2400000000000000000000000000000000000000000
SCALE: 1/3200000000000000000000000000000000000000000
SCALE: 1/4000000000000000000000000000000000000000000
SCALE: 1/4800000000000000000000000000000000000000000
SCALE: 1/6400000000000000000000000000000000000000000
SCALE: 1/8000000000000000000000000000000000000000000
SCALE: 1/9600000000000000000000000000000000000000000
SCALE: 1/12000000000000000000000000000000000000000000
SCALE: 1/16000000000000000000000000000000000000000000
SCALE: 1/20000000000000000000000000000000000000000000
SCALE: 1/24000000000000000000000000000000000000000000
SCALE: 1/32000000000000000000000000000000000000000000
SCALE: 1/40000000000000000000000000000000000000000000
SCALE: 1/48000000000000000000000000000000000000000000
SCALE: 1/64000000000000000000000000000000000000000000
SCALE: 1/80000000000000000000000000000000000000000000
SCALE: 1/96000000000000000000000000000000000000000000
SCALE: 1/120000000000000000000000000000000000000000000
SCALE: 1/160000000000000000000000000000000000000000000
SCALE: 1/200000000000000000000000000000000000000000000
SCALE: 1/240000000000000000000000000000000000000000000
SCALE: 1/320000000000000000000000000000000000000000000
SCALE: 1/400000000000000000000000000000000000000000000
SCALE: 1/480000000000000000000000000000000000000000000
SCALE: 1/640000000000000000000000000000000000000000000
SCALE: 1/800000000000000000000000000000000000000000000
SCALE: 1/960000000000000000000000000000000000000000000
SCALE: 1/1200000000000000000000000000000000000000000000
SCALE: 1/1600000000000000000000000000000000000000000000
SCALE: 1/2000000000000000000000000000000000000000000000
SCALE: 1/2400000000000000000000000000000000000000000000
SCALE: 1/3200000000000000000000000000000000000000000000
SCALE: 1/4000000000000000000000000000000000000000000000
SCALE: 1/4800000000000000000000000000000000000000000000
SCALE: 1/6400000000000000000000000000000000000000000000
SCALE: 1/8000000000000000000000000000000000000000000000
SCALE: 1/9600000000000000000000000000000000000000000000
SCALE: 1/12000000000000000000000000000000000000000000000
SCALE: 1/16000000000000000000000000000000000000000000000
SCALE: 1/20000000000000000000000000000000000000000000000
SCALE: 1/24000000000000000000000000000000000000000000000
SCALE: 1/32000000000000000000000000000000000000000000000
SCALE: 1/40000000000000000000000000000000000000000000000
SCALE: 1/48000000000000000000000000000000000000000000000
SCALE: 1/64000000000000000000000000000000000000000000000
SCALE: 1/80000000000000000000000000000000000000000000000
SCALE: 1/96000000000000000000000000000000000000000000000
SCALE: 1/120000000000000000000000000000000000000000000000
SCALE: 1/160000000000000000000000000000000000000000000000
SCALE: 1/200000000000000000000000000000000000000000000000
SCALE: 1/240000000000000000000000000000000000000000000000
SCALE: 1/320000000000000000000000000000000000000000000000
SCALE: 1/400000000000000000000000000000000000000000000000
SCALE: 1/480000000000000000000000000000000000000000000000
SCALE: 1/640000000000000000000000000000000000000000000000
SCALE: 1/800000000000000000000000000000000000000000000000
SCALE: 1/960000000000000000000000000000000000000000000000
SCALE: 1/1200000000000000000000000000000000000000000000000
SCALE: 1/1600000000000000000000000000000000000000000000000
SCALE: 1/2000000000000000000000000000000000000000000000000
SCALE: 1/2400000000000000000000000000000000000000000000000
SCALE: 1/3200000000000000000000000000000000000000000000000
SCALE: 1/4000000000000000000000000000000000000000000000000
SCALE: 1/4800000000000000000000000000000000000000000000000
SCALE: 1/6400000000000000000000000000000000000000000000000
SCALE: 1/8000000000000000000000000000000000000000000000000
SCALE: 1/9600000000000000000000000000000000000000000000000
SCALE: 1/12000000000000000000000000000000000000000000000000
SCALE: 1/16000000000000000000000000000000000000000000000000
SCALE: 1/20000000000000000000000000000000000000000000000000
SCALE: 1/24000000000000000000000000000000000000000000000000
SCALE: 1/32000000000000000000000000000000000000000000000000
SCALE: 1/40000000000000000000000000000000000000000000000000
SCALE: 1/48000000000000000000000000000000000000000000000000
SCALE: 1/64000000000000000000000000000000000000000000000000
SCALE: 1/80000000000000000000000000000000000000000000000000
SCALE: 1/96000000000000000000000000000000000000000000000000
SCALE: 1/120000000000000000000000000000000000000000000000000
SCALE: 1/160000000000000000000000000000000000000000000000000
SCALE: 1/200000000000000000000000000000000000000000000000000
SCALE: 1/240000000000000000000000000000000000000000000000000
SCALE: 1/320000000000000000000000000000000000000000000000000
SCALE: 1/400000000000000000000000000000000000000000000000000
SCALE: 1/480000000000000000000000000000000000000000000000000
SCALE: 1/640000000000000000000000000000000000000000000000000
SCALE: 1/800000000000000000000000000000000000000000000000000
SCALE: 1/960000000000000000000000000000000000000000000000000
SCALE: 1/1200000000000000000000000000000000000000000000000000
SCALE: 1/1600000000000000000000000000000000000000000000000000
SCALE: 1/2000000000000000000000000000000000000000000000000000
SCALE: 1/2400000000000000000000000000000000000000000000000000
SCALE: 1/3200000000000000000000000000000000000000000000000000
SCALE: 1/4000000000000000000000000000000000000000000000000000
SCALE: 1/4800000000000000000000000000000000000000000000000000
SCALE: 1/6400000000000000000000000000000000000000000000000000
SCALE: 1/8000000000000000000000000000000000000000000000000000
SCALE: 1/9600000000000000000000000000000000000000000000000000
SCALE: 1/12000000000000000000000000000000000000000000000000000
SCALE: 1/16000000000000000000000000000000000000000000000000000
SCALE: 1/20000000000000000000000000000000000000000000000000000
SCALE: 1/24000000000000000000000000000000000000000000000000000
SCALE: 1/32000000000000000000000000000000000000000000000000000
SCALE: 1/40000000000000000000000000000000000000000000000000000
SCALE: 1/48000000000000000000000000000000000000000000000000000
SCALE: 1/64000000000000000000000000000000000000000000000000000
SCALE: 1/80000000000000000000000000000000000000000000000000000
SCALE: 1/96000000000000000000000000000000000000000000000000000
SCALE: 1/120000000000000000000000000000000000000000000000000000
SCALE: 1/160000000000000000000000000000000000000000000000000000
SCALE: 1/200000000000000000000000000000000000000000000000000000
SCALE: 1/240000000000000000000000000000000000000000000000000000
SCALE: 1/320000000000000000000000000000000000000000000000000000
SCALE: 1/400000000000000000000000000000000000000000000000000000
SCALE: 1/480000000000000000000000000000000000000000000000000000
SCALE: 1/640000000000000000000000000000000000000000000000000000
SCALE: 1/800000000000000000000000000000000000000000000000000000
SCALE: 1/960000000000000000000000000000000000000000000000000000
SCALE: 1/1200000000000000000000000000000000000000000000000000000
SCALE: 1/1600000000000000000000000000000000000000000000000000000
SCALE: 1/2000000000000000000000000000000000000000000000000000000
SCALE: 1/2400000000000000000000000000000000000000000000000000000
SCALE: 1/3200000000000000000000000000000000000000000000000000000
SCALE: 1/4000000000000000000000000000000000000000000000000000000
SCALE: 1/4800000000000000000000000000000000000000000000000000000
SCALE: 1/6400000000000000000000000000000000000000000000000000000
SCALE: 1/8000000000000000000000000000000000000000000000000000000
SCALE: 1/9600000000000000000000000000000000000000000000000000000
SCALE: 1/12000000000000000000000000000000000000000000000000000000
SCALE: 1/16000000000000000000000000000000000000000000000000000000
SCALE: 1/20000000000000000000000000000000000000000000000000000000
SCALE: 1/24000000000000000000000000000000000000000000000000000000
SCALE: 1/32000000000000000000000000000000000000000000000000000000
SCALE: 1/40000000000000000000000000000000000000000000000000000000
SCALE: 1/48000000000000000000000000000000000000000000000000000000
SCALE: 1/64000000000000000000000000000000000000000000000000000000
SCALE: 1/80000000000000000000000000000000000000000000000000000000
SCALE: 1/96000000000000000000000000000000000000000000000000000000
SCALE: 1/120000000000000000000000000000000000000000000000000000000
SCALE: 1/160000000000000000000000000000000000000000000000000000000
SCALE: 1/200000000000000000000000000000000000000000000000000000000
SCALE: 1/240000000000000000000000000000000000000000000000000000000
SCALE: 1/320000000000000000000000000000000000000000000000000000000
SCALE: 1/400000000000000000000000000000000000000000000000000000000
SCALE: 1/480000000000000000000000000000000000000000000000000000000
SCALE: 1/640000000000000000000000000000000000000000000000000000000
SCALE: 1/800000000000000000000000000000000000000000000000000000000
SCALE: 1/960000000000000000000000000000000000000000000000000000000
SCALE: 1/1200000000000000000000000000000000000000000000000000000000
SCALE: 1/1600000000000000000000000000000000000000000000000000000000
SCALE: 1/2000000000000000000000000000000000000000000000000000000000
SCALE: 1/2400000000000000000000000000000000000000000000000000000000
SCALE: 1/3200000000000000000000000000000000000000000000000000000000
SCALE: 1/4000000000000000000000000000000000000000000000000000000000
SCALE: 1/4800000000000000000000000000000000000000000000000000000000
SCALE: 1/6400000000000000000000000000000000000000000000000000000000
SCALE: 1/8000000000000000000000000000000000000000000000000000000000
SCALE: 1/9600000000000000000000000000000000000000000000000000000000
SCALE: 1/12000000000000000000000000000000000000000000000000000000000
SCALE: 1/16000000000000000000000000000000000000000000000000000000000
SCALE: 1/20000000000000000000000000000000000000000000000000000000000
SCALE: 1/24000000000000000000000000000000000000000000000000000000000
SCALE: 1/32000000000000000000000000000000000000000000000000000000000
SCALE: 1/40000000000000000000000000000000000000000000000000000000000
SCALE: 1/48000000000000000000000000000000000000000000000000000000000
SCALE: 1/64000000000000000000000000000000000000000000000000000000000
SCALE: 1/80000000000000000000000000000000000000000000000000000000000
SCALE: 1/96000000000000000000000000000000000000000000000000000000000
SCALE: 1/120000000000000000000000000000000000000000000000000000000000
SCALE: 1/160000000000000000000000000000000000000000000000000000000000
SCALE: 1/200000000000000000000000000000000000000000000000000000000000
SCALE: 1/240000000000000000000000000000000000000000000000000000000000
SCALE: 1/320000000000000000000000000000000000000000000000000000000000
SCALE: 1/400000000000000000000000000000000000000000000000000000000000
SCALE: 1/480000000000000000000000000000000000000000000000000000000000
SCALE: 1/640000000000000000000000000000000000000000000000000000000000
SCALE: 1/800000000000000000000000000000000000000000000000000000000000
SCALE: 1/960000000000000000000000000000000000000000000000000000000000
SCALE: 1/1200000000000000000000000000000000000000000000000000000000000
SCALE: 1/1600000000000000000000000000000000000000000000000000000000000
SCALE: 1/2000000000000000000000000000000000000000000000000000000000000
SCALE: 1/2400000000000000000000000000000000000000000000000000000000000
SCALE: 1/3200000000000000000000000000000000000000000000000000000000000
SCALE: 1/4000000000000000000000000000000000000000000000000000000000000
SCALE: 1/4800000000000000000000000000000000000000000000000000000000000
SCALE: 1/6400000000000000000000000000000000000000000000000000000000000
SCALE: 1/8000000000000000000000000000000000000000000000000000000000000
SCALE: 1/9600000000000000000000000000000000000000000000000000000000000
SCALE: 1/12000000000000000000000000000000000000000000000000000000000000
SCALE: 1/16000000000000000000000000000000000000000000000000000000000000
SCALE: 1/20000000000000000000000000000000000000000000000000000000000000
SCALE: 1/24000000000000000000000000000000000000000000000000000000000000
SCALE: 1/32000000000000000000000000000000000000000000000000000000000000
SCALE: 1/40000000000000000000000000000000000000000000000000000000000000
SCALE: 1/48000000000000000000000000000000000000000000000000000000000000
SCALE: 1/64000000000000000000000000000000000000000000000000000000000000
SCALE: 1/80000000000000000000000000000000000000000000000000000000000000
SCALE: 1/96000000000000000000000000000000000000000000000000000000000000
SCALE: 1/120000000000000000000000000000000000000000000000000000000000000
SCALE: 1/160000000000000000000000000000000000000000000000000000000000000
SCALE: 1/200000000000000000000000000000000000000000000000000000000000000
SCALE: 1/240000000000000000000000000000000000000000000000000000000000000
SCALE: 1/320000000000000000000000000000000000000000000000000000000000000
SCALE: 1/400000000000000000000000000000000000000000000000000000000000000
SCALE: 1/480000000000000000000000000000000000000000000000000000000000000
SCALE: 1/640000000000000000000000000000000000000000000000000000000000000
SCALE: 1/800000000000000000000000000000000000000000000000000000000000000
SCALE: 1/960000000000000000000000000000000000000000000000000000000000000
SCALE: 1/1200000000000000000000000000000000000000000000000000000000000000
SCALE: 1/1600000000000000000000000000000000000000000000000000000000000000
SCALE: 1/2000000000000000000000000000000000000000000000000000000000000000
SCALE: 1/2400000000000000000000000000000000000000000000000000000000000000
SCALE: 1/3200000000000000000000000000000000000000000000000000000000000000
SCALE: 1/4000000000000000000000000000000000000000000000000000000000000000
SCALE: 1/4800000000000000000000000000000000000000000000000000000000000000
SCALE: 1/6400000000000000000000000000000000000000000000000000000000000000
SCALE: 1/8000000000000000000000000000000000000000000000000000000000000000
SCALE: 1/9600000000000000000000000000000000000000000000000000000000000000
SCALE: 1/12000000000000000000000000000000000000000000000000000000000000000
SCALE: 1/16000000000000000000000000000000000000000000000000000000000000000
SCALE: 1/20000000000000000000000000000000000000000000000000000000000000000
SCALE: 1/24000000000000000000000000000000000000000000000000000000000000000
SCALE: 1/32000000000000000000000000000000000000000000000000000000000000000
SCALE: 1/40000000000000000000000000000000000000000000000000000000000000000
SCALE: 1/48000000000000000000000000000000000000000000000000000000000000000
SCALE: 1/64000000000000000000000000000000000000000000000000000000000000000
SCALE: 1/80000000000000000000000000000000000000000000000000000000000000000
SCALE: 1/96000000000000000000000000000000000000000000000000000000000000000
SCALE: 1/120000000000000000000000000000000000000000000000000000000000000000
SCALE: 1/160000000000000000000000000000000000000000000000000000000000000000
SCALE: 1/200000000000000000000000000000000000000000000000000000000000000000
SCALE: 1/240000000000000000000000000000000000000000000000000000000000000000
SCALE: 1/320000000000000000000000000000000000000000000000000000000000000000
SCALE: 1/400000000000000000000000000000000000000000000000000000000000000000
SCALE: 1/480000000000000000000000000000000000000000000000000000000000000000
SCALE: 1/640000000000000000000000000000000000000000000000000000000000000000
SCALE: 1/800000000000000000000000000000000000000000000000000000000000000000
SCALE: 1/960000000000000000000000000000000000000000000000000000000000000000
SCALE: 1/1200000000000000000000000000000000000000000000000000000000000000000
SCALE: 1/1600000000000000000000000000000000000000000000000000000000000000000
SCALE: 1/2000000000000000000000000000000000000000000000000000000000000000000
SCALE: 1/2400000000000000000000000000000000000000000000000000000000000000000
SCALE: 1/3200000000000000000000000000000000000000000000000000000000000000000
SCALE: 1/4000000000000000000000000000000000000000000000000000000000000000000
SCALE: 1/4800000000000000000000000000000000000000000000000000000000000000000
SCALE: 1/6400000000000000000000000000000000000000000000000000000000000000000
SCALE: 1/8000000000000000000000000000000000000000000000000000000000000000000
SCALE: 1/9600000000000000000000000000000000000000000000000000000000000000000
SCALE: 1/12000000000000000000000000000000000000000000000000000000000000000000
SCALE: 1/16000000000000000000000000000000000000000000000000000000000000000000
SCALE: 1/20000000000000000000000000000000000000000000000000000000000000000000
SCALE: 1/24000000000000000000000000000000000000000000000000000000000000000000
SCALE: 1/32000000000000000000000000000000000000000000000000000000000000000000
SCALE: 1/40000000000000000000000000000000000000000000000000000000000000000000
SCALE: 1/48000000000000000000000000000000000000000000000000000000000000000000
SCALE: 1/64000000000000000000000000000000000000000000000000000000000000000000
SCALE: 1/80000000000000000000000000000000000000000000000000000000000000000000
SCALE: 1/96000000000000000000000000000000000000000000000000000000000000000000
SCALE: 1/120000000000000000000000000000000000000000000000000000000000000000000
SCALE: 1/160000000000000000000000000000000000000000000000000000000000000000000
SCALE: 1/200000000000000000000000000000000000000000000000000000000000000000000
SCALE: 1/240000000000000000000000000000000000000000000000000000000000000000000
SCALE: 1/320000000000000000000000000000000000000000000000000000000000000000000
SCALE: 1/400000000000000000000000000000000000000000000000000000000000000000000
SCALE: 1/480000000000000000000000000000000000000000000000000000000000000000000
SCALE: 1/640000000000000000000000000000000000000000000000000000000000000000000
SCALE: 1/800000000000000000000000000000000000000000000000000000000000000000000
SCALE: 1/960000000000000000000000000000000000000000000000000000000000000000000
SCALE: 1/1200000000000000000000000000000000000000000000000000000000000000000000
SCALE: 1/1600000000000000000000000000000000000000000000000000000000000000000000
SCALE: 1/2000000000000000000000000000000000000000000000000000000000000000000000
SCALE: 1/2400000000000000000000000000000000000000000000000000000000000000000000
SCALE: 1/3200000000000000000000000000000000000000000000000000000000000000000000
SCALE: 1/4000000000000000000000000000000000000000000000000000000000000000000000
SCALE: 1/4800000000000000000000000000000000000000000000000000000000000000000000
SCALE: 1/6400000000000000000000000000000000000000000000000000000000000000000000
SCALE: 1/8000000000000000000000000000000000000000000000000000000000000000000000
SCALE: 1/9600000000000000000000000000000000000000000000000000000000000000000000
SCALE: 1/12000000000000000000000000000000000000000000000000000000000000000000000
SCALE: 1/16000000000000000000000000000000000000000000000000000000000000000000000
SCALE: 1/20000000000000000000000000000000000000000000000000000000000000000000000
SCALE: 1/24000000000000000000000000000000000000000000000000000000000000000000000
SCALE: 1/32000000000000000000000000000000000000000000000000000000000000000000000
SCALE: 1/40000000000000000000000000000000000000000000000000000000000000000000000
SCALE: 1/48000000000000000000000000000000000000000000000000000000000000000000000
SCALE: 1/64000000000000000000000000000000000000000000000000000000000000000000000
SCALE: 1/80000000000000000000000000000000000000000000000000000000000000000000000
SCALE: 1/96000000000000000000000000000000000000000000000000000000000000000000000
SCALE: 1/120000000000000000000000000000000000000000000000000000000000000000000000
SCALE: 1/160000000000000000000000000000000000000000000000000000000000000000000000
SCALE: 1/200000000000000000000000000000000000000000000000000000000000000000000000
SCALE: 1/240000000000000000000000000000000000000000000000000000000000000000000000
SCALE: 1/320000000000000000000000000000000000000000000000000000000000000000000000
SCALE: 1/400000000000000000000000000000000000000000000000000000000000000000000000
SCALE: 1/480000000000000000000000000000000000000000000000000000000000000000000000
SCALE: 1/640000000000000000000000000000000000000000000000000000000000000000000000
SCALE: 1/800000000000000000000000000000000000000000000000000000000000000000000000
SCALE: 1/960000000000000000000000000000000000000000000000000000000000000000000000
SCALE: 1/1200000000000000000000000000000000000000000000000000000000000000000000000
SCALE: 1/1600000000000000000000000000000000000000000000000000000000000000000000000
SCALE: 1/2000000000000000000000000000000000000000000000000000000000

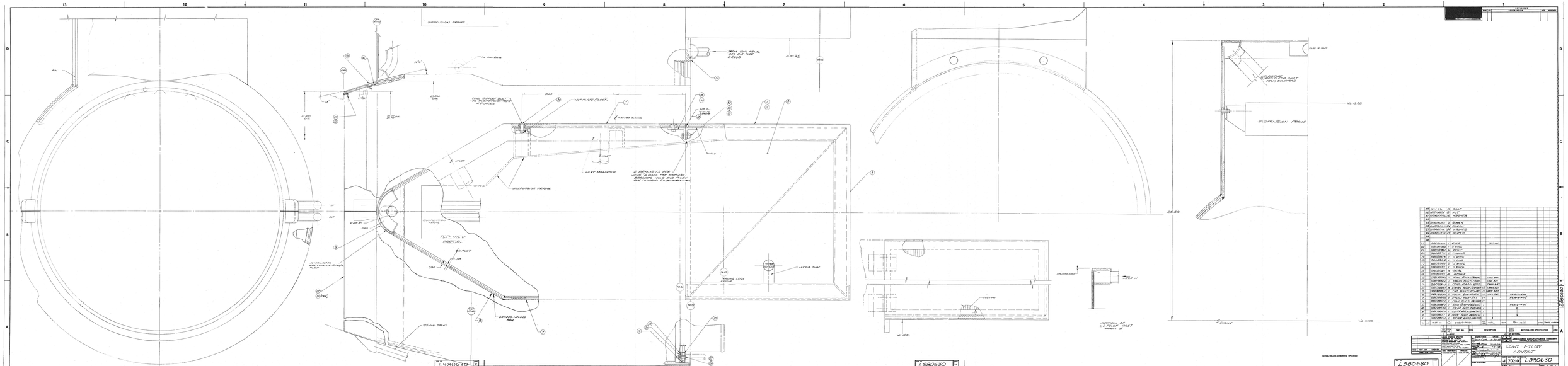
FIN
SUSPENSION FRAME
TOP VIEW PARTIAL
INLET
OUTLET
.125
.080
BRAZED HOLES ONLY
.753 DIA. SEAL
.125 HOLE DIA. FOR RIVETS, PLACES
.250 DIA. SEAL
.375 DIA. SEAL
.750 DIA. SEAL
.875 DIA. SEAL
.625 DIA. SEAL
.500 DIA. SEAL
.438 DIA. SEAL
.313 DIA. SEAL
.188 DIA. SEAL
.063 DIA. SEAL
.938 DIA. SEAL
.1.000 DIA. SEAL
.1.063 DIA. SEAL
.1.125 DIA. SEAL
.1.188 DIA. SEAL
.1.250 DIA. SEAL
.1.313 DIA. SEAL
.1.375 DIA. SEAL
.1.438 DIA. SEAL
.1.500 DIA. SEAL
.1.563 DIA. SEAL
.1.625 DIA. SEAL
.1.688 DIA. SEAL

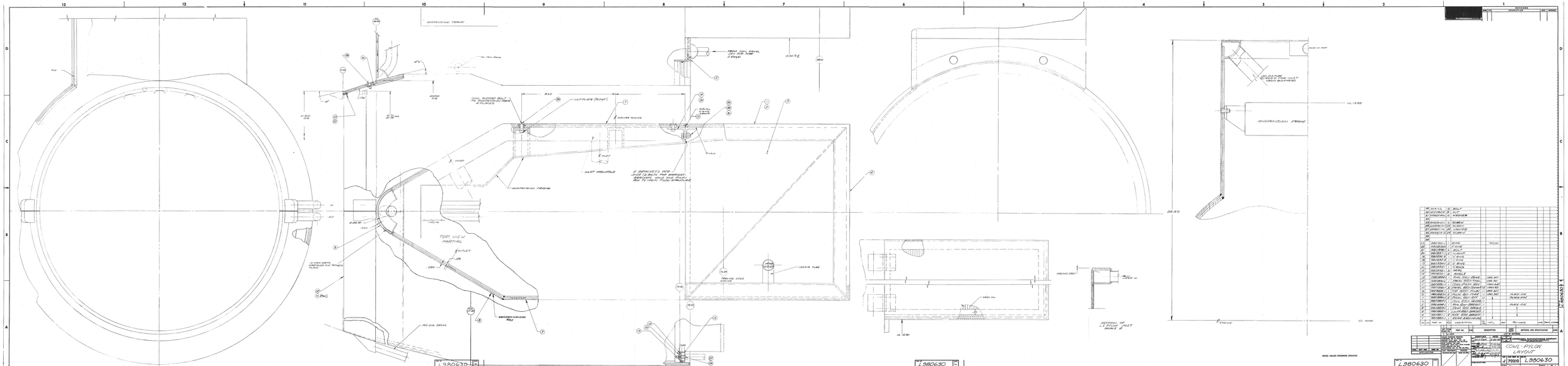

ITEM	QTY	PART NO.	DESCRIPTION	SPEC	MATERIAL AND SPECIFICATION	FINISH
1						
2						
3						
4						
5						
6						
7						
8						
9						
10						
11						
12						
13						
14						
15						
16						
17						
18						
19						
20						
21						
22						
23						
24						
25						
26						
27						
28						
29						
30						
31						
32						
33						
34						
35						
36						
37						
38						
39						
40						
41						
42						
43						
44						
45						
46						
47						
48						
49						
50						
51						
52						
53						
54						
55						
56						
57						
58						
59						
60						
61						
62						
63						
64						
65						
66						
67						
68						
69						
70						
71						
72						
73						
74						
75						
76						
77						
78						
79						
80						
81						
82						
83						
84						
85						
86						
87						
88						
89						
90						
91						
92						
93						
94						
95						
96						
97						
98						
99						
100						
101						
102						
103						
104						
105						
106						
107						
108						
109						
110						
111						
112						
113						
114						
115						
116						
117						
118						
119						
120						
121						
122						
123						
124						
125						
126						
127						
128						
129						
130						
131						
132						
133						
134						
135						
136						
137						
138						
139						
140						
141						
142						
143						
144						
145						
146						
147						
148						
149						
150						
151						
152						
153						
154						
155						
156						
157						
158						
159						
160						
161						
162						
163						
164						
165						
166						
167						
168						
169						
170						
171						
172						
173						
174						
175						
176						
177						
178						
179						
180						
181						
182						
183						
184						
185						
186						
187						
188						
189						
190						
191						
192						
193						
194						
195						
196						
197						
198						
199						
200						
201						
202						
203						
204						
205						
206						
207						
208						
209						
210						
211						
212						
213						
214						
215						
216						
217						
218						
219						
220						
221						
222						
223						
224						
225						
226						
227						
228						
229						
230						
231						
232						
233						
234						
235						
236						
237						
238						
239						
240						
241						
242						
243						
244						
245						
246						
247						
248						
249						
250						
251						
252						
253						
254						
255						
256						
257						
258						
259						
260						
261						
262						
263						
264						
265						
266						
267						
268						
269						
270						
271						
272						
273						
274						
275						
276						
277						
278						
279						
280						
281						
282						
283						
284						
285						
286						
287						
288						
289						
290						
291						
292						
293						
294						
295						
296						
297						
298						
299						
300						
301						
302						
303						
304						
305						
306						
307						
308						
309						
310						
311						
312						
313						
314						
315						
316						
317						
318						
319						
320						
321						
322						
323						
324						
325						
326						
327						
328						
329						
330						
331						
332						
333						
334						
335						
336						
337						
338						
339						
340						
341						
342						
343						
344						
345						
346						
347						
348						
349						
350						
351						
352						
353						
354						
355						
356						
357						
358						
359						
360						
361						
362						
363						
364						
365						
366						
367						
368						
369						
370						
371						
372						
373						
374						
375						
376						
377						
378						
379						
380						
381						
382						
383						
384						
385						
386						
387						
388						
389						
390						
391						
392						
393						
394						
395						
396						
397						
398						
399						
400						
401						
402						
403						
404						
405						
406						
407						
408						
409						
410						
411						
412						
413						
414						
415						
416						
417						
418						
419						
420						
421						
422						
423						
424						
425						
426						
427						
428						
429						
430						
431						
432						
433						
434						
435						
436						
437						
438						
439						
440						
441						
442						
443						
444						
445						
446						
447						
448						
449						
450						
451						
452						
453						
454						
455						
456						
457						
458						
459						
460						
461						
462						
463						
464						
465						
466						
467						
468						
469						
470						
471						
472						
473						
474						
475						
476						
477						
478						
479						
480						
481						
482						
483						
484						
485						
486						
487						
488						
489						
490						
491						
492						
493						
494						
495						
496						
497						
498						
499						
500						
501						
502						
503						
504						
505						
506						
507						
508						
509						
510						
511						
512						
513						
514						
515						
516						
517						
518						
519						
520						
521						
522						
523						
524						
525						
526						
527						
528						
529						
530						
531						
532						
533						
534						
535						
536						
537						
538						
539						
540						
541						
542						
543						
544						
545						
546						
547						
548						
549						
550						
551						
552						
553						
554						
555						
556						
557						
558						
559						
560						
561						
562						
563						
564						
565						
566						
567						
568						
569						
570						
571						
572						
573						
574						
575						
576						
577						
578						
579						
580						
581						
582						
583						
584						
585						
586						
587						
588						
589						
590						
591						
592						
593						
594						
595						
596						
597						
598						
599						
600						
601						
602						
603						
604						
605						
606						
607						
608						
609						
610						
611						
612						
613						
614						
615						
616						
617						
618						
619						
620						
621						
622						
623						
624						
625						
626						
627						
628						
629						
630						
631						
632						
633						
634						
635						
636						
637						
638						
639						
640						
641						
642						
643						
644						
645						
646						
647						
648						
649						
650						
651						
652						
653						
654						
655						
656						
657						
658						
659						
660						
661						
662						
663						
664						
665						
666						
667						
668						
669						
670						
671						
672						
673						
674						
675						
676						
677						
678						
679						
680						
681						
682						
683						
684						
685						
686						
687						
688						
689						
690						
691						
692						
693						
694						
695						
696						
697						
698						
699						
700						
701						
702						
703						
704						
705						
706						
707						
708						
709						
710						
711						
712						
713						
714						
715						
716						
717						
718						
719						
720						
721						
722						
723						
724						
725						
726						
727						
728						
729						
730						
731						
732						
733						
734						
735						
736						
737						
738						
739						
740						
741						
742						
743						
744						
745						
746						
747						
748						
749						
750						
751						
752						
753						
754						
755						
756						
757						
758						
759						
760						
761						
762						
763						
764						
765						
766						
767						
768						
769						
770						
771						
772						
773						
774						
775						
776						
777						
778						
779						
780						
781						
782						
783						
784						
785						
786						
787						
788						
789						
790						
791						
792						
793						
794						
795						
796						
797						
798						
799						
800						
801						
802						
803						
804						
805						
806						
807						
808						
809						
810						
811						
812						
813						
814						
815						
816						
817						
818						
819						
820						
821						
822						
823						
824						
825						
826						
827						
828						
829						
830						
831						
832						
833						
834						
835						
836						
837						
838						
839						
840						
841						
842						
843						
844						
845						
846						
847						
848						
849						
850						
851						
852						
853						
854						
855						
856						
857						
858						
859						
860						
861						
862						
863						
864						
865						
866						
867						
868						
869						
870						
871						
872						
873						
874						
875						
876						
877						
878						
879						
880						
881						
882						
883						
884						
885						
886						
887						
888						
889						
890						
891						
892						
893						
894						
895						
896						
897						
898						
899						
900						
901						
902						
903						
904						
905						
906						
907						
908						
909						
910						
911						
912						
913						
914						
915						
916						
917						
918						
919						
920						
921						
922						
923						
924						
925						
926						
927						
928						
929						
930						
931						
932						
933						
934						
935						
936						
937						
938						
939						
940						
941						
942						
943						
944						
945						
946						
947						
948						
949						
950						
951						
952						
953						
954						
955						
956						
957						
958						
959						
960						
961						
962						
963						
964						
965						
966						
967						
968						
969						
970						
971						
972						
973						
974						
975						
976						
977						
978						
979						
980						
981						
982						
983						
984						
985						
986						
987						
988						
989						
990						
991						
992						
993						
994						
995						
996						
997						
998						
999						
1000						

ITEM	QTY	PART NO.	DESCRIPTION	SPEC	MATERIAL AND SPECIFICATION	FINISH
1						
2						
3						
4						
5						
6						
7						
8						
9						
10						
11						
12						
13						
14						
15						
16						
17						
18						
19						
20						
21						
22						
23						
24						
25						
26						
27						
28						
29						
30						
31						
32						
33						
34						
35						
36						
37						
38						
39						
40						
41						
42						
43						
44						
45						
46						
47						
48						
49						
50						
51						
52						
53						
54						
55						
56						
57						
58						
59						
60						
61						
62						
63						
64						
65						
66						
67						
68						
69						
70						
71						
72						
73						
74						
75						
76						
77						
78						
79						
80						
81						
82						
83						
84						
85						
86						
87						
88						
89						
90						
91						
92						
93						
94						
95						
96						
97						
98						
99						
100						
101						
102						
103						
104						
105						
106						
107						
108						
109						
110						
111						
112						
113						
114						
115						
116						
117						
118						
119						
120						
121						
122						
123						
124						
125						
126						
127						
128						
129						
130						
131						
132						
133						
134						
135						
136						
137						
138						
139						
140						
141						
142						
143						
144						
145						
146						
147						
148						
149						
150						
151						
152						
153						
154						
155						
156						
157						
158						
159						
160						
161						
162						
163						
164						
165						
166						
167						
168						
169						
170						
171						
172						
173						
174						
175						
176						
177						
178						
179						
180						
181						
182						
183						
184						
185						
186						
187						
188						
189						
190						
191						
192						
193						
194						
195						
196						
197						
198						
199						
200						
201						
202						
203						
204						
205						
206						
207						
208						
209						
210						
211						
212						
213						
214						
215						
216						
217						
218						
219						
220						
221						
222						
223						
224						
225						
226						
227						
228						
229						
230						
231						
232						
233						
234						
235						
236						
237						
238						
239						
240						
241						
242						
243						
244						
245						
246						
247						
248						
249						
250						
251						
252						
253						
254						
255						
256						
257						
258						
259						
260						
261						
262						
263						
264						
265						
266						
267						
268						
269						
270						
271						
272						
273						
274						
275						
276						
277						
278						
279						
280						
281						
282						
283						
284						
285						
286						
287						
288						
289						
290						
291						
292						
293						
294						
295						
296						
297						
298						
299						
300						
301						
302						
303						
304						
305						
306						
307						
308						
309						

UNCLASSIFIED

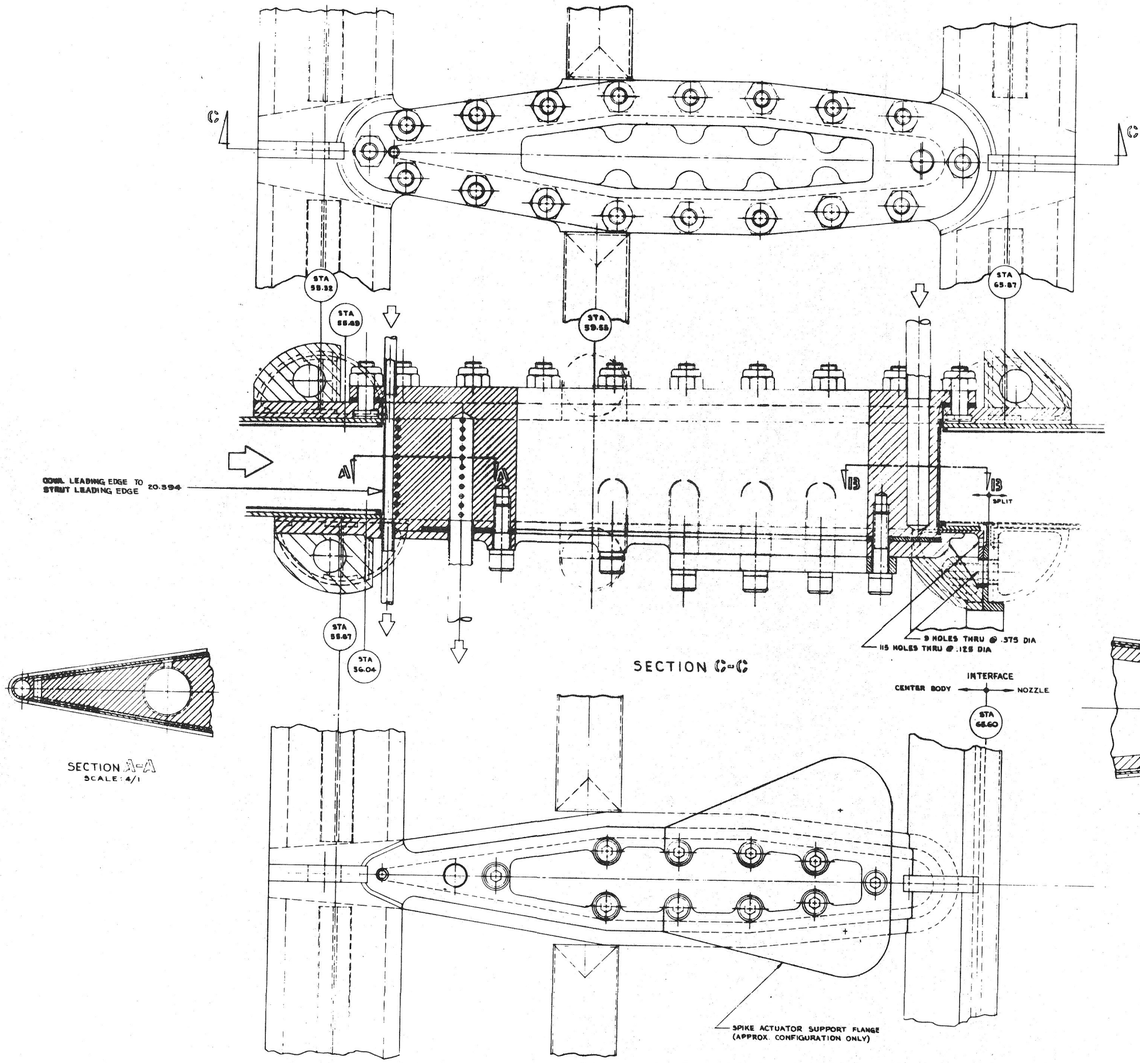

SECTION C-C

SECTION A-A
SCALE: 4/1

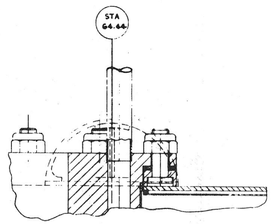

PROPOSED ALTERNATE
COOLING RING POSITION

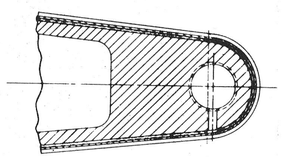

SECTION B-B
SCALE: 4/1

PROPRIETARY NOTICE
THIS LAYOUT DRAWING EMBODIES A PROPRIETARY DESIGN OWNED BY THE GARRETT CORPO-RATION AND IS LOANED SUBJECT TO THE AGREEMENT THAT IT SHALL NOT BE COPIED OR EXPRESSLY ADAPTED IN WHOLE OR IN PART, ALL RIGHTS ARE RESERVED BY THE GARRETT CORPORA-TION. THIS DRAWING SHALL BE RETURNED WHEN THE NEED FOR IT HAS BEEN CONCLUDED.

SIGNATURES	DATES	DATE STARTED	WITHDRAWN BY
DRN W. B. COOKE	4-20-67	4-20-67	
CHKD			
ENGR		DATE COMPLETED	WITHDRAWN BY
APPD			
APPD			
APPD			

SHEET 2500521-2500

FEATURES
REVISED AERODYNAMIC STRUT SHAPE

AIRESEARCH MANUFACTURING COMPANY
A DIVISION OF THE GARRETT CORPORATION
LOS ANGELES

LAYOUT

SUPPORT ASSY, STRUT, H.R.E.

SIZE	CODE IDENT NO.	DRAWING NO.
J	70210	L-980608

SCALE 1/1 WT SHEET 1 OF 1

UNCLASSIFIED

UNCLASSIFIED

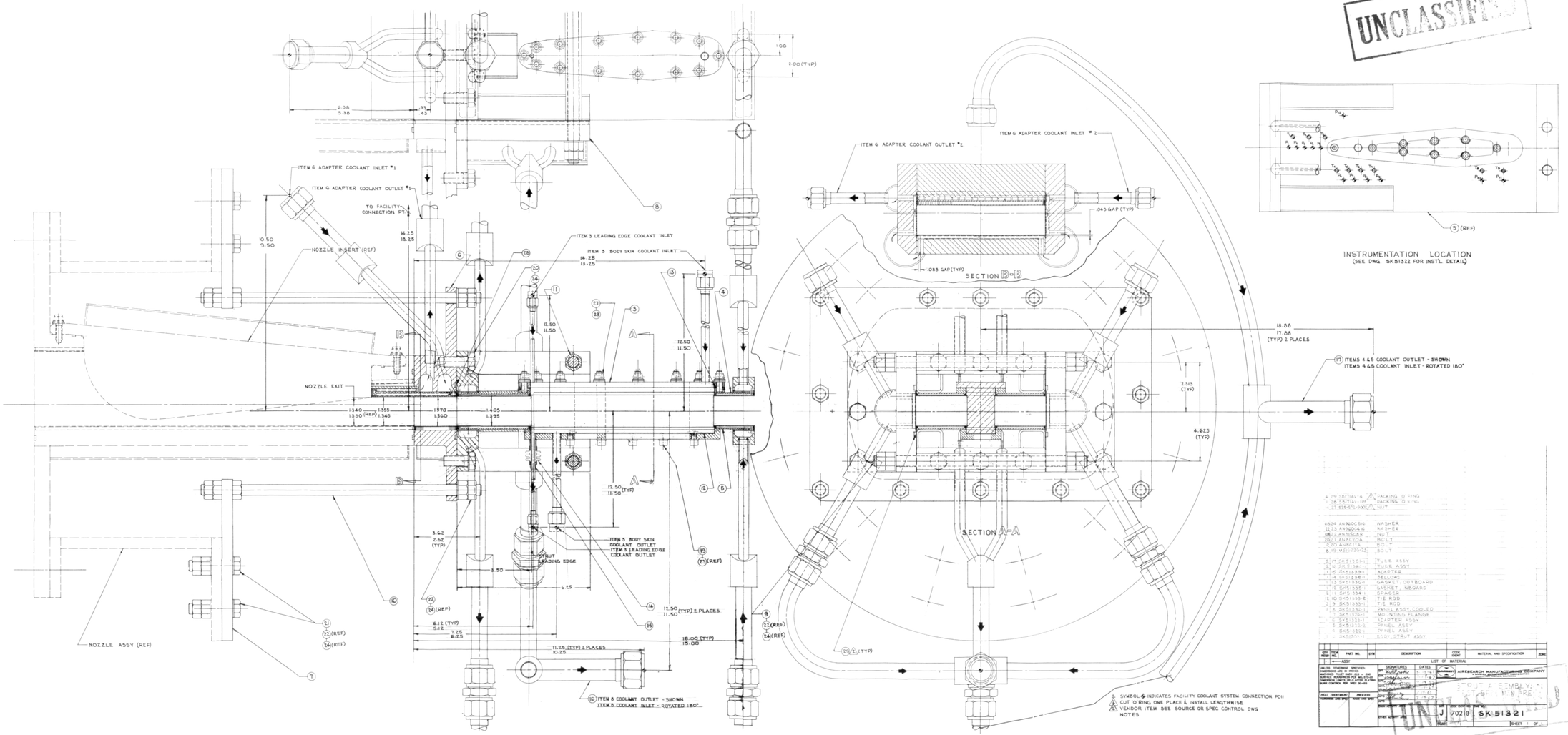

QTY ITEM REQD NO.	PART NO.	DTR	DESCRIPTION	CODE IDENT	MATERIAL AND SPECIFICATION	ZONE
←ASSY			LIST OF MATERIAL			
4 19 (REF)	AN6227A1-4	A	PACKING, O RING			
1 28 (REF)	AN6227A1-109		PACKING, O RING			
4 17	555-517-1900		NUT			
6	MS24693C81		WASHER			
12	AN960C416		WASHER			
48	AN315C8R		NUT			
2	AN5C8A		BOLT			
8	AN4C8A		BOLT			
8	MS21075C32		BOLT			
2	SK51351-1		TUBE ASSY			
2	SK51338-1		TUBE ASSY			
1	SK51339-1		ADAPTER			
1	SK51338-1		BELLOWS			
1	SK51353-1		GASKET, OUTBOARD			
1	SK51335-1		GASKET, INBOARD			
2	SK51334-1		SPACER			
12	SK51333-2		TIE ROD			
2	SK51333-1		TIE ROD			
1	SK51332-1		PANEL ASSY COOLED			
1	SK51336-1		MOUNTING FLANGE			
1	SK51322-1		ADAPTER ASSY			
1	SK51331-1		PANEL ASSY			
1	SK51332-1		PANEL ASSY			
1	AS1311-1		S-U-P STRUT ASSY			

	SIGNATURES	DATES
DRAWN		
CHECKED		
ENGR APPR		
MFG APPR		
QUAL APPR		
PROJ ENGR		

AIRESEARCH MANUFACTURING COMPANY
A DIVISION OF THE GARRETT CORPORATION
LOS ANGELES

CAGE CODE NO.	DWG NO.	REV
J 70210	SK51321	

SHEET 1 OF 1

UNCLASSIFIED

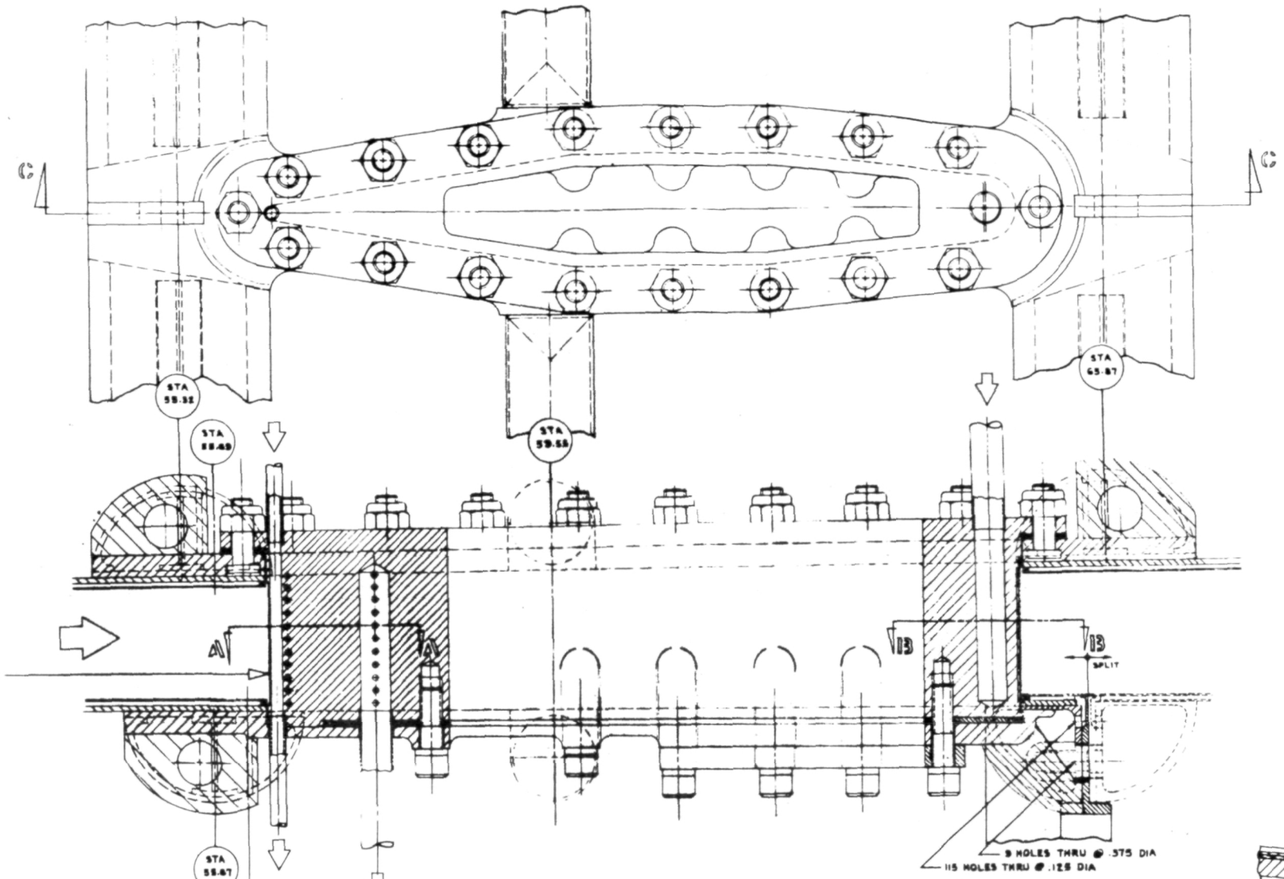

SECTION C-C

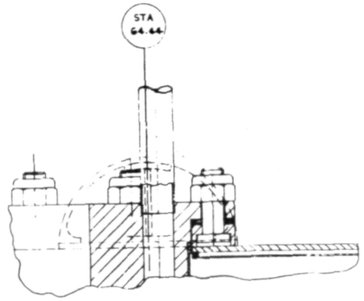

PROPOSED ALTERNATE COOLING RING POSITION

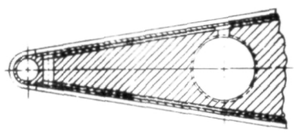

SECTION A-A
SCALE: 4/1

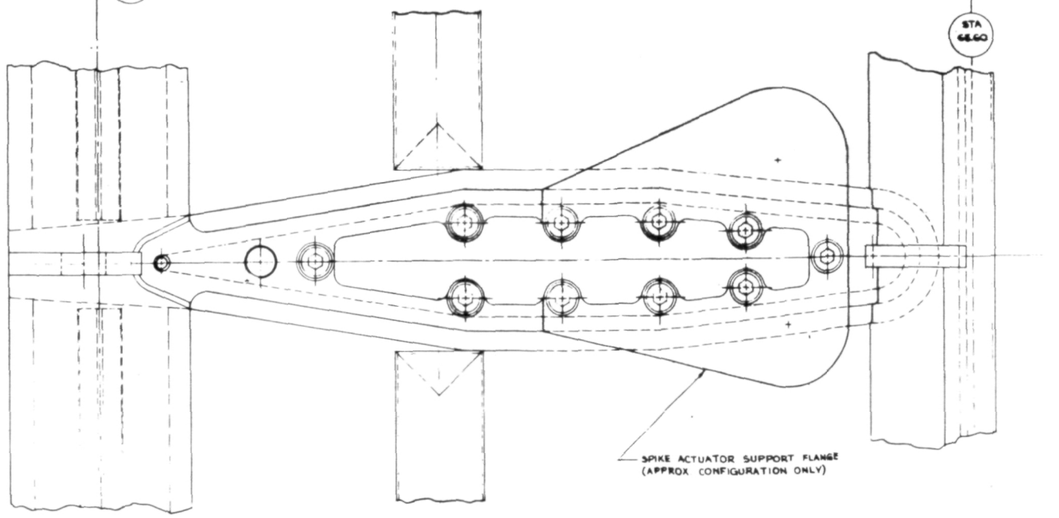

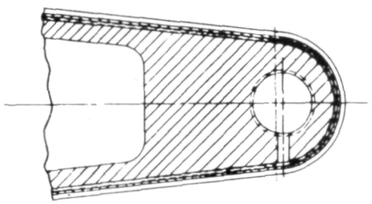

SECTION 13-13
SCALE: 4/1

PROPRIETARY NOTICE
THIS LAYOUT DRAWING EMBODIES A PROPRIETARY DESIGN OWNED BY THE GARRETT CORPORATION AND IS SUBMITTED UNDER A CONFIDENTIAL RELATIONSHIP. EXCEPT FOR USES EXPRESSLY GRANTED IN WRITING, ALL RIGHTS ARE RESERVED BY THE GARRETT CORPORATION. THIS DRAWING SHALL BE RETURNED WHEN THE NEED FOR IT HAS BEEN CONCLUDED.

AIRESEARCH MANUFACTURING COMPANY
A DIVISION OF THE GARRETT CORPORATION
LOS ANGELES, CALIFORNIA

LAYOUT

SIGNATURES	DATES	DATE STARTED	WITNESSED BY
DES W. R. COOKE	4-20-67	4-6-67	
DATE		DATE COMPLETED	WITNESSED BY
STRESS			
WEIGHT			
APPD		4-26-67	
APPD			
APPD		3402 250052-21-2500	

FEATURES
REVISED AERODYNAMIC STRUT SHAPE

SUPPORT ASSY, STRUT, H.R.E.

SIZE	CODE IDENT NO	DWG NO
J	70210	L-980608
SCALE	WT	SHEET OF

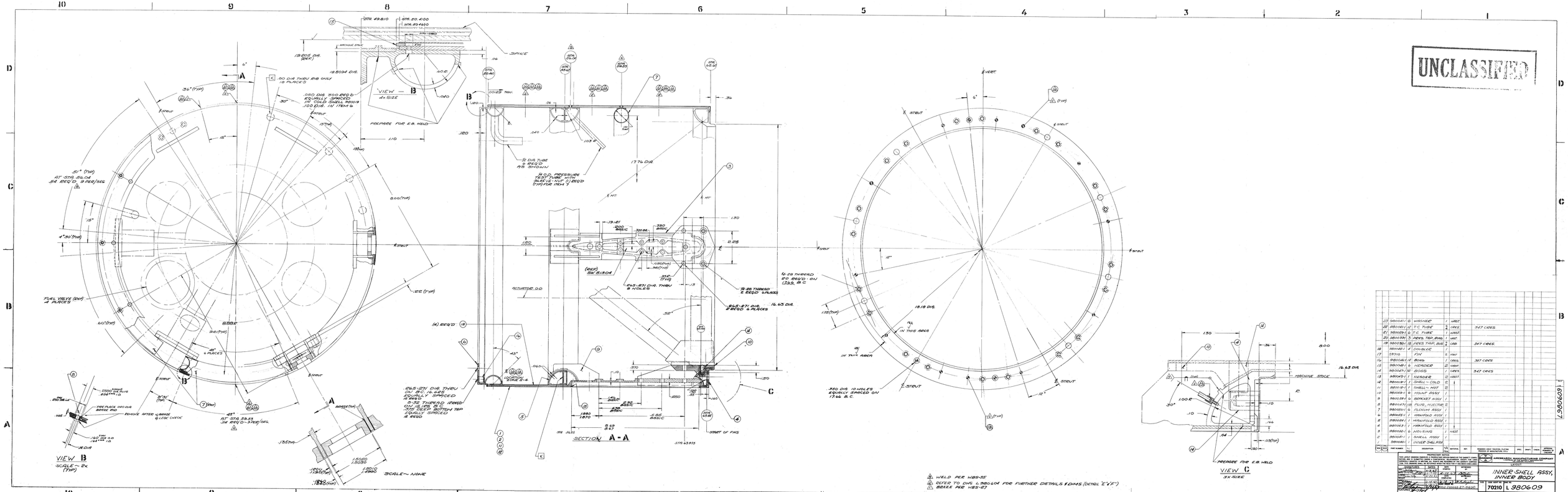

23	3800041	G	WASHER	1	MAT		
22	3800481	H	T.C. TUBE	3	CRES	347 CRES	
21	3800539	J	T.C. TUBE	1	MAT		
20	3800339	S	REVS. T&P. BRKT	1	MAT		
19	3800380	G	REVS. T&P. BUS	2	CRS	347 CRES.	
18	3800481	F	DOUBLER	1	MAT		
17	59310		PIN	8	MAT		
16	3800481	E	BOSS	1	CRES	347 CRES	
15	3800481	B	HEADER	2	MAT		
14	3800473	M	BOSS	1	CRES	347 CRES	
13	3800481	J	HEADER	2	MAT		
12	3800181	F	SHELL-COLD	1			
11	3800181	J	SHELL-HOT	1			
10	3800181	B	MOUNT ASSY	1			
9	3800589	K	BRACKET ASSY	1			
8	3800471	05	PLUG, INJECTOR	2			
7	3800551	K	PLENUM ASSY	1			
6	3800181	J	MANIFOLD ASSY	1			
5	3800181	J	MANIFOLD ASSY	1			
4	3800181	J	MANIFOLD ASSY	1			
3	3800182	G	HOUSING	1	MAT		
2	3800181	J	SHELL ASSY	1			
1	3800180	J	INNER SHELL ASSY	1			

REV	E.O.	PART NUMBER	CL	DESCRIPTION	QTY	MATERIAL	REF.

PROPRIETARY NOTICE
THIS LETTER DRAWING CONTAINS A PROPRIETARY DESIGN DISCLOSURE OF THE GARRETT CORPORATION AND IS LOANED SUBJECT TO THE AGREEMENT THAT IT SHALL NOT BE REPRODUCED, COPIED, OR USED IN WHOLE OR IN PART AS THE BASIS OF MANUFACTURE OR SALE OF ITEMS DEPICTED HEREIN WITHOUT WRITTEN PERMISSION OF THE GARRETT CORPORATION.

SIGNATURES	DATE
DRAWN [illegible]	4-8-82
CHECKED [illegible]	4-12-82
ENGR APPR [illegible]	4-12-82
PROJ ENGR [illegible]	4-12-82
QUALITY [illegible]	4-12-82
PROG MGR [illegible]	4-12-82

APPROVED
DATE
4-12-82

GARRETT TURBINE ENGINE COMPANY
A DIVISION OF THE GARRETT CORPORATION
PHOENIX, ARIZONA

TITLE
INNER SHELL ASSY, INNER BODY

SIZE 70210 | DWG NO. L 980609 | REV

SCALE 4/1 | WT | SHEET 1 OF 1

980609

UNCLASSIFIED

UNCLASSIFIED

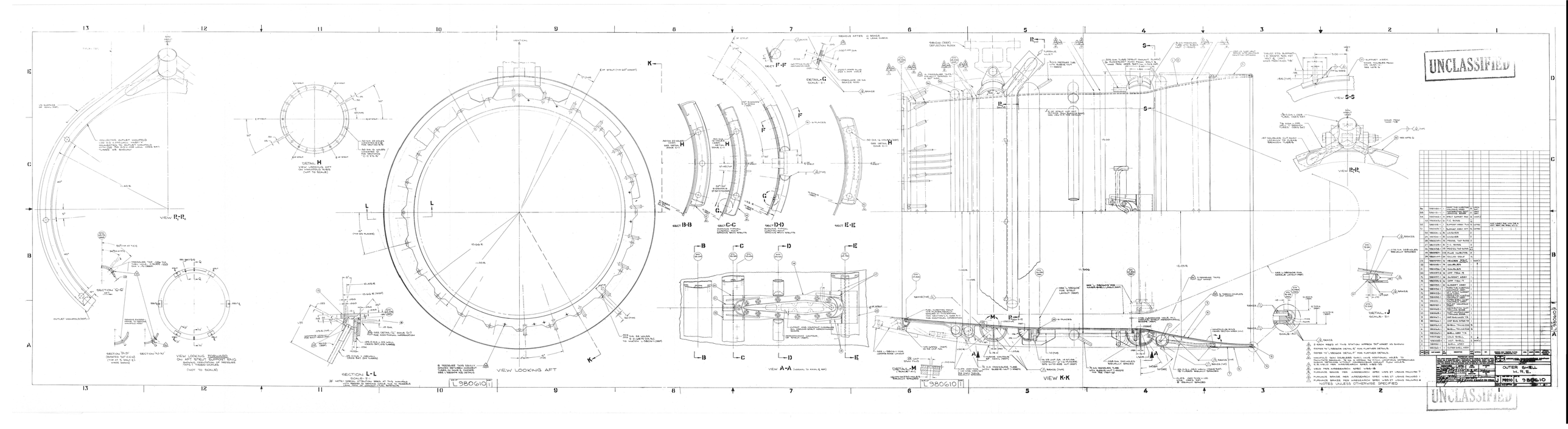
UNCLASSIFIED
VIEW R2-R2
SECTION Q-Q
SECTION T-U
VIEW LOOKING FORWARD
DETAIL H
SECTION L-L
VIEW LOOKING AFT
SECT F-F
DETAIL G
SECT B-B
SECT C-C
SECT D-D
SECT E-E
VIEW A-A
DETAIL M
VIEW K-K
VIEW S-S
VIEW R2-R2
DETAIL J
OUTER SHELL
MK 71 MOD 0
L 980610
UNCLASSIFIED

UNCLASSIFIED

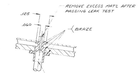

DETAIL D
SCALE - 4/1

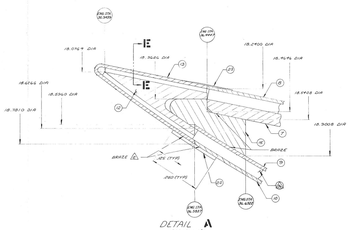

DETAIL A
SCALE - HALF

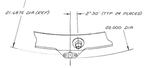

VIEW C-C

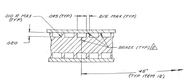

SECTION E-E

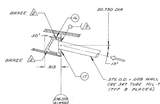

VIEW SHOWING INSTALLATION OF COOLANT INLET TUBE

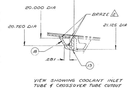

VIEW SHOWING COOLANT INLET TUBE & CROSSOVER TUBE CUTOUT

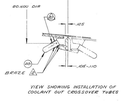

VIEW SHOWING INSTALLATION OF COOLANT OUT CROSSOVER TUBES

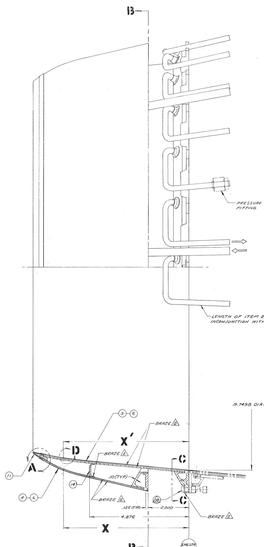

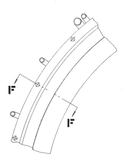

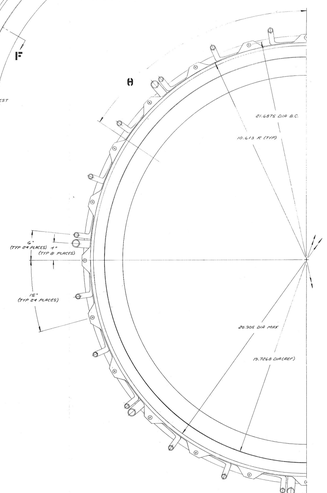

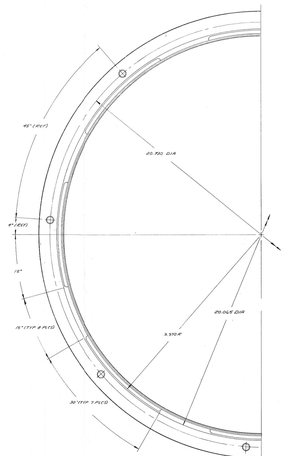

SECTION B-B

SYM	X	X'	θ	REMARKS
P_1	4.206	——	0°	HOT GAS STATIC PRESSURE
P_2	4.233	——	180°	
P_3	4.035	——	0°	
P_4	9.830	——	180°	
P_5	——	2.1170	0°	
P_6	——	2.2001	180°	
P_7	——	6.455	0°	
P_8	——	6.335	0°	
P_9	——	0.600	180°	
P_{10}	——	2.230	0°	
P_{11}	——	2.585	180°	HOT GAS STATIC PRESSURE
P_{12}	——	——	7°16'	COOLANT INLET STATIC PRESSURE
P_{13}	——	——	8°30'	
P_{14}	——	——	23°42'	
P_{15}	——	——	338°18'	
P_{16}	——	——	353°30'	
P_{17}	——	——	368°58'	
P_{18}	——	——	188°	COOLANT INLET STATIC PRESSURE
P_{19}	——	——	0°	COOLANT OUTLET STATIC PRESSURE
P_{20}	——	——	171°30	
P_{21}	——	——	351°4'	
P_{22}	——	——	186°4'	
P_{23}	——	——	374°	COOLANT OUTLET STATIC PRESSURE
T	2.000	——	180°	HOT WALL TEMPERATURE
T_1	3.600	——	180°	HOT WALL TEMPERATURE
T_2	11.780	——	0°	COLD WALL TEMPERATURE
T_3	9.730	——	0°	
T_4	3.793	——	0°	
T_5	——	1.990	0°	
T_6	——	9.780	0°	
T_7	——	9.730	0°	
T_8	——	3.000	0°	
T_9	2.780	——	180°	
T_{10}	3.780	——	180°	
T_{11}	9.780	——	180°	
T_{12}	9.730	——	180°	
T_{13}	2.780	——	180°	
T_{14}	9.780	——	270°	
T_{15}	——	2.780	270°	COLD WALL TEMPERATURE
T_{16}	——	——	4°30'	COOLANT INLET TEMPERATURE
T_{17}	——	——	349°30	COOLANT INLET TEMPERATURE
T_{18}	——	——	2°18'	COOLANT OUTLET TEMPERATURE
T_{19}	——	——	89°24'	
T_{20}	——	——	90°	
T_{21}	——	——	185°	
T_{22}	——	——	274°	
T_{23}	——	——	18°	COOLANT OUTLET TEMPERATURE
P_{24}	——	——	26°	COOLANT OUTLET STATIC PRESSURE
T_{24}	——	——	197°30	COOLANT OUTLET STATIC PRESSURE

PROVIDE CUTOUTS IN ITEM 14 — INLET MANIFOLD △ — OUTLET MANIFOLD △

PROVIDE CUTOUT IN ITEM 14 — INLET MANIFOLD △ — OUTLET MANIFOLD △ — OUTLET MANIFOLD △

△ HELD PER MBS 36.
△ BRAZE PER MBS 27.
REFER TO DRAWING L380610M (DETAILS 'A','C','F&G') FOR INSTALLATION DETAILS & DIMENSIONS.
NOTE: UNLESS OTHERWISE SPECIFIED.

19	305-04-960	4	NUT, PLATE	2				
18	2330B	24	PIN	24	MBS F		AMS 5534	
17	380609-1	3	TUBE, THERMOCOUPLE	3	CRES 347		MIL-T-8808 (SHIP SET)	
16	380608-1	1	MANIFOLD	1	MBS F		AMS 5536	
15	380607-1	1	MANIFOLD ASSY	1	MBS F		AMS 5534	
14	380638-1	1	SHELL, FIRST TAPE	1	MBS F		AMS 5534	
13	380638-1	1	SHELL, FIRST TAPE	1	MBS F		GD-3.76.3 CLASS 347	
12	380629-1	1	TUBE, THERMOWELL	1	MBS F		AMS 5536	
11	380640-1	1	MANIFOLD, INNER	1	MBS F		AMS 5534	
10	380639-1	1	MANIFOLD, OUTER	1	MBS F		AMS 5534	
9	380639-1	24	COLLAR	5	CRES 347		MIL-C-5241 - CLASS 2A	
8	380638-1	24	TUBE, CROSSOVER	2	CRES 347		MIL-T-8808 (SHIP SET)	
7	380638-1	1	FLANGE, INTL OUTLET	1	MBS F		AMS 5534	
6	380638-1	1	RING, FWD, OUTLET	1	MBS F		AMS 5534	
5	380638-1	1	RING, INTL, INLET	1	MBS F		AMS 5534	
4	380638-1	1	RING, FWD, INLET	1	MBS F		AMS 5534	
3	380638-1	1	RING, SUPPORT	1	MBS F		AMS 5534	
2	380638-1	1	RING, SUPPORT	1	MBS F		AMS 5534	
1	380638-1	1	SHELL, LEADING EDGE	1	MBS F		AMS 5534	
12	380638-1	8	SEGMENT, TIP	11	MBS F		AMS 5534	
11	380638-1	1	TIP ASSY	1				
10	380638-1	1	SHELL, MID OUTER	6	MBS F		AMS 5534	
9	380638-1	1	SHELL, COLD OUTER	6	MBS F		AMS 5534	
8	380638-1	1	SHELL, MID INNER	6	MBS F		AMS 5534	
7	380638-1	1	SHELL, COLD INNER	6	MBS F		AMS 5534	
6	380638-1	1	SHELL ASSY, OUTER	6				
5	380638-1	1	SHELL ASSY, INNER	6				
4	380638-1	1	BRAZE ASSY, OUTER	6				
3	380638-1	1	BRAZE ASSY, INNER	6				
2	380638-1	1	BRAZE ASSY	1				
1	380638-1	1	LEADING EDGE ASSY	1				

NO.	PART NUMBER	QTY.	DESCRIPTION	MATERIAL	REF.	UNLESS OTHERWISE SPECIFIED DIMENSIONS ARE IN INCHES TOLERANCES ARE	APPD.	DRAFT.	DATE

PROPRIETARY NOTICE
THIS DRAWING IS THE PROPERTY OF GENERAL ELECTRIC COMPANY AND IS LOANED SUBJECT TO AGREEMENT THAT NEITHER IT NOR THE INFORMATION IT DISCLOSES WILL BE USED, LOANED, COPIED, QUOTED OR DISCLOSED IN WHOLE OR IN PART EXCEPT AS AUTHORIZED IN WRITING BY GENERAL ELECTRIC COMPANY.

GENERAL ELECTRIC COMPANY
EVENDALE, OHIO

LAYOUT, CONL LEADING EDGE, H.P.E.

DESIGN APPROVAL		SIZE	CODE IDENT. NO.
DRAFTING APPROVAL		D	07916
STRESS APPROVAL		SCALE	DWG. NO. L380611
MFG. APPROVAL			
QUALITY CONTROL APPROVAL		DATE 7/7/67	SHEET 1 OF 1

UNCLASSIFIED

UNCLASSIFIED

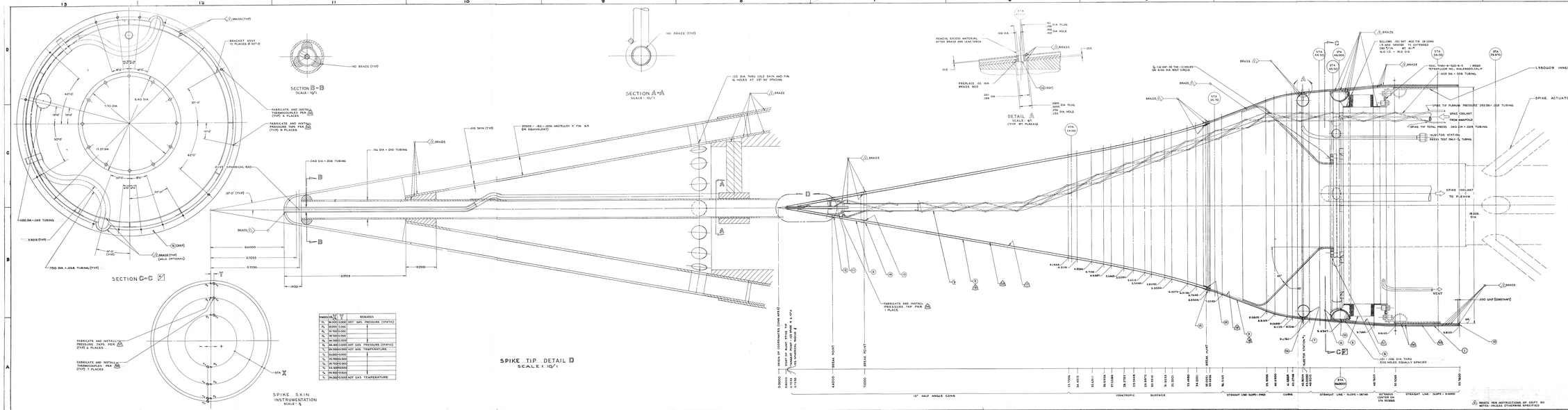
SECTION C-C
SECTION B-B
SCALE : 10/1
SECTION A-A
SCALE : 10/1
DETAIL A
SCALE : 4/1
(TYP 8PT PLACES)
SPIKE TIP DETAIL D
SCALE : 10/1
SPIKE SKIN
INSTRUMENTATION
SCALE : 1/4
BRAZE (TYP)
BRACKET ASSY
15 PLACES @ 30°-0'
FABRICATE AND INSTALL
THERMOCOUPLES PER
(TYP) 5 PLACES
FABRICATE AND INSTALL
PRESSURE TAPS PER
(TYP) 19 PLACES
.040 DIA x .008 TUBING
.156 DIA x .028 TUBING
.050 SKIN (TYP)
.125 SPHERICAL RAD
.100 DIA
.050 DIA
.055
.015
.025
.005
.035
.010
.020
.030
.040
.050
.060
.070
.080
.090
.100
.110
.120
.130
.140
.150
.160
.170
.180
.190
.200
.210
.220
.230
.240
.250
.260
.270
.280
.290
.300
.310
.320
.330
.340
.350
.360
.370
.380
.390
.400
.410
.420
.430
.440
.450
.460
.470
.480
.490
.500
.510
.520
.530
.540
.550
.560
.570
.580
.590
.600
.610
.620
.630
.640
.650
.660
.670
.680
.690
.700
.710
.720
.730
.740
.750
.760
.770
.780
.790
.800
.810
.820
.830
.840
.850
.860
.870
.880
.890
.900
.910
.920
.930
.940
.950
.960
.970
.980
.990
1.000
1.010
1.020
1.030
1.040
1.050
1.060
1.070
1.080
1.090
1.100
1.110
1.120
1.130
1.140
1.150
1.160
1.170
1.180
1.190
1.200
1.210
1.220
1.230
1.240
1.250
1.260
1.270
1.280
1.290
1.300
1.310
1.320
1.330
1.340
1.350
1.360
1.370
1.380
1.390